cGMP Signaling in Brown Adipocytes

Dissertation

zur

Erlangung des Doktorgrades (Dr. rer. nat.)

dei

Mathematisch-Naturwissenschaftlichen Fakultät

der

Rheinischen Friedrich-Wilhelms-Universität Bonn

vorgelegt von

Daniel Ray Rowland

aus

Wiesbaden-Frauenstein, Deutschland

Bonn 2024

Angefertigt mit Genehmigung der Mathematisch-Naturwissenschaftlichen Fakultät der Rheinischen Friedrich-Wilhelms-Universität Bonn

Gutachter/Betreuer: Prof. Alexander Pfeifer

Gutachter: Prof. Günther Weindl

Tag der Promotion: 30.10.2024

Erscheinungsjahr: 2024

Acknowledgments

First and foremost, I extend my deepest gratitude to Prof. Alexander Pfeifer. Your support, supervision, and mentorship have been the cornerstone of this thesis, making it all possible.

I also want to thank my second supervisor, Prof. Elvira Mass, for your valuable input and the stimulating scientific discussions. I am equally grateful to Prof. Günther Weindl for kindly agreeing to review this work.

I am thankful to the DFG and the GRK 1873 for their generous funding and the structured framework they provided. A special thanks to Elisabeth Mies-Klomfass for managing GRK 1873 and organizing crucial workshops that enhanced my scientific capabilities.

My sincere thanks go to Dennis de Conninck, who not only supervised much of this thesis but also meticulously proofread it. Your insights and ideas in the early stages were vital to the project's success. I am also grateful to Thorsten Gnad for his valuable contributions throughout the project and for helping with the proofreading.

I would like to acknowledge and thank the pharmacy students, Alina, Anna, and Nadine, who accompanied me on this PhD journey. Your curiosity and enthusiasm for science have been a great source of support and inspiration.

To my friends at IPT - Alex, Danli, Laura, Caro, Mickel, Zheming, and Nina - thank you for the support and the great time we had together.

I am profoundly grateful to my partner Hannah, who moved all the way to Bonn for me and has supported me wholeheartedly throughout this entire journey. Nobody helped me as much as you did to weather the ups and downs during this time. Thank you for always having my back.

Finally, my deepest gratitude goes to my parents. Since my childhood, you have always believed in me, instilling in me the unwavering conviction that I can achieve anything I set my mind to. Your continuous support has been my foundation, and without you, I wouldn't be where I am today.

Table of Contents

List of Abbreviations	III
List of Figures	VI
List of Tables	VIII
1. Introduction	1
1.1 Obesity – A global pandemic	1
1.2 Adipose tissue – brown, white, and beige	2
1.2.1 General	2
1.2.2 Anatomy of WAT and BAT	3
1.2.3 Transcriptional regulation of BAT	5
1.2.4 Role and function of BAT	6
1.2.5 BAT in humans	7
1.2.6 Pharmacological activation of BAT	8
1.3 cGMP signaling	10
1.3.1 cGMP as a drug target for cardiovascular and metabolic diseases	10
1.3.2 cGMP signaling overview	11
1.3.3 Natriuretic peptides	12
1.3.4 Nitric oxide	14
1.3.5 Protein kinase G	14
1.3.6 Phosphodiesterases	15
1.3.7 Compartmentalization of cyclic nucleotide signaling	17
1.4 Förster resonance energy transfer	20
2. Aim of the thesis	22
3. Materials and methods	23
3.1 Chemicals and reagents	23
3.1.1 Antibodies	23
3.1.2 Primers for qRT-PCR	23
3.1.3 Drugs	26
3.2 Animals	27
3.3 Cell Culture	31
3.3.1 Murine brown adipocyte culture	32
3.3.2 Human brown adipocyte culture	34
3.4 Oil Red O staining	36
3.5 Analysis of intracellular cAMP and cGMP concentrations via ELISA	37
3.6 In vitro lipolysis	37
3.7 RNA isolation, cDNA synthesis and qRT-PCR	38
3.7.1 Isolation of RNA	38

	3.7.2 Synthesis of complementary DNA	39
	3.7.3 Quantitative real-time polymerase chain reaction	39
	3.8 Protein isolation	40
	3.8.1 Isolation of proteins	41
	3.8.2 Quantification of protein content via Bradford Assay	42
	3.9 Sodium-dodecyl sulfate polyacrylamide gel electrophoresis and Western Blot	42
	3.9.1 Preparation of protein samples	43
	3.9.2 Sodium-dodecyl sulfate polyacrylamide gel electrophoresis	43
	3.9.3 Western Blotting	44
	3.10 Real-time imaging of cyclic nucleotides in BA via FRET	46
	3.10.1 FRET calculations	48
	3.11 Real-time imaging of cyclic nucleotides in human preBA and BA	49
	3.12 Development of organelle-targeted cGMP biosensors	50
	3.13 Statistical analysis	53
4.	. Results	54
	4.1 Expression of cGMP generators and PDEs in murine BA and BAT	54
	4.2 Establishing cGMP FRET measurements in murine preBA	58
	4.3 cGMP generators in murine preBA	60
	4.4 cGMP compartmentalization in murine preBA	65
	4.5 cGMP compartmentalization in murine BA	67
	4.6 Calcium cGMP crosstalk in murine preBA	69
	4.7 Calcium cGMP crosstalk in murine BA	72
	4.8 Role of PDE1 in murine BA differentiation	74
	4.9 Effect of calcium and PDE1 on murine BA differentiation	76
	4.10 Role of cGMP in inducing lipolysis in murine BA	77
	4.11 cGMP and cAMP crosstalk in murine preBA	78
	4.12 cGMP and cAMP crosstalk in murine BA	83
	4.13 Expression of cGMP generators and PDEs in human BA and BAT	87
	4.14 Real-time imaging of human preBA with the Green cGull biosensor	89
	4.15 Real-time imaging of human BA using the Green cGull biosensor	93
	4.16 Targeted cGMP sensors in hBA	95
5.	. Discussion	99
	5.1 cGMP compartmentalization in murine BA and the role of PDE1	99
	5.2 cGMP compartmentalization during BA differentiation	101
	5.4 cGMP synthesis in human adipocytes	106
	5.5 cGMP compartmentalization in human brown adipocytes	108
R	eferences	111
S	ummary	127

List of Abbreviations

AC Adenylate cyclase
ANOVA Analysis of variance
ANP Atrial natriuretic peptide
aP2 Fatty acid binding protein 4
APS Ammoniumperoxodisulphate

AT Adipose tissue

ATGL Adipose triglyceride lipase

BA Brown adipocytes
BAT Brown adipose tissue
BMI Body-Mass-Index

BNP Brain-type natriuretic peptide

BP Base pairs

BSA Bovine serum albumin CaM Calcium-calmodulin

cAMP Cyclic adenosine monophosphate

CE Cold exposure

C/EBP CCAAT/enhancer-binding proteins

CFP Cyan fluorescent protein

cGMP Cyclic guanosine monophosphate

CI Confidence interval
CN Cyclic nucleotide
CNG Cyclic nucleotide-ga

CNG Cyclic nucleotide-gated CNO Clozapine-N-oxide

Ct Cycle threshold

CNP

CTEPH Chronic thromboembolic pulmonary hypertension

DEA-NO Diethylamine NONOate
DEPC-H₂O Diethylpyrocarbonat-H₂O
DETA-NO Diethylenetriamine NONOate
DMEM Dulbecco's Modified Eagle Medium

DMSO Dimethyl sulfoxide

DREADD Designer receptor exclusively activated by designer drugs

C-type natriuretic peptide

EC₅₀ Half maximal effective concentration

ED Erectile dysfunction

EDTA Ethylene diamine tetraacetic acid

EE Energy expenditure

ELISA Enzyme-linked immunosorbent assay eNOS Endothelial nitric oxide synthase

EtOH Ethanol

FDG Fluorodeoxyglucose FFA Free fatty acids

FRET Förster resonance energy transfer

GC Guanylate cyclase

GPCR G-protein-coupled receptors hBA Human brown adipocyte

HEPES N-(2-hydroxyethyl)-piperazine-N'-2-ethansulfonic acid

HFD Heart failure HFD High-fat diet

HPRT Hypoxanthine-guanine phosphoribosyltransferase

HSL Hormone-sensitive lipase IBMX Isobutylmethylxanthine

iNOS Inducible nitric oxide synthase

LB Lysogeny broth

mRNA Messenger ribonucleic acid MSC Mesenchymal stem cells

NE Norepinephrine
NEP Neprilysin

nNOS Neuronal nitric oxide synthase

NO Nitric oxide

NOS Nitric oxide synthase NP Natriuretic peptide

NPRA Natriuretic peptide receptor A
NPRB Natriuretic peptide receptor B
NPRC Natriuretic peptide receptor C
NST Nonshivering thermogenesis

p38 MAPK p38 mitogen-activated protein kinase
PAGE Polyacrylamide gel electrophoresis
PAH Pulmonary arterial hypertension

PDE Phosphodiesterase

PDEI Phosphodiesterase inhibitor
PET Positron emission tomography

PFA Paraformaldehyde
PGC1α PPARγ coactivator 1α
PKA Protein kinase A
PKG Protein kinase G

PPARy Peroxisome proliferator-activated receptor gamma

PRDM16 PR domain containing 16
P/S Penicillin and streptomycin
preBA Premature BA (BA progenitors)
ROCK Rho-associated protein kinase

RT Room temperature
SDS Sodium dodecyl sulfate
SEM Standard error of the mean
SGC Soluble guanylate cyclase
SNS Sympathetic nervous system
ST Shivering thermogenesis
T2DM Type 2 diabetes mellitus

TAE Triiodothyronine TRIS-acetate-EDTA

TBST Tris-buffered saline with tween 20 TEMED N-N-N'-N'-tetramethyl ethylene diamine

TF Transcription factors

UCP1 Uncoupling protein 1
WA White adipocytes
WAT White adipose tissue

WATg Gonadal white adipose tissue
WATi Inguinal white adipose tissue
WHO World Health Organization

WT Wild type

YFP Yellow fluorescent protein

 $\beta\text{-AR} \hspace{1cm} \beta\text{-adrenoceptors}$

List of Figures

Figure 1: Global prevalence of overweight or obesity as reported by the WHO in 2021	2
Figure 2: Schematic depiction of white, beige, and brown adipocytes	3
Figure 3: Location of ATs in humans and mice	4
Figure 4: Function of BAT	7
Figure 5: cGMP generators and effectors	17
Figure 6: Expression of cGMP-related genes in murine preBA and BA	55
Figure 7: Effect of cold exposure on BAT PDE mRNA expression	55
Figure 8: Effect of murine BA differentiation on NPR mRNA abundance	56
Figure 9: Relative mRNA expression ratios of the NPRs during differentiation of murine B	3A57
Figure 10: Expression of sGC-subunit coding genes during differentiation of murine BA	58
Figure 11: Pseudo-colored confocal fluorescence images of cGi-500 murine preBA	58
Figure 12: Real-time cGMP dynamics in murine preBA expressing the cGi-500 FRET biosensor	59
Figure 13: DEA-NO and CNP dose-response curves in murine preBA	60
Figure 14: Basal cGMP levels in murine preBA and BA	61
Figure 15: Real-time measurements of cGMP synthesis in cGi-500 preBA versus BA	63
Figure 16: cGMP synthesis quantification in murine preBA and BA via ELISA	64
Figure 17: Regulation of NPRB-cGMP versus sGC-cGMP by PDEs in murine preBA	66
Figure 18: Regulation of GC-associated cGMP pools by PDEs in murine BA	68
Figure 19: Gαq-calcium cGMP crosstalk in murine preBA	70
Figure 20: Role of PDE1 in mediating calcium cGMP crosstalk in murine preBA	71
Figure 21: Role of PDE1 in mediating calcium cGMP crosstalk in murine BA	73
Figure 22: GC-specific effects of PDE1 inhibition on murine BA adipogenic and thermoge marker mRNA expression	
Figure 23: NPRB-specific effect of PDE1 inhibition on murine BA adipogenic and thermogenic marker protein expression	75
Figure 24: Dependence of calcium-induced impairment of murine BA differentiation on PI	
Figure 25: Individual and additive effects of cGMP on lipolysis in murine BA	78
Figure 26: cGMP-cAMP crosstalk in murine epac1-camps preBA	79
Figure 27: Effect of adrenergic stimulation on cGMP-cAMP crosstalk in murine preBA	80
Figure 28: Role of PDE3 in cGMP-cAMP crosstalk in murine preBA	81
Figure 29: Role of PDE2 in cGMP-cAMP crosstalk in murine preBA	82
Figure 30: Basal effect of PDE2 or PDE3 inhibition on cytosolic cAMP levels murine preB	3A 82
Figure 31: Crosstalk between cGMP and cAMP in fully differentiated murine BA	84
Figure 32: β-AR specific cGMP-cAMP crosstalk in murine BA	86
Figure 33: Effect of PDE2 inhibition in altering the β -AR specific cGMP-cAMP crosstalk in	
murine BA	87

Figure 34: mRNA expression of sGC and NPR-related genes in human BA	88
Figure 35: PDE expression in human BA and BAT	89
Figure 36: Fluorescence image of human preBA transduced with the Green cGull intensiometric biosensor	90
Figure 37: Fluorescence response of Green cGull expressing human preBA to cGMP-inducing drugs	90
Figure 38: Real-time measurements of cGMP synthesis in human preBA	91
Figure 39: Real-time measurements of cGMP synthesis in human BA	93
Figure 40: Regulation of NPRA-cGMP by PDEs in human BA	94
Figure 41: Role of PDE1 in Calcium cGMP crosstalk in human BA	95
Figure 42: Fluorescence image of human preBA transduced with the Green cGull-NLS intensiometric biosensor	96
Figure 43: Targeted and untargeted Green cGull dose-response curves in human preBA t	to 97
Figure 44: cGMP synthesis at different cell organelles in human preBA	98
Figure 45: Fluorescence traces of DEA-NO induced cGMP synthesis at different cell organelles in human preBA	98
Figure 46: Schematic depiction of the association of different cGMP pools with their speci	ific .103

List of Tables

Table 1: Primary antibodies	23
Table 2: Secondary antibodies	23
Table 3: Primers for quantitative real-time polymerase chain reaction (qRT-PCR)	23
Table 4: Drugs used for experiments	26
Table 5: List of mice used	28
Table 6: Primers and amplification products for R26-CAG-cGI500 genotyping	29
Table 7: Mixture for R26-CAG-cGi500 genotyping via PCR	29
Table 8: PCR program for genotyping of R26-CAG-cGi500 mice	30
Table 9: Recipe for TAE buffer 50x	30
Table 10: PCR products for WT, heterozygous, and homozygous R26-CAG-cGi500 mice	30
Table 11: BA isolation buffer	32
Table 12: BA isolation buffer ready to use	32
Table 13: BA culture medium	32
Table 14: BA growth medium	33
Table 15: BA freezing medium	34
Table 16: BA differentiation medium	34
Table 17: BA induction medium	34
Table 18: hBA proliferation medium	35
Table 19: hBA differentiation medium	35
Table 20: hBA induction medium ready to use	35
Table 21: PFA 4% solution	36
Table 22: Oil Red O stock solution	36
Table 23: Oil Red O working dilution	36
Table 24: Lipolysis medium	37
Table 25: cDNA Synthesis Program	39
Table 26: Primer mastermix for qRT-PCR	40
Table 27: qRT-PCR program with melting curve	40
Table 28: RIPA buffer recipe	41
Table 29: Lysis buffer recipe	41
Table 30: Coomassie Solution Recipe	42
Table 31: 3x Laemmli buffer recipe	43
Table 32: Composition of the separating gel	44
Table 33: Composition of the stacking gel	44
Table 34: 10x electrophoresis buffer recipe	44
Table 35: 1x Transfer buffer recipe	45
Table 36: 10x Tris-buffered saline (TBS) recipe	45
Table 37: TBS-Tween (TBST) recipe	46

Table 38:	Blocking buffer	.46
Table 39:	Stripping buffer recipe	.46
Table 40:	Ringer's solution recipe	.47
Table 41:	Restriction digestion mixture	.51
Table 42:	Ligation mixture	.51
Table 43:	LB+ medium	.52
Table 44:	Ampicillin LB+ plates	.52
Table 45:	Glycerol stock recipe	.52
Table 46:	Green cGull biosensors characteristics:	.97

1. Introduction

1.1 Obesity – A global pandemic

The world is experiencing a global obesity pandemic¹. Obesity is characterized by an imbalance between energy intake and energy expenditure (EE), whereby the former exceeds the latter, leading to the storage of excess energy in the form of fat². This imbalance is caused by our modern increasingly sedentary lifestyles, overeating of energy-dense food, and reduced physical activity³.

The Body-Mass-Index (BMI) is used to classify obesity and overweight. A BMI above or equal to 25 and below 30 is considered overweight / pre-obese, while a BMI above or equal to 30 is considered obese⁴. Obesity is a central risk factor for cardiometabolic diseases, such as hypertension, dyslipidemia, heart disease, ischemic strokes, type 2 diabetes mellitus, and even certain types of cancer^{5,6}. These cardiometabolic diseases are the leading cause of global mortality and morbidity, placing obesity at the forefront of global causes of death⁷. The World Health Organization (WHO) reported in 2021 that the rate of obesity had nearly tripled since 1975, with more than 1.9 billion people being overweight globally, of which 650 million were obese in 2016² (Figure 1). This worsening trend is predicted to continue into the foreseeable future^{7,8}. Alarmingly, on the global scale, more deaths occur as a consequence of excess consumption of food than from malnutrition⁸, a situation that has never been observed throughout human history. Consequently, obesity does not only represent a major burden for each affected individual but also for public healthcare systems. Although obesity represents one of the most urgent issues for global health, there remains an unmet need for novel treatment options⁹.

Obvious approaches to combat the obesity pandemic include the reduction of energy intake, as well as the increase of energy expenditure, via diet and exercise. However, global and regional efforts to improve nutrition awareness or to increase physical activity have proven ineffective^{2,7}. Furthermore, a transition away from the modern sedentary lifestyle seems unlikely.

A well-established treatment option for obesity is bariatric surgery. However, bariatric surgery is invasive and poses significant risks for patients undergoing the treatment¹⁰. Therefore, it is essential to improve our understanding of the underlying causes of obesity and to explore potential non-invasive pharmacological treatment approaches. One relevant target tissue for these treatment approaches is brown adipose tissue (BAT).

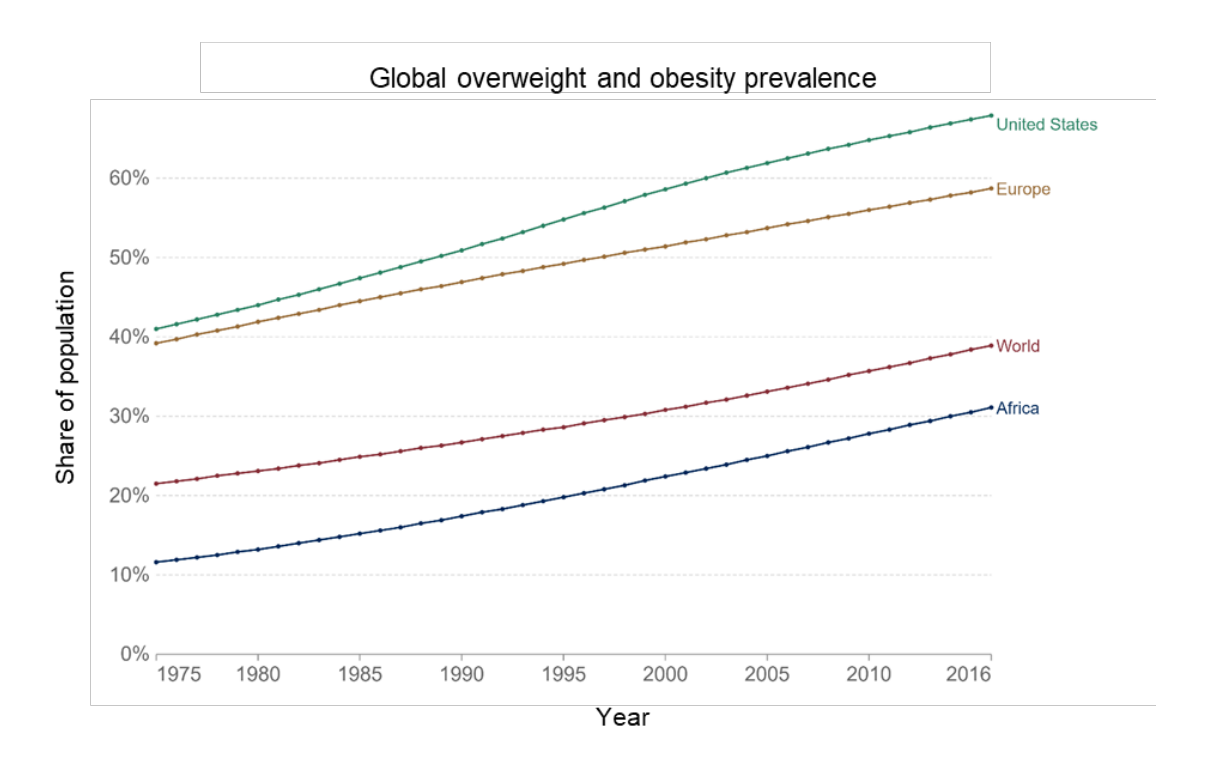


Figure 1: Global prevalence of overweight or obesity as reported by the WHO in 2021 The figure was adapted from ourworldindata.org using data from WHO².

1.2 Adipose tissue – brown, white, and beige

1.2.1 General

In mammals, the adipose organ is made up of at least two different types of tissue: White adipose tissue (WAT) and BAT¹¹. While WAT represents the primary form of energy storage, BAT is specialized for EE, where calories are burned to produce heat via a process called nonshivering thermogenesis (NST)^{12,13}. Beyond storing triglycerides during energy abundance and releasing lipids as well as enzymatically hydrolyzing them during nutrient deficits, WAT is also an important endocrine organ¹⁴. The hormones secreted from WAT are called "adipokines". Some of the most well understood adipokines are adiponectin and leptin, which influence appetite, satiety, and insulin-sensitivity and -secretion^{14,15}.

In contrast to WAT, BAT is highly innervated by the sympathetic nervous system and thoroughly vascularized, which ensures a sufficient supply of oxygen and nutrients for thermogenesis¹¹. While white adipocytes (WA) store lipids in large single lipid droplets (unilocular), brown adipocytes (BA) are multilocular containing multiple smaller lipid droplets, thus increasing the relative surface area of the droplets, enabling more rapid degradation¹⁶. Additionally, BA are distinct from WA in that their more abundant mitochondria are enriched with the uncoupling protein 1 (UCP1). UCP1, localized at the inner mitochondrial membrane, uncouples substrate oxidation within the respiratory chain from ATP production, producing heat instead^{13,16} (Figure 2). BA are, thus, equipped with substantial respiratory capacity¹³. It is from the high content of mitochondria, which are rich in iron, that BAT gains its distinct brown

color. Apart from WA and BA, another type of adipocyte has been described – the beige or brite adipocyte^{13,16}. These beige adipocytes share many characteristics with BA, such as high expression levels of UCP1, a multilocular / paucilocular appearance, and a high mitochondria content^{13,17}. Beige adipocytes are sometimes called inducible brown adipocytes because they can be derived from fully mature WA via a process called transdifferentiation¹⁷. Transdifferentiation mainly occurs in response to prolonged sympathetic stimulation of a WAT depot, for example, during extended periods of cold exposure (CE)^{16,17}. Transdifferentiation from WA to beige adipocytes gives rise to brown-like cell clusters in WAT depots, resulting in a browner appearance of WAT which is hence called browning^{18,19}. However, the origin of beige adipocytes remains controversial, with some potentially arising de-novo from distinct progenitors, instead of transdifferentiating from reprogrammed WA²⁰. Even though beige and brown adipocytes share many characteristics, they represent different cell types with unique transcriptomic signatures^{13,16,21}.

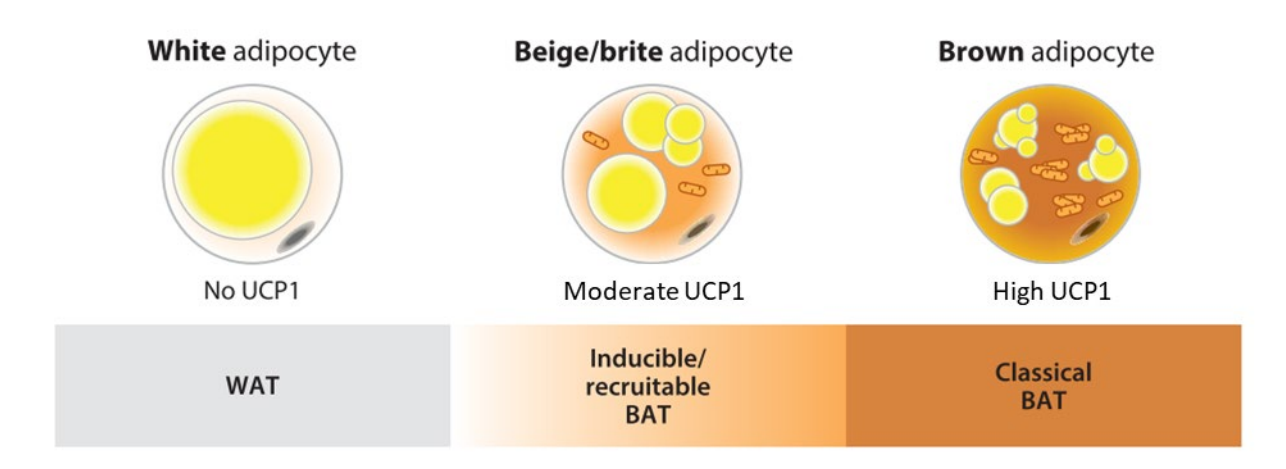


Figure 2: Schematic depiction of white, beige, and brown adipocytes

The types of adipocytes are characterized by distinct differences in morphology and function. WA mainly consist of one large unilocular lipid droplet without any notable UCP1 expression, while beige and brown adipocytes have multilocular lipid droplets and an increased amount of mitochondria rich in UCP1. The figure has been adapted from Pfeifer and Hoffmann 2015¹³.

1.2.2 Anatomy of WAT and BAT

Both BAT and WAT have distinct anatomical features and locations. In general, the adipose organ is composed of several subcutaneous and visceral depots. Rodents possess two main subcutaneous fat depots – an anterior and a posterior. The anterior region lies at the base of the forelimbs and occupies the dorsal body region around the scapulae, the cervical area, and the axillary and proximal regions of the forelimbs. The posterior region is located at the base of the hind legs and consists of a single tissue band¹¹. This depot is oftentimes classified as inguinal white adipose tissue (WATi) and frequently used for experiments, due to its high potential for browning²². On the other hand, the visceral depots are located at the thorax and the abdominal cavity or around the kidneys (perirenal) as well as around the gonads

(perigonadal, WATg)¹¹. WATg is commonly used in experiments as a "pure" form of WAT, as it has a limited potential for transdifferentiation of WA to beige adipocytes²².

Contrarily, BAT is mainly found in the interscapular, subscapular, perirenal, periaortal, and mediastinal regions of mice^{11,16}. However, BA can also be found in WAT depots, especially after CE or otherwise increased tonus of the sympathetic nervous system (SNS)^{13,22}. Among all murine BAT depots, the interscapular represents the largest and is, therefore, commonly used to isolate cells or tissue. The interscapular BAT is connected via the Sulzer vein to the systemic blood circulation, allowing efficient heat distribution from this thermogenic tissue throughout the entire body²³. Newborn humans also possess a relatively large interscapular BAT depot. In adult humans, on the other hand, the interscapular BAT depot has been degraded. Instead, their BAT depots are mainly located in the neck, the supraclavicular, periaortic, paravertebral, and perirenal regions (Figure 3).

Regarding their cellular composition, adipose tissues (ATs) show a surprising degree of heterogeneity. Cellular populations include adipocytes, endothelial cells, fibroblasts, noradrenergic neurons, stem cells, and various immune cells, such as macrophages. Although adipocytes constitute approximately 90% of the adipose tissue volume, they might make up less than 50% of the total number of cells in murine WAT and BAT^{24,25}.

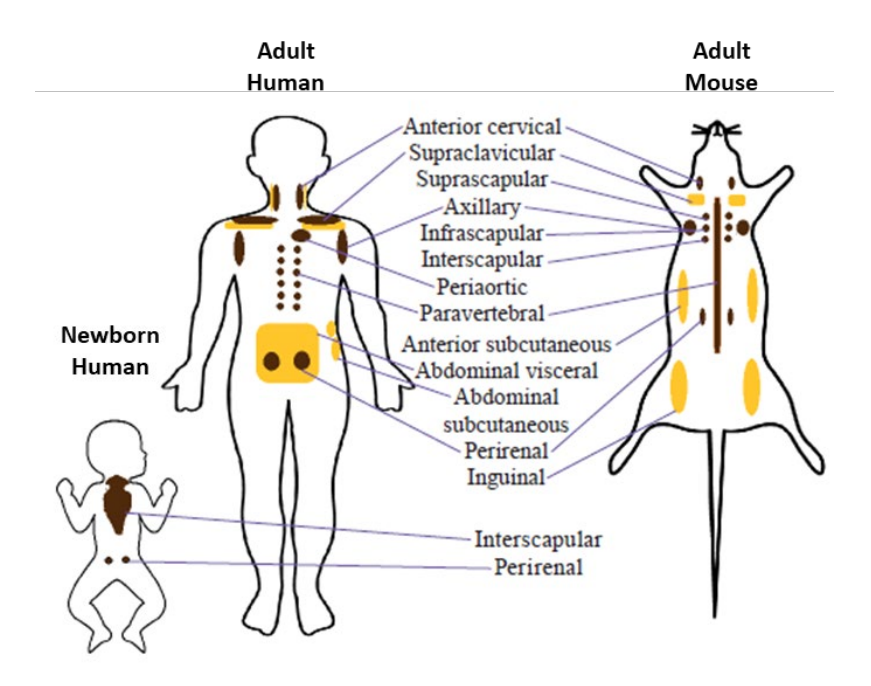


Figure 3: Location of ATs in humans and mice

Both mice and newborn humans possess a main interscapular BAT depot, whereas in adult humans BAT is mainly found in the supraclavicular and anterior cervical region. Adapted from Chernukha *et al.* 2022²⁶.

1.2.3 Transcriptional regulation of BAT

Adipocytes, which represent the largest cellular population in ATs, both by volume as well as cell number, are derived from multipotent mesenchymal stem cells (MSC)²⁷. The process of mesenchymal stem cells differentiating into adipocytes is called adipogenesis and is at the basis of AT formation and development^{28,29}. The process of adipogenesis can be subdivided into two distinct phases. Initially, MSCs commit towards preadipocytes. Should the cellular environment be suitable, the differentiation of preadipocytes into fully mature lipid-laden adipocytes is subsequently initiated³⁰.

The most central and vital transcription factors (TFs) for adipogenesis are peroxisome proliferator-activated receptor gamma (PPARγ) and CCAAT/enhancer-binding proteins (C/EBPs)²⁸. As such, they are considered master regulators of adipogenesis. Studies have shown that cells lacking either of these TFs can no longer undergo adipogenesis^{31–33}. C/EBPα acts together with PPARγ to enable differentiation into mature adipocytes³⁴, while PPARγ specifically controls the terminal differentiation of preadipocytes into mature adipocytes.

In more detail, adipogenesis is controlled by a transcriptional cascade. This cascade is initiated by the upregulation of C/EBP β and C/EBP δ . This, in turn, induces upregulation of PPAR γ and C/EBP α , which leads to the expression of several downstream targets, such as fatty acid binding protein 4 (FABP4; also called adipocyte protein2 or aP2) and, in the case of BA, UCP1, which are essential for adipocyte function³⁰.

Besides adipogenesis, another process that is of major importance for the maturation of BA and, thus, the development of BAT, is thermogenesis. The most important TFs for the thermogenic development of BAT are PPAR γ coactivator 1 α (PGC1 α), C/EBP β , and transcription factor PR domain containing 16 (PRDM16)³⁵.

Beyond C/EBPs and PPARs, a multitude of other TFs that are relevant for the development of AT exist. Some of the better-known TFs include zinc finger protein 423, cAMP response element-binding protein, activating transcription factor 4, and signal transducer and activator of transcription 5A³⁰.

More than a decade ago, the importance of cyclic guanosine monophosphate (cGMP) for the differentiation of BA was shown. cGMP can affect mitochondrial biogenesis as well as the adipogenic and thermogenic programs of adipocytes via different pathways. The most prominent of these pathways are downstream of cGMP-mediated protein kinase G (PKG) phosphorylation. In 2009 Haas *et al.* demonstrated that PKG controls insulin signaling via inhibiting RhoA / Rho-associated kinase (ROCK), thus reducing the inhibitory effects of ROCK on insulin receptor substrate-1 and activating the phosphoinositide 3-kinase-Akt cascade, thereby controlling both the adipogenic and thermogenic programs in BA³⁶. An additional

cGMP-PKG dependent pathway, relevant for the thermogenic program of BA, was described by Bordicchia *et al.* in 2012, where PKG activation led to phosphorylation of p38 mitogen-activated protein kinase (p38 MAPK)³⁷.

Taken together, the thermogenic and adipogenic programs of adipocytes are connected, highly complex, and at the core of AT development with cGMP being of central importance for both programs.

1.2.4 Role and function of BAT

Both humans and mice are endothermic animals, meaning that body temperature is kept relatively constant, regardless of environmental conditions. To enable heat production and, thus, maintain body temperature in cold environments, two main processes are utilized: shivering thermogenesis (ST) and NST38,39. ST is an involuntary subconscious process, in which skeletal muscle fibers contract repeatedly without performing physical work, but still produce heat³⁹. The energy consumption in the form of ATP results in heat dissipation throughout the body. Before the body relies on ST, BAT-fueled NST regulates body temperature, whereby the mitochondrial respiratory chain is uncoupled via UCP1³⁹. In normal cellular respiration, electrons are transported along a chain of mitochondrial proteins at the inner mitochondrial membrane. This process leads to the formation of a proton gradient in which H⁺ ions accumulate in the intermembrane space between the inner and outer mitochondrial membrane, ultimately leading to the formation of ATP via ATP-synthase. However, UCP1, a protein located at the inner mitochondrial membrane, allows protons to re-enter the mitochondrial matrix without passing through the ATP-synthase and thus without producing ATP. Instead, the proton leakage via UCP1 leads to a more rapid electron flow through the respiratory chain. The resulting energy is then dissipated as heat 13,40. If NST is not sufficient to keep the body temperature at appropriate levels, ST and NST can work in tandem to enhance heat production¹².

The activation of BAT, for example in response to cold, is mainly mediated by the SNS via the neurotransmitter norepinephrine (NE)⁴¹. NE binds to the β -adrenoceptors (β -ARs), and G-Protein-coupled receptors (GPCR), thereby liberating their $G_{\alpha s}$ subunit and allowing it to stimulate the adenylate cyclase (AC) to start producing cyclic adenosine monophosphate (cAMP) from ATP. cAMP, in turn, activates protein kinase A (PKA) leading to the phosphorylation of many downstream effectors, such as perilipin, hormone-sensitive lipase (HSL), and adipose triglyceride lipase (ATGL) resulting in enhanced lipolysis^{42,43} ^{44,45}(Figure 4). The free fatty acids (FFA) released by this process subsequently serve as fuel for mitochondrial β -oxidation, but also as activators of UCP1 within the inner mitochondrial membrane, thereby fueling NST and enhancing EE⁴⁰.

While acute CE activates BAT leading to enhanced substrate oxidation and heat production, chronic CE induces the thermogenic gene expression program via cAMP response element-binding protein and p38 MAPK^{46,47}. This program enhances the thermogenic capacity of brown fat by several processes, such as PRDM16 activation, which ultimately stimulates the expression of UCP1¹⁹ (Figure 4). Furthermore, this thermogenic program in WA is responsible for the cold-induced adaptation of WAT, where it adopts a brown-like phenotype (browning)^{18,48}.

Beyond being a thermogenic tissue and a sink for excess calories, BAT has recently gained appreciation as a vital endocrine organ⁴⁹ that is involved in promoting cardiovascular health. Consequently, patients with metabolically active BAT are leaner and less likely to suffer from cardiovascular complications, such as stroke or cardiac arrest, as well as metabolic conditions, like type 2 diabetes mellitus (T2DM)⁵⁰.

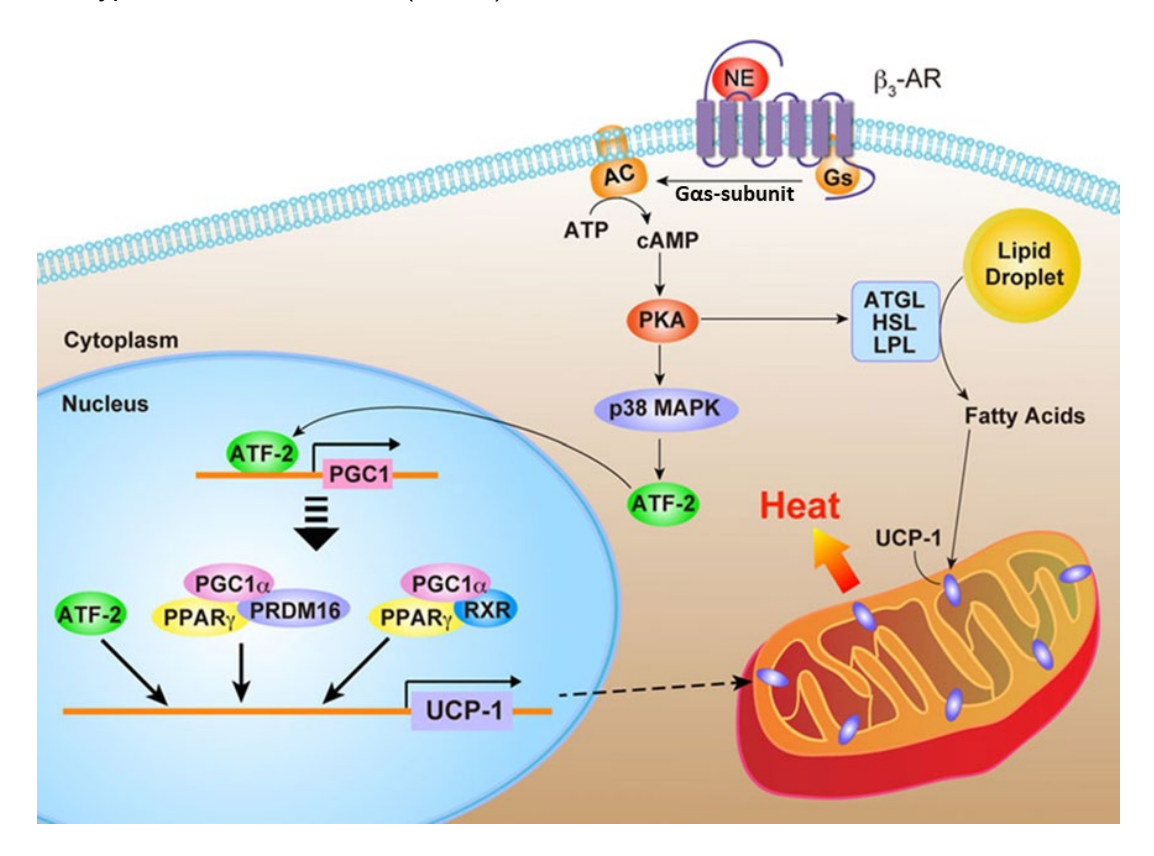


Figure 4: Function of BAT

NE binds to β_3 -ARs thus activating the AC via the G_{α s}-subunit, thereby increasing cAMP levels. cAMP in turn activates PKA, which phosphorylates ATGL, HSL, and LPL which all stimulate lipolysis and hence the release of FFA. These FFA subsequently activate UCP1, fueling thermogenesis. On the other hand, longer sympathetic activation (for example, long-term cold exposure) leads to PKA-mediated phosphorylation of p38 MAPK and, thus, transcriptional upregulation of the thermogenic protein UCP1. Adapted from Merlin *et al.* 2015⁵¹.

1.2.5 BAT in humans

Most of our insights into BAT thermogenesis come from studies with rodents, such as mice. Consequently, our knowledge of the function and characteristics of BAT in humans remains limited. Similar to rodents, newborn humans possess significant amounts of BAT, which is vital for the regulation of body temperature during neonatal life⁵². Until approximately 2010 it was believed that BAT would quickly disappear postpartum and play no or only a negligible role in adult humans⁵³. Thus, only very few researchers even considered BAT a potential target for novel obesity therapies in humans⁵³. However, around 2010 this view was challenged, when metabolically active BAT was found in adult humans via fluorodeoxyglucose (FDG) positron emission tomography (PET) by multiple groups, elevating the field of BAT research to prominence^{54–57}. These experiments identified that the main sites of FDG uptake were in the supraclavicular, para-aortic, suprarenal, and cervical regions⁵⁷. Other studies demonstrated that this FDG uptake was enhanced at lower environmental temperatures and reduced by pretreatment with adrenergic blockers, indicating similar behavior of metabolically active BAT in humans as in rodents^{46,58,59}. Since then, a multitude of PET scans have furthered our anatomical and pharmacological understanding of BAT⁵⁰. Importantly, BAT activity is reduced in obese patients, as well as in older patients^{52,60,61}. Furthermore, metabolically active BAT is found more frequently in females, compared to males⁶⁰. Interestingly, the occurrence of BAT increases in colder winter months compared to warmer summer months, providing further evidence of the association between cold and BAT activity⁵⁰. The therapeutic potential of BAT as a caloric sink was highlighted when it was estimated that complete activation of BAT could result in EE equivalent to roughly four kg of fat tissue per year⁵⁷. Overall, we can conclude from these studies that adult humans indeed possess metabolically active BAT, which can be stimulated either by physiological cues, such as cold, but also by pharmacological means^{42,56,62}. This highlights BAT as a potential target for the development of novel treatment approaches for obesity and its associated comorbidities. However, using CE as a large-scale public health measure to treat obesity, remains unfeasible, thus necessitating the establishment of pharmacological approaches to either activate pre-existing or recruit additional beige or brown AT.

1.2.6 Pharmacological activation of BAT

Since CE is the most well-studied physiological activator of BAT and also a potent mechanism for the recruitment of new beige adipocytes in WAT, the most obvious pharmacological approach for BAT activation or beige adipocyte recruitment are sympathomimetic drugs. However, sympathomimetic drugs, without specific modes of drug delivery to the adipose tissue or other mechanisms to specifically target AT, demonstrate substantial side effects on the cardiovascular system, such as hypertension and tachycardia $^{63-65}$. A possible solution to this problem was the development of relatively selective β_3 -AR-agonists, a receptor that is highly expressed in adipocytes but less so in the cardiovascular system. One such compound is Mirabegron, which was developed for the treatment of an overactive bladder 66 . Indeed, high doses (200 mg) of Mirabegron were effective in stimulating human BAT thermogenesis and in

improving resting metabolic rate⁶³. However, Mirabegron and similar compounds still demonstrated significant cardiovascular side effects, such as tachycardia and hypertension^{63–65}. Considering the people most in need of obesity treatments (obese, elderly men) represent a group with a particularly high risk for major adverse cardiovascular events, the application of β -AR-agonists and, thus, the risk of causing unwanted cardiovascular events seems highly problematic. Therefore, the identification of novel non-adrenergic regulators of BAT activity or BA differentiation represents an essential step toward developing a feasible method for utilizing BAT to treat obesity.

Beyond adrenergic agonists several other factors have been identified to be capable of either activating BAT, inducing browning of WAT, or recruiting new BA by improving the differentiation of BA progenitor cells (preBA). The most promising candidates include adenosine^{67–69}, inosine⁶⁹, bile acids^{70–72}, and treatments conveying their effects via the cyclic nucleotide (CN) cGMP, such as natriuretic peptides (NPs) and nitric oxide (NO)^{37,73–76}.

For example, the purine nucleoside adenosine synergistically increases lipolysis with NE in murine and human ATs⁶⁷. Furthermore, adenosine enhances the expression of thermogenic marker genes in murine and human BA via the GPCR A2A⁶⁷. Importantly, mice lacking the A2A receptor exhibit reduced BAT thermogenesis⁶⁷. Newer studies have additionally highlighted the role of the A2B receptor in mediating adenosine's effects on BAT⁶⁸. Intriguingly, equally impressive results have been obtained with the adenosine metabolite inosine⁶⁹.

The thyroid hormone triiodothyronine (T3) is well established as a key regulator of whole-body energy utilization and heat generation, regulating transcription by signaling via thyroid receptors^{77–80}. Especially in BAT, T3 is known to stimulate thermogenesis by inducing the expression of UCP1⁸¹. On the other hand, in the absence of T3, the thermogenic capacity of BAT is drastically reduced⁸². Additionally, disruption of T3 signaling leads to impaired adipogenesis, lipogenesis, and mitochondrial biogenesis^{82–84}. T3 has also been demonstrated to cause browning of WAT by activating key TFs such as PRDM16 and PGC1α thus driving mitochondrial biogenesis and the thermogenic program in beige adipocytes⁸⁵. Thyroid status is also highly correlated to BAT activity in mice, as hyperthyroid mice showed increased BAT volume and activity⁸². Lastly, T3 is implied to sensitize adipocytes to adrenergic stimulation, one reason why it is commonly used for the *in vitro* differentiation of BA⁸⁶.

1.3 cGMP signaling

1.3.1 cGMP as a drug target for cardiovascular and metabolic diseases

Like cAMP, cGMP is a second messenger, enabling cells to react to external stimuli, without requiring those stimuli to permeate into the cell itself⁸⁷. In the 1950s, Earl Sutherland discovered the first CN, cAMP^{88,89}. Shortly after in 1963, the second second messenger, cGMP, was discovered in rat urine and also synthesized^{90,91}. cGMP regulates a myriad of different pathways in various organs. The most prominent organ system affected by cGMP is the cardiovascular system^{92–96}. Here, cGMP mediates several effects, such as promoting vasodilation, natriuresis, antifibrotic and antihypertrophic effects as well as regulating cardiac contractility^{92–97}. Additionally, enhancement of cGMP signaling has been shown to be beneficial for pathologies such as heart failure (HF), pulmonary arterial hypertension (PAH), and chronic thromboembolic pulmonary hypertension (CTEPH)^{92,94,96,98}.

Various drugs have been approved in the context of different cardiovascular diseases and hypertensive disorders. Both Riociguat and Vericiguat (sGC stimulators) have been approved by the FDA for the treatment of PAH and, in the case of Vericiguat, also for HF^{94,98}. Furthermore, the combination of Sacubitril (a neprilysin (NEP) inhibitor, which blocks the degradation of natriuretic peptides) in combination with Valsartan (an Angiotensin 1 receptor antagonist) has been introduced as a breakthrough for the treatment of HF, especially in patients with a reduced ejection fraction⁹⁴. On the other hand, drugs blocking the degradation of cGMP, via phosphodiesterase (PDE) inhibition, have also been shown to be promising for treating various disorders. PDE 5 inhibitors, such as Sildenafil, Tadalafil, Vardenafil, and Avanafil have all been accepted as standard treatments for erectile dysfunction (ED), though this class of drugs was originally intended as a treatment option for hypertension^{99–101}. Sildenafil and Tadalafil additionally received approval as PAH and CTEPH treatments¹⁰², with Tadalafil also being accepted as a treatment for benign prostatic hyperplasia (BPH)^{102–107}. Taken together, the importance of cGMP in the context of the cardiovascular system is unquestionable.

In addition to the cardiovascular system, various other types of tissues in which cGMP plays a crucial role have been identified. Among these, are the ATs, especially BAT^{36,75,108}. cGMP is able to stimulate BAT-based EE via an entirely different mechanism than cAMP^{36,37}. From a mechanistic point of view, it has been demonstrated that cGMP signaling depends on PKG-mediated activation of p38 MAPK, which enhances the adipogenic and thermogenic transcriptional program of BA as well as mitochondrial biogenesis³⁷. As such, cGMP-PKG signaling is vital for the differentiation of BA progenitors into fully mature BA³⁶. Additionally, newborn mice lacking PKG have significantly reduced body temperatures, especially in the interscapular area, due to decreased BAT activity³⁶. The importance and druggability of the

cGMP signaling axis in the context of BAT development has also been demonstrated via the pharmacological activation of sGC with the sGC-stimulator Bay 41-8543, which resulted in increased EE and reduced weight gain of mice on a high fat diet due to enhanced cGMP-PKG signaling⁷⁵. Affirmingly, mice lacking sGC displayed reduced core body temperature and BA progenitor cells from these mice could not differentiate into mature adipocytes in vitro⁷⁵. While these studies highlight the relevance of cGMP for the development of healthy functioning BAT, other studies have found that, contrary to cAMP, cGMP does not stimulate lipolysis in murine adipocytes but instead only in those of primates 109-111. Further studies suggested, that this might be due to the about 100-fold higher expression of the clearance receptor for natriuretic peptides, natriuretic peptide receptor C (NPRC) in murine adipocytes^{109,112}. Ultimately a NPRC knockout model found that cultured adipocytes from these cells do indeed respond to atrial natriuretic peptide (ANP) with increased lipolysis, just like primate adipocytes, however, these results remain controversial as other cGMP-inducing drugs, such as NO-donors, also do not induce lipolysis in murine BA³⁷. Importantly, cGMP does not cause the typical cardiovascular side effects, such as tachycardia and hypertension, seen with cAMP-based treatments. Instead, cGMP-based treatments are frequently used against hypertension, as in the case of PAH or CTEPH. The safety profile and high importance of cGMP for BAT development and function highlight cGMP signaling as a potential target for BAT-based treatments of obesity.

1.3.2 cGMP signaling overview

cGMP is synthesized from guanosine triphosphate by three different guanylate cyclases (GCs)¹¹³. The first source of cGMP is the soluble guanylate cyclase (sGC), which is activated by NO^{112,113}. The other two are both membrane-bound (particulate) natriuretic peptide receptors, which are activated by natriuretic peptides^{114,115}. ANP and brain-type natriuretic peptide (BNP) both bind to and activate natriuretic peptide receptor A (NPRA), while C-type natriuretic peptide (CNP) activates natriuretic peptide receptor B (NPRB) and potentially also the clearance receptor NPRC, which might also harbor some signaling properties^{115–119}.

The physiological agonist for the sGC is NO. In mammals, NO can be endogenously produced by three different NO synthases (NOS)¹²⁰. First, there is the endothelial NOS (eNOS), secondly the neuronal NOS (nNOS) and thirdly the inducible NOS (iNOS)¹²¹. All three NO synthases utilize L-arginine and molecular oxygen as substrates and require cofactors, such as reduced nicotinamide adenine dinucleotide phosphate, flavin adenine dinucleotide, flavin mononucleotide, and (6R-)5,6,7,8-tetrahydrobiopterin^{121,122}. sGC is a heterodimeric hemeprotein complex consisting of an α -subunit (either α_1 or α_2) and a heme-containing β -subunit (either β_1 or β_2)^{123–126}. To date, two isoforms of each subunit, α_1 and α_2 as well as β_1 or β_2 respectively, have been identified in both humans and mice^{127–129}. Accordingly, four different variations of sGC could theoretically be assembled, a combination of α_1 with either β_1 or β_2 and α_2 with either β_1 or β_2 . In vivo, the $\alpha_1\beta_1$ sGC isoform is the most commonly found

isoform¹³⁰, being especially highly expressed in organs such as the lung and liver¹³¹. On the other hand, the $\alpha_2\beta_1$ sGC isoform is less abundant, but nevertheless highly expressed in the brain, uterus, and placenta^{123,129,131–133}. While the β_2 subunit has been identified on the level of mRNA, its function and capability to form functional sGC proteins *in vivo* remains controversial.^{123,133} Depending on the environment, the Fe²⁺-containing heme can either be present in a reduced or oxidized state. In the reduced state, sGC can be activated by NO. However, upon oxidation to Fe³⁺, the heme group loses its NO binding site and, thus, becomes unresponsive to NO^{134–136}. In addition, sGC transcription and mRNA stability are also affected by oxidative stress¹³⁷. Oxidative stress is, therefore, associated with several cardiovascular diseases^{138,139}. Interestingly, high levels of reactive oxygen species, and thus oxidative stress, can be observed during obesity leading to a higher degree of Fe²⁺ oxidation and, thus, reduced NO sensitivity¹⁴⁰.

Besides sGC stimulators, which sensitize sGC to NO and are thus partially heme-dependent, sGC activators, which can activate the sGC even in the oxidized state regardless of the bound heme, have been developed 141–144. Indeed, studies have demonstrated that under pathological conditions associated with oxidative stress, sGC-activators can be more potent than sGC-stimulators 145,146. Based on these findings it might seem more prudent to investigate sGC-activators instead of sGC-stimulators for potential cGMP-based treatments of obesity, as the AT of obese patients will be exposed to significant amounts of oxidative stress. Yet, none of these sGC activators, such as Cinaciguat (Bay 58-2667), have been approved for clinical usage to date.

The downstream signaling effects of cGMP are mainly mediated by three different effectors¹⁴⁷. The most prominent is the protein kinase G (PKG), of which two different isoforms exist (PKG1 and PKG2)^{36,148,149}. PKG phosphorylates a variety of different substrates, thereby regulating a myriad of processes, such as platelet aggregation, blood pressure, learning, metabolic control, and also adipocyte differentiation^{36,129,150}. The other two cGMP targets are cyclic nucleotide-gated (CNG) channels^{151,152} and the CN-degrading phosphodiesterases, especially PDE2 and PDE3¹⁵³ as well as PDE5¹⁵⁴. PDEs are unique in the sense that they are CN degrading enzymes that in some cases can also be activated or inhibited by cGMP, thus, affecting the levels of cAMP, via a process known as CN crosstalk^{153,155}.

1.3.3 Natriuretic peptides

The most prominent function of NPs are their effects on the renal system. They mediate natriuresis, diuresis, suppress the renin-angiotensin-aldosterone system, and also induce vasodilation^{156–158}. However, NPs can regulate metabolic functions as well. They promote lipolysis in primate adipocytes, but not in murine adipocytes unless they lack NPRC^{37,109,111,159}. Furthermore, they regulate mitochondrial respiration^{160,161}. Interestingly, low levels of NPs are

found in the plasma of obese patients or patients suffering from metabolic syndrome or T2DM¹⁶². There are three types of NPs: ANP, BNP, and CNP¹⁶³. ANP is mainly produced in the atria and BNP is found primarily in the left ventricle 164. However, both are released from the left ventricle during HF, which explains why HF patients usually show high ANP and BNP plasma levels and why these NPs and their progenitors (NT-proBNP) are used as biomarkers for HF^{165,166}. CNP on the other hand is produced in endothelial cells as well as chondrocytes and the kidney^{167–169}. In the context of AT, the expression in endothelial cells is highly important, as endothelial cells are one of the most abundant and well-studied cell populations in the AT^{163,170,171}. ANP and BNP bind to NPRA, CNP binds to NPRB, yet all of them bind to NPRC¹¹⁴. At high concentrations, BNP can also bind to NPRB^{114,172}. All three receptors are transmembrane receptors. NPRA and NPRB contain intracellular guanylate cyclases, enabling cGMP synthesis. NPRC, though, does not have an intracellular GC and, thus, has no GC activity^{173,174}. NPRC was, therefore, thought to function as a clearance receptor^{112,172}. However, alternative signaling pathways involving NPRC have been demonstrated recently 175-177. For example, infusing mice with cANF⁴⁻²³, a selective NPRC agonist, resulted in a reduction of body temperature and thermogenesis, via a G_{αi} mediated reduction of cAMP-PKA signaling. Additionally, in isolated adipocytes, cANF⁴⁻²³ mediated NPRC activation abolished NE-induced upregulation of thermogenic markers and reduced mitochondrial density¹⁷⁵. These findings highlight that NPRC is more than a clearance receptor and instead also has considerable capacity to signal via Gαi.

NEP represents another mechanism for NP signaling termination. NEP is a neutral endopeptidase, which is involved in the degradation of various peptides, such as angiotensin, but also NPs^{178,179}. Because pharmacological inhibition of NEP increases the circulating concentrations of angiotensin, NEP is combined with an AT1-receptor antagonist (Valsartan) in the treatment of HF, to prevent unwanted side effects of angiotensin, such as hypertension^{94,180,181}.

NPRA is mainly found in vascular smooth muscle cells, endothelium, the heart, the nervous system, and the kidney. It is also found in AT ^{37,163,182}. Stimulation of NPRA has been reported to prevent cardiac hypertrophy and mediate antifibrotic effects, as well as stimulate lipolysis in primate adipocytes or murine adipocytes lacking NPRC^{37,109,110}.

NPRB is mainly expressed in vascular smooth muscle cells, the endothelium and the peripheral vasculature, long bones, as well as in the heart and the AT^{114,163,169,183}. Treatment with CNP or similar analogues promotes antifibrotic effects and modulates heart contractility¹⁸⁴⁻¹⁸⁶. Furthermore, NPRB has profound effects on promoting long-bone growth^{76,183}. Consequently, mice lacking NPRB are affected by dwarfism¹⁸³. Contrarily, mice treated with CNP or a CNP analogue are significantly larger than control animals⁷⁶. Indeed,

these observations have led to the development and approval of Vosoritide, a CNP analogue authorized for the treatment of achondroplasia in children¹⁸⁷.

NPs have been studied extensively as potential candidates for the treatment of HF. ANP analogues, such as Anaritide and Carperitide have failed to show reliable beneficial effects on HF^{188,189}. In the recent past BNP analogues, such as Nesiritide, were approved for the treatment of acute decompressed HF. However, longer-term studies found no lasting beneficial effects but instead found considerable adverse effects^{190,191}. Cenderitide, a CNP analogue that can activate both NPRA and NPRB and is resistant to degradation via NEP, was also developed^{76,192}. However, none of these peptides represent first-line treatment options for HF¹⁹³. Instead, more promising results have been obtained by enhancing the endogenous NP signaling with NEP inhibitors^{94,180,181}.

1.3.4 Nitric oxide

NO was discovered as an endothelium-derived smooth muscle relaxation factor ¹⁹⁴. However, its functions extend far beyond simple relaxation of the non-striated musculature ¹⁹⁵. As mentioned above, NO can be produced via three different NOSs: nNOS, eNOS, and iNOS. All are found in cardiomyocytes ¹⁹⁶. eNOS and iNOS seem to be the most relevant in AT due to their relatively high expression, as well as the large content of endothelial cells in the AT ^{170,197,198}. Interestingly, CE, which leads to the activation of BAT, increases eNOS expression in BAT ¹⁹⁸. NOS are oxidoreductase homodimer enzymes that possess an oxygenase domain but also a reductase domain ^{121,195,199}. These two domains are divided by a linker, which binds and is activated by calcium-calmodulin (CaM)²⁰⁰. Consequently, NOS are activated upon an increase in the intracellular calcium concentration. Such calcium increases are oftentimes the consequence of $G_{\alpha q}$ -signaling resulting in the IP₃-mediated release of calcium from intracellular stores, such as the endoplasmic or sarcoplasmic reticulum. NO is a lipophilic gaseous molecule, which allows it to diffuse through cell membranes, thus, enabling it to act as a paracrine signal from endothelial cells to various surrounding cells ¹⁹⁵. In AT, these surrounding cells are mainly adipocytes, smooth muscle cells, and sympathetic neurons ^{11,170}.

1.3.5 Protein kinase G

PKGs are homodimeric serine/threonine kinases²⁰¹. In mammals, two splice variants of the *Prkg1* gene are expressed leading to the expression of two different PKG1 splice variants, PKG1 α and PKG1 β ²⁰². Furthermore, a second PKG isoform, PKG2, which is encoded by the *Prkg2* gene exists²⁰³. PKG1 is mainly expressed in cardiac muscle, smooth muscle, the endothelium of the vasculature, platelets, nerve cells, the kidney, and adipocytes^{36,204,205}. The importance of PKG in the context of BAT is highlighted by the fact that mice lacking PKG1 show dramatically reduced thermogenesis and body temperature as well as far lower expression of the key thermogenic protein UCP1 in BAT³⁶. On the other hand, global

overexpression of PKG1 shows opposite effects, such as increasing mitochondrial biogenesis, upregulating thermogenic and adipogenic markers in BAT, and increasing thermogenesis and, thus, elevating body temperature. Consequently, PKG1 overexpressing mice are leaner than WT littermates and protected against weight gain on a high-fat diet (HFD)^{160,206}.

PKG1 also plays a major role in WA. As such, the cGMP-PKG1 axis has been shown to play an important part in enhancing adipogenesis, mitochondrial biogenesis, thermogenic gene expression, and even browning of WAT^{37,108}. In contrast, overexpression of PKG1 in WA also influences the endocrine role of WA, leading to reduced expression of pro-inflammatory cytokines such as interleukin-6^{108,207}. Taken together, these findings highlight the pivotal role of the cGMP-PKG1 signaling cascade for the development and function of BAT and WAT.

In contrast, PKG2 is mainly found in the kidney, intestinal mucosa, and long bones. The importance of PKG2 for long bone growth is highlighted by the fact that mice lacking PKG2 are affected by dwarfism²⁰³. These findings, along with the aforementioned observations that CNP treatment of mice enhances long bone growth led to the development of CNP analogues for long bone growth disorders, such as achondroplasia¹⁸⁷.

To conclude, while cGMP and PKG1 signaling have most prominently been investigated in the context of the cardiovascular system, their importance in the metabolic processes of AT should not be underestimated.

1.3.6 Phosphodiesterases

PDEs are enzymes that hydrolyze phosphodiester bonds in CN, such as cAMP and cGMP, leading to the formation of AMP and GMP, respectively^{208,209}. Over the last decades, eleven major PDE families have been categorized, with various subfamilies and splice variants²¹⁰. These families differ in multiple ways from one another, most prominently in their substrate specificity and affinity. PDE 1, 2, 3, 10, and 11 are dual-specific, which means that they hydrolyze both cAMP and cGMP. On the other hand, PDE 4, 7, and 8 are selective for cAMP, while PDE 5, 6, and 9 are selective for cGMP^{210,211}. PDEs contain a catalytic domain and a regulatory N-terminal domain. The catalytic domain binds the CNs for hydrolysis. PDE inhibitors also target the catalytic domain of PDEs^{210,211}. The development of specific PDE inhibitors is possible, due to the amino acids in the binding region of the catalytic domain being different between PDE families, enabling inhibitor specificity. The N-terminal region is also responsible for the sub-cellular localization of the different PDEs²¹².

PDE 1, 2, 3, 5, and 9 are the PDEs that are both expressed in AT and are either dual-specific or selective for cGMP.

PDE1 has three isoforms: PDE1A, 1B and 1C. All of these are dual-specific PDEs catalyzing the hydrolysis of both cAMP and cGMP²¹³. A unique feature of PDE1 is that its regulatory

domain includes two binding sites for Calcium/CaM, which, upon binding, activate the enzyme, leading to increased CN degradation²¹⁴. This interaction is crucial for facilitating the crosstalk between calcium signaling and CN. Furthermore, PDE1 contains a PKA phosphorylation site, which can reduce its sensitivity for Calcium/CaM²¹⁵. Various inhibitors of PDE1 exist, such as Vinpocetine, Nimodipine, and Iti-214^{216,217}.

While there is only one isoform of PDE2, PDE2A, this subtype has three splice variants, PDE2A1, 2, and 3^{218,219}. The regulatory region of PDE2 contains two GAF domains, A and B²²⁰. PDE2 has a comparable kinetic profile regarding cAMP versus cGMP degradation, with V_{max} and K_m being similar²¹⁰. However, cGMP can not only bind to the catalytic domain to be hydrolyzed but also to the GAF-B domain²²⁰. By binding to the GAF-B domain, cGMP enhances the degradation of cAMP^{153,221,222}. Consequently, PDE2 is one of the main mediators of cGMP to cAMP crosstalk and is, thus, an interesting cGMP downstream effector, by which cGMP accelerates cAMP degradation^{153,221,222}. A commonly used PDE2 inhibitor is Bay 60-7550^{153,223}.

PDE3 has two isoforms, 3A and 3B. Like PDE2, both PDE3 isoforms play a major role in CN crosstalk^{210,224}. However, while PDE2-mediated CN crosstalk depends on the allosteric modulation of PDE2, PDE3-mediated crosstalk is competitive²¹⁰. In detail, PDE3 has a similar K_m for cAMP and cGMP, but the V_{max} is approximately 10-fold higher for cAMP^{208,210}. Consequently, binding of cGMP to PDE3 blocks the enzyme for a longer period of time, preventing further degradation of cAMP. Thus, PDE3A and PDE3B represent additional downstream effectors of cGMP that allow cGMP to modulate cAMP levels^{153,222}. Cilostamide is a commonly used PDE3 inhibitor^{153,225}.

To summarize, the effect of cGMP on cAMP depends on two PDEs mediating opposite effects. cGMP can activate PDE2 leading to decreased levels of cAMP. On the other hand, cGMP can also inhibit PDE3, leading to increased cAMP levels (Figure 5). Which effect dominates, might depend on the expression of the relevant PDEs, as well as their subcellular compartmentalization.

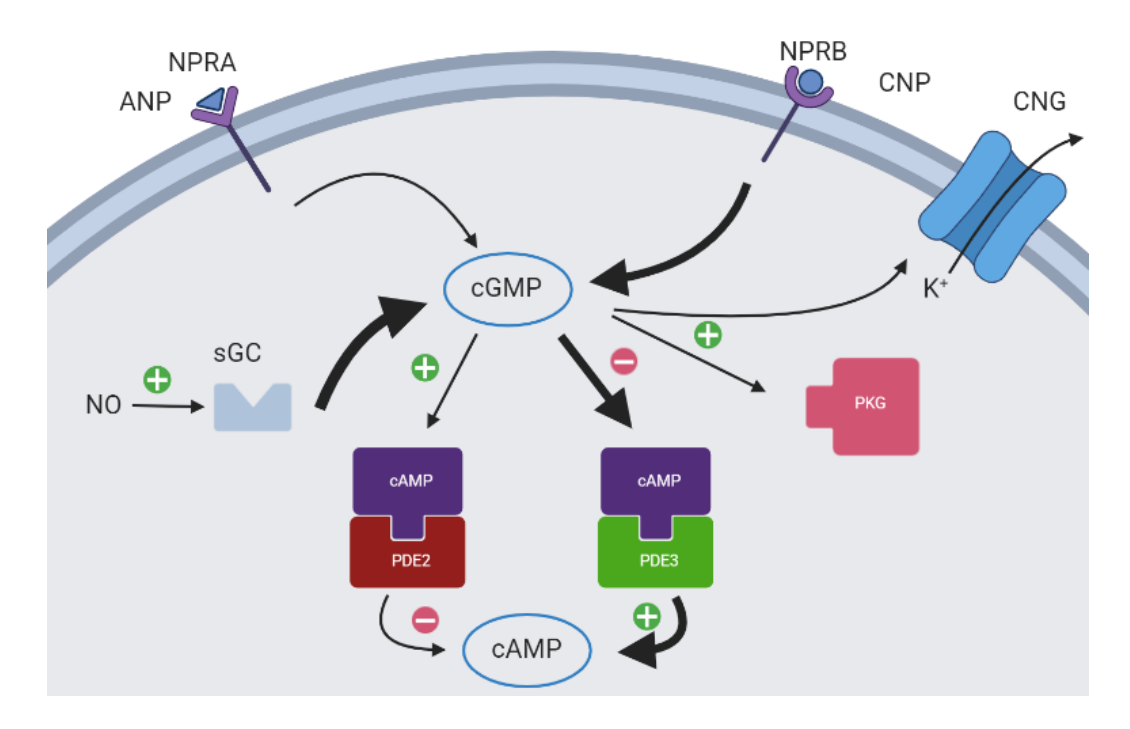


Figure 5: cGMP generators and effectors

cGMP can be produced from three different sources, NPRA, NPRB, and sGC. cGMP has three main downstream effectors, CNG channels, PKG, and PDEs. cGMP can allosterically activate PDE2 to enhance cAMP degradation, or competitively inhibit PDE3 to decrease cAMP degradation. Created with BioRender.com.

PDE5 has three different isoforms, PDE5A1, 2, and 3, and is cGMP selective²¹⁰. The regulatory domain contains a phosphorylation site for PKG1. PKG1-mediated phosphorylation increases the enzymatic activity of PDE5 and, hence, the rate of cGMP degradation¹⁵⁴. This mechanism represents a negative feedback loop, by which higher cGMP levels elevate PKG1 activity leading to increased phosphorylation of PDE5, thereby stimulating degradation of cGMP and, thus, terminating the signal¹⁵⁴. There are various commonly used and clinically approved PDE5 inhibitors available, mainly for the treatment of ED or PAH, such as Sildenafil, Tadalafil, Avanafil, or Vardenafil^{226,227}.

PDE9 has only one isoform, PDE9A, but several different splice variants. PDE9 is cGMP selective²¹⁰. While PDE9A mRNA expression levels are fairly low in adipocytes, recent publications have highlighted its pivotal role in AT function. Mice lacking PDE9, or mice receiving a PDE9 inhibitor, were protected from weight gain on HFD, and their expression of thermogenic genes in the AT was enhanced^{73,74}. The most commonly used PDE9 inhibitors for basic research are PF-7943 and Bay 73-6691⁷⁴.

1.3.7 Compartmentalization of cyclic nucleotide signaling

CNs mediate a myriad of different cellular functions in response to countless different stimuli. With more than 1000 GPCRs having been identified, researchers have wondered for years how signal fidelity and accurate coordination could be achieved considering that so many different receptors signal via only two cyclic nucleotides^{228–230}. How could this be the case, if

the CN were to just freely diffuse throughout the cell? Shouldn't the activation of any $G_{\alpha s}$ - or $G_{\alpha i}$ -coupled receptor lead to exactly the same response? How can a cell generate such diverse effects in response to the same second messenger? Consequently, scientists have speculated that some form of sub-cellular architecture that promotes signal fidelity and coordination must exist^{231,232}. Indeed, we now know, that the answers to these questions lie in the precise segregation of the different pathways by a specific spatial and temporal sub-cellular regulation of the production and degradation of these second messengers. This concept is termed compartmentalization²³³.

cAMP was discovered more than 60 years ago by Earl Sutherland, who was later awarded the Nobel prize for his discovery⁸⁹. However, the concept of compartmentalization of this second messenger was postulated many years later. In the 1980s, Hayes as well as Buxton and Brunton observed that in cardiac myocytes catecholamines and prostaglandins raise cellular cAMP to similar levels, but have distinct functional effects^{232,234}. When going into detail they found that hearts stimulated with Isoproterenol contract more forcefully (positive inotropic effect), whereas prostaglandin did not affect contractility, even though it also raised cAMP to a similar degree^{232,234}. Clearly, the model of linear transduction of the messenger from the receptor to everywhere in the cell at the same time was too simplistic to explain this phenomenon. Considering that CNs diffuse rapidly at 200-700 µm per second, something must be limiting their diffusion within the cell²³⁰. It has become accepted that PDEs are vital regulators that restrict the spatial diffusion of CN by acting as barriers, thus, locally confining CN concentrations^{185,235,236}. Specifically, it is believed that PDEs are critical for creating pools of locally enriched CN levels associated with downstream effectors. These are called signalosomes^{229,237}. Though the role of PDEs in maintaining compartmentalization is well accepted, other mechanisms that might be essential for buffering CN diffusion speed remain controversial. In the following years, several observations have been made that lend credibility to the concept of CN compartmentalization. For example, recent observations have shown that the distribution of GPCRs and ACs is not homogenous throughout the cell, but instead, certain areas enriched with either one or both were found^{231,238–240}.

On the other hand, the concept of cGMP compartmentalization remains far less well-understood. cGMP was identified in rat urine in 1963, slightly later than cAMP⁹⁰. The fact that some sources of cGMP, namely the particulate GCs or NPRs, are associated with the plasma membrane and other sources of cGMP, namely the sGC, are cytosolic, hints at a possibility for compartmentalization similar to that of cAMP. However, the concept of cGMP compartmentalization took shape decades later than for cAMP. The first indication of cGMP compartmentalization was observed in 1990 when researchers found that NO-mediated cGMP was found in the soluble- as well as particulate fraction of frog ventricle lysates, while NPR-mediated cGMP was found only in the particulate fraction²⁴¹. More convincingly, a

functional role of cGMP compartmentalization was found in 2006, approximately 20 years after the work of Hayes, Buxton, and Brunton on cAMP compartmentalization. In this publication, Liliana Castro and Rodolphe Fischmeister demonstrated that cGMP derived from membrane-bound NPRs activated also membrane-bound CNG channels, while cGMP from the sGC did not²³³. This work in cardiomyocytes suggested the existence of some membrane-associated, NP-mediated cGMP compartment that is separated from the cytosolic sGC-associated compartment via PDEs. From this point onwards, the concept of cGMP compartmentalization almost exclusively explored the context cardiomyocytes 185,186,223,242. Further research in cardiomyocytes demonstrated that depending on which cyclase generates cGMP, different PDE subsets are involved in the degradation of these specific cGMP pools¹⁸⁵. Moreover, it has been shown that depending on which pool of cGMP is stimulated, PKG can target different proteins for phosphorylation^{185,186,243}. Recently, research from the Nikolaev lab has demonstrated the physiological relevance of the compartmentalization of NP-associated cGMP in cardiomyocytes, by revealing that only NPRB-cGMP results in positive inotropic effects, but NPRA-cGMP does not 185. This highlights a further separation of membrane-associated cGMP compartments between the different NPs and explains why multiple previous studies could not find any effects of ANP or BNP but could find an effect of CNP on contractility. Regarding the subcellular localization of cGMP compartments, great advances have lately been achieved by utilizing targeted biosensors. With these, researchers could demonstrate that the cGMP compartment at phospholamban varies considerably from the cytosolic compartment in regard to which PDEs are involved in cGMP degradation¹⁸⁶.

The critical role of PDEs in the compartmentalization of cGMP has been demonstrated by various recent publications 185,186,244,245. As such, PDE5 has been shown to mainly regulate the sGC-cGMP pool in cardiomyocytes 233, but in a model of cardiac hypertrophy, it also regulates the NPRA-cGMP pool, indicating remodeling of the sub-cellular architecture of cGMP compartmentalization during pathological conditions 246. PDE2 has been implicated to be associated with the NPRA-cGMP pool in cardiomyocytes, while PDE3 has been shown to preferentially associate with the NPRB-cGMP pool 185. Further work focusing more on cellular organelles has demonstrated that in cardiomyocytes PDE9 regulates a NPR-cGMP pool located at the mitochondria 74,247. However, how the cGMP moves from the NPR at the membrane to its mitochondrial compartment, remains completely unclear.

Taken together, scientists have generated convincing evidence for the compartmentalization of cAMP and cGMP in cardiomyocytes. However, the field of cGMP compartmentalization still lags far behind that of cAMP compartmentalization. Furthermore, the concept of cGMP compartmentalization has remained confined to very few types of cells, almost exclusively focusing on cardiomyocytes or other cells of the heart, such as cardiac fibroblasts or pericytes.

It remains to be proven that this concept is universally applicable to other cell or tissue types. The existence and the role of cGMP compartmentalization in adipocytes so far remains completely unknown. Over the recent years the most influential method to investigate CN compartmentalization has been the application of genetically encoded Förster Resonance Energy Transfer (FRET) biosensors.

1.4 Förster resonance energy transfer

The discovery of FRET²⁴⁸ and the development of genetically encoded FRET biosensors has been one of the most important developments in the field of CN compartmentalization²⁴⁹. FRET enables the measurement of various molecules, such as cAMP and cGMP, in living cells or tissues with high spatial and temporal resolution, without disturbing the physiological equilibrium of the cell^{250–252}. Consequently, FRET remains one of the most frequently used methods for investigating sub-cellular CN dynamics to this date^{253–255}.

Theodor Förster was the first to describe this non-radiative form of energy transfer between two fluorophores in 1940²⁴⁸. FRET is based on the interaction of dipoles coupling to one another within the different fluorophores²⁵¹. Typically, a FRET biosensor consists of three different components. A binding domain, which binds the molecule of interest, often based on the structure of a typical downstream effector of the molecule of interest, such as PKG or a PDE. This binding domain is usually flanked by two different fluorophores. One of these fluorophores acts as an energy donor, being excited by high-energy light with a short wavelength, while the other acts as an energy acceptor, emitting lower-energy light of a longer wavelength²⁴⁹. For FRET to occur, two main criteria must be met. First, the emission spectrum of the donor and excitation spectrum of the acceptor must show significant overlap, as is the case for the fluorophore pair cyan fluorescent protein (CFP = donor) and yellow fluorescent protein (YFP = acceptor)²⁵⁶. Secondly, these fluorescent proteins have to be in close proximity (approximately less than 10 nm apart)²⁴⁹. Furthermore, when choosing fluorophores for sensor design, one has to consider two disruptive factors. One is the excitation crosstalk phenomenon, where the excitation wavelength does not only excite the donor but to a lesser extent also the acceptor fluorophore, resulting in FRET-independent acceptor emission. The second factor is donor bleed-through, where a fraction of the donor emission can also be detected in the acceptor channel, resulting again in FRET independent signal from the acceptor fluorophore. Ever since GFP was first genetically cloned, countless fluorescent proteins and, thus, also FRET biosensors have been developed^{257–260}. Many of these show improved characteristics and are better suited for FRET than fluorescent proteins of previous generations. The main areas in which the field of fluorescent proteins has shown improvement, are reduced donor photobleaching and optimized emission and excitation spectra, minimizing bleed-through and fluorophore crosstalk²⁵⁹. FRET biosensors have benefited from the

improvement of the physicochemical characteristics of fluorescent proteins. However, FRET biosensors have additionally been improved by optimization of their ligand binding domains, yielding sensors with vastly different sensitivities, affinities, and dynamic ranges, suitable for a multitude of applications in different cell types^{254,260–262}.

Upon binding of the molecule of interest to the binding domain of a FRET biosensor, a conformational change is induced. This conformational change moves the two fluorophores either closer to one another, resulting in increased FRET efficiency, or further apart from one another, resulting in decreased FRET efficiency. Sensors that display increased FRET efficiency in response to increased concentrations of the molecule of interest are called "gain of FRET sensors", while in "loss of FRET sensors" less FRET occurs when the molecule of interest binds^{254,263}. Two prominent FRET sensors for cAMP and cGMP are epac1-camps and cGi-500, respectively. Both are loss of FRET sensors and both utilize the CFP and YFP fluorophore pair^{261,264}. Thus, upon binding of cAMP or cGMP to the sensor, FRET efficiency decreases. As a consequence, in response to increasing concentrations of these CN, the CFP emission (FRET donor) will increase, while the YFP emission (FRET acceptor) will decrease. Usually, FRET measurements are displayed as a ratio between the emission of both fluorophores. By displaying the ratio of the CFP/YFP signal, the result will correlate to the concentration of the CN, i.e. a higher CFP/YFP ratio indicates higher levels of the respective CN and vice versa.

When such FRET biosensors are expressed in the cell, they usually distribute rather evenly throughout the cytosol. However, using targeting sequences, FRET sensors can also be targeted to certain cell organelles, or even sub-cellular nanodomains, spanning only a few dozen nm in distance^{185,186}. Even more impressively, by fusing FRET sensors linked to receptors or PDEs via linkers of a predefined nanometer length, termed "nanorulers", the size of CN nanodomains can be precisely mapped²⁶⁵. Indeed, the use of nanorulers demonstrated that nanodomains truly deserve their name, with them being often less than 60nm across²⁶⁵.

Today, FRET is mainly used for two distinct applications. Firstly, to investigate whether two different proteins interact with one another. For this application, one of the proteins of interest is fused to a donor fluorophore, while the other is fused to an acceptor fluorophore²⁶⁶. If these proteins localize closely to one another, as they would if they interact with one another, FRET will occur and an acceptor emission will be detected. The other main application of FRET is with biosensors, measuring (intra-)cellular molecules in real-time. In this dissertation, the epac1-camps cAMP and cGi-500 cGMP biosensors were utilized to investigate the compartmentalization of cGMP as well as the crosstalk between cGMP and cAMP in both murine and human preBA and BA.

2. Aim of the thesis

The main goal of this thesis is to elucidate cGMP compartmentalization and signaling in adipocytes by utilizing FRET-based cGMP and cAMP biosensors.

In detail, the aims of the thesis are:

- 1. Investigate the existence, architecture, and regulation of cGMP compartmentalization in murine and human BA and identify the various relevant components.
- 2. Analyze how BA differentiation alters cGMP signaling and compartmentalization.
- 3. Study whether distinct cGMP compartments have different effects on BA function and differentiation.
- 4. Probe whether a CN crosstalk exists in BA and, if so, whether it shows compartment-specific effects between cGMP and cAMP.
- 5. Explore species-specific differences between cGMP compartmentalization and signaling in murine versus human preBA and BA.

3. Materials and methods

3.1 Chemicals and reagents

If not mentioned otherwise, chemicals were purchased either at Merck (Darmstadt), Sigma-Aldrich (München), Calbiochem (Darmstadt), Carl Roth GmbH (Karlsruhe) and VWR (Darmstadt). The Milli-Q Water Purification System (Merck EMD Millipore) was used to desalt and purify water (= millipore water). If not specified otherwise, millipore water was used for all experiments.

3.1.1 Antibodies

Table 1: Primary antibodies

Target Protein	Host Species	Dilution	Manufacturer	Cat. No
aP2	Rabbit	1:1000	Santa Cruz	sc-18661
			Biotechnology	
UCP1	Rabbit	1:1000	Thermo Fisher	PA1-24894
			Scientific	
Calnexin	Rabbit	1:1000	Sigma	208880

Primary antibodies were diluted in 5% milk in tris-buffered saline with tween 20 (TBST).

Table 2: Secondary antibodies

Target species	Dilution	Conjugation to	Manufacturer	Cat. No
Rabbit	1:10000	HRP	Cell Signaling	7074

Secondary antibodies were diluted in 5% milk in TBST.

3.1.2 Primers for qRT-PCR

Primers were ordered and synthesized by Microsynth. Stock solutions were prepared at a concentration of 10 μ M by diluting the lyophilized primers in Diethylpyrocarbonat-H₂O (DEPC-H₂O). Primer stocks were stored at -20°C.

Table 3: Primers for quantitative real-time polymerase chain reaction (qRT-PCR)

Name	Species	Sequence 5' to 3'
UCP1 forward	murine	TAAGCCGGCTGAGATCTTGT
UCP1 reverse	murine	GGCCTCTACGACTCAGTCCA
HPRT forward	murine	GTCCCAGCGTCGTGATTAGC
HPRT reverse	murine	TCATGACATCTCGAGCAAGTCTTT
aP2 forward	murine	GCGTGGAATTCGATGAAATCA
aP2 reverse	murine	CCCGCCATCTAGGGTTATGA
PGC1a forward	murine	GCACACCGCAATTCTCCCTTGTA
PGC1a reverse	murine	ACGCTGTCCCATGAGGTATTGACCA

PDE1a forward	murine	GGTCTTTGCAGCTGCCATTC
PDE1a reverse	murine	ATAGCAACGTCCGACCTCGT
PDE1b forward	murine	AGTTGCTGACTCGGCATAGC
PDE1b reverse	murine	CCCATAGCCTGTCTCCAAGG
PDE1c forward	murine	AACCCTCGTGGGAAGAACTC
PDE1c reverse	murine	TTCCGGTGTTGGAGTGATCC
PDE2a forward	murine	CTAGGCGCCGTTATCGACAT
PDE2a reverse	murine	ACACACCAGTCTGGACTCCC
PDE3a forward	murine	CCCCGTCTGTCATATGTAG
PDE3a reverse	murine	AGGTAACTTGAGAAGTGTCATCT
PDE3b forward	murine	TTTCCCGAGAACAGATGATCC
PDE3b reverse	murine	TGCGAGCTTCATTTAGCACTG
PDE5a forward	murine	TGTATGAGGCCCTGACCCAC
PDE5a reverse	murine	GGCAGTTTGTACACGGGGAG
PDE6a forward	murine	CTTTTGTCTATAAGGAGTTCTCCCG
PDE6a reverse	murine	TCAGCTACTGGATGCAACAGG
PDE6b forward	murine	CTGGGAAGTCCAGAGCAAGG
PDE6b reverse	murine	CCATCATGGGAATGGGCTGT
PDE6c forward	murine	GACCAAAGACTCCAGATGGCA
PDE6c reverse	murine	GCTGGAGGTGACGGAATCAC
PDE9a forward	murine	TGTGGCCTCCAGGAGAAGT
PDE9a reverse	murine	TGCGGCATTGATCTGGTAT
PDE10a forward	murine	CTATCGGCGGGTTCCTTACC
PDE10a reverse	murine	CAGACACGCAATTAGCAGGC
PDE11a forward	murine	ATTAGCCACAGACCTCACGC
PDE11a reverse	murine	AACACATCTCGGTGGCTTGT
NPRA forward	murine	TGGGCGAGGCTCCAATTATG
NPRA reverse	murine	CCACGAGGTTGCCCTTATAG
NPRB forward	murine	GAGTCGAATGGCCAAGCTCT
NPRB reverse	murine	TTCATCTCCACATCCCCACG
NPRC forward	murine	ATGGCCTTCTACTTTTCAGGAA
NPRC reverse	murine	TCTCGCAGCTCTCGATG
Gucy1a1 forward	murine	GCCCACCACATACAGGTTA
Gucy1a1 reverse	murine	GGAAGTTTGGTGGAAGCTCC
Gucy1a2 forward	murine	GCAAAGCCCATTGCTCTGAT
Gucy1a2 reverse	murine	TGCCTATCCGCATCTGAATTG
	1	· ·

Gucy1b1 forward	murine	TGCTTACGTCTCAAAGGCCA
Gucy1b1 reverse	murine	CCAGGTTCATCACACTTGGT
Gucy1b2 forward	murine	TGTATGCCATGCTGCAA
Gucy1b2 reverse	murine	ACACGTCTCGAATTCTCCTG
hNPRA forward	human	ACCGAAGCTTTCAAGGTGTGA
hNPRA reverse	human	GCACCATTCTCGGGATCCAT
hNPRB forward	human	GCTGAGGCCTTTGACAGTGT
hNPRB reverse	human	TCATTAAGAAGTGTCACTACCTG
hNPRC forward	human	TTGCCATGACTGATGTGGAG
hNPRC reverse	human	AGGGCCCCAAGGATATTTGA
hGucy1a1 forward	human	ATGGAGAACCTATCAAGATGCG
hGucy1a1 reverse	human	GCCAGAGTGACATTGTTTCCA
hGucy1a2 forward	human	GCTGGGCGAGAGCATCAG
hGucy1a2 reverse	human	TTCTGCATCCCTGTAACCAATAA
hGucy1b1 forward	human	TGTCTTCTCGCTGGTTCGTC
hGucy1b1 reverse	human	CATCCAACAATCCTTCCTTGCT
hPDE1a forward	human	CACCACGTGAGTGCAGCTTA
hPDE1a reverse	human	CTAGGTTCCGAAGATCCCTC
hPDE1b forward	human	GTGGTCAGCTTTCGTTCCAC
hPDE1b reverse	human	CATCTGGTTGGTGATGCCACT
hPDE1c forward	human	AAGACAGGAGTGGCGAACTG
hPDE1c reverse	human	TTGGTGGTTCCGGTATGCTC
hPDE2a forward	human	GAGAGGCACCACTTTGCTCA
hPDE2a reverse	human	ATGCGCTGATAGTCCTTCCG
hPDE3a forward	human	CTGCAGCCATGCACGATTAT
hPDE3a reverse	human	ATCGTTATATAGCACCGCCTG
hPDE3b forward	human	CCTTGTATTTCCAGAGAACAGAT
hPDE3b reverse	human	CAACTCCATTTCCACCTCCAG
hPDE5a forward	human	AGCACTGTACATTAAGAGGCG
hPDE5a reverse	human	CAAGCTGTCATCAGCATTGCC
hPDE6a forward	human	AAGGGCTACCGCAAGATCAC
hPDE6a reverse	human	TTCAGCTTTCCCGTCACCAG
hPDE6b forward	human	TCCAGAGCAAGGTCGCAC
hPDE6b reverse	human	GCCTTGTTCCGGTCCATCA
hPDE6c forward	human	TCAAAGTGATTCCGACGCCT
hPDE6c reverse	human	AAGTATTCATCCGCAGGGGC
	1	

hPDE9a forward	human	ACGCCATGAAAGAGTTACAGAA
hPDE9a reverse	human	GCTTTCCTCAGGCACAGTCT
hPDE10a forward	human	AATTCTGGGCTGAGGGTGAT
hPDE10a reverse	human	CACGGCATTGTAGAACCCAA
hPDE11a forward	human	TCTGTGGCTCTTGATGTGCTAT
hPDE11a reverse	human	CTGACACCAGAGGGATGTTGG

3.1.3 Drugs

Table 4: Drugs used for experiments

Compound	Function	Manufacturer	Product	Experimental
name			number	concentration
ANP	NPRA Agonist	Tocris	Cat. No. 1906	100 nM
			(human)	
			Cat. No. 1912	
			(mouse)	
CNP	NPRB Agonist	Tocris	Cat. No. 3520	100 nM
DEA-NO	Short-acting	MedChemExpress	ArtNr.: HY-	100 μΜ
	NO-donor		131925	
DETA-NO	Long-acting	MedChemExpress	ArtNr.: HY-	10 μΜ
	NO-donor		136278	
Norepinephrine	Adrenoceptor	Sigma-Aldrich	A9512-5G	100 nM, 1 μM
	Agonist			
Forskolin	Adenylate	Sigma-Aldrich	F6886-10MG	1–10 μΜ
	Cyclase			
	Activator			
Isoproterenol	β-	Sigma-Aldrich	I6504-1G	100 nM
	Adrenoceptor-			
	Agonist			
CGP 20712A	β1-	Sigma-Aldrich	C231-10MG	100 nM
	Adrenoceptor-			
	Antagonist			
ICI 118551	β2-	MedChemExpress	ArtNr.: HY-	50 nM
	Adrenoceptor-		13951	
	Antagonist			
CL 316243	β3-	Sigma-Aldrich	C5976-5MG	10 μΜ
	Adrenoceptor-			
	Agonist			

Iti-214	PDE1-	MedChemExpress	ArtNr.: HY-	100 nM
	Antagonist		12501A	
Bay 60-7550	PDE2-	MedChemExpress	ArtNr.: HY-	100 nM
	Antagonist		14992	
Cilostamide	PDE3-	MedChemExpress	ArtNr.: HY-	10 μΜ
	Antagonist		101312	
Avanafil	PDE5-	MedChemExpress	ArtNr.: HY-	1 μΜ
	Antagonist		18252	
Bay 73-6691	PDE9-	MedChemExpress	ArtNr.: HY-	10 μΜ
	Antagonist		104028	
IBMX	Pan PDE	Sigma-Aldrich	I5879-5G	100 μΜ
	Antagonist			
Ionomycin	Calcium-	MedChemExpress	ArtNr.: HY-	100 nM
	Ionophore		13434	
CNO	Gq-DREADD	MedChemExpress	ArtNr.: HY-	1 μΜ
	Agonist		17366	

Unless mentioned otherwise, the concentrations listed here were used for all experiments.

3.2 Animals

C57BL/6J mice, ordered from Charles River, were considered wild-type (WT) mice. The mice^{261,264} reporter were generated by targeted integration of a Cre recombinase-activatable expression cassette driven by the cytomegalovirus early enhancer/chicken β-actin/β-globin promoter into the Rosa26 locus. A more detailed description of the generation of this transgenic mouse line can be found in M. Thunemann's Ph.D. thesis²⁶⁷. These mice were generously provided by Robert Feil. The epac1-camps reporter mice^{256,268} were generated via pronuclear injection of one-cell-stage mouse embryos with the construct, containing the epac1-camps sequence under the control of the hybrid CMV enhancer/chicken β-actin (CAG) promoter. These mice were generously provided by Viacheslav Nikolaev.

Table 5: List of mice used

Mouse Line	Genetic	Source
	Background	
Wild type (WT)	C57BL/6J	Charles River
CAG-epac1-	FVB/N	Viachslav Nikolaev ²⁶⁸
camps		
R26-CAG-cGi500	C57BL/6JCrl	Robert Feil, Martin
		Thunemann ²⁶⁴

Mice were housed and bred at the animal facility of the LIMES Institute, University of Bonn. They had access to standard rodent chow and water ad libitum. Tissues and cells were isolated, unless stated otherwise, from male mice aged 8-12 weeks.

3.2.1 Genotyping

Materials and equipment:

- Acetic acid (Roth, Cat. No. 3738.4)
- Centrifuge (Eppendorf, Cat. No. 5415R)
- EDTA (Roth, Cat.No. 8043.2)
- Electrophoresis chamber, RunOne™ Electrophoresis System (Embi Tec)
- Ethanol (EtOH) (Roth, Cat. No. 9065.4)
- Ethidium bromide solution 10mg/ml (Roth, Cat. No. 2218.1)
- Gel casting chambers, RunOne™ Agarose Gel Casting Systeme (Embi Tec)
- Microwave (Severin)
- OneTaq® Quick Load® 2x MM w/Std Buffer (New England BioLabs, Cat. No. M0486S)
- Phire Tissue Direct PCR Master Mix (ThermoFisher Scientific, Cat. No. F170L)
- 2-Propanol (Roth, Cat. No. 6752.4)
- Proteinase K (Roche, Cat. No. 03115828001)
- QuantityOne® Software (BioRad)
- Reaction tube 1.5 ml (Sarstedt, Cat. No. 72706)
- Roti®- Phenol/chloroform/isoamyl alcohol (Roth, Cat. No. A156.2)
- Sodium dodecyl sulfate (SDS) (Roth, Cat. No. 2326.2)
- Sodium chloride (NaCl) (Roth, Cat. No. 3957.1)
- Thermocycler Biometra (Analytik Jena)
- Thermomixer (Eppendorf)
- Tris (Roth, Cat. No. AE15.3)
- Tris HCl (Roth, Cat. No. 9090.3)
- UV light transilluminator, GelDoc®XR (BioRad)

3.2.1.1 Isolation of DNA from biopsies and amplification via PCR

For genotyping, a small piece of biopsied earlobe was digested in 500 μ l proteinase K-buffer at 55°C at 550 rpm in a thermomixer (Eppendorf) overnight. The digestion was then terminated by increasing the temperature to 99°C for 20 minutes. Afterwards, 500 μ l of Roti®-Phenol/Chloroform/Isoamyl alcohol was added, and the samples were shaken. Then, the samples were centrifuged for 15 minutes at 15000 g, and the upper aqueous phase was transferred to a new microcentrifuge tube. 500 μ l of chloroform was added to the aqueous phase and the samples were shaken vigorously for 15 seconds, and then centrifuged again for 15 minutes at 15000 g. The upper phase was again transferred to a new microcentrifuge tube, and 800 μ l of isopropanol was added. After careful mixing, samples were centrifuged for 10 minutes at 15000 g and then washed in 70% EtOH. After pelleting the DNA by centrifugation for 10 minutes at 15000 g, samples were dried for 30 minutes and then resuspended in 30 μ l of H₂O. Afterwards, DNA was amplified using specific primers via PCR.

Table 6: Primers and amplification products for R26-CAG-cGI500 genotyping

Name	Primer Sequence (5' → 3')
ROSA10	CTCTGCTGCCTCCTGGCTTCT
ROSA11	CGAGGCGGATCACAAGCAATA)
ROSA4	TCAATGGGCGGGGTCGTT

ROSA10 and ROSA11 amplify a 330 bp fragment of the wild-type ROSA26 locus, while ROSA10 and ROSA4 amplify a 250 bp fragment of the R26-CAG-cGi500 allele. For experiments, homozygous R26-CAG-cGi500 transgenic mice, showing a 250 bp fragment, but not a 330 bp fragment were used.

Table 7: Mixture for R26-CAG-cGi500 genotyping via PCR

Substance	Volume [µl]
gDNA	1
2x Phire tissue direct PCR master mix	10
Primer ROSA10 (10 μM)	1
Primer ROSA11 (10 μM)	1
Primer ROSA4 (10 μM)	1
H ₂ O	6

Table 8: PCR program for genotyping of R26-CAG-cGi500 mice

Step	Time [s]	Temperature [°C]	
1	300	94°C	
2	10	94°C	_
3	30	65°C	35 cycles
4	30	72°C	
5	300	72°C	
6	∞	4°C	

3.2.1.2 Agarose gel electrophoresis

Agarose gel electrophoresis was used to analyze PCR amplification products. 1 g of agarose was dissolved in 50 ml of 1x TRIS-Acetate-EDTA (TAE) buffer, yielding a 2% agarose solution. Subsequently, ethidium bromide (800 ng/ml) was added and the gels were solidified in casting chambers. Next, the agarose gels were loaded with the samples. The loaded gel was then placed into an electrophoresis chamber containing 1x TAE buffer. Afterwards, gel electrophoresis was performed at room temperature (RT) and 100 V. After the run finished, DNA bands were visualized using an UV light transilluminator (GelDoc®XR, BioRad) and QuantityOne® software (BioRad).

Table 9: Recipe for TAE buffer 50x

Substance	Quantity
Tris	2 M
Acetic acid	5.71%
Na ₂ -EDTA	50 mM

Substances were dissolved in H_2O and stored at RT. 50x TAE buffer was diluted in millipore water at a 1:50 ratio to the final concentration of 1x.

Table 10: PCR products for WT, heterozygous, and homozygous R26-CAG-cGi500 mice

Name	Genotype	PCR Product size [bp]
CAG-cGi-500	WT	330
	Heterozygous	250 and 330
	Homozygous	250

3.3 Cell Culture

Materials and equipment:

- 3,3′,5-Triiodo-L-thyronine sodium salt (Sigma-Aldrich, Cat. No. T6397)
- 3-Isobutyl-1-methylxanthine (IBMX; Sigma-Aldrich, Cat. No. I5879)
- 6 well TC plates (Sarstedt, Cat. No. 83.3920)
- 6 well TPP plates (TPP Techno Plastic Products AG, Cat. No. 92406)
- 10 cm² TC dishes, Standard (Sarstedt, Cat. No. 83.3902)
- 12 well TC plates (Sarstedt, Cat. No. 83.3921)
- Autoclave, Varioklav 135 T (Faust)
- Bovine Serum Albumin (BSA; Sigma-Aldrich, Cat. No. A7030)
- Canulaes (Braun, Sterican 0,90 x 40 mm, Cat. No. 4657519)
- Centrifuge, Biofuge Primo (Heraeus)
- Collagenase, Type II (Worthington, Cat. No. CLS2)
- Conical tubes, 15 ml and 50 ml volume (Sarstedt, Cat. No. 62.554.502, 62.547.254)
- Countess Automated Cell Counter (Invitrogen, Cat. No. C10227)
- Cryogenic vials (Sarstedt, Cat. No. 72.379.992)
- Dexamethasone (Sigma-Aldrich, Cat. No. D4902)
- Dimethyl sulfoxide (DMSO; Roth, Cat. No. A994)
- Dulbecco's Modified Eagle's Medium (DMEM), high glucose, GlutaMAX(TM) (Gibco, Cat. No. 31965)
- DMEM, high glucose, GlutaMAX(TM), pyruvate (Gibco, Cat. No. 61966)
- DMEM/F-12 (1:1) (Gibco, Cat. No. 11039-047)
- Fetal Bovine Serum (FBS) (Biochrom, Cat. No. S0015)
- FGF-1 (rh) (Immuno Tools, Cat. No. 11343555)
- Human Transferrin (Lonza, Cat. No. CC-4205)
- Incubator, HERAcell® 150 (Heraeus)
- Insulin solution human (Insulin; Sigma-Aldrich, Cat. No, 19278)
- Laminar air flow, HerasafeTM (Heraeus)
- Microscope, LEICA DMIL (Leica Microsystems GmbH)
- 30 μM and 100 μM nylon meshes (Millipore, Cat. No. NY3002500, NY1H00010)
- Penicillin/streptomycin (P/S) (Merck, Cat. No. A2213)
- PBS (see section 3.2.12)
- Reaction tube 1.5 ml (Sarstedt, Cat. No. 72706)
- Rosiglitazone (Sigma-Aldrich, Cat. No. R2408)
- Scissors, forceps (Fine science tools)
- Serological pipettes 5ml, 10ml, 25ml (Sarstedt, Cat. No. 86.1253.001, 86.1254.001, 86.1685.001)

- Syringe filter 0.22 μm (VWR, Cat. No. 514-0061)
- Syringes 5 ml (BD Discardit II, Cat. No. 309050)
- T175 tissue culture flasks (Sarstedt, Cat. No. 83.3912.002)
- Trypan Blue Stain (Gibco, Cat. No. 15250)
- Trypsin-EDTA (0.05%), phenol red (Trypsin; Gibco, Cat. No. 25300054)

3.3.1 Murine brown adipocyte culture

WT BA were isolated from interscapular BAT of neonatal C57BL/6J mice. cGi-500 BA were isolated from interscapular BAT of neonatal R26-CAG-cGI500 mice. Epac1-camps BA were isolated from interscapular BAT of neonatal CAG-epac1-camps mice.

3.3.1.1 Isolation and immortalization of brown preadipocytes

Table 11: BA isolation buffer

Substance	Quantity
NaCl	123 mM
KCI	5 mM
CaCl2	1.3 mM
Glucose	5 mM
HEPES	100 mM

Substances were dissolved in H_2O . Afterwards, the pH was adjusted to 7.4 and the solution was sterile filtered.

Table 12: BA isolation buffer ready to use

Substance	Quantity
BSA	1.5%
Collagenase II	2 mg/ml

BSA and collagenase type II were added immediately before use. Then the solution was sterile filtered again.

Table 13: BA culture medium

Substance	Quantity
FBS	10%
HEPES	10 mM
Insulin	4 nM
P/S	1%
Sodium-Ascorbate	25 μg/ml
Т3	4 nM

Supplements were dissolved in DMEM, high glucose, GlutaMAX(TM), (Gibco, Cat. No. 61965).

BAT from the interscapular region of newborn mice was dissected with surgical scissors. Surrounding tissues were removed. The tissues of three to four mice were pooled and then mechanically minced with surgical scissors in a sterile petri dish. Afterwards, the minced tissues were transferred into a falcon containing 3 ml of BA isolation buffer ready to use (containing BSA and Collagenase II) and digested in a water bath set to 37°C for 30 minutes. The digestion mixture was vigorously shaken every 5 minutes. After the digestion, the mixture was filtered using a 100 µm nylon mesh to remove any remaining undigested clumps. The resulting cell suspension was then incubated on ice for 30 minutes. Afterwards to upper phase containing fat and mature adipocytes was removed. The middle phase containing the stromal vascular fraction was then filtered through 30 µm nylon mesh and centrifuged at 700 g for 10 minutes. The resulting cell pellet was then resuspended in 2 ml auf BA culture medium and plated in a 6 well tissue culture (TC) plate. For each sacrificed mouse one well was filled (i.e. a pool of four sacrificed mice yielded four wells). The cells were then placed in an incubator for 24 hours at 37°C, 5% CO₂. After one day, cells were immortalized using 200 ng of Simian Virus 40 (SV40) large T-antigen under the control of phosphoglycerate kinase (PGK) promoter per well. 24 hours after lentiviral transduction, the virus-containing media was substituted with a regular BA culture medium and the cells were grown to confluency.

3.3.1.2 Expansion and freezing of brown preadipocytes

Once the cells reached around 70-90% confluency, they were washed two times with PBS at RT and detached from the TC dish by adding 0.5 ml Trypsin per well, while incubating at 37°C for 3 minutes. After the incubation, trypsin was inactivated by the addition of 2 ml BA growth medium. The obtained cell suspension was centrifuged at 300 g for 5 minutes, afterwards the pellet was re-suspended in BA growth medium. The number of cells was then counted using trypan blue stain and the Countess Automated Cell Counter. Cells were then either frozen in cryogenic vials containing BA growth medium with 10% DMSO (= BA freezing medium) or reseeded onto 10 cm² TC dishes at a density of 500.000 cells per plate, corresponding to approximately 10% confluency. Vials intended for storage were frozen at -80°C for 24 hours and then stored at -150°C. Each splitting of cells using trypsin was considered one passage, with newly isolated adipocytes being considered passage 0. Passage four brown adipocytes were used for experiments.

Table 14: BA growth medium

Substance	Quantity
FBS	10%
P/S	1%

Supplements were added to DMEM, high glucose, GlutaMAX(TM) (Gibco, Cat. No. 61965).

Table 15: BA freezing medium

Substance	Quantity
DMSO	10%

Supplements were freshly added to the BA growth medium before use.

3.3.1.3 Differentiation of brown preadipocytes into brown adipocytes

Cells were seeded (considered as day -4) on TC plates in BA growth medium at a density of ~160.000 cells per well of a 6 well or ~80.000 cells per well of a 12 well plate and incubated at 37°C and 5% CO₂. After 48 hours (day -2) BA growth medium was exchanged for BA differentiation medium. Further 48 hours later, the medium was replaced with BA induction medium (day 0) initiating the differentiation program of preBA to BA. Afterwards, cells were cultured in BA differentiation medium from day 2 until day 7 with the medium being replaced every second day. Experiments with preBA were performed on day -2 before the addition of the differentiation medium. Experiments with BA were performed on day 7.

Table 16: BA differentiation medium

Substance	Quantity
FBS	10%
Insulin	1 nM
P/S	1%
Т3	20 nM

Substances were added to DMEM, high glucose, GlutaMAX(TM) (-) pyruvate. Differentiation medium was used for a maximum of one month, starting on the day of T3 dissolution.

Table 17: BA induction medium

Substance	Quantity
Dexamethasone	1 μΜ
IMBX	0.5 mM

Substances were added to the BA differentiation medium. Induction Medium was made freshly immediately before use.

3.3.2 Human brown adipocyte culture

Stromal vascular fraction cells obtained from biopsies of human supraclavicular brown adipose tissue (Ethical registration no. 076/18) were isolated according to previously established methods.²⁶⁹

For the differentiation of human preBA into fully mature human BA (hBA), 500.000 human preBA were seeded onto 12 well plates in hBA proliferation medium. The proliferation medium was replaced every other day until the cells reached full confluency. Two days after reaching 100% confluency, hBA were stimulated by changing the medium to hBA induction medium.

The day of induction was considered day 0. Three days post-induction, the hBA differentiation medium, with an additional 200 nM Rosiglitazone, was applied to the cells.

Subsequently, the differentiation process was maintained for an additional nine days by substituting the medium with fresh hBA differentiation medium (without Rosiglitazone) every third day. Experiments were performed on day 12 of differentiation.

Table 18: hBA proliferation medium

Substance	Quantity
FBS	10%
P/S	1%
FGF-1	1 nM

Substances were added to DMEM/F-12 (Gibco, Cat. No. 11039-047). FGF-1 was added freshly before every use.

Table 19: hBA differentiation medium

Substance	Quantity
P/S	1%
Dexamethasone	0.1 μΜ
Insulin	100 nM
Т3	2 nM
Transferrin	10 μg/ml

Substances were added to DMEM/F-12 (Gibco, Cat. No. 11039-047). Insulin, T3, and Transferrin were added freshly before every use. On day 3 of differentiation (after completion of the induction step) an additional 200 nM Rosiglitazone was added.

Table 20: hBA induction medium ready to use

Substance	Quantity
Rosiglitazone	200 nM
IBMX	540 μM

Substances were added to the hBA differentiation medium freshly before every use.

3.4 Oil Red O staining

Materials and equipment:

- Oil Red O (Sigma-Aldrich, Cat. No. O9755)
- Paraformaldehyde (PFA) (Roth, Cat. No. 0335.3)
- PBS (see table 19)
- 2-Propanol (Roth, Cat. No. 6752.4)
- Epson Perfection V370 Photo scanner

Cells were washed twice with PBS and then fixed with PFA 4% for 15 minutes at RT. After removal of the PFA, cells were washed two times with PBS again, covered with Oil Red O working dilution, and incubated for 2 hours at RT. Afterwards, the Oil Red O working dilution was carefully washed off with distilled water. Plates were dried at RT. Images were acquired by scanning the whole plates using a standard office scanner (Epson).

Table 21: PFA 4% solution

Substance	Quantity
Paraformaldehyde	40 g
PBS 10x	100 ml
H ₂ O	900 ml

PFA was dissolved in H₂O pH 10,0 under constant stirring. After the PFA was completely dissolved, 10x PBS was added. This PFA was then immediately used within a single day.

Table 22: Oil Red O stock solution

Substance	Quantity
Oil Red O	0.5 g
Isopropanol 99%	100 ml

Dye and isopropanol were mixed and stirred overnight. This stock solution was then stored at RT

Table 23: Oil Red O working dilution

Substance	Quantity
Oil Red O stock solution	6 ml

Immediately before use Oil Red O stock solution was diluted in a ratio of 3:2 with H_2O and filtered twice through filter papers.

3.5 Analysis of intracellular cAMP and cGMP concentrations via ELISA Materials and equipment:

- Direct cAMP ELISA Kit (Enzo, Cat. No. ADI-901-066)
- Monoclonal cGMP EIA Kit No Acetylation (New East Biosciences, Cat. No. 80103)
- Enspire® microplate reader (Perkin Elmer, Cat. No. 2300-0000
- PBS (see section 3.2.12)
- Reaction tube 1.5 ml (Sarstedt, Cat. No. 72706)
- Ultra-Turrax®, T8, IKA, Staufen

Cells were treated with various compounds for 5 minutes in regular media (BA growth media for preBA and BA differentiation media for BA). Afterwards, cells were washed with PBS twice and then lyzed with 0.1 M HCl, taking care that all cells had the same drug incubation time. After 10 minutes of HCl incubation for preBA or 20 minutes for BA, cells were collected using a cell scraper. The cell suspension was then sonicated for complete lysis. Cell debris were centrifuged at 600 g. The supernatant was then used for analysis. Samples were analyzed using the Direct cAMP Enzyme-Linked Immunosorbent Assay (ELISA) Kit, following the manufacturer's instructions. Measurement of optical density was performed at 405 nm using the Enspire plate reader (Perkin Elmer). Data analysis was carried out according to the specifications of the manufacturer via a standard curve. The cAMP concentration was then normalized to the protein content of each well, as determined by the Bradford assay.

3.6 In vitro lipolysis

Materials and equipment:

- 96 well plates (Sarstedt, Cat. No. 83.3924)
- Bovine serum albumin (BSA) (Sigma-Aldrich, Cat. No. A7030)
- DMEM (Gibco, Cat. No. 21063)
- Enspire® microplate reader (Perkin Elmer, Cat. No. 2300-0000)
- Free glycerol reagent (Sigma-Aldrich, Cat. No. F6428)
- Glycerol standard (Sigma-Aldrich, Cat. No. G7793)
- Incubator, HERAcell® 150 (Heraeus)
- Reaction tube 1.5 ml (Sarstedt, Cat. No. 72706)

Table 24: Lipolysis medium

BSA 2%	Substance	Quantity
	BSA	2%

BSA was dissolved in DMEM (Gibco, Cat. No. 21063).

BA were washed two times with lipolysis medium and wells were refilled with 300 μ l of lipolysis medium for 12 well plates, or 600 μ l for 6 well plates containing the compounds to be studied. Cells were then incubated at 37°C, 5% CO₂ for 2 hours for murine BA or 4 hours for human BA. Afterwards, the free glycerol content of the supernatant was measured. For this 40 μ l of conditioned lipolysis medium was combined with 60 μ l of free glycerol reagent. Blanks were pipetted using 40 μ l of unconditioned lipolysis medium with 60 μ l of glycerol reagent. Glycerol standard concentration was prepared by mixing 5 μ l of glycerol standard with 95 μ l free glycerol reagent. After all samples were added the plate was incubated for 5 minutes at 37°C. Absorption was measured in an Enspire microplate reader (Perkin Elmer) at 540 nm. Blanks were subtracted. Glycerol content was calculated according to the manufacturer's instructions. Results for each sample were normalized to protein concentration as determined via Bradford assay.

3.7 RNA isolation, cDNA synthesis and qRT-PCR

Materials and equipment:

- Centrifuge (Eppendorf, Cat. No. 5415R)
- Chloroform (Roth, Cat. No. 6340.1)
- Diethylpyrocarbonate (DEPC; Roth, Cat. No. K028.1)
- Ethanol (EtOH) (Roth, Cat. No. 9065.4)
- InnuSOLV RNA Reagent (Analytik Jena AG, Cat. No. 845-SB-2090100)
- Nanodrop200 Spectrophotometer (ThermoScientific)
- 2-Propanol (Roth, Cat. No. 6752.4)
- Reaction tube 1.5 ml (Sarstedt, Cat. No. 72706)
- Real-time PCR machine, HT7900 (Applied Biosystems)
- SYBR-Green PCR master mix (Applied Biosystems, Cat. No. 4309155)
- Thermocycler Biometra TOne (Analytik Jena)
- Thermomixer comfort (Eppendorf, Cat. No. 2050-120-04)
- Protoscript® II First Strand cDNA Synthesis Kit (New England BioLabs, Cat. No. E6560S)
- Ultra-Turrax®, T8, IKA, Staufen

3.7.1 Isolation of RNA

RNA extraction from cells or tissues was performed using innuSOLV RNA Reagent. To initiate cell lysis, 1 ml of innuSOLV RNA Reagent was added to the cells. For tissues, an additional step involved using an Ultra-Turrax® to mash the tissue in 1 ml innuSOLV RNA Reagent. The resulting lysates were then transferred to reaction tubes, and 200 μ l of cold chloroform (at -20°C) was added to each sample. Following vigorous shaking for 15 seconds, the samples were left at room temperature for 5 minutes for phase separation to occur.

Subsequently, the lysed cells were centrifuged at 4° C and 13000 g for 20 minutes. The upper phase, which contained the RNA, was carefully separated from other cellular components, such as lipids, DNA, or proteins. This upper phase was then moved to new reaction tubes and combined with 500 μ l of cold isopropanol to induce RNA precipitation. The mixture was centrifuged for 10 minutes at 4° C and 13000 g. After removing the supernatant, the resulting RNA pellet was subjected to three washes with 75% EtOH (diluted in DEPC-H₂O), followed by air drying and dissolution in 30 μ l DEPC-H₂O. Finally, the concentration of RNA was determined using a Nanodrop spectrophotometer.

3.7.2 Synthesis of complementary DNA

1000 ng of RNA were transcribed to complementary DNA (cDNA) using Protoscript® II First Strand cDNA Synthesis Kit according to the manufacturer's instructions. The following program was used for the thermocycler:

Table 25: cDNA Synthesis Program

Step	Time [minutes]	Temperature [°C]
1	5	25
2	60	42
3	5	80
4	∞	4

The obtained cDNA was diluted to a final concentration of 2.5 ng/µl.

3.7.3 Quantitative real-time polymerase chain reaction

10 ng of cDNA was combined with 5 μ I of SYBR Green PCR mastermix containing the relevant primer pair [1 μ M] and amplified using a HT7900 instrument (Applied Biosystems).

Quantitative real-time PCR (qPCR) was conducted utilizing SYBR green, a dye that generates a fluorescent signal upon binding to double-stranded DNA. The intensity of fluorescence is directly correlated with the quantity of double-stranded DNA present in the reaction at each time point, enabling real-time monitoring of the PCR process. This method involves tracking the number of cycles required to achieve an automatically determined signal threshold (= cycle threshold, Ct), allowing for accurate quantification of the initial template amount.

The threshold was determined via the second derivative maximum method. This automated method calculates the Ct by identifying the point at which the second derivative of the real-time fluorescence intensity curve reaches its peak value, or in other words, the cycle at which the rate of fluorescence increase is at its highest point²⁷⁰.

To serve as an internal control, the amplification of the hypoxanthine-guanine phosphoribosyltransferase (*Hprt*) gene was measured for murine and human samples.

In this context, the Ct value of an internal control (*Hprt*) was subtracted from the Ct value of the target gene, resulting in the calculation of a Δ Ct value. Since Ct values are logarithmic (to the base of 2), the difference between Δ Ct values from the gene to be investigated and the endogenous control yields the relative proportion of target mRNA abundance in those samples. This proportion is obtained by raising 2 to the power of the negative Δ Ct (2- Δ Ct).

Table 26: Primer mastermix for qRT-PCR

Substance	Quantity
ABI SYBR Green	10 ng
Forward Primer	500 nM
Reverse Primer	500 nM

The components were diluted in DEPC- H_2O . The total volume used per well of a 384 well plate was 9 μ l.

Table 27: qRT-PCR program with melting curve

Step	Time [s]	Temperature [°C]	
1	600	95	
2	15	95	40 cycles
3	60	60	40 cycles
Melting curv	/e:		
4	1	95	
5	15	65	
6	-	95	

The melting curve data was acquired during the ramp from 65°C to 95°C between steps 5 and 6.

3.8 Protein isolation

Materials and equipment:

- BioPhotometer D30 (Eppendorf)
- Bovine Serum Albumin (BSA) (Roth GmbH, Cat. No. 8076.3)
- Cell scraper (Labomedic, Cat. No. 2015217)
- Centrifuge 5430R (Eppendorf)
- Complete protease inhibitor cocktail (Roche, Cat. No. 04693116001)
- Coomassie brilliant blue G-250 (Merck, Cat. No. 1.15444.0025)
- Deoxycholic acid sodium salt (Roth, Cat. No. 3484.2)
- Ethanol (EtOH) (Roth, Cat. No.9065.4)
- Minispin centrifuge (Sigma-Aldrich, Cat. No. Z606235)
- Nonidet® P 40 Substitute (NP-40) (Fluka BioChemika, Cat. No. 74385)

- Ortho-Phosphoric acid 85% (Roth, Cat. No. 6366.1)
- PBS (see section 3.2.12)
- Reaction tube 1.5 ml (Sarstedt, Cat. No. 72706)
- Syringe filter 0.22 μm (VWR, Cat. No. 514-0061)
- Sodium dodecyl sulfate (SDS) (Roth, Cat. No. 2326.2)
- Sodium chloride (NaCl) (Roth, Cat. No. 3957.1)
- Sodium fluoride (NaF) (Roth, Cat. No. 2618.1)
- Tris HCl (Roth, Cat. No.9090.3)
- Tri-Sodiummonovanadate (Na3VO4) (Roth, Cat. No. 0735.1)
- Ultra-Turrax® (T8, IKA, Staufen)

3.8.1 Isolation of proteins

Cells were washed with PBS twice. Next cold lysis buffer was added to the cells (200 μ l per well for 6 well plates, 100 μ l per well for 12 well plates). Cells were scraped off the cell culture plates and transferred into a reaction tube. Afterwards, they were sonicated and kept on ice for 15 minutes. Then they were centrifuged for 20 minutes at 4°C and 13000 g. The clear middle phase was transferred into a new reaction tube and stored at -80°C or used directly. The upper phase containing lipids and the lower phase containing cellular debris were discarded.

Table 28: RIPA buffer recipe

Substance	Quantity
Deoxycholic acid sodium salt	0.5%
NaCl	150 mM
NP-40	1%
Sodium dodecyl sulfate (SDS)	0.1%
Tris HCI (pH 7.5)	50 mM

All substances were dissolved in H_2O . Afterwards, the solution was sterile-filtered and stored at $4^{\circ}C$.

Table 29: Lysis buffer recipe

Substance	Quantity
Complete® EDTA free	40 µl
NaF	10 mM
Na ₃ VO ₄	1 mM

All substances were added to 1 ml RIPA buffer freshly before use.

3.8.2 Quantification of protein content via Bradford Assay

Table 30: Coomassie Solution Recipe

Substance	Quantity
Coomassie brilliant blue G-250	0.01%
EtOH	5%
Phosphoric acid	8.5%

The components were dissolved in H₂O. The solution was stored at 4°C.

 $2~\mu l$ of protein lysate was diluted with $98~\mu l$ 0.15M NaCl solution and $900~\mu l$ Coomassie solution and kept at RT for 1 minute. Absorbance was measured with a BioPhotometer at 595 nm and protein amount was quantified using a BSA standard calibration curve. 100 μl 0.15 M NaCl with $900~\mu l$ Coomassie solution was used as a blank.

3.9 Sodium-dodecyl sulfate polyacrylamide gel electrophoresis and Western Blot

Materials and equipment:

- Acrylamide Rotiphorese® Gel 30 (37.5:1), (Roth, Cat. No. 3029.1)
- SuperSignal[™] West Femto Maximum Sensitivity Substrate (Thermo Fisher, Cat. No. 34094)
- Bromophenol blue (Roth, Cat. No. T116.1)
- Color protein Broad Range (New England Bio Labs, Cat. No. 0021405)
- Centrifuge (Eppendorf)
- Electrophoresis power supply, EV202 (Sigma-Aldrich)
- Electrophoresis/western blotting system: Mini Trans-Blot® Cell system (BioRad)
- Glas plates mini Protean® (Bio Rad, Cat. No. 1653312)
- Glycerol (Roth, Cat. No. 3908.3)
- LAS 4000 mini (GE Healthcare Life Sciences)
- 2-Mercaptoethanol (Sigma-Aldrich, Cat. No. M3148)
- Nitrocellulose blotting membranes (GE Lifesciences, Cat. No. A29434120)
- N-N-N'-N'-Tetramethyl ethylene diamine (TEMED) (Sigma-Aldrich, Cat. No. T7024)
- Nonfat dried milk powder (PanReac AppliChem, Cat. No. A0830)
- Sodium chloride (NaCl) (Roth, Cat. No. 3957.1)
- Sodium-dodecyl sulfate (SDS) (Roth, Cat. No. 2326.2)
- Thermomixer (Eppendorf)
- Tris (Roth, Cat. No. AE15.3)
- Tris HCl (Roth, Cat. No. 9090.3)
- WhatmanTM gel blot paper (GE Lifesciences, Cat. No. 10426892)

3.9.1 Preparation of protein samples

Protein concentrations were adjusted to 40 μ g per sample by diluting them with lysis buffer. Next, 3x concentrated loading buffer (3x Laemmli) was added at one-third of the final volume to achieve a final concentration of 1x. β -mercaptoethanol was added to the protein solution (5%) to cleave disulfide bonds by reducing them to thiols. The final sample contained 40 μ g of protein at a volume of 30 μ l. Subsequently, the samples were heated to 95°C for 5 minutes to destroy the secondary and tertiary structures.

Table 31: 3x Laemmli buffer recipe

Substance	Quantity
Bromophenol blue	0.015%
Glycerol	20%
SDS	17%
Tris-HCI (pH=6.8)	125 mM

The components were dissolved in H₂O and the buffer was stored at -20°C.

3.9.2 Sodium-dodecyl sulfate polyacrylamide gel electrophoresis

The gels for sodium-dodecyl sulfate polyacrylamide gel electrophoresis (SDS-PAGE) are produced through radical polymerization. Acrylamide functions as the gel-forming agent. The polymerization is initiated by introducing N-N-N'-N'-tetramethyl ethylene diamine (TEMED) as a catalyst and ammoniumperoxodisulphate (APS) as a radical initiator. The polyacrylamide gels were poured by combining the compounds listed below. TEMED was added last, as it starts the polymerization. Immediately after the TEMED addition, the liquid gels were poured between glass plates in gel casting stands. Once the separating gel was poured, isopropanol was added to enable smooth polymerization of the uppermost part of the gel. Once the polymerization of the separating gel was completed, the isopropanol was removed using Whatman papers. Then TEMED was added to the stacking gel mixture, which was then added on top of the separating gel. Gel combs were then immediately added and the gel was allowed to fully polymerize.

Table 32: Composition of the separating gel

Substance	8%	10%	12%	15%
H ₂ O	4.6 ml	4 ml	3.3 ml	2.3 ml
30% Acrylamide	2.7 ml	3.3 ml	4 ml	5 ml
1.5M Tris (pH=8.8)	2.5 ml	2.5 ml	2.5 ml	2.5 ml
20% ammonium persulfate (APS)	0.05 ml	0.05 ml	0.05 ml	0.05 ml
N-N-N'-N'-Tetramethyl ethylene diamine (TEMED)	6 µl	4 µl	4 µl	4 µl

TEMED was added last. Immediately after the TEMED addition, the gel was poured.

Table 33: Composition of the stacking gel

Substance	Quantity
H ₂ O	3.4 ml
30% Acrylamide	0.83 ml
1M Tris (pH=8.8)	0.63 ml
20% ammonium persulfate	0.05 ml
N-N-N'-N'-Tetramethyl ethylene	6 µl
diamine (TEMED)	

TEMED was added last. Immediately after the TEMED addition, the gel was poured.

After completion of polymerization, denatured protein samples were loaded into the pockets of the stacking gel. SDS-PAGE was performed in 1x electrophoresis buffer at 100V for 60-120 minutes, depending on the acrylamide gel content and the size of proteins to be analyzed, at RT using the Mini Trans-Blot® Cell system.

Table 34: 10x electrophoresis buffer recipe

Substance	Quantity
Glycine	2 M
SDS	0.1%
Tris	250 mM

The substances were dissolved in H_2O and pH was adjusted to 8.3. Before usage electrophoresis buffer was diluted with deionized H_2O to a final concentration of 1x.

3.9.3 Western Blotting

Following the completion of SDS-PAGE, the Western Blotting procedure was performed to transfer the proteins from the gel onto a nitrocellulose membrane. The gels were placed into the Mini Trans-Blot® Cell system transfer setup, positioned between sponges and Whatman papers, with a nitrocellulose membrane placed on top of the gel. Protein transfer was facilitated

by applying a 300 mA transverse electric field for 90 minutes in a cold transfer buffer. Once the transfer was finalized, the membranes were blocked with the blocking buffer for 1 hour.

After blocking, the membranes were immersed in a primary antibody solution overnight at 4°C with gentle agitation. Primary antibodies were prepared in blocking buffer at a 1:1000 dilution unless mentioned otherwise. Post-incubation, the membranes underwent three consecutive 5 minute washes with TBST. Following this, the membranes were exposed to the HRP-conjugated secondary antibodies, diluted in blocking buffer, for a 1 hour incubation at RT. Following secondary antibody incubation, the membranes were washed three additional times with TBST for 5 minutes each. Finally, proteins were visualized with SuperSignal West Femto Maximum Sensitivity Substrate (approximately 1 ml per membrane) in the ImageQuant LAS 4000 mini (GE Healthcare Life Sciences).

The quantification of bands was performed using ImageJ's gel function with background subtraction. After visualization and quantification, the membranes were stripped by applying a stripping buffer for 30 minutes, followed by another set of three 5 minute washes with TBST. The membranes were then blocked again for 1 hour and subsequently exposed to a fresh primary antibody solution in a blocking buffer for the detection of the next protein of interest. This cycle was repeated until all desired proteins were detected. If protein sizes differed substantially, the membranes were appropriately cut, and the proteins were detected simultaneously in their corresponding antibody solutions.

If not indicated otherwise, Calnexin was detected as an endogenous loading control, and individual protein expression levels were then normalized to Calnexin.

Table 35: 1x Transfer buffer recipe

Substance	Quantity
10x Electrophoresis buffer	10%
Methanol	20%

The substances were dissolved in H2O.

Table 36: 10x Tris-buffered saline (TBS) recipe

Substance	Quantity
Tris	24.3 g
NaCl	80 g

The substances were dissolved in H2O and the pH was adjusted to 8.0 using HCl.

Table 37: TBS-Tween (TBST) recipe

Substance	Quantity
Tween-20	1 ml
10x TBS	100 ml

The substances were dissolved in H2O.

Table 38: Blocking buffer

Substance	Quantity
Non-fat dry milk powder	5 g
TBST	100 ml

Table 39: Stripping buffer recipe

Substance	Quantity
Glycine	2 M
SDS	1%

The substances were dissolved in H₂O and pH was adjusted to 2.0 using HCl.

3.10 Real-time imaging of cyclic nucleotides in BA via FRET

Materials and equipment:

- μ-Slide 8 well ibiTreat (ibidi GmbH, Gräfelfing, Germany), Cat. No. 80826
- μ-Dish 35 mm, high ibiTreat (ibidi GmbH, Gräfelfing, Germany), Cat. No. 81156-400
- Calcium chloride dihydrate (Roth), Cat. No. T885.1
- Glucose, waterfree (Roth), Cat. No. X997.2
- HEPES (Sigma-Aldrich), Cat. No. H4034
- ImageJ Software including Add-on Fiji
- ImmersolTM 518 F/30°C (Carl Zeiss Microscopy Gmbh, Jena, Germany), Cat. No. 444970-9000-000
- Magnesium chloride hexahydrate (Roth), Cat. No. A-537.1
- Potassium chloride (Roth), Cat. No. 6781.1
- Sodium chloride (NaCl) (Roth, Cat. No. 3957.1)

One million passage four transgenic cGi-500 preBA or passage four transgenic epac1-camps preBA were thawed and resuspended in 10 ml of BA growth medium. The cell suspension was then centrifuged at 300 g for 5 minutes. The supernatant was discarded. Afterwards, the cell pellet was resuspended in 5 ml of BA growth medium. Of this suspension 500 μ l (containing approximately 100.000 cells) were added onto round glass coverslips (ibiTreat, μ -Dish 35 mm, high), taking care that the droplet does not spill over the glass bottom in the center of the dish, to ensure that all cells adhere to the area suitable for imaging. 6 hours later cell attachment was verified and then 1.5 ml of BA growth medium was added to the cells.

48 hours afterwards (day -2) FRET experiments were performed. BA GM was replaced with 900 μl Ringer's solution. The drugs of interest were diluted in Ringer's solution to a concentration corresponding to 10-12x of the experimental concentration, depending on their order of application (first compounds 10x, second compounds 11x, third compounds 12x). 100 μl of the respective compound was then added to the sample, representing a 1:10 dilution of the 10x compound, or a 1:11, or 1:12 dilution of the second or third compound, respectively. IBMX + either CNP, ANP or DEA-NO (for cGi-500) or IBMX + Forskolin (for epac1-camps) was added at the end of the measurement to ensure that the cells remained functional, and that the sensor did not become fully saturated throughout the experiment.

For experiments with fully differentiated BA, one million cells were seeded on a 6 well plate and differentiated according to the aforementioned protocol. On day 5 of differentiation, the cells were detached from the plate by adding 500 μ l of trypsin and incubating for 5 minutes at 37° C. Afterwards cells were transferred to a falcon and diluted in 27 ml of BA differentiation medium. Centrifugation was then performed at 300 g for 10 minutes. The cell pellet was resuspended in the BA differentiation medium. Cells were counted and 500 μ l, containing approximately 150.000 cells were then reseeded onto round glass coverslips (ibiTreat, μ -Dish 35 mm, high), again taking care that the cells attach to the central area, suitable for imaging. The differentiation then continued until day 7, when cells were imaged in Ringer's solution, as mentioned above.

Table 40: Ringer's solution recipe

Substance	Quantity
NaCl	140 mM
KCI	2.8 mM
MgCl2 6 x H₂O	2 mM
CaCl2 2 x H₂O	1 mM
HEPES	10 mM
D+ Glucose	10 mM

The substances were dissolved in 100 ml H₂O and pH was adjusted to 7.4 using HCl.

FRET measurements were performed with an inverted microscope (Leica DMI 4000 B, Leica), beam splitter (DualView-A, Photometrics) with a dcrx505 dichroic mirror, and ET480/40 plus ET535/30 emission filters (Chroma Technologies) and a T510lpxrxt-UF2 long pass filter (Chroma Technologies) and scientific complementary metal—oxide—semiconductor camera (sCMOS) (Photometrics Prime sCMOS) connected to a computer via the interface of an Arduino UNO I/O switchboard. As a light source CoolLED pE-100, 440 nm was used. An oil immersion 63x objective was used.

As software Micromanager 2.0 Beta, coupled with ImageJ was used. The settings were Binning 1*1, Preset State 1, and exposure time 100 ms. As a ROI the entire imaged area was selected, taking the average values of all visible cells (approximately 5-10 cells). An LED intensity of 40% was used, which yielded an ideal trade-off between signal-to-noise ratio and photobleaching. The LED emission at 440 nm excited the CFP, with FRET transferring energy to YFP to a degree depending on the concentration of cGMP or cAMP. CFP and YFP signals were measured, background subtracted (if the background was visible within the field of view) and then the CFP/YFP ratio was calculated and normalized to the baseline value (the mean of the 50 seconds before the addition of the first drug). FRET measurements took between 600-1200 seconds. Images were acquired every 10 seconds. It was assured that a stable baseline of the CFP/YFP ratio had been reached before new compounds were added to the cells. Ringer's solution served as a vehicle control. If the effect of compounds, which were dissolved in DMSO, was being studied, the same amount of DMSO was added to the Ringer's solution serving as vehicle control.

3.10.1 FRET calculations

- 1. Individual CFP and YFP signals were determined via ImageJ as mean gray values. As ROI the entire image was chosen.
- 2. CFP and YFP background signals were determined and subtracted from the individual CFP and YFP signals.
- 3. The baseline FRET ratio (R0) was calculated by taking the geometric mean of the 5 frames (50 seconds) before the addition of the first compound (for example the mean CFP/YFP ratio from frames 15-19, if the compound were to be added at Frame 20).
- 4. All CFP/YFP ratios from the measurement were normalized via division by R0. These normalized FRET ratios are represented as FRET ratio traces in the results.
- 5. The CFP/YFP ratio of the first compound was calculated by taking the geometric mean of the normalized CFP/YFP ratio of the 5 frames before the addition of the second compound (for example frames 45-49). This was considered R1.
- 6. The difference between R1 and R0 was considered dR1 and when divided by R0 represents the relative change in FRET over baseline as a consequence of the first drug application. This value was multiplied by 100 to represent the FRET change in %.

Drug 1 Effect =
$$\frac{R1 - R0}{R0} * 100 \%$$

For all experiments concerned with cGMP or cAMP generators, this FRET change over baseline, induced by the agonist (i.e. NO or NE) is displayed.

7. If a second compound was investigated (for example a PDE inhibitor) the same calculation was performed for drug 2, with R2 representing the geometric mean CFP/YFP ratio of the five frames before the addition of the positive control (for example frame 75-79). R1 was used as the reference ratio to determine the additive effect of the second drug over the effect caused by the first drug.

Drug 2 Effect =
$$\frac{R2 - R1}{R0} * 100 \%$$

For all experiments concerned with the PDE effect on cAMP or cGMP levels, this drug 2 effect was determined for an individual PDE (i.e. PDE3) and also for IBMX. The IBMX response was considered 100% (i.e. total PDE inhibition) and the individual PDE effect was divided by the IBMX effect. The result was then multiplied by 100% to obtain a result representing PDE inhibition as a percentage of total PDE inhibition.

Individual PDE effect relative to IBMX =
$$\frac{\text{Drug 2 Effect (individual PDEI)}}{\text{Drug 2 Effect (IBMX)}} * 100 \%$$

3.11 Real-time imaging of cyclic nucleotides in human preBA and BA Materials and equipment:

- LSM 700 VRGB (445), ZEN 2010, laser scanning confocal microscope (Carl Zeiss Microscopy GmbH, Jena, Germany), Cat. No. 000000-1865-957
- μ-Slide 8 well ibiTreat (ibidi GmbH, Gräfelfing, Germany), Cat. No. 80826
- µ-Dish 35 mm, high ibiTreat (ibidi GmbH, Gräfelfing, Germany), Cat. No. 81156-400
- Calcium chloride dihydrate (Roth), Cat. No. T885.1
- Glucose, waterfree (Roth), Cat. No. X997.2
- HEPES (Sigma-Aldrich), Cat. No. H4034
- ImmersolTM 518 F/30°C (Carl Zeiss Microscopy Gmbh, Jena, Germany), Cat. No. 444970-9000-000
- Magnesium chloride hexahydrate (Roth), Cat. No. A-537.1
- Potassium chloride (Roth), Cat. No. 6781.1
- Sodium chloride (NaCl) (Roth, Cat. No. 3957.1)

For real-time single fluorophore-based cGMP imaging human preBA were thawed and suspended in 10 ml of hBA proliferation medium. Afterwards, the suspension was centrifuged at 300 g for 5 minutes. The supernatant was discarded, and the cell pellet was resuspended in hBA proliferation medium. Cells were then counted, and the final volume was adjusted to a

cell density of 100.000 cells per ml of medium. 200 μ l of this suspension (containing approximately 20.000 cells) was then added to each well of an ibidi μ -Slide 8 well high plate. The cells were then incubated at 37°C and 5% CO₂ for 6 hours. After 6 hours 20 ng of Green cGull lentiviral particles were added to each well to transduce the cells. After 72-96 hours human Green cGull preBA were imaged using a confocal microscope. For this, the medium was again exchanged with Ringer's solution.

For hBA, cells were seeded in the same way as mentioned above. 2 days after reaching confluency human preBA were induced with hBA induction medium and differentiation was carried out as described above. On day 9 of differentiation, the cells were transduced with 20 ng of Green cGull lentivirus. After 72-96 hours Green cGull hBA were imaged using a confocal microscope. For this, the medium was again exchanged with Ringer's solution.

A 20x magnification objective was used (EC Plan-Neofluar 20x/0.50 M27). The excitation wavelength was 488 nm. Laser Intensity was 20%. The gain was set to 600. During the time series, an image was acquired every 10 seconds. The total experiment duration was between 600 and 1200 seconds. ROIs were placed around single cells. The experiments and data analyses were performed analogously to the above-mentioned FRET measurements, the only difference being that mean fluorescence intensity was measured here instead of a fluorescence ratio.

3.12 Development of organelle-targeted cGMP biosensors

Materials and equipment:

- 100 mm dish, Sarstedt, Cat. No. 83.1802.001
- Agar-Agar, Carl Roth, Cat. No. 2266.3
- Bsrgl-HF Restriction-Enzyme (NEB), Cat. No. R3575S
- Electrophoresis chamber: RunOne™ Electrophoresis System, Embi Tec, San Diego, CA, USA
- Gel casting chambers: RunOne™ Agarose Gel Casting System, Embi Tec, San Diego, CA, USA
- Illustra™ GFX™ PCR DNA and Gel Band Purification Kit, GE Healthcare Europe GmbH, Freiburg, Cat. No. 28-9034-70
- Incubator: AL01-07-100, Advantage Lab, Schilde, Belgium Microwave oven: Severin Elektrogeräte GmbH, Sundern Spectrophotometer:
- NanoDrop 2000, ThermoFischer Scientific
- NucleoBond® Xtra Maxi Plus, Macherey-Nagel GmbH, Düren, Cat. No. 740416.50
- T4 DNA ligase, Invitrogen, Karlsruhe, Cat. No. 15224-041
- UV light transilluminator, GelDoc® XR, BioRad, München
- Xhol Restriction Enzyme (NEB), Cat. No. R0146M
- XL1-Blue Supercompetent cells, Agilent Technologies, Ratingen, Cat. No. 200236

The original Green cGull biosensor vector was obtained from Addgene²⁷¹. This vector was then subcloned into the rrl-CMV lentiviral backbone²⁷² to allow for lentiviral transduction of cells and was kindly provided by Dennis de Coninck.

For the nuclear-targeted Green cGull a nuclear-localization-sequence (NLS) targeting sequence was chosen (PKKKRKV)²⁷³ and added C-terminally to the biosensor. Complementary oligonucleotides coding for the targeting sequence and resulting in appropriate overhangs for the insertion into the Green cGull-rrl-CMV vector were ordered from Microsynth.

The sequence of the forward oligonucleotide was:

(5' to 3') GTACCCCAAGAAGAAGAAGGAAGGTGGAGGACGCCTAA. The sequence for the reverse oligo was (5' to 3') TCGATTAGGCGTCCTCCACCTTCCTCTTCTTCTTGGG.

Next, the rrl-CMV-Green-cGull plasmid was digested with the restriction enzymes BsrgI and XhoI (according to the manufacturer's instructions, NEB) overnight at 37°C resulting in sticky ends complementary to the overhang of the hybridized targeting oligonucleotides.

Table 41: Restriction digestion mixture

Substance	Quantity
DNA	1 µg
10X rCutSmart Buffer	5 μΙ
BsrGI-HF	1.0 µl (20 units)
Xhol	1.0 µl (20 units)

Substances were dissolved in nuclease-free water to a final volume of 50 µl.

Afterwards, the restriction digestion mixture was cleaned via agarose gel electrophoresis. Subsequently, ligation was performed with a 1:5 molecular ratio of vector to insert (the hybridized oligonucleotides), using 50 ng of vector DNA, at 16°C overnight (according to manufacturer's instructions).

Table 42: Ligation mixture

Substance	Quantity
T4 DNA Ligase Buffer (10X)	2 µl
Vector DNA (4 kb)	50 ng (0.020 pmol)
Insert DNA	0.10 pmol
T4 DNA Ligase	1 μΙ

Substances were dissolved in nuclease-free water to a final volume of 20 µl.

After that, the ligase enzyme was heat-inactivated at 65° C for 10 minutes. Next, bacteria were transformed via heat shock with 10 μ l of the ligation mix and cultured for 1 hour in LB (+) media, and then plated on ampicillin-containing agar plates.

Table 43: LB+ medium

Substance	Quantity
NaCl	0.5%
Peptone	1%
Yeast extract	0.5%
Glucose	0.1%

The substances were dissolved in H₂O, adjusted to pH 7.5, and autoclaved.

Table 44: Ampicillin LB+ plates

Substance	Quantity
Agar-agar	1.5%
Ampicillin	50 µg

The Agar-agar was dissolved in LB+ medium, autoclaved, and poured into 100 mm Petri dishes. Ampicillin was added after autoclaving.

The next day three colonies were picked and sequenced by Microsynth. Glycerol stocks were prepared of the successful mutants and DNA amplification via NucleoBond Xtra Maxi was performed (according to the manufacturer's instructions).

Table 45: Glycerol stock recipe

Substance	Quantity
Bacteria containing LB+ medium	500 μΙ
Glycerol (50%)	500 μΙ

The Glycerol stocks were frozen and stored at -80°C.

Lastly, lentiviruses were prepared based on 300 µg of the cleaned CMV-rrl-Green-cGull-NLS plasmid.

The membrane-targeted biosensor rrl-CMV-Green-cGull-CAAX was prepared in the same way. The CAAX motif (CVIM) together with a short linker was added C-terminally to the biosensor²⁷⁴. For this, the following oligonucleotides were ordered from Microsynth:

The sequence of the forward oligonucleotide was (5' to 3'):

GTACAAGAAGAAAAAGAAAGAAGTCAAAGACAAAGTGTGTAATTATGTAAC.

The sequence for the reverse oligonucleotide was: (5' to 3'):

TCGAGTTACATAATTACACACTTTGTCTTTGACTTCTTTTTCTTTTTCTT.

3.13 Statistical analysis

All statistical analyses were performed in GraphPad Prism 8 software. Various appropriate different statistical tests were used, as implied in the corresponding figure legends. Data are represented as mean ± SEM in the case of bar charts. The boxes of box-plots represent the range between the 25th and 75th percentile. Whiskers represent the range to the minimum and maximum value. The horizontal line in the box-plot represents the median. EC₅₀ values were calculated by using a non-linear four-parameter regression in GraphPad Prism 8. "n" represents experiment samples from individually differentiated cells from different pools. In the live-cell imaging experiments using the confocal microscope and the Green cGull biosensor "n" refers to an individual cell being imaged.

4. Results

4.1 Expression of cGMP generators and PDEs in murine BA and BAT

Previous publications have demonstrated the pivotal role of the cGMP-PKG signaling cascade for the differentiation of BA, mitochondrial biogenesis, and BAT function. Initially, a broad gene expression screening for GCs and cGMP- and dual-specific PDEs was performed via qRT-PCR to investigate the abundance of these different cGMP-generating and degrading enzymes. Adipocyte precursor cells isolated from transgenic cGi-500 FRET reporter mice were cultured, differentiated, and analyzed either on day -2 of the differentiation protocol as premature BA (= preBA) or on day 7 as mature BA (= BA). High expression levels of *Nprb* were found in preBA (2^{-dCt} = 0.235 relative mRNA expression to *Hprt*), while on the other hand, in fully differentiated lipid-laden BA, *Nprb* expression levels were significantly reduced (2^{-dCt} = 0.050 to *Hprt*) (Figure 6A). Conversely, *Npra* expression levels showed a trend of being upregulated upon differentiation (2^{-dCt} = 0.002 versus 0.003, p = 0.06), but were in general low compared to *Nprb* and *Nprc*. Importantly, the genes *Gucy1a1* and *1b1*, which code for the sGC subunits, were highly upregulated upon BA differentiation (*Gucy1a1* 120-fold, *Gucy1b1* 12-fold, Figure 6A), whereas *Gucy1a2* was equally expressed in preBA as well as in BA, indicating that both sGC variants are present throughout BA differentiation.

Taken together, these results indicate that cGMP generation in murine preBA might differ from BA, with preBA possibly deriving most of their cGMP from the CNP-NPRB pathway, while BA might derive more of their cGMP via the NO-sGC pathway and possibly the ANP-NPRA pathway. However, this hypothesis is based solely on mRNA expression levels and has to be substantiated with further experiments.

Since PDEs have particularly many isoforms, primers that target the most conserved regions of the respective PDEs were designed to detect the expression levels of as many of the various isoforms and splice variants as possible. Regarding PDE mRNA expression levels, Pde3b, Pde3a, and Pde1a were highly expressed in preBA and BA (Figure 6B). Furthermore, Pde3a was upregulated upon BA differentiation ($2^{-dCt} = 0.019$ versus 0.066 relative mRNA expression to Hprt), while Pde1a showed a trend of being upregulated upon differentiation ($2^{-dCt} = 0.028$ versus 0.075, p =0.07). Due to these expression data, and, concerning previously reported roles of PDEs in BA metabolism, the focus of the project was placed on PDE1, 2, 3, 5, and 9.

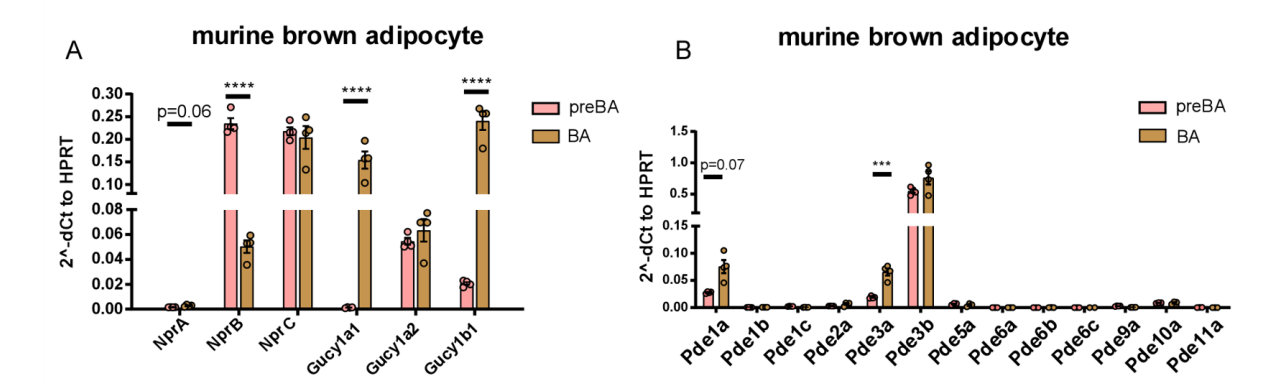


Figure 6: Expression of cGMP-related genes in murine preBA and BA

A mRNA expression normalized to *Hprt* of guanylate cyclases and the clearance receptor *Nprc* in murine preBA (day -2) and BA (day 7). **B** mRNA expression normalized to *Hprt* of dual- and cGMP-specific PDEs in murine preBA (day -2) and BA (day 7). Bar graphs are represented as mean \pm SEM. Multiple t-tests with Holm-Sidak correction for multiple comparisons. n=4, p* \leq 0.05, p** \leq 0.01, p*** \leq 0.001, p**** \leq 0.0001.

Since BAT is a highly heterogeneous tissue consisting of various cell types besides adipocytes, RNA-sequencing was employed to evaluate how PDE expression patterns might differ between BA and BAT. Analogous to BA, Pde3b was highly expressed in BAT, and Pde1a and Pde3a were abundant as well (Figure 7). Additionally, appreciable levels of Pde5a, Pde10a, and Pde11a expression could also be detected. The difference in expression patterns between BA and BAT suggests that Pde5a, 10a, and 11a might be predominantly expressed in non-adipocytes, such as smooth muscle cells, endothelial cells, or noradrenergic neurons. Interestingly, Pde1a (27.42 \pm 1.684 versus 16.93 \pm 0.865 reads, p = 0.0065) and Pde1b (3.50 \pm 0.277 versus 2.064 \pm 0.1752 reads, p = 0.0253) were the only PDEs that showed significantly altered gene expression upon activation of BAT via CE (Figure 7). As both genes are downregulated, this could indicate a role of these PDEs as a thermogenic brake on BAT activity, which gets released upon CE-mediated BAT activation.

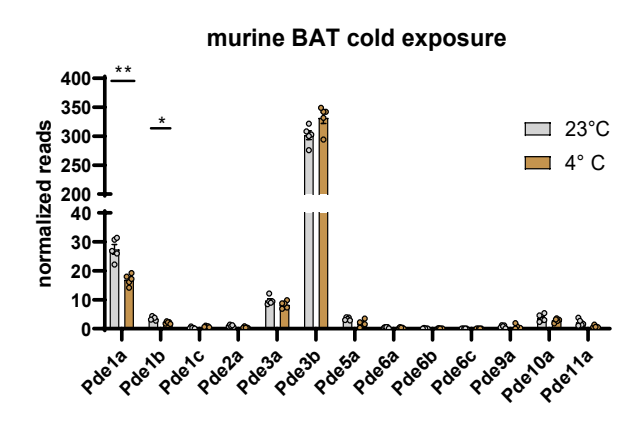


Figure 7: Effect of cold exposure on BAT PDE mRNA expression

Gene expression of PDEs in murine BAT isolated from mice kept either at 23°C or 4°C detected by bulk RNA sequencing. Bar graphs are represented as mean \pm SEM. Multiple t-tests with Holm-Sidak correction for multiple comparisons. n = 5, p* \leq 0.05, p** \leq 0.01, p*** \leq 0.001, p**** \leq 0.0001.

Differentiation of BA is regulated by a complex transcriptional cascade leading ultimately to the development of fully differentiated, lipid-laden BA. During this process specific genes are up or downregulated, sometimes only for short periods of time. Since previous research has highlighted the role of the cGMP-signaling cascade for the differentiation of BA³⁶ and our results have shown that the expression of GCs differs between preBA and BA, their expression during the course of differentiation was analyzed next.

Therefore, RNA was isolated from BA at different time points during their differentiation (day -2, 0, 2, 4, and 7). qRT-PCR revealed that certain genes coding for GCs are upregulated only momentarily during differentiation. This effect was especially striking for *Npra*. While *Npra* expression levels are relatively low in preBA and BA, a 74-fold upregulation was observed at day 4 of differentiation (Figure 8A). Interestingly, this upregulation was transient and almost entirely nullified by day 7. The other natriuretic peptide receptors, *Nprb* and the clearance receptor *Nprc*, also showed differential expression patterns. *Nprb* expression generally decreased during the final stages of differentiation but was strongly upregulated during day 0 (Figure 8B), while *Nprc* was upregulated at days 0, 2, and 4, but returned to its original expression levels at day 7 (Figure 8C).

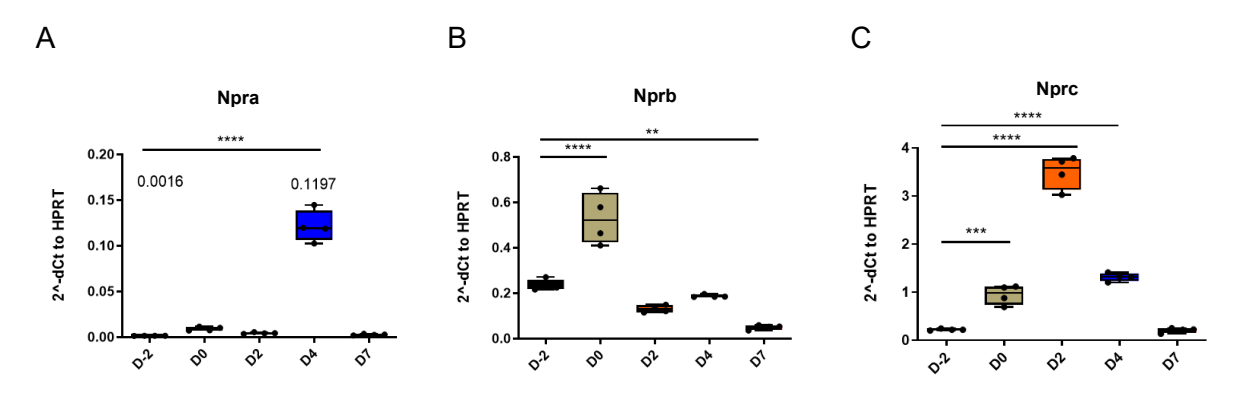


Figure 8: Effect of murine BA differentiation on NPR mRNA abundance

A, **B**, **C** mRNA expression normalized to *Hprt* of *Npra* (A), *Nprb* (B), and *Nprc* (C) in murine BA isolated at different time points during differentiation (day -2, 0, 2, 4, 7). Box-plots are represented as median \pm min/max. One-way ANOVA followed by post-hoc Tukey correction for multiple comparisons. n = 4, $p^* \le 0.05$, $p^{***} \le 0.01$, $p^{****} \le 0.001$.

The Npra/Nprc³⁷ ratio is often used to assess the sensitivity of a tissue or cells towards natriuretic peptides, as it relates the levels of the respective cGMP-producing receptor to the clearance receptor. High ratios suggest high sensitivity. Intriguingly, the Npra/Nprc ratio reaches its maximum around day 4, while the Nprb/Nprc ratio peaks in preBA (Figure 9A, B). These expression data might indicate that preBA are especially sensitive to NPRB-mediated cGMP, while NPRA-mediated cGMP plays a role later during differentiation.

Npra/Nprc expression

Nprb/Nprc expression

Nprb/Nprc expression

Nprb/Nprc expression

Figure 9: Relative mRNA expression ratios of the NPRs during differentiation of murine BA

A Relative mRNA expression to *Hprt* of NPRs in murine (pre)BA for *Npra/Nprc*. **B** Relative mRNA expression to *Hprt* of NPRs in murine (pre)BA for *Nprb/Nprc*. RNA was isolated at different time points during differentiation (day -2, 0, 2, 4, 7). Box-plots are represented as median \pm min/max. One-way ANOVA followed by post-hoc Tukey correction for multiple comparisons. n = 4, $p^* \le 0.05$, $p^{***} \le 0.01$, $p^{****} \le 0.001$, $p^{****} \le 0.0001$.

In parallel to the membrane-bound GCs, the genes coding for the intracellular sGC subunits *Gucy1a1*, *1a2*, and *1b1* also showed altered gene expression during BA differentiation, with their expression generally increasing throughout differentiation while remaining elevated in fully differentiated BA compared to preBA. In more detail, *Gucy1a1* was upregulated 161.3-fold, 132.3-fold, and 120.2-fold at days 0, 4, and 7, respectively (Figure 10A). *Gucy1a2*'s differential expression was less pronounced as it was only upregulated 2.3-fold at day 0 and 2.6-fold at day 4 (Figure 10B). Expression of *Gucy1b1*, on the other hand, behaved similarly to *Gucy1a1*, being upregulated 14.5-fold, 12.1-fold, and 11.6-fold at days 0, 4, and 7, respectively (Figure 10C).

In conclusion, these experiments demonstrate that the expression of GCs and *Nprc* are highly variable during BA differentiation. Before induction of differentiation (day 0), *Nprb* showed high expression levels which consistently decreased during the subsequent differentiation; whereas *Npra* was briefly highly upregulated around day 4 but returned to baseline levels towards the end of BA differentiation. *Gucy1a1*, *Gucy1a2*, and *Gucy1b1* are all significantly upregulated throughout differentiation. This suggests that the dynamics of cGMP synthesis are altered during BA differentiation. However, to confirm this hypothesis the second messenger cGMP must be measured directly.

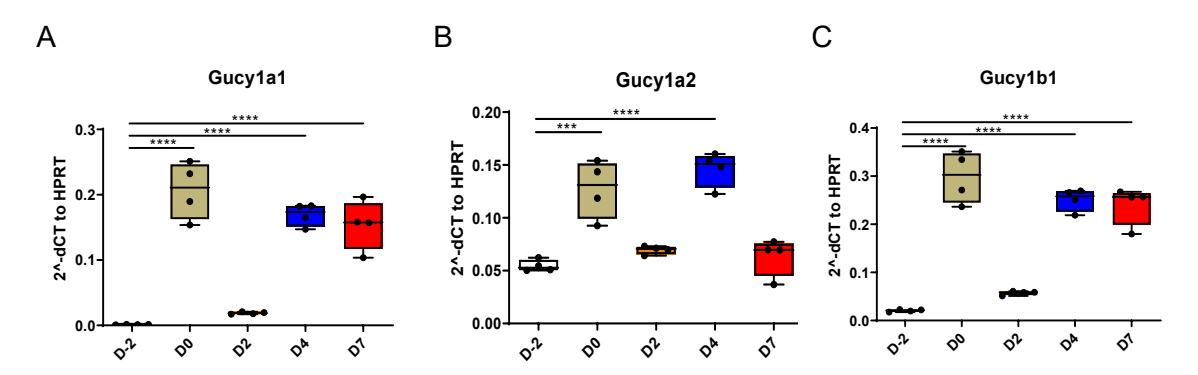


Figure 10: Expression of sGC-subunit coding genes during differentiation of murine BA

A, **B**, **C** Relative mRNA expression to *Hprt* of *Gucy1a1* (A), *1a2* (B) or *1b1* (C) in murine BA isolated at different time points during differentiation (day -2, 0, 2, 4, 7). Box-plots are represented as median \pm min/max. One-way ANOVA followed by post-hoc Tukey correction for multiple comparisons. n = 4, p* \leq 0.05, p** \leq 0.01, p**** \leq 0.001.

4.2 Establishing cGMP FRET measurements in murine preBA

To investigate the spatio-temporal dynamics of cGMP synthesis and hydrolysis, BA progenitors were isolated from newborn transgenic mice expressing the cytosolic cGi-500 FRET biosensor, allowing live monitoring of intracellular cGMP levels. Since cGMP plays a pivotal role in BA differentiation, preBA were investigated first. The cGi-500 preBA displayed a homogenous distribution of the CFP (excitation 445 nm, emission at 488nm) and YFP (excitation at 488 nm, emission at 555 nm) signals within all isolated cells (Figure 11A - C).

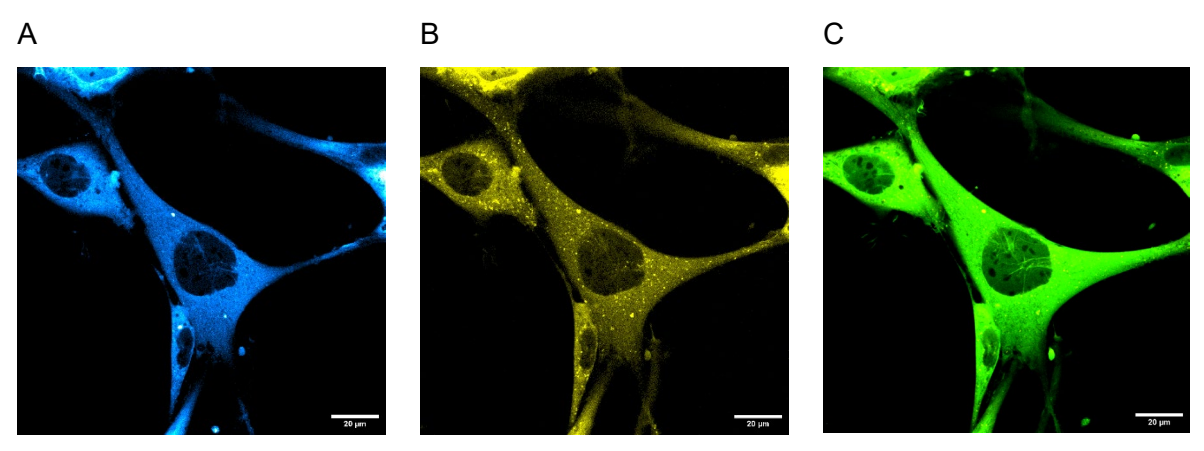


Figure 11: Pseudo-colored confocal fluorescence images of cGi-500 murine preBA A CFP emission from preBA (excitation 445 nm, emission 488 nm). **B** YFP emission from preBA (excitation 488 nm, emission at 555 nm). **C** Overlay of CFP and YFP images.

Upon stimulation of preBA with the NO-donor Diethylamine NONOate (DEA-NO) (100 μ M), which in turn activates the sGC, a decrease in YFP emission as well as an increase in CFP emission, and, thus, a decrease in the intramolecular FRET efficiency (Figure 12), was observed. This results in an increased CFP/YFP ratio which corresponds to an increase in cytosolic cGMP. Importantly, upon addition of CNP and IBMX an additional increase in CFP/YFP ratio and accordingly in cytosolic cGMP was observed, demonstrating that DEA-NO

treatment by itself does not saturate the cGi-500 sensor in murine preBA (Figure 12). Consequently, these initial experiments demonstrate that cGi-500 preBA can be used to investigate the spatio-temporal dynamics of cGMP turnover and compartmentalization in preBA.

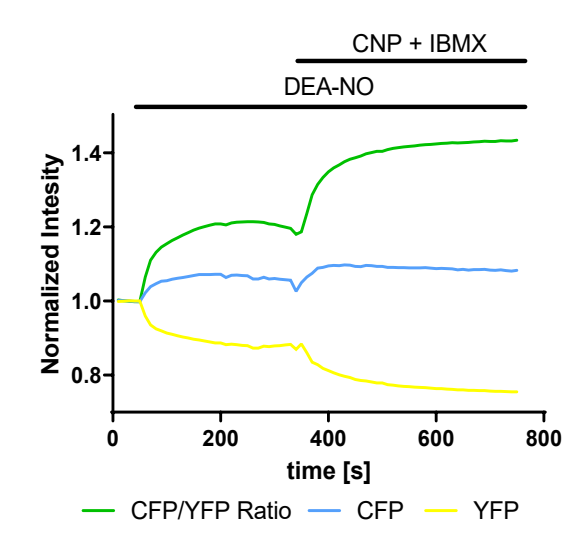


Figure 12: Real-time cGMP dynamics in murine preBA expressing the cGi-500 FRET biosensor CFP (blue) and YFP (yellow) traces as well as the CFP/YFP ratio (green) of cGi-500 murine preBA upon stimulation with DEA-NO (100 μ M) and subsequent application of CNP (100 nM) + IBMX (100 μ M) to achieve the maximum activation of the sensor.

To identify the optimal concentration of cGMP-inducing compounds to use in the subsequent studies, dose-response experiments were performed with DEA-NO and CNP. These experiments showed that DEA-NO reaches its maximum response at a concentration of 1 μ M with an EC₅₀ of 0.09 μ M (Figure 13A). CNP on the other hand reached its maximum response at 0.1 μ M with an EC₅₀ of 0.02 μ M (Figure 13B). Perfusion with ANP induced no detectable change in FRET efficiency. Therefore, no dose-response curve could be generated for ANP. Based on these observations, CNP was used at a concentration of 100 nM.

Considering its relatively short half-life of only approximately 2 minutes at 37°C and pH 7.4^{275} , DEA-NO was used at a 100x higher concentration than the concentration that yielded the maximum response, i.e. 100 μ M. This ensures that enough active DEA-NO was available until the end of the measurements. As FRET measurements take up to 12 additional minutes after the initial DEA-NO addition, representing around 6 compound half-lifes, an initial treatment with 100 μ M DEA-NO will maintain a concentration of at least 1.56 μ M throughout the entire measurement, leading to constant maximum activation of the sGC. No toxic effects of DEA-NO were observed at any concentration (data not shown).

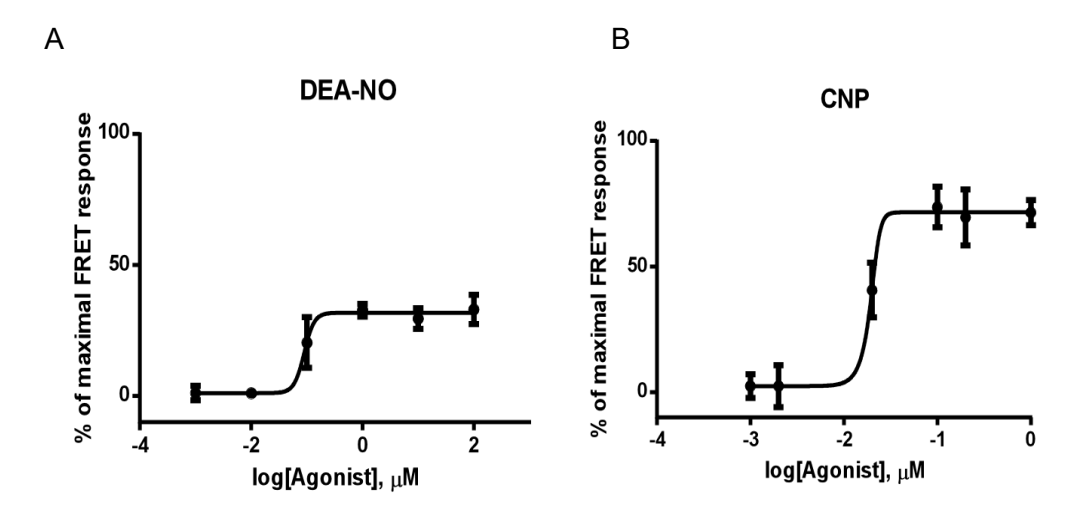


Figure 13: DEA-NO and CNP dose-response curves in murine preBA

A Dose-response curve for DEA-NO in cGi-500 preBA (EC $_{50}$ = 0.09 μ M). **B** Dose-response curve for CNP in cGi-500 preBA (EC $_{50}$ = 0.02 μ M). Data points are depicted as means \pm SEM. n = 3-4.

4.3 cGMP generators in murine preBA

Since the expression pattern of the cGMP-generating enzymes differ considerably between preBA and BA, the differences on the molecular levels of the second messenger cGMP itself were characterized next. First, the basal cytosolic cGMP levels were determined via FRET by measuring the CFP/YFP ratio of untreated preBA and fully differentiated BA. Similarly, to preBA, BA displayed a homogenous cytosolic fluorescent signal (Figure 14A, B). However, neither the lipid droplets, characteristic for BA, nor the nucleus, showed any fluorescence, demonstrating that the cGi-500 biosensor remains confined to the cytosol (Figure 14A, B). Importantly, the basal CFP/YFP ratio was significantly higher in fully differentiated BA than in preBA (0.865 \pm 0.014 versus 0.746 \pm 0.012, p < 0.0001) (Figure 14C), indicating higher basal cGMP levels in BA than in preBA. These results were then verified by ELISA, which detected a 12.1-fold increase in basal cGMP levels, from 2.23 \pm 0.70 pmol cGMP/mg protein to 26.99 \pm 4.81 pmol cGMP/mg protein (p = 0.0005), upon differentiation of preBA to BA (Figure 14D).

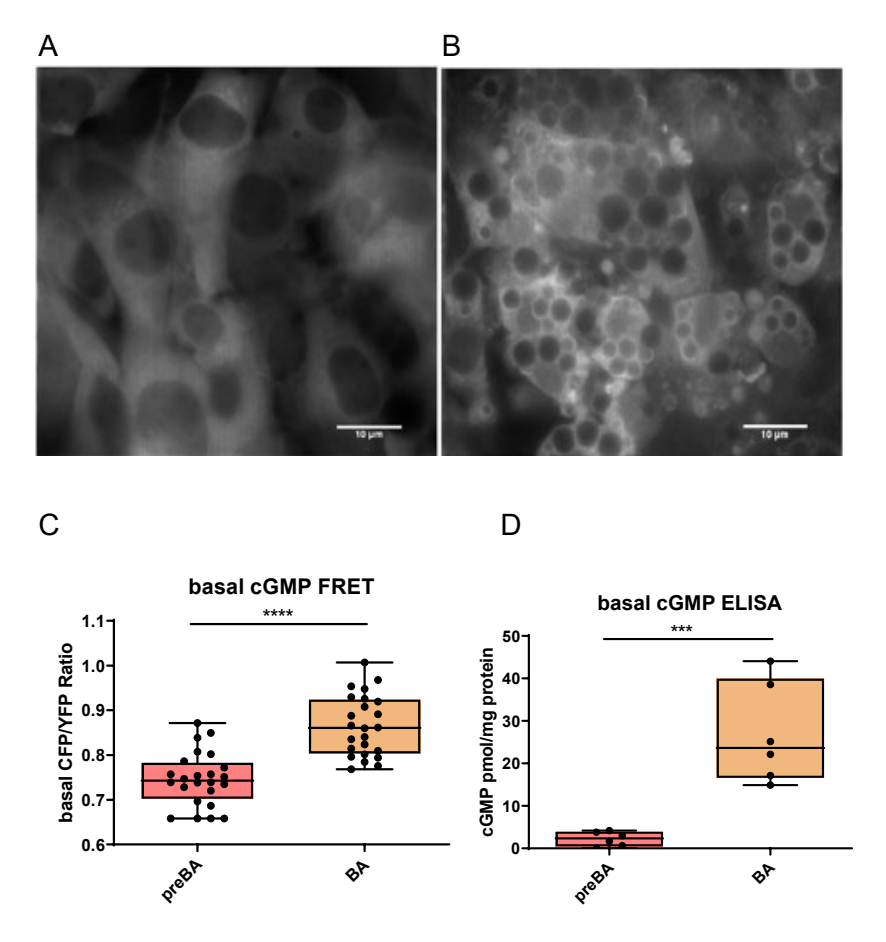


Figure 14: Basal cGMP levels in murine preBA and BA

A, **B** CFP channel images from murine preBA (A) and BA (B). **C** Quantification of basal CFP/YFP FRET ratio in untreated preBA and BA. **D** Quantification of basal cGMP in preBA and BA via ELISA. Box-plots are represented as median \pm min/max. Two-tailed students t-test. n = 24 for C, n = 6 for D, $p^* \le 0.05$, $p^{**} \le 0.01$, $p^{****} \le 0.0001$.

Next, differences between preBA and BA on the level of cGMP synthesis in response to the activation of individual GCs were scrutinized. To this end, cGi-500 preBA and BA were initially perfused with either ANP, CNP, or DEA-NO and subsequently with the pan-PDE-inhibitor IBMX plus either DEA-NO (in case ANP or CNP were used first) or CNP (in case DEA-NO was used first) to elicit a maximum response. Alternatively, Ringer's solution was used as a vehicle control. Both DEA-NO and CNP evoked a significant increase in cytosolic cGMP, whereas ANP did not induce any detectable increase in cytosolic cGMP in preBA (Figure 15A). In detail, quantification of the change in FRET ratio in response to ANP, CNP, or DEA-NO (Figure 15C) revealed that CNP treatment resulted in the highest increase of cGMP levels in preBA (29.99 \pm 1.58% CFP/YFP ratio increase), DEA-NO stimulation caused a more moderate cGMP increase (9.14 \pm 1.12%) and ANP treatment yielded no significant change in FRET ratio (1.18 \pm 1.19%). In addition to the GC expression pattern on the mRNA level, these data further substantiate that CNP-NPRB constitutes the main source of cGMP in preBA and NO-sGC is a viable secondary stimulus for cGMP generation. ANP-mediated stimulation of NPRA, on the

other hand, does not contribute significantly to cGMP production in the cytosolic compartment of murine preBA.

Based on the altered expression of GCs in fully differentiated BA, it was hypothesized that the dynamics of cGMP synthesis in BA might be altered compared to preBA. To explore this concept, fully differentiated lipid-laden BA were treated as described for preBA and FRET measurements were performed. The dynamics of cGMP generation indeed changed significantly compared to preBA. In murine BA, DEA-NO induced the greatest increase of cytosolic cGMP ($17.46 \pm 0.90\%$ CFP/YFP ratio increase), followed by ANP ($9.06 \pm 0.74\%$) and finally CNP ($5.46 \pm 0.58\%$) (Figure 15B, D). These results partially fit the GC mRNA expression data in BA, as the genes coding for the sGC are highly upregulated upon BA differentiation, while *Nprb* is downregulated. Surprisingly ANP induces a larger increase in cytosolic cGMP in BA than CNP, even though *Npra* mRNA expression levels remain rather low in BA compared to *Nprb*.

In conclusion, these results indicate that upon BA differentiation cGMP synthesis via GCs is altered considerably, with NO-GC-cGMP being the main source of cGMP in murine BA, while CNP-NPRB-cGMP represents the main source of cGMP in preBA. Although NPRA stimulation did not induce a meaningful elevation of cGMP levels in preBA, it induced a strong cGMP increase in BA. Thus, the dynamics of cGMP generation switch from mainly being CNP mediated in preBA to mainly being NO and ANP mediated in BA.

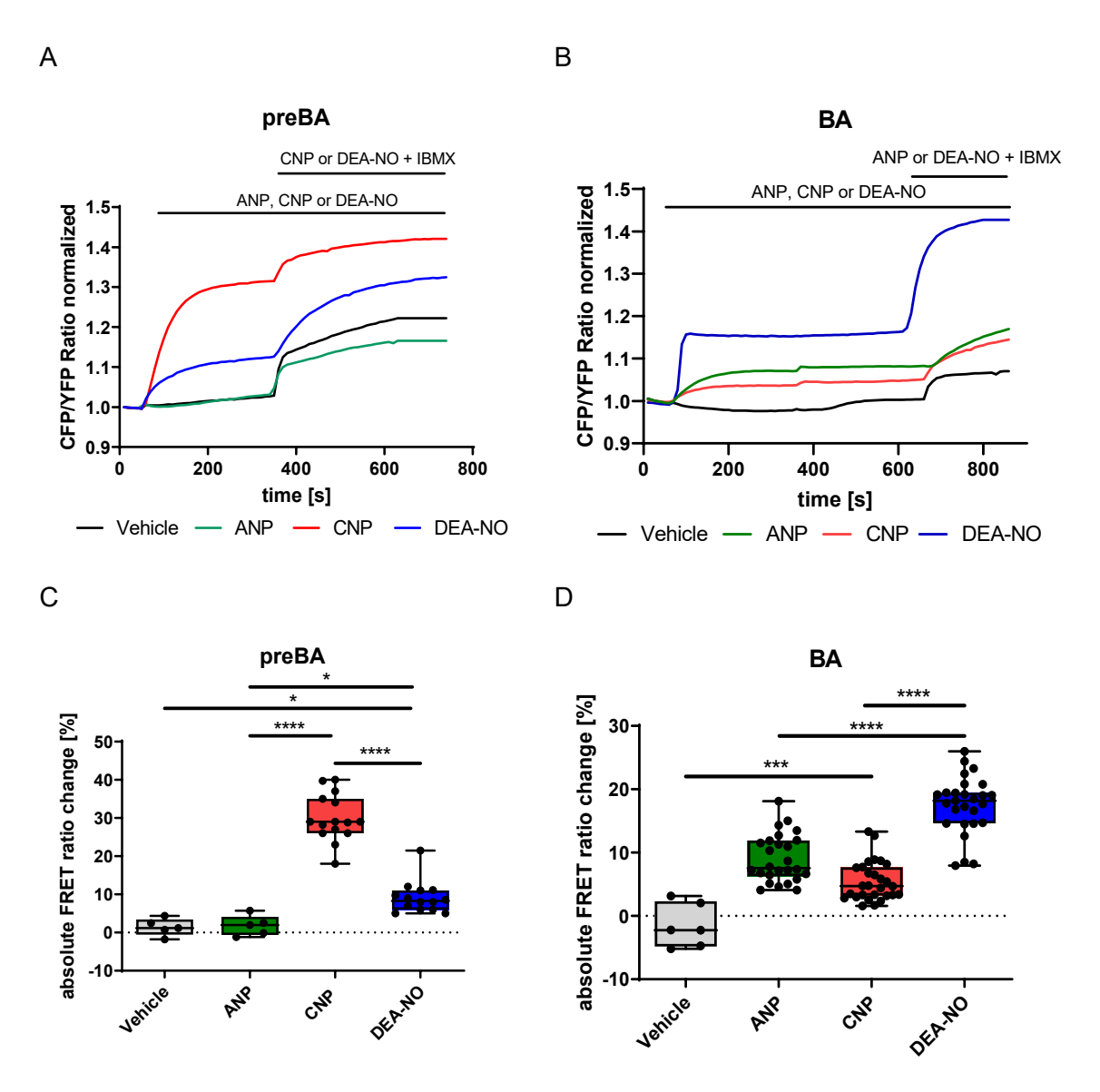


Figure 15: Real-time measurements of cGMP synthesis in cGi-500 preBA versus BA

A Representative FRET ratio traces from cGi-500 preBA upon stimulation with either ANP (100 nM), CNP (100 nM), DEA-NO (100 μ M), or vehicle with subsequent maximum stimulation with either CNP (if DEA-NO was applied first) or DEA-NO (if ANP or CNP was applied first) + IBMX (100 μ M). **B** Representative FRET ratio traces from fully differentiated cGi-500 murine BA upon stimulation with either ANP, CNP, DEA-NO, or vehicle with subsequent maximum stimulation with either CNP (if DEA-NO was applied first) or DEA-NO (if ANP or CNP was applied first) + IBMX. **C** Quantification of FRET ratio changes in cGi-500 preBA to ANP, CNP, DEA-NO, or vehicle in cGi-500 preBA as absolute FRET ratio change. **D** Quantification of FRET ratio changes in fully differentiated cGi-500 BA to ANP, CNP, DEA-NO, or vehicle as absolute FRET ratio change. Box-plots are represented as median \pm min/max. One-way ANOVA with post-hoc Tukey correction for multiple comparisons. n = 5-15 for A and C, n = 6-28 for B and D, p* \leq 0.05, p** \leq 0.01, p*** \leq 0.001, p**** \leq 0.0001.

To verify the results for the cGMP generators obtained with FRET microscopy in BA before and after differentiation, an additional detection method was employed. Murine preBA and BA cGMP levels were quantified using ELISA after 5 minutes of stimulation with either CNP or DEA-NO. Comparable to the previous FRET experiments, CNP-mediated NPRB stimulation resulted in the greatest increase in cytosolic cGMP in preBA while DEA-NO induced a more moderate increase in cytosolic cGMP (69.30 \pm 5.57 pmol/mg protein for CNP versus 11.65 \pm 2.243 pmol/mg protein for DEA-NO) (Figure 16A). In BA on the other hand, DEA-NO treatment resulted in the largest rise of cytosolic cGMP levels, while CNP induced a smaller increase in cGMP (513.0 \pm 55.69 pmol/mg protein for DEA-NO versus 93.50 \pm 16.78 pmol/mg protein for CNP) (Figure 16B). These results further substantiate the previous hypothesis, that, upon differentiation of BA, cGMP generation switches from being predominantly mediated via CNP-NPRB to NO-sGC. However, CNP still increased cGMP levels in murine BA more than 3-fold over baseline, albeit not significantly. Interestingly, IBMX by itself had no effect on cGMP levels in either preBA or BA, suggesting that cGMP degradation via PDEs without previous stimulation is relatively low in murine preBA and BA.

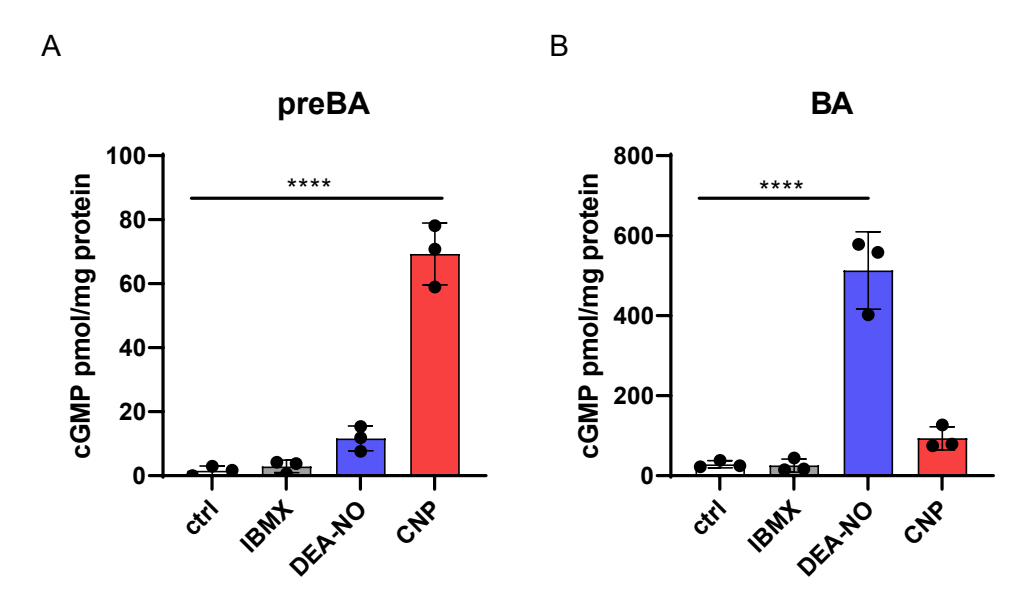


Figure 16: cGMP synthesis quantification in murine preBA and BA via ELISA

A, **B** Quantification of cGMP in preBA (A) and BA (B) via ELISA for cells treated with either IBMX (100 μ M), DEA-NO (100 μ M), or CNP (100 nM) for 5 minutes. One-way ANOVA comparing everything to ctrl followed by post-hoc Dunnet correction for multiple comparisons. n = 3, p* \leq 0.05, p** \leq 0.01, p*** \leq 0.001, p**** \leq 0.0001.

4.4 cGMP compartmentalization in murine preBA

To explore cGMP compartmentalization in adipocytes, the degradation of cytosolic cGMP via PDEs was analyzed. It was hypothesized that cGMP generated from different GCs might interact with different PDEs, thus providing evidence for cGMP compartmentalization. To investigate this hypothesis cGi-500 preBA were first treated either with CNP or DEA-NO to elicit cGMP synthesis. Then, the cells were perfused with different specific inhibitors of expressed cGMP-specific and dual-specific PDEs, including Iti-214 (100 nM) for inhibition of PDE1, Bay 60-7550 (100 nM) for inhibition of PDE2, Cilostamide (10 μ M) for inhibition of PDE3, Avanafil (1 μ M) for inhibition of PDE5 and Bay 73-6691 (10 μ M) for inhibition of PDE9 or IBMX (100 μ M) to inhibit all PDEs (Figure 17A-D). The individual effect of single PDEs on cGMP levels were compared and normalized to that of total PDE inhibition evoked by IBMX application (Figure 17B, D). NPRB-cGMP was mainly degraded via PDE1 (55.36 \pm 6.42% of IBMX) and PDE3 (49.79 \pm 4.80% of IBMX), whereas inhibition of PDE2, 5, and 9 had no detectable effect on CNP-induced cGMP levels (Figure 17A, B). On the other hand, sGC-cGMP was regulated by PDE3 (50.03 \pm 4.10% of IBMX) and PDE9 (54.63 \pm 6.77% of IBMX), but not by PDE1 (Figure 17C, D).

In sum, NPRB-derived cGMP is regulated mainly via PDE1 and PDE3 while sGC-derived cGMP is mainly regulated by PDE3 and PDE9, indicating that distinct cGMP pools exist in murine preBA, which are regulated by different PDEs, a hallmark of subcellular compartmentalization.

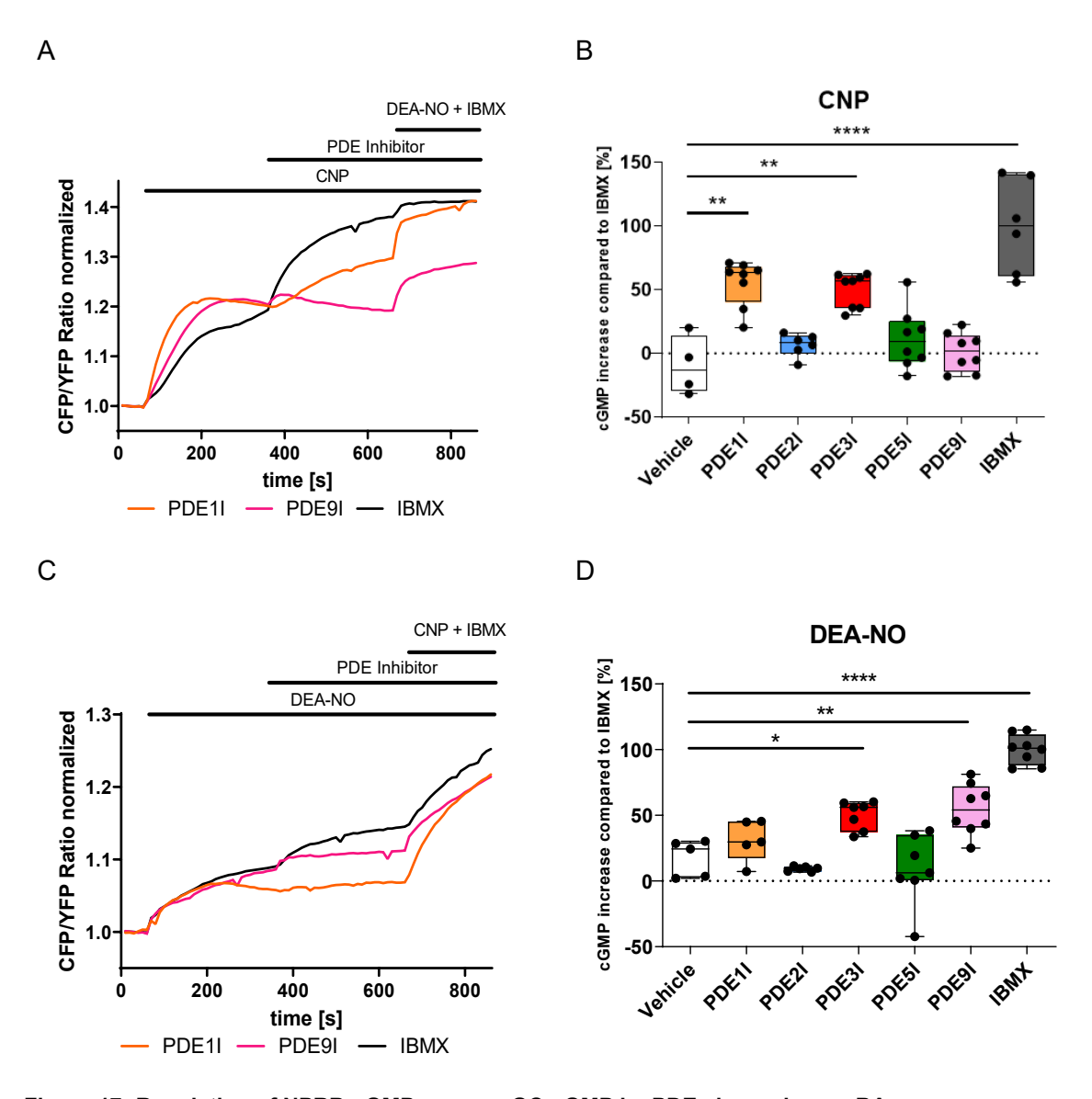


Figure 17: Regulation of NPRB-cGMP versus sGC-cGMP by PDEs in murine preBA

A, C Representative FRET ratio traces from cGi-500 murine preBA upon stimulation with either CNP (100 nM) (A) or DEA-NO (100 μM) (C) with subsequent application of either PDE1I Iti-214 (100 nM), PDE9I Bay 73-6691 (10 μM) or pan PDE Inhibitor IBMX (100 μM). **B, D** Quantification of FRET ratio changes to either PDE1I Iti-214, PDE2I Bay 60-7550 (100 nM), PDE3I Cilostamide (10 μM), PDE5I Avanafil (1 μM), PDE9I Bay 73-6691, or IBMX after previous application of either CNP (B) or DEA-NO (D) in relation to complete PDE Inhibition by IBMX. Box-plots are represented as median \pm min/max. One-way ANOVA followed by post-hoc Tukey correction for multiple comparisons. n = 4-8, p* \leq 0.05, p** \leq 0.01, p**** \leq 0.001, p***** \leq 0.0001.

4.5 cGMP compartmentalization in murine BA

Considering that the effectiveness of different GC stimulators on cGMP synthesis is altered upon BA differentiation, it was hypothesized that the regulation of discrete cGMP pools by PDEs might also change during BA differentiation. To this end, similar FRET experiments were performed with fully differentiated murine cGi-500 BA.

The ANP-NPRA-cGMP pool was mainly regulated by PDE3 ($47.88 \pm 4.84\%$ of IBMX) and PDE9 ($42.73 \pm 8.04\%$ of IBMX) and to a lesser extent by PDE2 ($28.38 \pm 3.46\%$ of IBMX), while PDE 1 and 5 showed no activity after ANP stimulation of murine BA (Figure 18A, B).

On the other hand, cGMP from NPRB mainly interacted with PDE1 ($28.41 \pm 8.25\%$ of IBMX) and PDE3 ($36.00 \pm 4.84\%$ of IBMX), similarly to preBA (Figure 18C, D). Importantly, PDE2 and PDE9, which had high activity in degrading cGMP from ANP-NPRA, had no significant activity in degrading NPRB-cGMP (Figure 18C, D).

Surprisingly, NO-sGC-cGMP was degraded mainly by PDE2 ($49.42 \pm 3.02 5$ of IBMX) and PDE3 ($34.68 \pm 3.74\%$ of IBMX). However, PDE9, which was strongly involved in regulating NO-sGC-cGMP in murine preBA, did not regulate NO-sGC-cGMP in BA (Figure 18E, F).

In conclusion, these results indicate that the regulation of cGMP pools by PDEs is also altered during BA differentiation. Notably, the NO-sGC-cGMP pool interacted with a different subset of PDEs, namely PDE2 and PDE3 in murine BA contrary to preBA, where PDE3 and PDE9 were the major contributors to NO-sGC-cGMP degradation. Furthermore, the NPRA-cGMP pool was regulated by other PDEs than the NPRB-cGMP pool in BA, indicating a spatial division between NPRA and NPRB-induced cGMP.

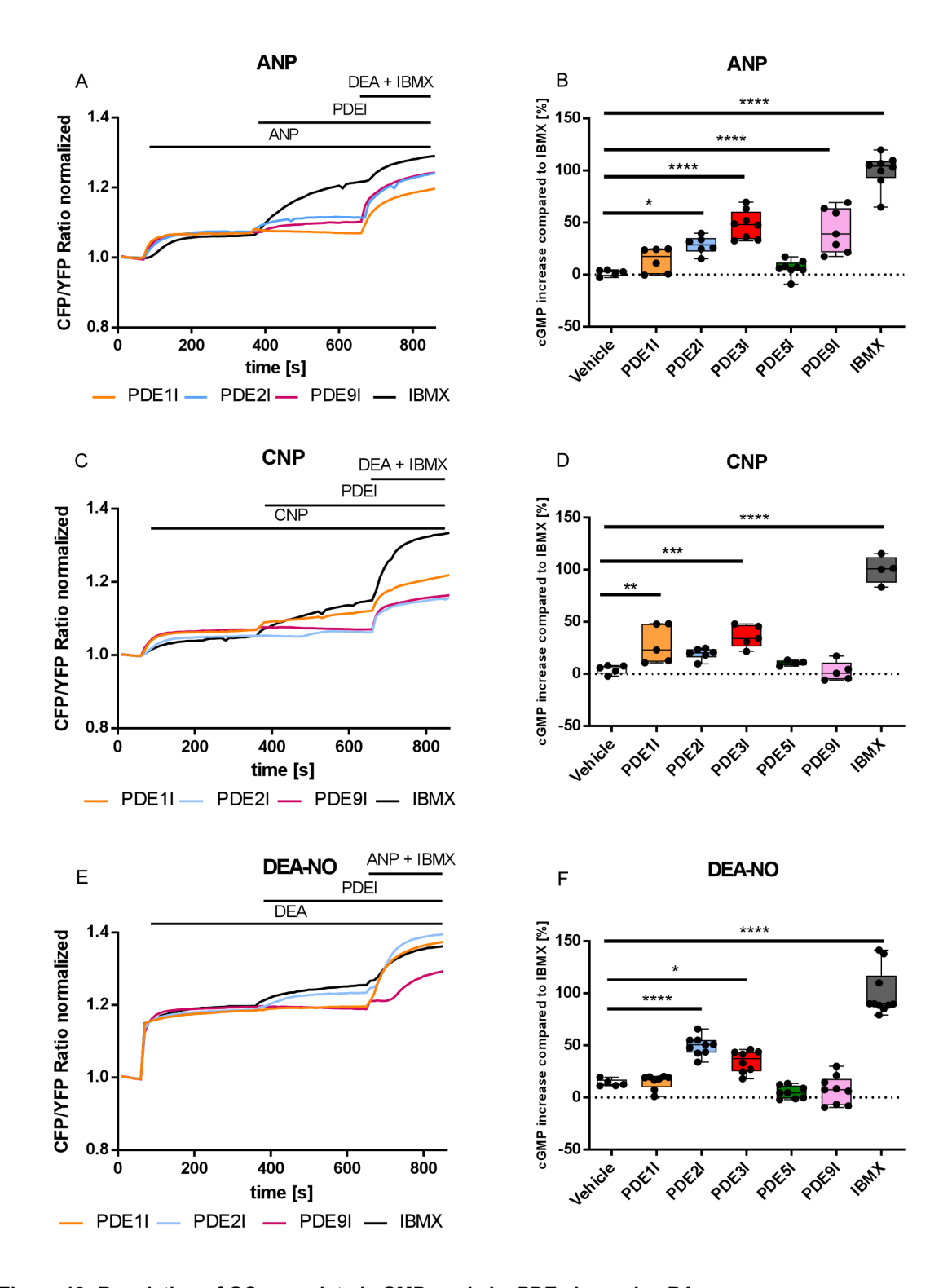


Figure 18: Regulation of GC-associated cGMP pools by PDEs in murine BA

A, **C**, **E** Representative FRET ratio traces from cGi-500 BA upon stimulation with either ANP (100 nM) (A) or CNP (100 nM) (C) or DEA-NO (100 μ M) (E) with subsequent application of either PDE1I Iti-214 (100 nM), PDE2I Bay 60-7550 (100 nM) PDE9I Bay 73-6691 (10 μ M) or pan PDE Inhibitor IBMX (100 μ M). **B**, **D**, **F** Quantification of FRET ratio changes to either PDE1I, PDE2I, PDE3I Cilostamide (10 μ M), PDE5I AvanafiI (1 μ M), PDE9I or IBMX after previous application of either ANP (B) CNP (D) or DEA-NO (F) relative to complete PDE Inhibition by IBMX. Box-plots are represented as median \pm min/max. One-way ANOVA followed by post-hoc Tukey correction for multiple comparisons. n = 5-10, p* \leq 0.05, p** \leq 0.01, p*** \leq 0.001, p**** \leq 0.0001.

4.6 Calcium cGMP crosstalk in murine preBA

Having identified PDE1 as a specific regulator of CNP-NPRB-cGMP in both murine preBA and BA and considering that previous studies have shown that PDE1 can be activated by calcium/calmodulin^{208,214}, it was hypothesized that calcium might mediate compartment-specific cGMP regulation via PDE1.

Thus, cGi-500 transgenic preBA were transduced with lentiviruses to overexpress Gq-DREADD (Designer receptor exclusively activated by designer drugs), a receptor that, upon binding of its ligand Clozapine-N-oxide (CNO), signals via the $G_{\alpha q}$ -pathway, thus leading to an increase in intracellular calcium²⁷⁶. These preBA were then treated with either CNP or DEA-NO, to selectively activate either NPRB or sGC. Subsequently, the cells were perfused with CNO to induce $G_{\alpha q}$ -mediated calcium influx.

Importantly $G_{\alpha q}$ -mediated calcium only decreased cGMP from NPRB (from 24.46% FRET change to baseline before CNO to 16.86% FRET change to baseline after CNO, p < 0.0001), but not from sGC (from 10.30% FRET change to baseline before CNO to 11.04% FRET change to baseline after CNO, p = 0.2709) (Figure19A, B). To interrogate, whether this $G_{\alpha q}$ -cGMP crosstalk was indeed mediated by PDE1 the same experiment was repeated with or without simultaneous PDE1 inhibition using the specific PDE1I Iti-214 (100 nM) together with CNP. Critically, it was observed that inhibition of PDE1 before CNO application completely abolished the calcium-mediated effect on cGMP (from 34.13% FRET change to baseline before CNO to 34.36% FRET change to baseline after CNO) (Figure 19C, D).

To ensure that the observed effect was indeed due to calcium itself and not other downstream components of the $G_{\alpha q}$ -signaling pathway, the same experiment was repeated with lonomycin (100 nM) instead of CNO in non-transduced cGi-500 preBA. Ionomycin is a calcium lonophore, that causes rapid, $G_{\alpha q}$ -independent, increases in intracellular calcium²⁷⁷. Indeed, similar results were obtained with lonomycin, which led to a significant reduction in CNP-mediated cGMP (from 30.50% FRET change to baseline before lonomycin to 22.67% FRET change to baseline after lonomycin, p = 0.0004), but no reduction in cGMP from DEA-NO (from 9.83% FRET change to baseline before lonomycin to 12.33% FRET change to baseline after lonomycin, p = 0.1810) (Figure 20B). Again, the effect of lonomycin on cGMP from NPRB was completely abolished after previous PDE1 inhibition (Figure 20C, D)

Taken together, these results further substantiate the hypothesis that PDE1 specifically associates and regulates NPRB-mediated cGMP, but not NO-sGC-mediated cGMP in murine preBA. Furthermore, the data demonstrate a cGMP pool-specific calcium/cGMP crosstalk, in which calcium modulates exclusively the CNP-NPRB-cGMP pool in a PDE1-dependent manner in preBA.

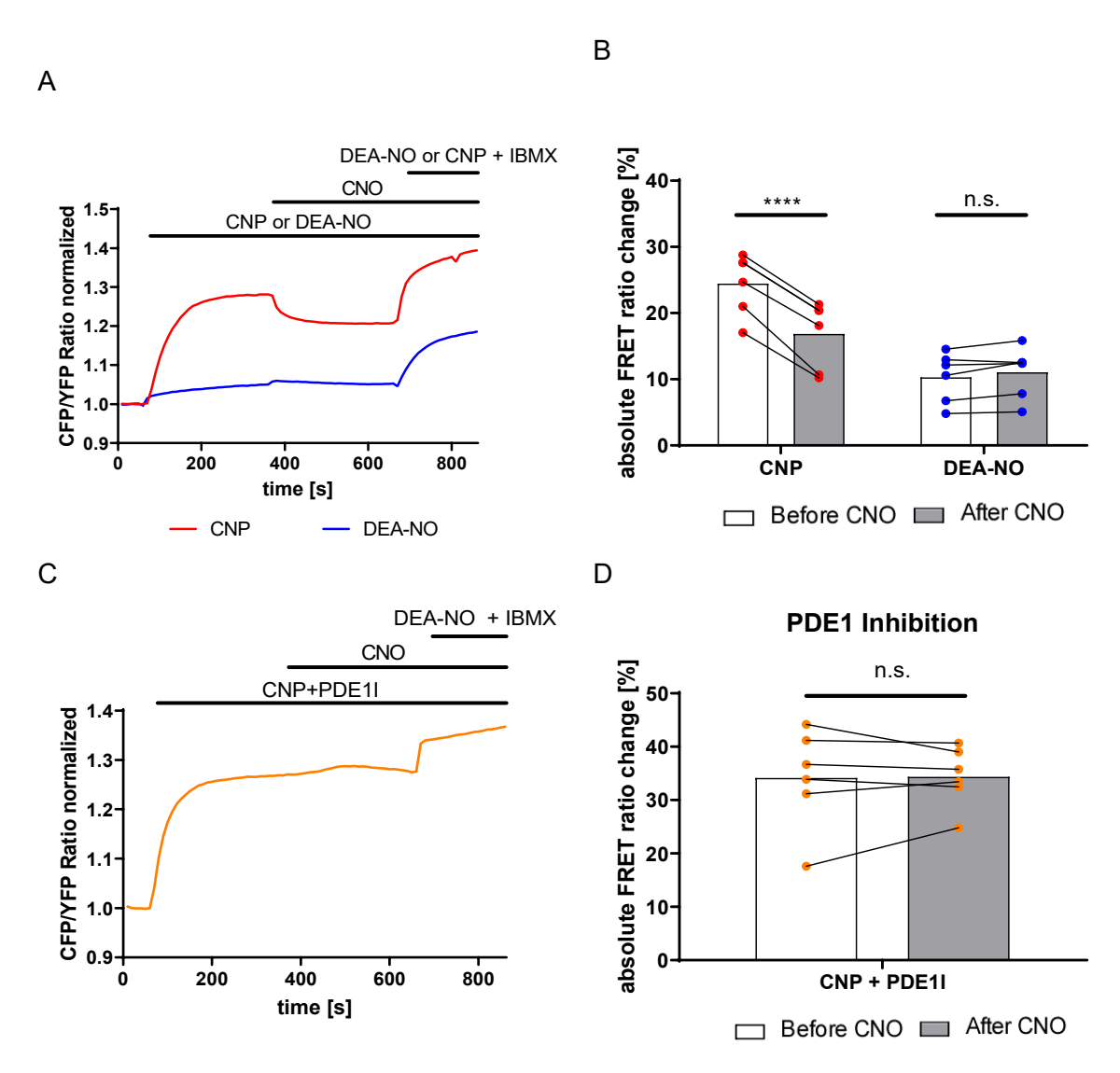


Figure 19: $G_{\alpha q}$ -calcium cGMP crosstalk in murine preBA

A Representative FRET ratio traces from Gq-DREADD-cGi-500 preBA perfused with either CNP (100 nM) or DEA-NO (100 μM) and subsequent application of CNO (1 μM) and then either DEA-NO or CNP + IBMX (100 μM) to elicit a maximum response. **B** Quantification of FRET ratio change to baseline from Gq-DREADD-cGi-500 preBA treated with either CNP or DEA-NO and subsequent application of CNO to induce calcium influx. **C** Representative FRET ratio traces from Gq-DREADD-cGi-500 preBA perfused with CNP + PDE1I Iti-214 (100 nM) and subsequent application of CNO and then DEA-NO + IBMX to elicit a maximum response. **D** Quantification of FRET ratio change to baseline in response to CNO from Gq-DREADD-cGi-500 preBA perfused with CNP + PDE1I Iti-214, and afterwards CNO to elicit calcium influx. Paired results in B and D are connected and represent FRET ratio changes in % over baseline throughout the same measurement at different time points, either before or after CNO addition. Two-way repeated-measures ANOVA followed by post-hoc Sidak correction for multiple comparisons for B. Two-tailed students t-test repeated measures for D. n = 5-6, p* \leq 0.05, p** \leq 0.01, p**** \leq 0.001, p**** \leq 0.0001.

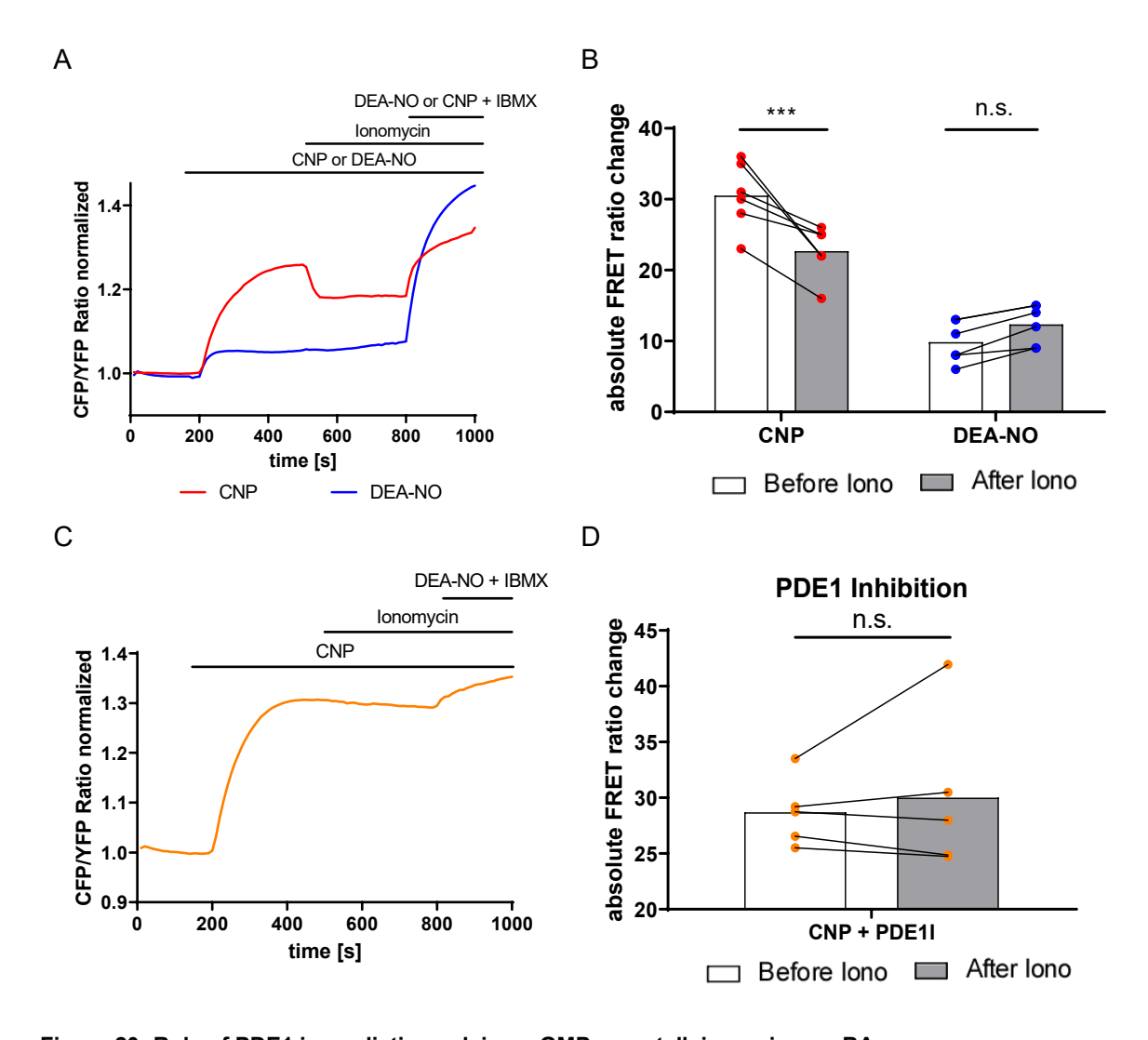


Figure 20: Role of PDE1 in mediating calcium cGMP crosstalk in murine preBA

A Representative FRET ratio traces from cGi-500 preBA perfused with either CNP (100 nM) or DEA-NO (100 μM) and subsequent application of lonomycin (100 nM) and then either DEA-NO or CNP + IBMX (100 μM) to elicit a maximum response. B Quantification of FRET ratio change to baseline from cGi-500 preBA treated with either CNP or DEA-NO and subsequent application of lonomycin to induce calcium influx. C Representative FRET ratio traces from cGi-500 preBA perfused with CNP + PDE11 Iti-214 (100 nM) and subsequent application of lonomycin and then DEA-NO + IBMX to elicit a maximum response. D Quantification of FRET ratio change to baseline in response to lonomycin from cGi-500 preBA perfused with CNP + PDE11 Iti-214, and afterwards lonomycin to elicit calcium influx. Paired results in B and D are connected and represent FRET ratio changes in % over baseline throughout the same measurement at different time points, either before or after lonomycin addition. Two-way repeated-measures ANOVA followed by post-hoc Sidak correction for multiple comparisons for B. Two-tailed students t-test repeated measures for D. n = 5-6, p* ≤ 0.05, p** ≤ 0.01, p*** ≤ 0.001, p**** ≤ 0.001.

4.7 Calcium cGMP crosstalk in murine BA

Having found that cGMP generation and regulation are altered upon BA differentiation, the calcium-cGMP crosstalk was next investigated in fully differentiated murine BA. Importantly, a significant interaction between lonomycin-induced calcium and cGMP was again observed for CNP-NPRB-cGMP (from 3.26% FRET change to baseline before lonomycin to 1.89% FRET change to baseline after lonomycin, p = 0.0004) but not for DEA-NO-sGC mediated cGMP (from 13.29 FRET change to baseline before lonomycin to 13.87% FRET change to baseline after lonomycin, p = 0.1277) (Figure 21B). Additionally, lonomycin-induced calcium also had a profound effect on ANP-NPRA-cGMP (from 11.91% FRET change to baseline before lonomycin to 7.17% FRET change to baseline after lonomycin, p < 0.0001) (Figure 21A, B), demonstrating a significant interaction between calcium and NPRA and NPRB-mediated cGMP in murine BA.

Again, the same experiment was repeated in the presence of the PDE1 inhibitor Iti-214. Importantly, PDE1 inhibition completely abolished the effect lonomycin-induced calcium had on both NPRA or NPRB-mediated cGMP (Figure 21C, D).

Consequently, these results indicate that PDE1 is the key mediator of calcium-cGMP crosstalk also in murine BA. Interestingly, PDE1 was able to degrade NPRA-cGMP upon activation by calcium, even though it did not interact with NPRA-cGMP in its non-activated state (see Figure 18A, B).

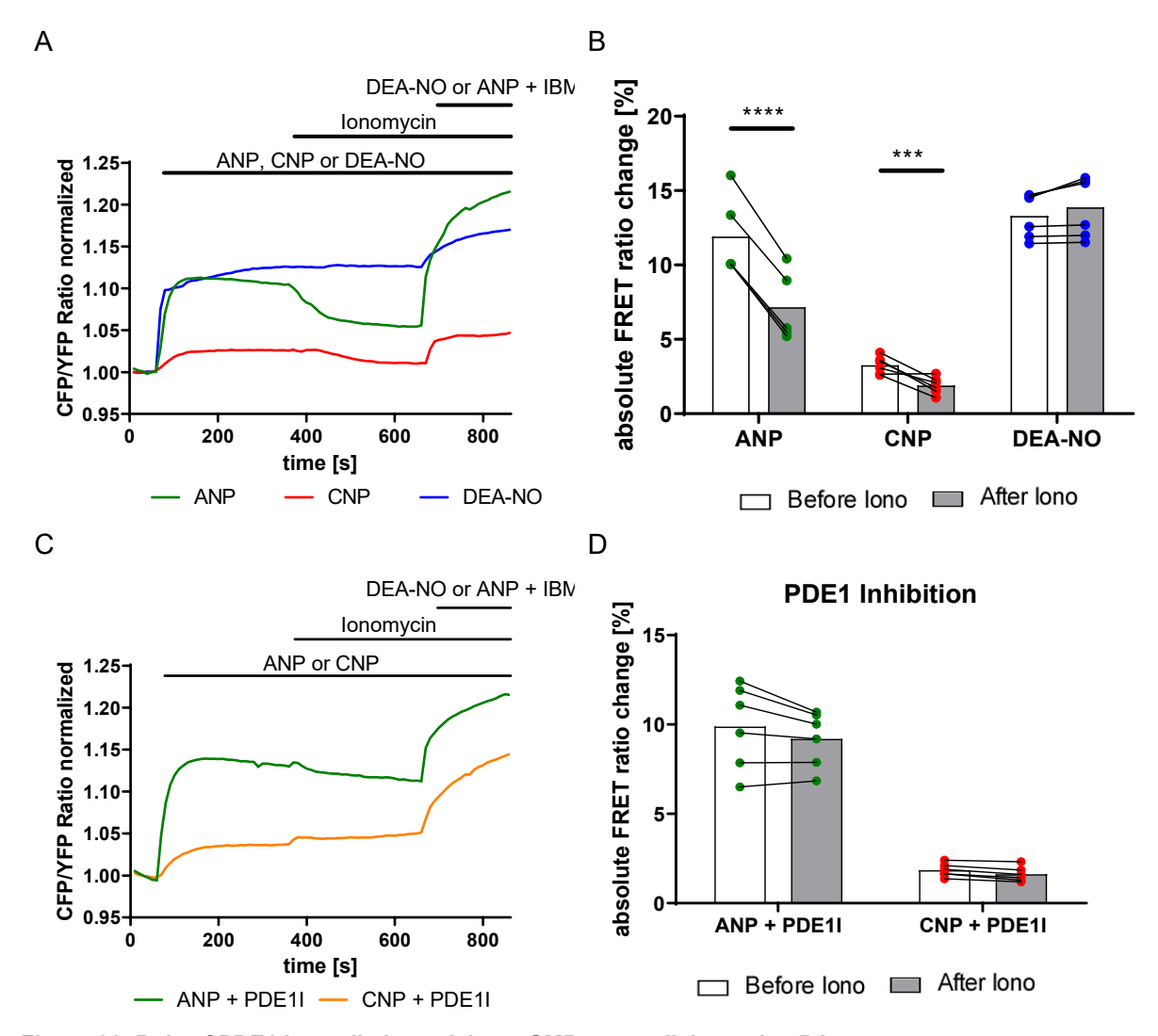


Figure 21: Role of PDE1 in mediating calcium cGMP crosstalk in murine BA

A, C Representative FRET ratio traces from cGi-500 BA perfused with either ANP (100 nM), CNP (100 nM), or DEA-NO (100 μ M) without (A) or with (C) previous PDE1 inhibition via Iti-214 (100 nM) treatment, and subsequent application of Ionomycin (100 nM) and then either DEA-NO or ANP + IBMX (100 μ M) to elicit a maximum response. **B** Quantification of FRET ratio change to baseline from cGi-500 BA treated with either CNP or DEA-NO and subsequent application of Ionomycin to elicit a calcium signal. **D** Quantification of FRET ratio change to baseline from cGi-500 BA with concomitant inhibition of PDE1 with Iti-214 together with either ANP or CNP and subsequently treated with Ionomycin to elicit calcium influx. Paired results in B and D are connected and represent FRET ratio changes in % over baseline throughout the same measurement at different time points, either before or after Ionomycin addition. Two-way repeated measures ANOVA followed by post-hoc Sidak correction for multiple comparisons. n = 5-6, p* \leq 0.05, p** \leq 0.01, p**** \leq 0.001, p***** \leq 0.0001.

4.8 Role of PDE1 in murine BA differentiation

Having found that PDE1 specifically associates with NPRB-induced cGMP but not NO-sGC-cGMP, it was hypothesized that PDE1 inhibition via Iti-214 would enhance only the effects of CNP on the differentiation of BA. To explore this hypothesis, preBA were treated with ANP, CNP, or Diethylenetriamine NONOate (DETA-NO) (a long-acting NO-donor), with or without concomitant PDE1 inhibition via Iti-214, for a total of 9 days (day -2 to day 7). The experiment was concluded on day 7 by isolating mRNA and protein samples.

mRNA expression of the key thermogenic marker Ucp1 was significantly increased by ANP treatment (p = 0.0482) and showed a tendency of being upregulated by CNP and DETA-NO treatment (Figure 22A). Key adipogenic marker aP2 mRNA expression was upregulated by CNP and DETA-NO treatment (p = 0.0054 and 0.0002, respectively) and showed a trend of being upregulated by ANP (p = 0.0825) (Figure 22B). Importantly, concomitant PDE1 inhibition by Iti-214 only showed an additive effect on Ucp1 and aP2 mRNA expression when cells were treated with CNP (p = 0.0105 for Ucp1, p < 0.0001 for aP2), but not with ANP or DETA-NO, further highlighting the specific interaction between NPRB-cGMP and PDE1 (Figure 22A, B).

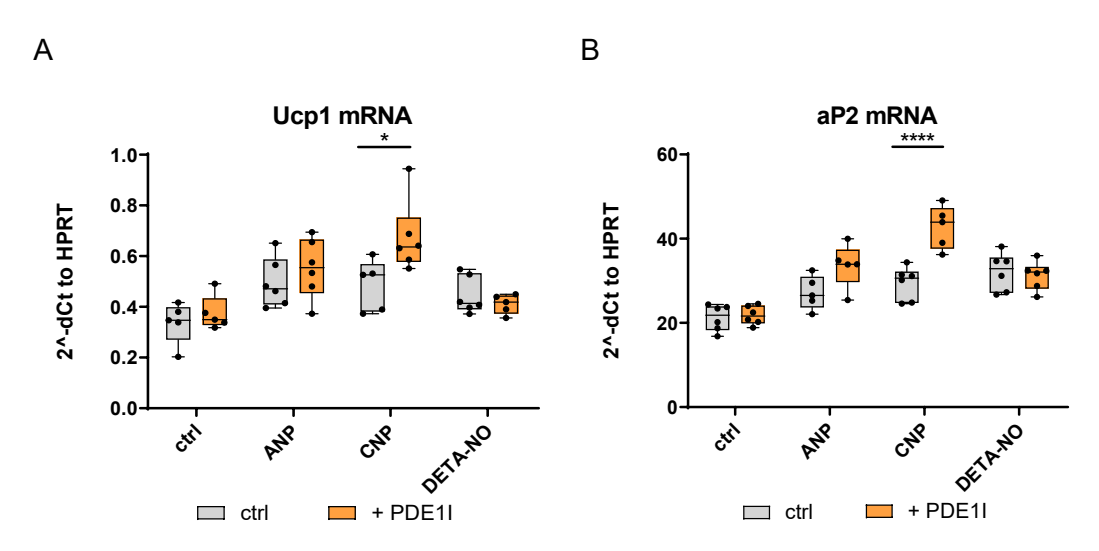


Figure 22: GC-specific effects of PDE1 inhibition on murine BA adipogenic and thermogenic marker mRNA expression

A, **B** Ucp1 (A) and aP2 (B) mRNA expression in murine brown adipocytes chronically treated (day -2 to day 7) with either ANP (100 nM), CNP (100 nM) or DETA-NO (10 μ M) \pm PDE1I Iti-214 (100 nM). Box-plots are represented as median \pm min/max. Two-way ANOVA followed by post-hoc Sidak correction for multiple comparisons. n = 4-6, $p^* \le 0.05$, $p^{**} \le 0.01$, $p^{***} \le 0.001$, $p^{****} \le 0.0001$.

Regarding protein expression similar results were obtained. ANP, CNP, and DETA-NO all enhanced UCP1 protein expression (UCP1: p = 0.0082 for ANP, p < 0.0001 for CNP and p = 0.0312 for DETA-NO). aP2 protein expression showed a tendency of being upregulated by ANP, CNP, and DETA-NO. Importantly, PDE1 inhibition via Iti-214 only demonstrated significant additive effects in combination with CNP (p = 0.0024), but not for ANP or

DETA-NO (Figure 23A, B, C). Furthermore, PDE1 inhibition enhanced CNP-induced lipid accumulation in BA, a hallmark of enhanced BA differentiation (Figure 23D).

Taken together, these findings provide further evidence that PDE1 specifically regulates NPRB-mediated cGMP and highlight the functional relevance of cGMP compartmentalization for murine BA differentiation.

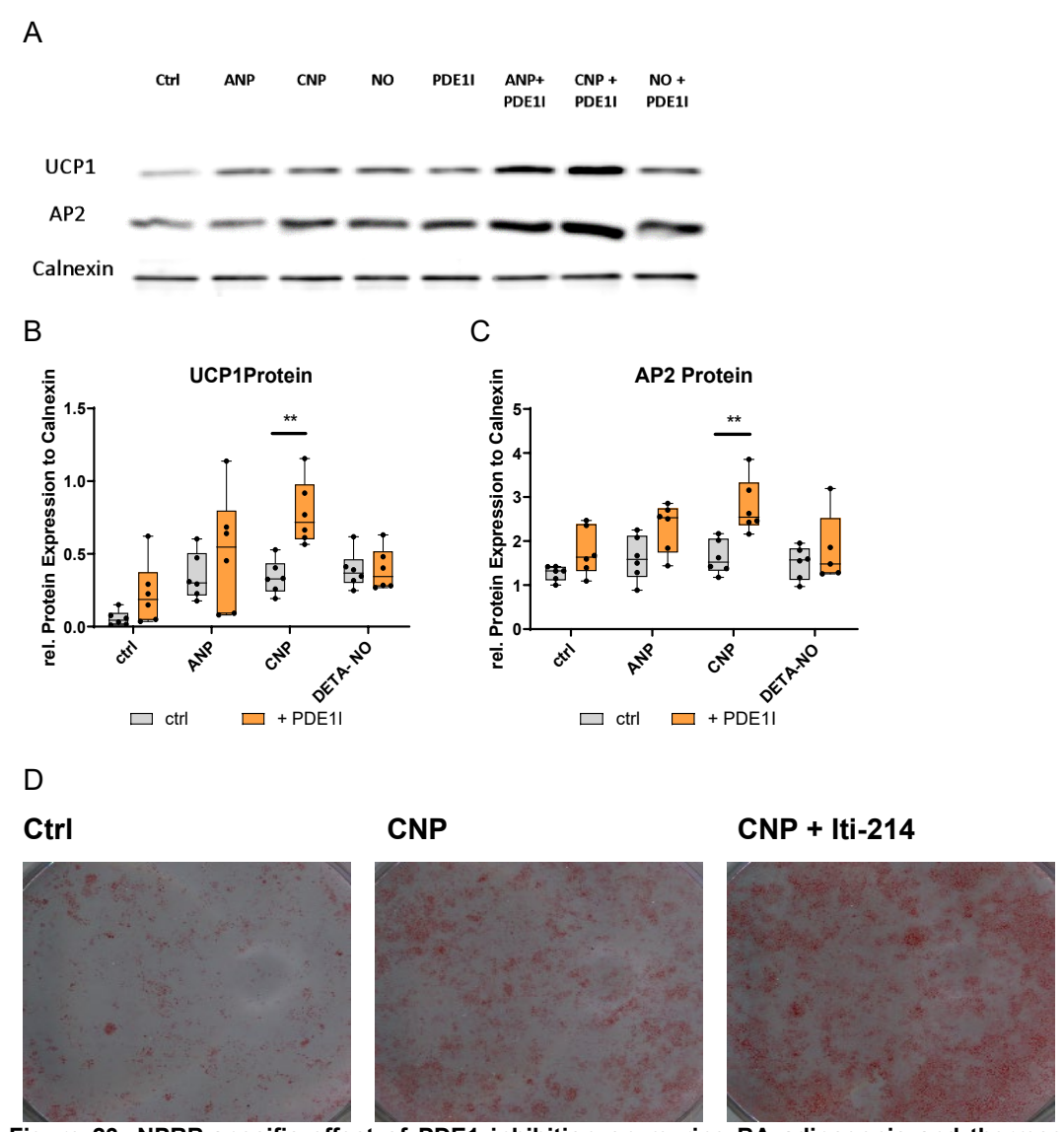


Figure 23: NPRB-specific effect of PDE1 inhibition on murine BA adipogenic and thermogenic marker protein expression

A Representative western blot image of UCP1, aP2, and Calnexin protein expression in murine BA chronically treated (day -2 to day 7) with vehicle, ANP (100 nM), CNP (100 nM), or DETA-NO (10 μ M) \pm PDE1I Iti-214 (100 nM). **B**, **C** Quantification of UCP1 (B) and aP2 (C) protein expression in BA chronically treated (day -2 to day 7) with either vehicle, ANP, CNP, or DETA-NO \pm PDE1I Iti-214. **D** Oil-Red-O Staining of BA chronically treated (day -2 to day 7) with vehicle, CNP, or CNP + Iti-214. Box-plots are represented as median \pm min/max. Two-way ANOVA followed by post-hoc Sidak correction for multiple comparisons. n = 5-6, p* \leq 0.05, p*** \leq 0.01, p**** \leq 0.001.

4.9 Effect of calcium and PDE1 on murine BA differentiation

Having observed the profound calcium-cGMP crosstalk in murine preBA and BA, it was next explored whether calcium could affect the differentiation of BA in a PDE1-dependent manner. To this end, BA were chronically treated (day -2 to day 7) with either lonomycin (100 nM) with or without concomitant application of the PDE1-inhibitor Iti-214 (100 nM) in the presence or absence of CNP (100 nM).

Indeed, chronic treatment with Ionomycin by itself reduced mRNA expression of thermogenic marker Ucp1 and adipogenic marker aP2 significantly. Also, the expression of Pgc1a was reduced, albeit not significantly (Figure 24A, B, C). The same pattern was observed in cGMP-stimulated conditions in the presence of CNP. CNP by itself enhanced Ucp1, aP2, and Pgca1a mRNA expression (Figure 24A, B, C). Concomitant treatment with Ionomycin significantly reduced the expression of Ucp1 mRNA by 72% and that of aP2 by 60%. mRNA expression of Pgc1a showed a non-significant trend of being reduced.

Importantly, in the presence of the PDE1I Iti-214, the detrimental effect of lonomycin on the differentiation of BA was significantly blunted for all three markers, although not completely rescued (Figure 24A, B, C).

These data highlight the fact that calcium impairs the adipogenic and thermogenic differentiation capacity of murine BA both in the presence or absence of CNP-induced cGMP. Critically, PDE1 is a central mediator of this crosstalk, as PDE1 inhibition blunted the detrimental effects of calcium on BA differentiation. However, PDE1 inhibition did not entirely abrogate the effects of lonomycin indicating that there are PDE1-independent mechanisms by which calcium can affect BA differentiation.

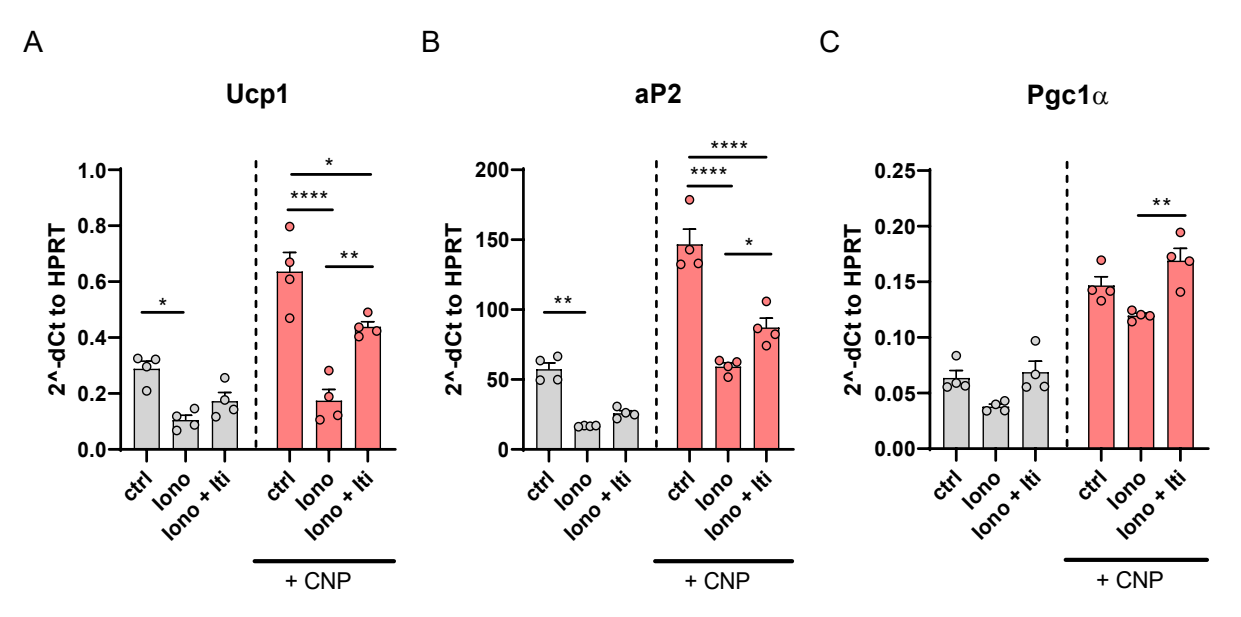


Figure 24: Dependence of calcium-induced impairment of murine BA differentiation on PDE1

A, **B**, **C** Ucp1 (A) aP2 (B) and $Pgc1\alpha$ (C) mRNA expression in brown adipocytes chronically treated (day -2 to day 7) with any combination of CNP (100 nM), Ionomycin (100 nM) and PDE1I Iti-214 (100 nM). Bar graphs represent mean \pm SEM. Two-way ANOVA followed by post-hoc Sidak correction for multiple comparisons. n = 4, $p^* \le 0.05$, $p^{***} \le 0.001$, $p^{****} \le 0.001$, $p^{****} \le 0.0001$.

4.10 Role of cGMP in inducing lipolysis in murine BA

Previous research has established that cGMP induces lipolysis in primate adipocytes but not in murine adipocytes¹⁰⁹. For some time, this difference was believed to be due to a higher expression of the clearance receptor NPRC in murine versus primate adipocytes. However, if this were the case, non-NP sources of cGMP, such as NO or 8-Br-cGMP (a membrane-permeable cGMP analogue) should induce lipolysis in murine BA.

Thus, it was investigated whether non-NP sources of cGMP could induce lipolysis in murine BA. Importantly, no source of cGMP, nor 8-Br-cGMP itself induced lipolysis in murine BA, while NE increased lipolysis by 2.753 ± 0.4028 -fold (Figure 25A).

However, it is known that cGMP can interact with PDE2, via allosteric activation, and PDE3, via competitive inhibition, thereby modulating cAMP levels. Based on this information, it was hypothesized that in the presence of a cAMP-inducing stimulus, such as NE, cGMP might have additive effects on lipolysis in murine BA. To test this hypothesis, fully differentiated murine BA were treated for two hours with either 8-Br-cGMP, NE, or both.

As expected, NE, but not 8-Br-cGMP, enhanced lipolysis of murine BA. However, when 8-Br-cGMP and NE were combined an additional increase in lipolysis was observed (NE: 1.996 ± 0.099 relative glycerol release to vehicle, NE + 8-Br-cGMP: 2.602 ± 0.142 relative glycerol release to vehicle, p = 0.0119), indicating an additive effect of cGMP on NE induced lipolysis (Figure 25B).

Taken together, these results demonstrate that by itself cGMP does not induce lipolysis in murine BA, highlighting a critical species difference between mice and primates. However, cGMP can enhance lipolysis in tandem with a cAMP-inducing stimulus, such as NE. These results suggest a possible crosstalk between cGMP and cAMP in murine BA, where cGMP-mediated inhibition of PDE3 possibly outweighs the cGMP-induced activation of PDE2.

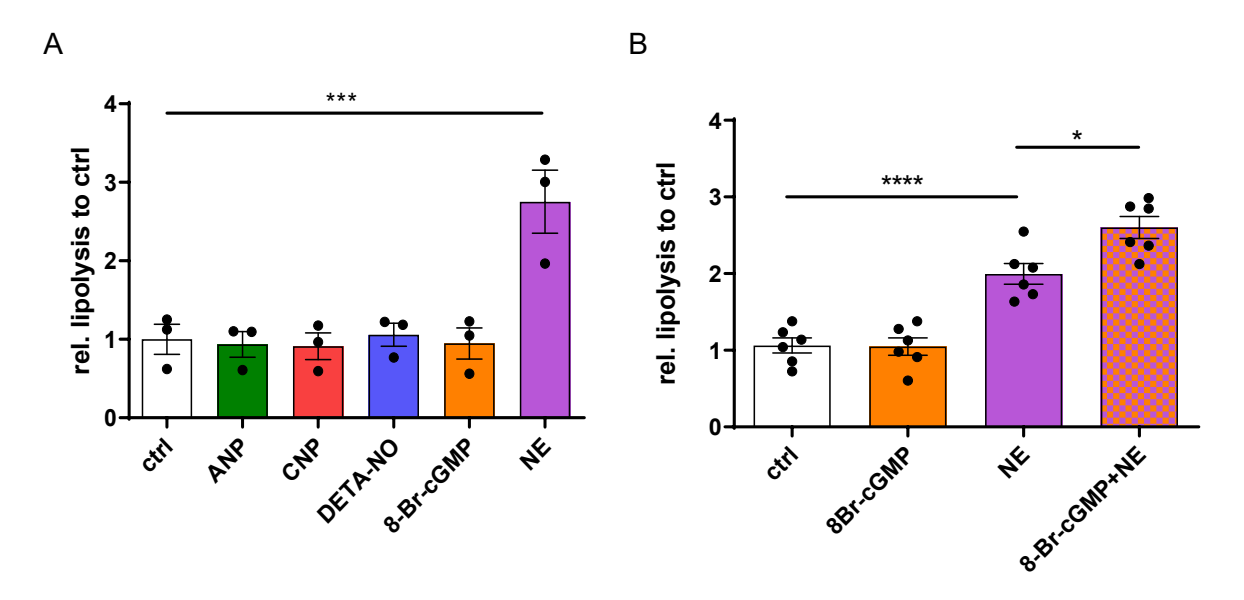


Figure 25: Individual and additive effects of cGMP on lipolysis in murine BA

A Relative glycerol release of murine BA after 120 minutes of treatment with either ANP (100 nM), CNP (100 nM), DETA-NO (10 μ M), 8-Br-cGMP (200 μ M) or NE (1 μ M). **B** Relative glycerol release of murine BA after 120 minutes of treatment with either 8-Br-cGMP, NE, or both. Data were normalized to protein content and then normalized to the vehicle control. Bar graphs represent mean \pm SEM. One-way ANOVA followed by post-hoc Tukey correction for multiple comparisons. n = 3 for A, n = 6 for B, p* \leq 0.05, p** \leq 0.01, p*** \leq 0.001, p**** \leq 0.0001.

4.11 cGMP and cAMP crosstalk in murine preBA

Both PDE2 and PDE3 are expressed in murine preBA and BA. Furthermore, FRET measurements have demonstrated that these PDEs, especially PDE3, are involved in the degradation of cGMP in these cells. Additionally, 8-Br-cGMP enhanced NE-mediated lipolysis, possibly suggesting a cGMP-cAMP crosstalk via these PDEs.

To interrogate the possible crosstalk between cGMP and cAMP, FRET measurements with preBA isolated from transgenic mice expressing the cAMP FRET biosensor epac1-camps were performed. With these cells the changes in intracellular cytosolic cAMP can be monitored in real-time and, thus, the crosstalk between cGMP and cAMP can be probed.

These epac1-camps preBA were treated with either ANP, CNP, or DEA-NO at day -2 and changes in intramolecular FRET efficiencies, which correspond to changes in cytosolic cAMP levels, were monitored. Subsequently, cells were perfused with the AC-activator Forskolin together with IBMX to elicit a maximum response.

Indeed, both CNP ($4.379 \pm 0.568\%$ FRET ratio change) and DEA-NO ($3.715 \pm 0.602\%$ FRET ratio change), but not ANP ($1.527 \pm .0380\%$ FRET ratio change compared to vehicle $1.198 \pm 0.172\%$ FRET ratio change) resulted in increased cytosolic cAMP levels (Figure 26A, B). Additionally, distinct kinetics of the interaction between the two cyclic nucleotides were observed. NO-sGC-derived cGMP caused a more rapid rise in cAMP levels ($0.0616 \pm 0.0059\%$ FRET ratio change per second), compared to NPRB-cGMP ($0.0312 \pm 0.0050\%$ FRET ratio change per second) (Figure 26C).

Together, these findings demonstrate that a positive crosstalk between cGMP and cAMP (i.e. cGMP increases cAMP levels) exists in murine preBA, even without a simultaneous adrenergic stimulation via NE. Furthermore, the interaction between sGC-cGMP with cAMP is more rapid than that of NPRB-cGMP with cAMP, possibly indicating a spatially closer association of sGC-cGMP with PDE3 and cAMP compared to NPRB-cGMP.

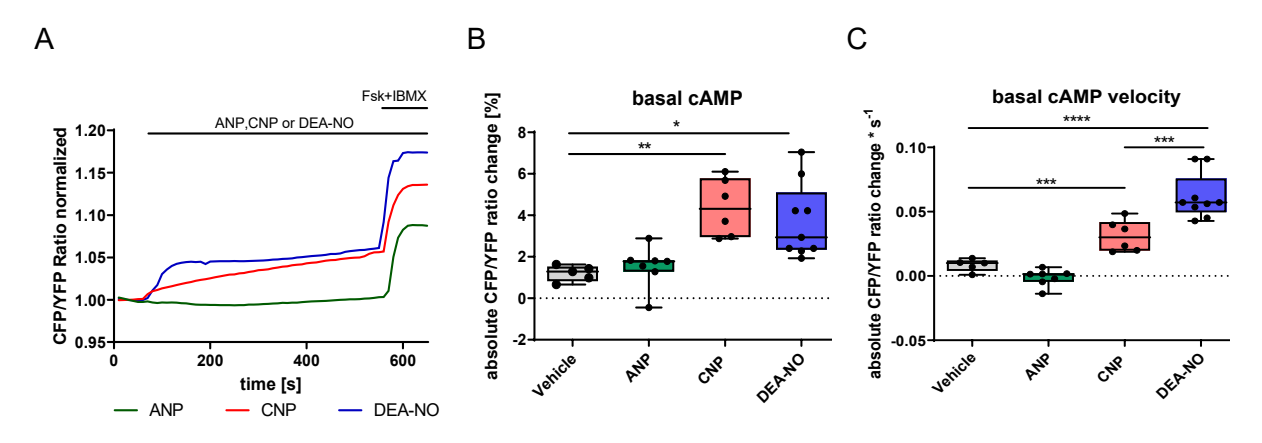


Figure 26: cGMP-cAMP crosstalk in murine epac1-camps preBA

A Representative FRET ratio traces from epac1-camps preBA upon stimulation with either vehicle, ANP (100 nM), CNP (100 nM), or DEA-NO (100 μ M) with subsequent maximum stimulation with IBMX (100 μ M) + Forskolin (10 μ M). **B** Quantification of FRET ratio changes to vehicle, ANP, CNP, or DEA-NO in epac1-camps preBA as absolute FRET ratio change. **C** Quantification of the velocity of FRET ratio change (as average FRET ratio change per second for the first 50 seconds after treatment) after previous vehicle, ANP, CNP, or DEA-NO stimulation. Box-plots are represented as median \pm min/max. One-way ANOVA followed by post-hoc Tukey correction for multiple comparisons. n = 6-9, $p^* \le 0.05$, $p^{***} \le 0.01$, $p^{****} \le 0.001$, $p^{****} \le 0.0001$.

Next, it was interrogated, whether the cGMP-cAMP crosstalk might be altered in the presence of a cAMP-enhancing adrenergic stimulus, such as NE. To this end, preBA were treated with Isoproterenol (100 nM) to induce β -AR mediated cAMP synthesis before being stimulated with ANP, CNP, or DEA-NO. As expected, Isoproterenol induced an elevation in cytosolic cAMP levels (Figure 27A). Following the trend observed in Figure 26, CNP and DEA-NO further increased Isoproterenol induced cAMP levels (CNP: 4.377 \pm 0.2581% FRET ratio change versus DEA-NO: 3.592 \pm 0.2942% FRET ratio change), whereas ANP did not (ANP: 1.837 \pm 0.2926% FRET ratio change versus vehicle: 1.667 \pm 0.110% FRET ratio change). Again, DEA-NO induced a more rapid rise in intracellular cAMP than CNP

(DEA-NO: $0.0805 \pm 0.0099\%$ FRET ratio change per second versus CNP: $0.0415 \pm 0.0058\%$ FRET ratio change per second) (Figure 27C).

In sum, these experiments show that the cGMP-cAMP crosstalk is also relevant during adrenergic stimulation and that sGC-cGMP leads to a more rapid cAMP increase in murine preBA in these conditions as well. Mechanistically, this positive crosstalk might be explained by the cGMP-mediated inhibition of PDE3 outweighing the cGMP-induced activation of PDE2. However, this hypothesis can only be scrutinized by the use of individual PDE inhibitors.

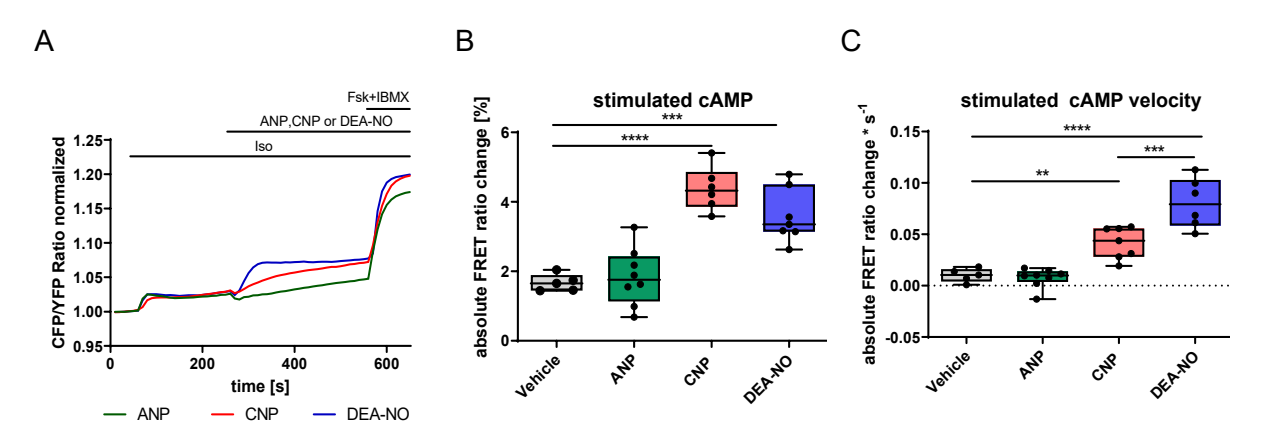


Figure 27: Effect of adrenergic stimulation on cGMP-cAMP crosstalk in murine preBA

A Representative FRET ratio traces from epac1-camps preBA upon stimulation with either vehicle, ANP (100 nM), CNP (100 nM), or DEA-NO (100 μ M) after previous stimulation with Isoproterenol (100 nM) and subsequent maximum stimulation with IBMX (100 μ M) + Forskolin (10 μ M). **B** Quantification of FRET ratio changes to vehicle, ANP, CNP, or DEA-NO in epac1-camps preBA after previous treatment with Isoproterenol as absolute FRET ratio change. **C** Quantification of the velocity of FRET ratio change (as average FRET ratio change per second for the first 50 seconds) after vehicle, ANP, CNP, or DEA-NO stimulation, after previous Isoproterenol stimulation. Box-plots are represented as median \pm min/max. One-way ANOVA followed by post-hoc Tukey correction for multiple comparisons. n = 5-8, p* \leq 0.05, p*** \leq 0.01, p**** \leq 0.001, p**** \leq 0.0001.

To explore the role of PDE2 and PDE3 in the observed cGMP-cAMP crosstalk and to exclude an unspecific activation of the epac-1camps FRET sensor directly via cGMP instead of cAMP, the previous experiments were repeated in the presence of either a PDE2 or PDE3 inhibitor.

Importantly, prior inhibition of PDE3 with cilostamide completely abrogated the cGMP-cAMP crosstalk, demonstrating sufficient specificity of the epac1-camps biosensor for cAMP over cGMP, as well as the pivotal role of PDE3 in the cGMP-cAMP crosstalk (Figure 28A-C). Additionally, immediately after the application of cGMP-inducing agents, a transient drop in FRET ratio was observed, indicating a temporary decrease in intracellular cAMP (Figure 28A). This might be due to more rapid allosteric activation of PDE2 via cGMP compared to the competitive inhibition of PDE3.

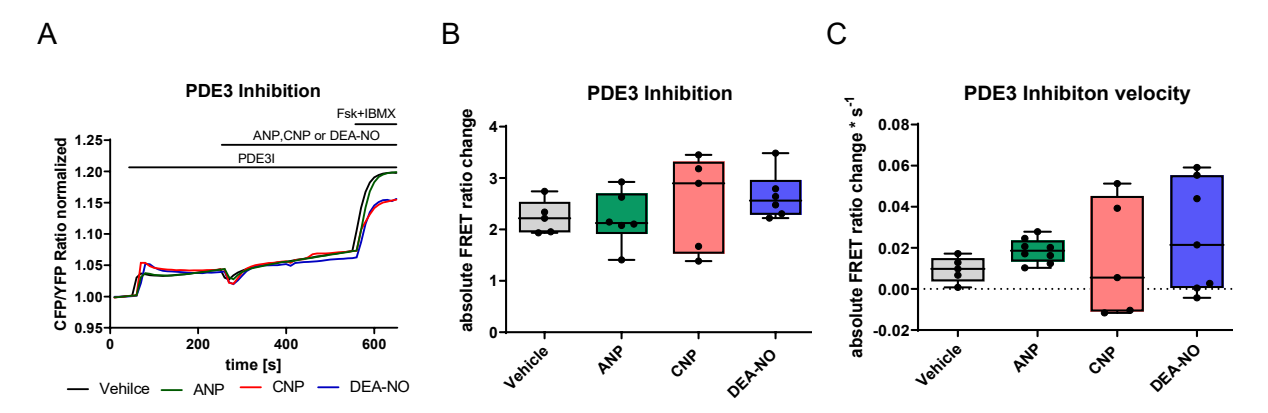


Figure 28: Role of PDE3 in cGMP-cAMP crosstalk in murine preBA

A Representative FRET ratio traces from epac1-camps preBA upon stimulation with either vehicle, ANP (100 nM), CNP (100 nM), or DEA-NO (100 μ M) after previous inhibition of PDE3 with Cilostamide (10 μ M) and subsequent maximum stimulation with IBMX (100 μ M) + Forskolin (10 μ M). **B** Quantification of FRET ratio changes to vehicle, ANP, CNP, or DEA-NO, after previous PDE3 inhibition with Cilostamide in epac1-camps preBA as absolute FRET ratio change. **C** Quantification of the velocity of FRET ratio change (as average FRET ratio change per second for the first 50 seconds) upon vehicle, ANP, CNP, or DEA-NO stimulation, after previous PDE3 inhibition with Cilostamide. Box-plots are represented as median \pm min/max. One-way ANOVA followed by post-hoc Tukey correction for multiple comparisons. n = 5-6, p* \leq 0.05, p** \leq 0.01, p**** \leq 0.001, p***** \leq 0.0001.

While PDE3 inhibition completely abolished CN crosstalk, PDE2 inhibition by Bay 60-7550 did not alter the CN crosstalk (Figure 29A-C). In this PDE2-inhibited state, epac1-camps preBA still displayed a strong increase of intracellular cAMP in response to CNP or DEA-NO, but not to ANP (Figure 29B). Again, the DEA-NO mediated cAMP increase was more rapid than the one induced by CNP.

Overall, these results indicate, that in murine preBA cGMP mainly affects cAMP levels via PDE3 inhibition, while the effect transmitted via PDE2 activation is marginal.

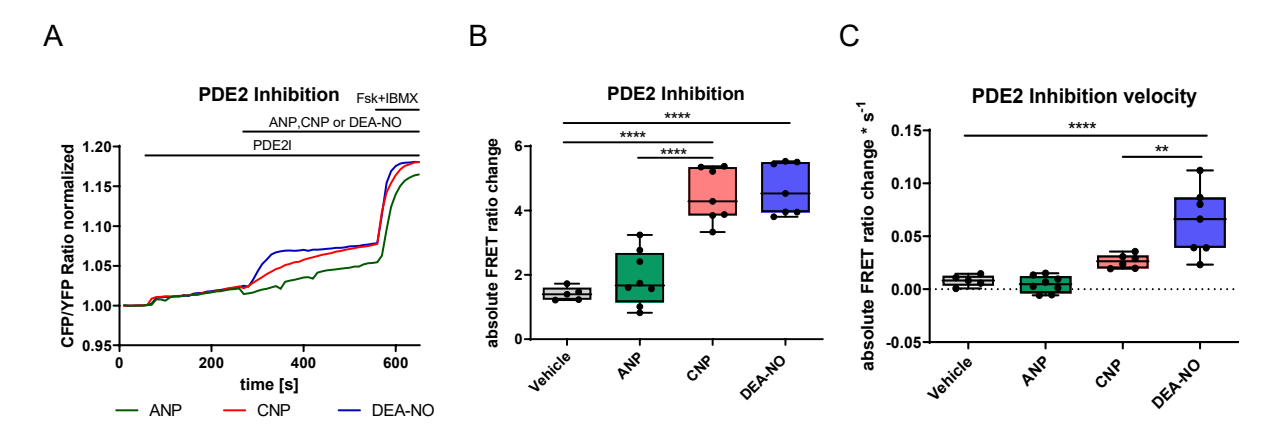


Figure 29: Role of PDE2 in cGMP-cAMP crosstalk in murine preBA

A Representative FRET ratio traces from epac1-camps preBA upon stimulation with either vehicle, ANP (100 nM), CNP (100 nM) or DEA-NO (100 μ M) after previous inhibition of PDE2 with Bay 60-7550 (100 nM) and subsequent maximum stimulation with IBMX (100 μ M) + Forskolin (10 μ M). **B** Quantification of FRET ratio changes to vehicle, ANP, CNP or DEA-NO, after previous PDE2 inhibition with Bay 60-7550 in epac1-camps preBA as absolute FRET ratio change. **C** Quantification of the velocity of FRET ratio change (as average FRET ratio change per second for the first 50 seconds) upon vehicle, ANP, CNP or DEA-NO stimulation, after previous PDE2 inhibition with Bay 60-7550. Box-plots are represented as median \pm min/max. One-way ANOVA followed by post-hoc Tukey correction for multiple comparisons. n = 5-8, p* \leq 0.05, p** \leq 0.01, p**** \leq 0.001, p***** \leq 0.0001.

Additionally, at basal cAMP levels, PDE3 inhibition caused a significant increase in intracellular cytosolic cAMP ($2.881 \pm 0.2291\%$ FRET ratio change), unlike PDE2 inhibition ($1.150 \pm 0.1599\%$ compared to vehicle $1.144 \pm 0.1638\%$) (Figure 30). Indicating that PDE3, but not PDE2, is significantly involved in the degradation of cAMP at steady-state cAMP levels in murine preBA.

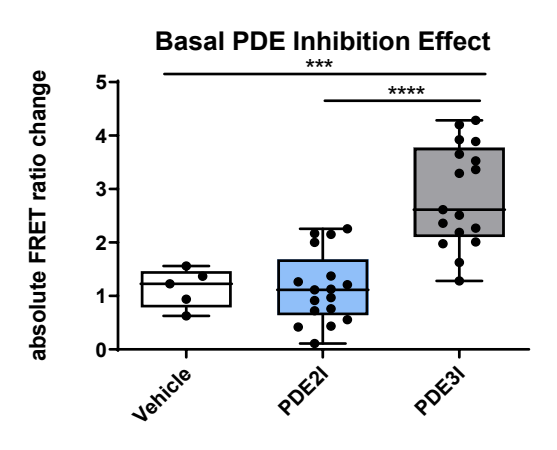


Figure 30: Basal effect of PDE2 or PDE3 inhibition on cytosolic cAMP levels murine preBA

Quantification of FRET ratio changes to either vehicle, PDE2 inhibition via Bay 60-7550 (100 nM) or PDE3 inhibition via Cilostamide (10 μ M). Box-plots are represented as median \pm min/max. One-way ANOVA followed by post-hoc Tukey correction for multiple comparisons. n = 5-17, p* \leq 0.05, p** \leq 0.01, p*** \leq 0.001, p**** \leq 0.0001.

4.12 cGMP and cAMP crosstalk in murine BA

Having found a pronounced crosstalk between cGMP and cAMP in preBA it was inquired whether this crosstalk might also exist in fully differentiated BA. Considering PDE2 showed a strong association with sGC-cGMP and also NPRA-cGMP in BA, it was hypothesized that the dynamics of the CN crosstalk might be reversed in BA.

To this end, transgenic epac1-camps BA were fully differentiated *in vitro*, with FRET measurements being performed on day 7. Interestingly, even when PDE2 and PDE3 were fully inhibited – which should abolish all mechanisms of CN crosstalk – DEA-NO still induced increases in the CFP/YFP FRET ratio, indicating an increase in intracellular cytosolic cAMP (Figure 31A). Importantly, this effect was not observed, when PDE2 and PDE3 were not inhibited $(0.5485 \pm 0.3943\% \text{ FRET ratio}$ change for no PDE inhibition versus $9.444 \pm 0.6562\%$ for PDE2 + PDE3 inhibition) (Figure 31A, B).

A possible explanation could be, that at the considerably higher cGMP levels in murine BA, compared to preBA, epac1-camps might also be activated by cGMP, and not only by cAMP. Previous research has already described the imperfect specificity of epac1-camps at higher cGMP concentrations²⁵⁶. By inhibiting both PDE2 and PDE3 – two of the main PDEs involved in sGC-cGMP degradation – the cGMP levels in BA might be increased by NO to such an extent that unspecific binding to the epac1-camps biosensor occurs.

These results indicate that the epac1-camps biosensor is unsuited to measure the CN crosstalk in BA. Thus, a different approach was chosen to analyze the CN crosstalk in BA.

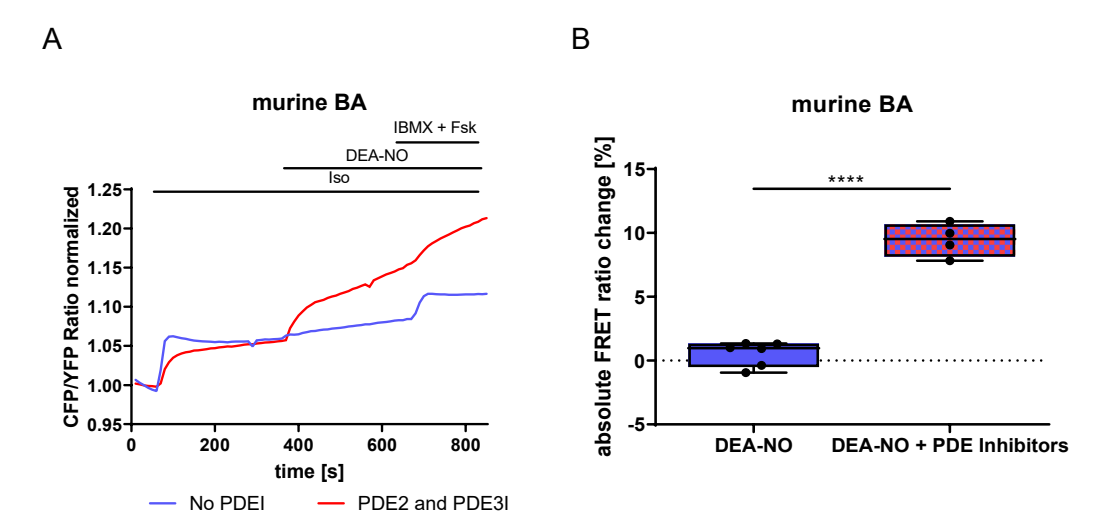


Figure 31: Crosstalk between cGMP and cAMP in fully differentiated murine BA

A Representative FRET ratio traces from epac1-camps BA upon stimulation with Isoproterenol (100 nM) and then with DEA-NO (100 μ M) with or without previous inhibition of PDE2 with Bay 60-7550 (100 nM) and PDE3 with Cilostamide (10 μ M) and subsequent maximum stimulation with IBMX (100 μ M) + Forskolin (10 μ M). B Quantification of FRET ratio changes from epac1-camps BA upon stimulation with DEA-NO with or without previous inhibition of PDE2 with Bay 60-7550 and PDE3 with Cilostamide. Box-plots are represented as median \pm min/max. One-way ANOVA followed by post-hoc Tukey correction for multiple comparisons. n = 4-6, $p^* \le 0.05$, $p^{***} \le 0.01$, $p^{****} \le 0.001$, $p^{*****} \le 0.0001$.

As an alternative approach to characterize the CN crosstalk in BA, two methods that supplement each other were chosen. The aforementioned lipolysis assay to measure cAMP-PKA mediated glycerol release as well as a cAMP-ELISA, to directly measure cAMP.

cGMP by itself does not stimulate lipolysis in BA (see Figure 25A, B), but in the presence of a cAMP stimulus, such as NE or Isoproterenol, cGMP can further enhance cAMP-mediated lipolysis, possibly indicating CN crosstalk in BA (see Figure 25B and Figure 26-29). Additionally, previous publications have demonstrated that cAMP does not freely diffuse within BA, but instead forms distinct subcellular clusters associated with distinct β -AR and PDEs²⁷⁸. Consequently, the crosstalk between cGMP and cAMP might vary depending on which subcellular pool of cGMP and cAMP interact with one another.

To test this hypothesis fully mature BA were first treated with either Isoproterenol (a rather unspecific β_1 and β_2 agonist, 100 nM) + β_2 -Antagonist ICI 118551 (50 nM) to specifically activate β_1 -Receptors, Isoproterenol (100 nM) + β_1 -Antagonist CGP 207102A (100 nM) to specifically activate β_2 -Receptors, or CL 316243 (10 μ M a specific β_3 -agonist) to specifically activate β_3 -receptors. After 5 minutes of incubation, samples were taken, and intracellular cAMP levels were determined by ELISA.

As expected, activation of each β -AR increased intracellular cAMP abundance (Vehicle: 1,166 ± 0,1159 pmol cAMP/mg protein, β_1 : 27,19 ± 2,445 pmol cAMP/mg protein, β_2 : 7,03 ± 1,423 pmol cAMP/mg protein, β_3 : 39,21 ± 0,9516 pmol cAMP/mg protein) (Figure 32). Interestingly, the cAMP elevation induced by β_2 - and β_3 -AR activation was significantly greater than that mediated by β_1 -AR activation. This indicates that in murine BA, β_2 and β_3 receptors are the main source of cAMP, while β_1 -AR activation induces a smaller, yet still significant, increase in intracellular cAMP.

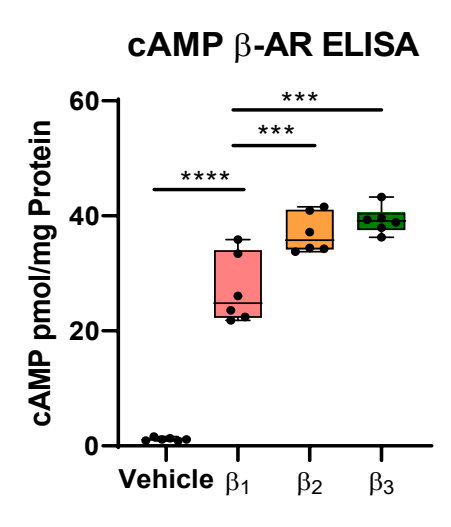


Figure 32: cAMP elevations in BA in response to activation of individual $\beta\text{-AR}$

Measurement of intracellular cAMP levels of murine BA via ELISA after 5 minutes of incubation with either vehicle, Isoproterenol (100 nM) + β_2 -Antagonist ICI 118551 (50 nM, for β_1 activation), Isoproterenol + β_1 Antagonist CGP 207102A (100 nM, for β_2 activation), or CL 316243 (10 μ M, for β_3 activation). Box-plots are represented as median \pm min/max. One way ANOVA followed by post-hoc Tukey correction for multiple comparisons. n = 6, $p^* \le 0.05$, $p^{***} \le 0.01$, $p^{****} \le 0.001$, $p^{*****} \le 0.0001$.

Subsequently, to test whether the distinct subcellular pools of both cAMP and cGMP interact in a compartment-specific manner with one another, the aforementioned specific β -AR stimuli were combined with each of the different cGMP generators, ANP, CNP or DEA-NO and their combined effect on both intracellular cAMP levels and lipolytic activity gauged.

Similar to the situation to preBA, induction of cGMP generally led to further increases of intracellular cAMP in the presence of β -AR stimulation in murine BA (Figure 33A-C), possibly indicating a crosstalk that is mainly mediated via cGMP-induced inhibition of PDE3, resulting in reduced cAMP degradation. In more detail, ANP showed significant additive effects on both cAMP levels and lipolysis together with β_1 (Figure 33A, D) and β_3 (Figure 33C, F) activation, but only a trend with β_2 activation (Figure 33B, E). CNP on the other hand, only enhanced β_1 -mediated cAMP levels, but not β_1 mediated lipolysis (Figure 33A, D). Surprisingly, DEA-NO enhanced β_1 -mediated lipolysis, but decreased both β_2 -mediated cAMP levels and lipolysis, while not interacting with β_3 -derived cAMP at all (Figure 33A-F). These data suggest that

sGC-cGMP interacts with different pools of cAMP via different PDEs (mainly PDE3 inhibition for β_1 -AR and PDE2 activation for β_2 -AR).

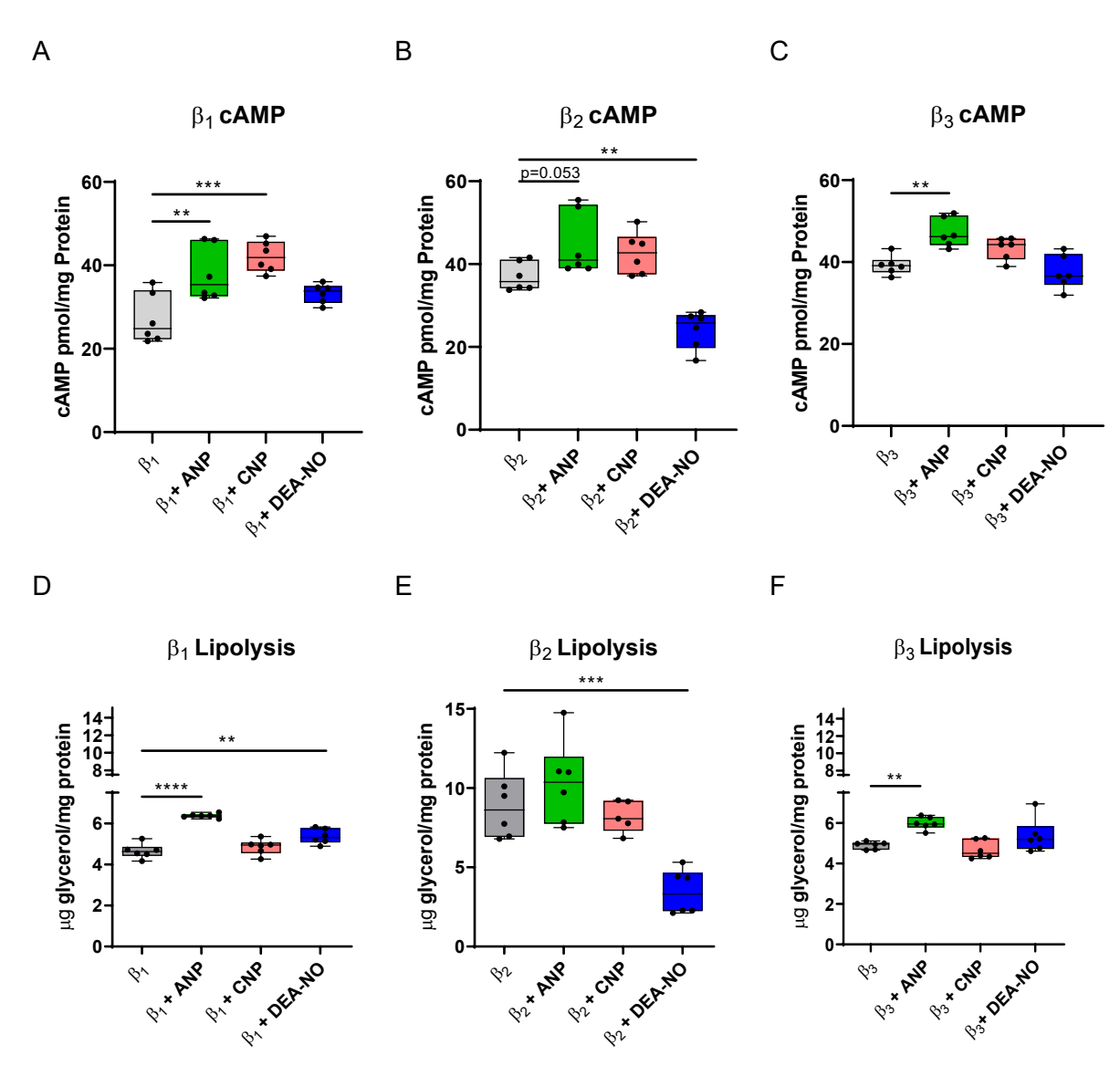


Figure 32: β-AR specific cGMP-cAMP crosstalk in murine BA

A, B, C Measurement of intracellular cAMP levels of murine BA, after 5 minutes of incubation with either Isoproterenol (100 nM) + $β_2$ -Antagonist ICI 118551 (50 nM for $β_1$ -activation), Isoproterenol + $β_1$ -Antagonist CGP 207102A (100 nM for $β_2$ -activation), or CL 316243 (for $β_3$ -activation), each with or without concomitant treatment with either ANP (100 nM), CNP (100 nM) or DEA-NO (100 μM) **D, E, F** Measurement of released glycerol after 2 hours of incubation with either Isoproterenol + $β_2$ -Antagonist ICI 118551 (for $β_1$ -activation), Isoproterenol + $β_1$ -Antagonist CGP 207102A (for $β_2$ -activation), or CL 316243 (for $β_3$ -activation), each with or without concomitant treatment with either ANP, CNP or DETA-NO (10 μM). Box-plots are represented as median ± min/max. One-way ANOVA followed by post-hoc Tukey correction for multiple comparisons. n = 5-6, $ρ^* ≤ 0.05$, $ρ^{***} ≤ 0.01$, $ρ^{****} ≤ 0.001$, $ρ^{*****} ≤ 0.0001$.

Furthermore, the unique interaction of NO-mediated cGMP with β_2 -cAMP was entirely dependent on PDE2, as concomitant inhibition of PDE2 completely abolished the sGC-cGMP mediated reduction in β_2 induced lipolysis (Figure 34B). Besides the prominent interaction between NO-cGMP and β_2 -AR-cAMP, inhibition of PDE2 had little effect on CN crosstalk, as PDE2 inhibition did not alter the crosstalk between cGMP and β_1 -AR-cAMP (Figure 34A). However, while ANP by itself already enhanced β_3 -AR mediated lipolysis (Figure 33F), this effect was further enhanced with concomitant PDE2 inhibition (Figure 34C), possibly indicating that the interaction between ANP-cGMP and β_3 -AR-cAMP depends on both PDE2 and PDE3.

Taken together, these results show that a crosstalk between cGMP and cAMP exists in murine BA, influencing intracellular cAMP levels and lipolysis. Importantly, the data demonstrate that the crosstalk between cGMP and cAMP is specific for distinct cGMP- and cAMP-pools. sGC-cGMP enhances cAMP signals and lipolysis from β_1 -AR while diminishing cAMP signals and lipolysis from β_2 -AR. The findings also highlight that the interaction between the different pools of cGMP and cAMP can depend on either PDE2, PDE3, or both simultaneously, further adding to the complexity of CN compartmentalization.

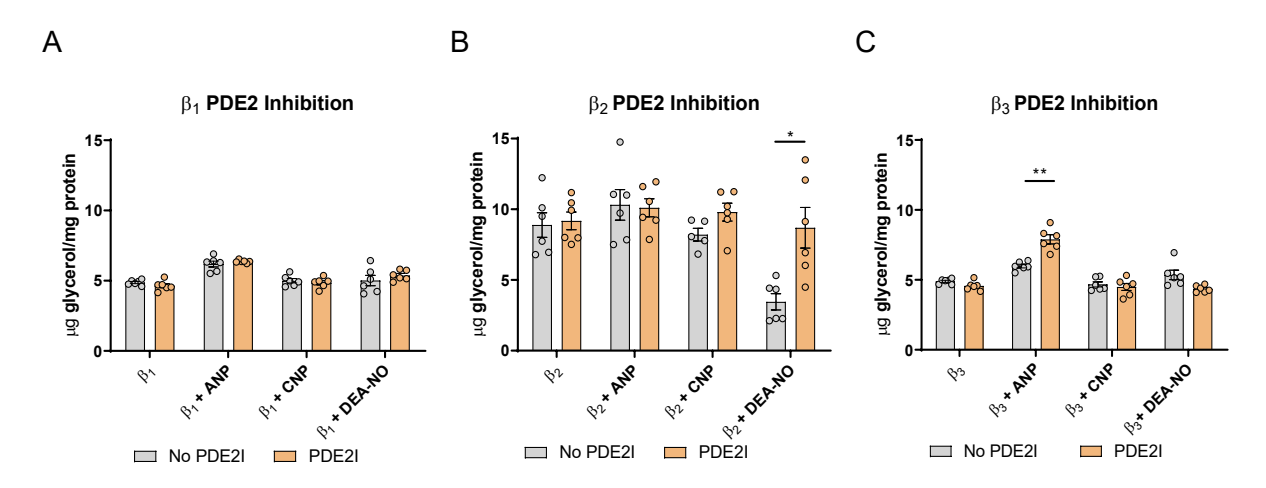


Figure 33: Effect of PDE2 inhibition in altering the β -AR specific cGMP-cAMP crosstalk in murine BA

A, **B**, **C** Measurement of released glycerol after 2 hours of incubation with either Isoproterenol (100 nM) + $β_2$ -Antagonist ICI 118551 (100 nM for $β_1$ -activation), Isoproterenol + $β_1$ -Antagonist CGP 207102A (50 nM for $β_2$ -activation), or CL 316243 (10 μM for $β_3$ -activation), each with or without concomitant treatment with either ANP (100 nM), CNP (100 nM) or DETA-NO (10 μM) in presence or absence of PDE2 inhibitor Bay 60-7550 (100 nM). Bar graphs are represented as mean ± SEM. Multiple t-tests with Holm-Sidak correction for multiple comparisons. n = 5-6, p* ≤ 0.05, p** ≤ 0.01, p**** ≤ 0.001, p**** ≤ 0.0001.

4.13 Expression of cGMP generators and PDEs in human BA and BAT

To evaluate the transferability of the previous studies in mice to humans, it was next investigated how cGMP production, degradation, and compartmentalization might differ between the two species. Again, gene expression of the relevant GCs was investigated via qRT-PCR in BA of human origin. Brown adipocyte progenitors (human preBA) were isolated from the BAT of the parathyroidal region of patients undergoing neck surgery and then

differentiated in vitro into fully mature human BA (hBA). Afterwards, RNA was isolated, and cDNA was synthesized. The gene expression studies revealed considerable differences regarding GC expression between human and murine BA.

While BA from mice mainly express *Gucy1a1*, *1a2*, and *1b1* mRNA (suggesting cGMP generation mainly via NO, as confirmed by FRET and ELISA), the BA from human subjects had low expression levels for these sGC-associated genes. However, hBA displayed high mRNA expression levels for the NP-receptors, *NPRA*, and even more so *NPRB* and *NPRC* (Figure 35A). Intriguingly, the *NPRA/NPRC* and *NPRB/NPRC* expression ratio was almost an order of magnitude greater in hBA, compared to murine BA (Figure 35B, C).

These findings might suggest a greater sensitivity to NPR signaling in hBA, compared to murine BA, as the NPRs containing a GC are more highly expressed relative to the clearance receptor in hBA versus murine BA.

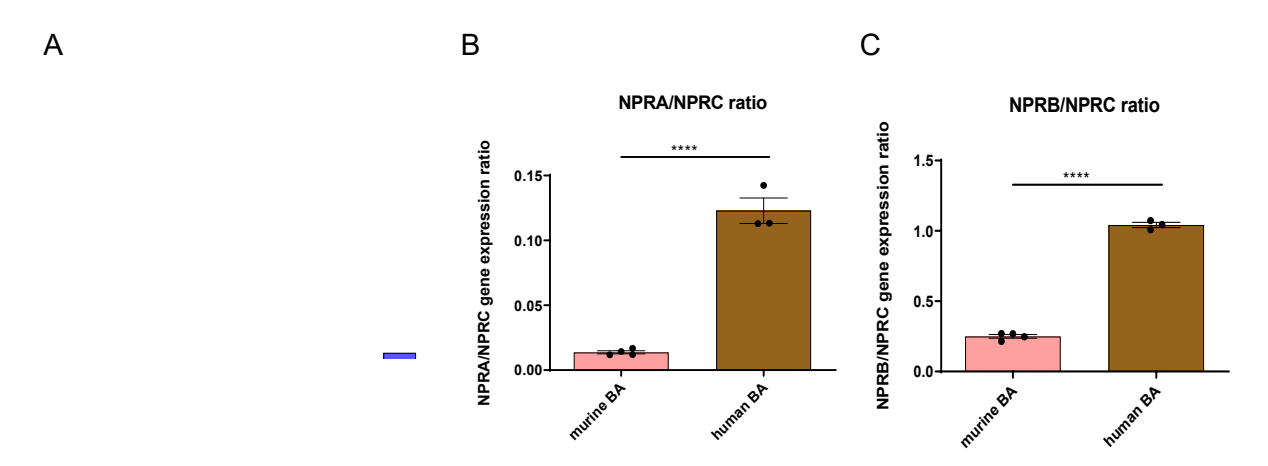


Figure 34: mRNA expression of sGC and NPR-related genes in human BA

A Relative mRNA expression to *HPRT* of GCs and the clearance receptor *NPRC* in human BA **B**, **C** Relative mRNA expression ratio of NPRs in human and murine BA (B: *NPRA/NPRC*, C: *NPRB/NPRC*). Bar graphs are represented as mean \pm SEM. Two-tailed students t-test. n = 3-4, p* \leq 0.05, p** \leq 0.01, p*** \leq 0.001, p**** \leq 0.0001.

Additionally, the expression patterns of cGMP- or dual-specific PDEs were also analyzed in fully differentiated hBA and compared to those of murine BA.

PDE3B was also the most highly expressed PDE in hBA, similar to murine BA. Unlike murine BA, PDE1A showed low expression levels in hBA. However, PDE1B was highly expressed in hBA, contrary to murine BA. Interestingly, PDE5A, a cGMP-specific PDE, was highly expressed in hBA, unlike murine BA. Additionally, PDE9A, 10 A, and 3A were also expressed in hBA (Figure 36A).

In summary, the PDE expression patterns differ between murine BA and hBA, especially concerning PDE1A, 1B, and 5A.

BAT is made up of more than one cell type, which might mean that PDE expression patterns differ between human BAT and hBA. To evaluate this possibility, the PDE expression patterns of hBA were compared to the expression patterns in human BAT found in RNA-sequencing data from the BATLAS Project²⁷⁹.

Similarly, to hBA, high expression levels were found for PDE3B and PDE1B. However, the expression of PDE5A was lower in human BAT than in human BA, while the expression of PDE2A was considerably higher in human BAT (Figure 36B). These findings might suggest, that PDE2A is mainly expressed by other cell types, which are not adipocytes, present in human BAT.

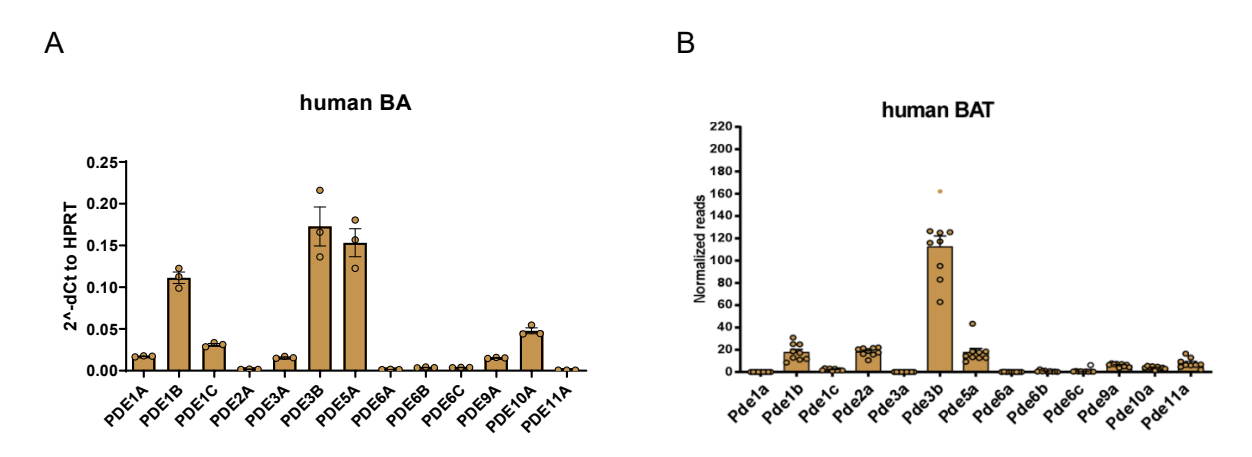


Figure 35: PDE expression in human BA and BAT

A Relative mRNA expression to HPRT of dual- and cGMP-specific PDEs in human BA. **B** Normalized reads from RNA-Sequencing data set of dual- and cGMP-specific PDEs in human BAT taken from the BATLAS Project. Bar graphs are represented as mean \pm SEM. n = 3 for A, n = 9 for B.

4.14 Real-time imaging of human preBA with the Green cGull biosensor

To perform real-time cGMP measurements in human preBA and hBA, cells were transduced via lentivirus to express the single-fluorophore, intensiometric, cGMP biosensor Green cGull²⁷¹. This sensor can be efficiently expressed in human preBA and hBA via lentivirus (transduction efficiency > 70%) and has the advantage over cGi-500 of having a far greater dynamic range (up to 700% signal intensity change versus around 10-50% ratio change for cGi-500). Furthermore, the higher EC₅₀ value of Green cGull (1.03 μ M versus 500 nM for cGi-500) enables the analysis of cGMP in cells with higher basal cGMP levels²⁷¹.

Cells were imaged 72 hours after lentiviral transduction either as human preBA or fully differentiated hBA. Importantly, at basal cGMP levels (in the absence of any cGMP-inducing drugs) the cells expressing Green cGull are very dim, and, thus, impossible to distinguish from untransduced cells. This necessitates high transduction efficiency to guarantee the presence of multiple Green cGull expressing cells in the field of view during measurements. When human preBA are treated with CNP, their fluorescence signal (measured at 520 nm) greatly increases, making the transduced cells clearly visible. (Figures 37 and 38). The time course

and the change in fluorescence intensity in response to either CNP or IBMX are indicated in Figure 38, revealing high transduction efficiency and the high degree of fluorescence intensity change (20-600%) of Green cGull expressing human preBA.

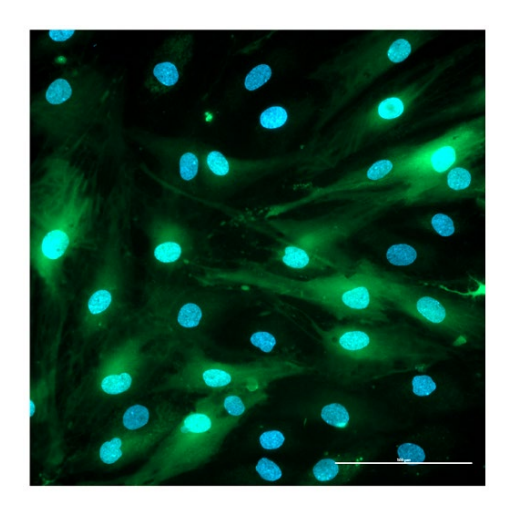


Figure 36: Fluorescence image of human preBA transduced with the Green cGull intensiometric biosensor

Transduction was performed via lentivirus (20 ng for each well of an Ibidi μ -Slide 8 well dish) 72 hours before imaging. Cells were nuclear stained with Hoechst (1 μ g/ml) immediately before imaging. The image depicts human preBA at 40x magnification.

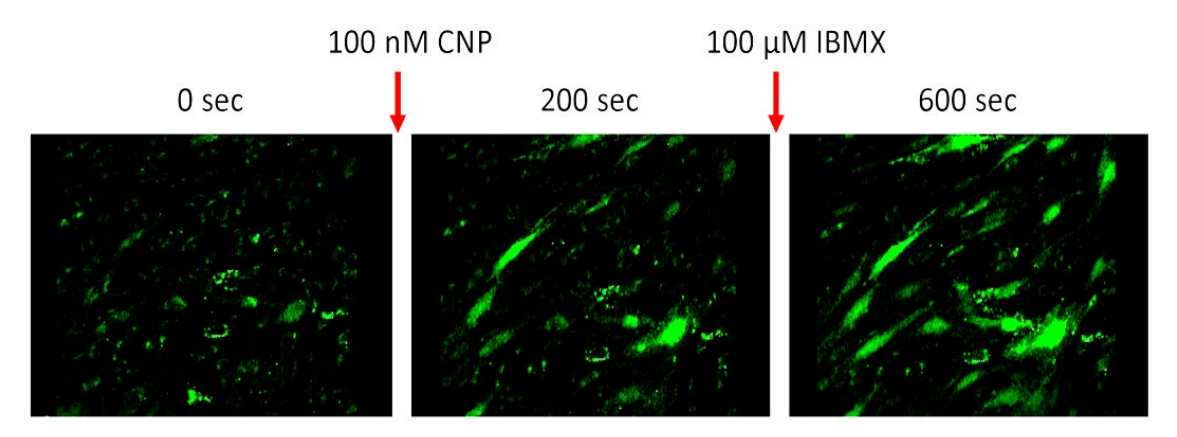


Figure 37: Fluorescence response of Green cGull expressing human preBA to cGMP-inducing drugs

Transduction was performed via lentivirus (20 ng for each well of an Ibidi μ -Slide 8 well dish) 72 hours before imaging. During imaging, cells were treated, when indicated, with either CNP (100 nM) or IBMX (100 μ M). The image depicts human preBA at 10x magnification.

To characterize the mechanisms of cGMP synthesis in human preBA, Green cGull expressing human preBA were either treated with ANP, CNP, or DEA-NO, similarly to the previous murine FRET experiments. The signal intensity change of the Green cGull sensor was then measured over the course of 600 seconds, with an image being acquired every 10 seconds. IBMX + CNP was used to elicit a maximum response for initial treatment with DEA-NO and ANP, while ANP + IBMX was used for cells initially treated with CNP.

Importantly, the data indicate that similar to murine preBA, CNP is also the main source of cGMP in human preBA (198.8 \pm 13.00% fluorescence intensity change over baseline) (Figure 39A, B). However, unlike murine preBA, DEA-NO did not induce any measurable change in cGMP levels (-2.66 \pm 1.01% fluorescence intensity change over baseline). Furthermore, ANP induced a significant increase in intracellular cGMP in human preBA, unlike murine preBA (88.87 \pm 9.46% fluorescence intensity change over baseline), albeit to a lesser extent than CNP.

Overall, cGMP synthesis is considerably different in human versus murine preBA. In murine preBA CNP and NO are the main sources of cGMP, while in human preBA CNP and ANP are most important, and NO is ineffective at inducing cytosolic cGMP elevations.

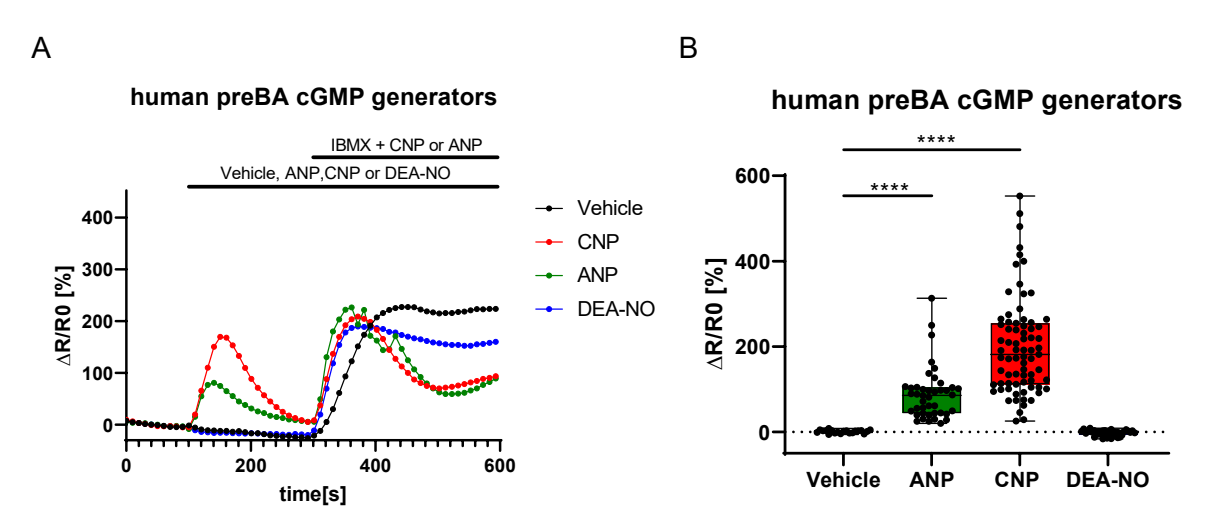


Figure 38: Real-time measurements of cGMP synthesis in human preBA

A Representative fluorescence intensity traces from Green cGull expressing human preBA upon stimulation with either vehicle, ANP (100 nM), CNP (100 nM), or DEA-NO (100 μ M) with subsequent maximum stimulation with either CNP (if DEA-NO or ANP was applied first) or ANP (if CNP was applied first) + IBMX (100 μ M). **B** Quantification of absolute fluorescence change over baseline from Green cGull expressing human preBA to vehicle, ANP, CNP, or DEA-NO. Box-plots are represented as median \pm min/max. One-way ANOVA with post-hoc Tukey correction. n = 42-75, $p^* \le 0.05$, $p^{***} \le 0.01$, $p^{****} \le 0.001$, $p^{*****} \le 0.0001$.

After characterizing cGMP synthesis in human preBA, the dynamics of cGMP degradation were analyzed next. To this end, similar experiments were performed as in murine preBA. Green cGull expressing human preBA were first stimulated with either CNP or ANP to induce cGMP elevations and then perfused with individual PDE inhibitors or IBMX. Since the Green cGull expression levels varied considerably between individual cells the effect of each PDE inhibitor was normalized to the maximum PDE inhibition effect obtained via IBMX at the end of the measurement in that particular cell.

cGMP induced via CNP was mainly degraded via PDE5 (68.89 \pm 1.71% of IBMX) and PDE9 (62.04 \pm 3.05% of IBMX) and to a lesser extent via PDE1 (39.75 \pm 1.90% of IBMX) and PDE2 (27.95 \pm 2.96% of IBMX) (Figure 40A, B). This is in stark contrast to murine preBA, where

PDE1 and PDE3, but not PDE5 or PDE9 were involved in cGMP degradation. Additionally, ANP-NPRA-cGMP was degraded by different PDEs than CNP-NPRB-cGMP in human preBA. ANP-NPRA-cGMP was predominantly degraded via PDE1 (52.96 \pm 1.61% of IBMX) and PDE9 (46.02 \pm 1.98% of IBMX) and to a lesser extent PDE2 (29.25 \pm 2.66% of IBMX) and PDE5 (25.75 \pm 2.26% of IBMX) (Figure 40C, D).

In summary, these results demonstrate that cGMP compartmentalization also exists in human preBA, as cGMP synthesized via different GCs interacts with different subsets of PDEs. Furthermore, the data show that the regulation of CNP-NPRB-cGMP via PDEs differs between murine and human preBA. PDE5 and 9 were most important for NPRB-cGMP degradation in human preBA, while PDE1 and 3 were the central NPRB-cGMP regulating PDEs in murine preBA.

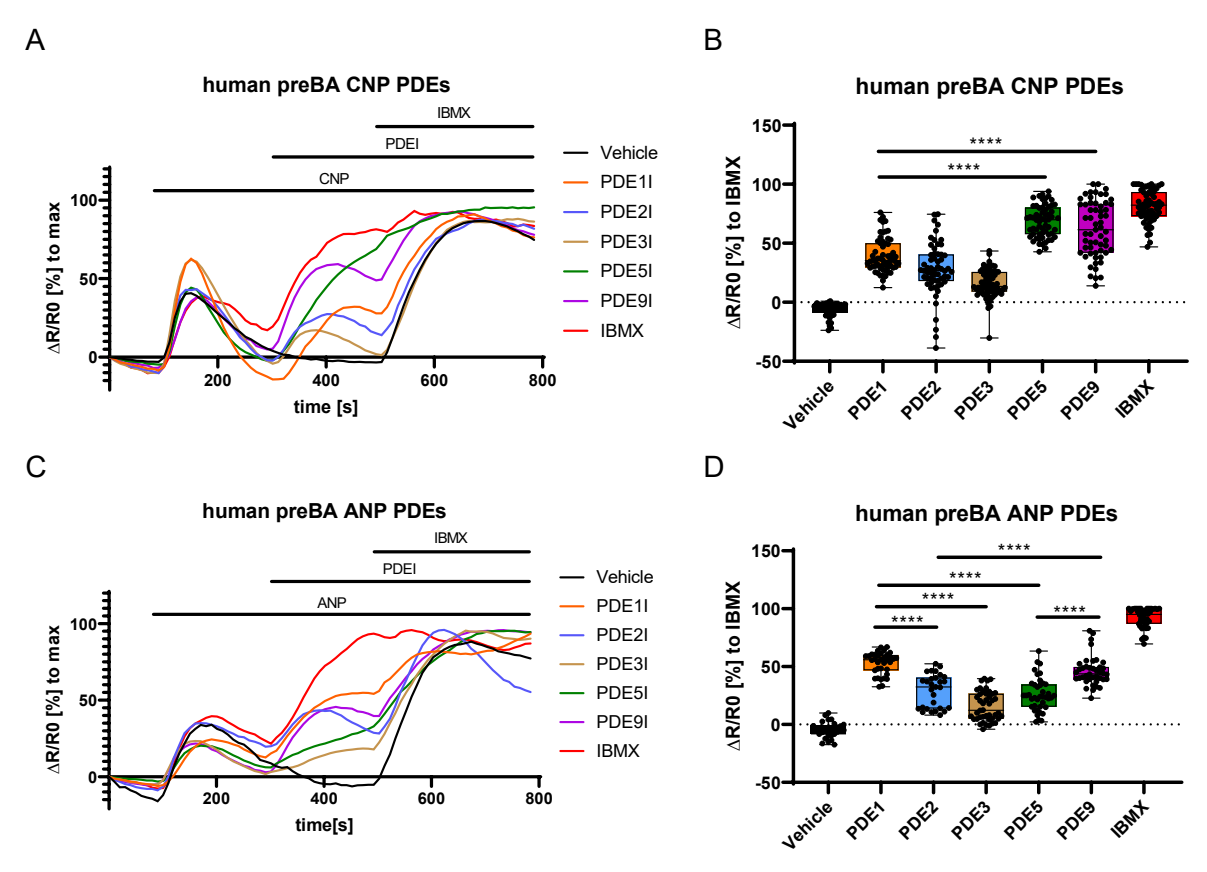


Figure 39: Differential regulation of NPRA-cGMP versus NPRB-cGMP by PDEs in human preBA

A, C Representative fluorescence intensity traces from Green cGull human preBA upon stimulation with either CNP (100 nM, A) or ANP (100 nM, C) with subsequent application of either PDE1I Iti-214 (100 nM), PDE2I Bay 60-7550 (100 nM), PDE3I Cilostamide (10 μ M), PDE5I Avanafil (1 μ M), PDE9I Bay 73-6691 (10 μ M) or pan PDE Inhibitor IBMX (100 μ M). **B, D** Quantification of fluorescence change of human preBA in response to PDE1I, PDE2I, PDE3I, PDE5I, PDE9I or IBMX after previous application of either CNP (B) or ANP (D) in relation to complete PDE Inhibition by IBMX. Box-plots are represented as median \pm min/max. One-way ANOVA followed by post-hoc Tukey correction for multiple comparisons. n = 30-72, p* \leq 0.05, p** \leq 0.01, p**** \leq 0.001, p***** \leq 0.0001.

4.15 Real-time imaging of human BA using the Green cGull biosensor

As cGMP synthesis and degradation changed considerably over the course of murine BA differentiation, it was speculated that this might also be the case in human BA. To this end, human BA were differentiated into fully mature lipid-laden multilocular hBA.

In the first attempts to stably express Green cGull in hBA, the lentiviral transduction was performed one day after seeding, when the cells were still in a progenitor state (human preBA). However, in this case, very few lipid-laden mature hBA expressed the sensor at the end of the differentiation process. Instead, undifferentiated fibroblasts showed a strong fluorescence signal, possibly indicating that the successful transduction with Green cGull impaired hBA differentiation. Instead, hBA were transduced via lentivirus 72 hours before imaging, when the cells were already almost fully differentiated hBA. In this case, high transduction efficiency was achieved in the multilocular mature hBA. Afterwards, on day 12 of the differentiation protocol, intensiometric cGMP measurements were performed similarly to Figures 39 and 40. Importantly, the dynamics of cGMP generation in hBA were significantly different than in human preBA. Only ANP induced detectable cGMP signals in hBA (146.9 ± 23.56% fluorescence intensity change over baseline), while neither CNP nor DEA-NO induced any significant increase in fluorescence over vehicle (Figure 41A, B).

This observation indicates that in human BA, similarly to murine BA, a switch in cGMP synthesis occurs upon BA differentiation. In human BA cGMP synthesis switches from CNP-NPRB to ANP-NPRA, unlike murine BA where cGMP synthesis switched from CNP-NPRB to NO-sGC and to a lesser extent ANP-NPRA. Interestingly, NO neither induced significant cGMP synthesis in human preBA or hBA.

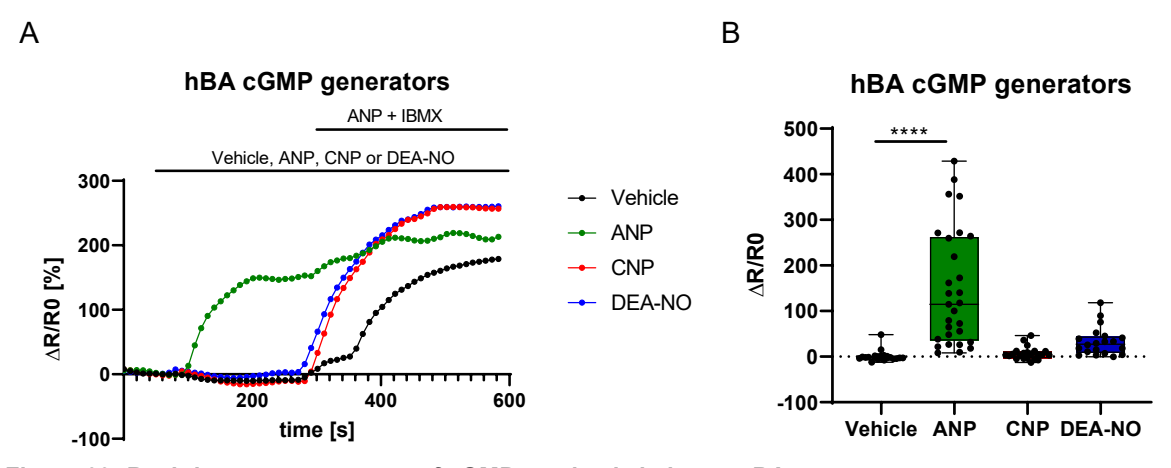


Figure 39: Real-time measurements of cGMP synthesis in human BA

A Representative fluorescence intensity traces from fully differentiated Green cGull hBA upon stimulation with either vehicle, ANP (100 nM), CNP (100 nM), or DEA-NO (100 μ M) with subsequent maximum stimulation with ANP + IBMX (100 μ M). **B** Quantification of absolute fluorescence change over baseline of fully differentiated Green cGull expressing human BA to vehicle, ANP, CNP, or DEA-NO. Box-plots are represented as median \pm min/max. Two-tailed students t-test. n = 42-75. p* \leq 0.05, p** \leq 0.01, p*** \leq 0.001, p**** \leq 0.0001.

Next, it was investigated which PDEs regulate the NPRA-cGMP pool in hBA. In hBA, ANP-NPRA-cGMP was mainly regulated via PDE 1 (72.26 \pm 3.80% of IBMX) and PDE3 (63.01 \pm 1.69% of IBMX) and to a lesser extent PDE2 (26.20 \pm 3.30% of IBMX) and PDE5 (25.29 \pm 3.03% of IBMX), but not PDE9 (Figure 42A, B). This is in contrast to human preBA, where PDE1 and PDE9, but not PDE3 were involved in NPRA-cGMP degradation.

Taken together these results highlight that, similarly to murine BA, the architecture of cGMP compartmentalization changes considerably upon BA differentiation. Furthermore, the data indicate that human and murine BA differ strongly from one another, both in cGMP synthesis via GCs but also concerning cGMP degradation via PDEs. However, cGMP appears to be compartmentalized in both murine and human preBA and BA.

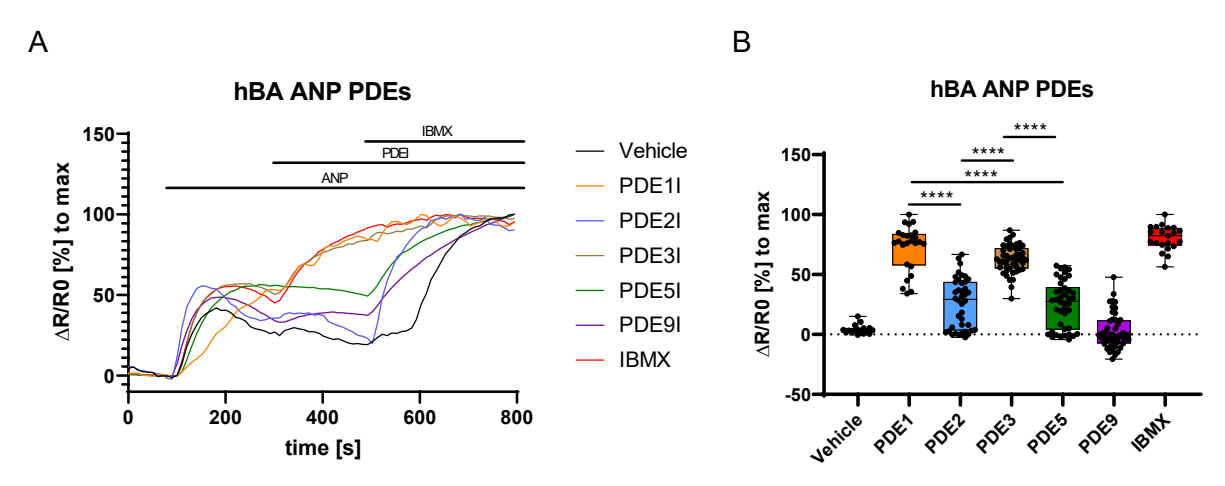


Figure 40: Regulation of NPRA-cGMP by PDEs in human BA

A Representative fluorescence intensity traces from Green cGull hBA upon stimulation with ANP (100 nM) with subsequent application of either PDE1I Iti-214 (100 nM), PDE2I Bay 60-7550 (100 nM), PDE3I Cilostamide (10 μ M), PDE5I Avanafil (1 μ M), PDE9I Bay 73-6691 (10 μ M) or pan PDE Inhibitor IBMX (100 μ M). **B** Quantification of fluorescence change of hBA in response to PDE1I, PDE2I, PDE3I, PDE5I, PDE9I, or IBMX after previous application of ANP in relation to complete PDE Inhibition by IBMX. Box-plots are represented as median \pm min/max. One-way ANOVA followed by post-hoc Tukey correction for multiple comparisons. n = 20-48, p* \leq 0.05, p** \leq 0.01, p**** \leq 0.001, p**** \leq 0.0001.

Since PDE1 was one of the main regulators of NPRA-cGMP in hBA, it was hypothesized that PDE1 might also facilitate a crosstalk between calcium and NPRA-cGMP in hBA. To probe this hypothesis, fully differentiated Green cGull hBA were first treated with ANP to initiate cGMP synthesis. Afterwards, the cells were perfused with lonomycin to induce calcium elevations. Importantly, a pronounced decrease in cGMP levels in response to lonomycin was observed (Figure 43A, B). Interestingly, this lonomycin-mediated cGMP decrease was far greater in hBA than in murine BA, almost entirely abrogating the cGMP signal, possibly indicating very tight control of NPRA-cGMP via PDE1 in hBA. Furthermore, if PDE1 was inhibited via Iti-214 preincubation, the calcium cGMP crosstalk was completely abolished, again indicating that PDE1 is critical for this effect.

In summary, these results demonstrate that calcium and NPR-mediated cGMP crosstalk is also present in hBA, similar to murine BA. Additionally, the data further substantiate the strong association between NPRA-cGMP and PDE1 in hBA, similar to fully differentiated murine BA.

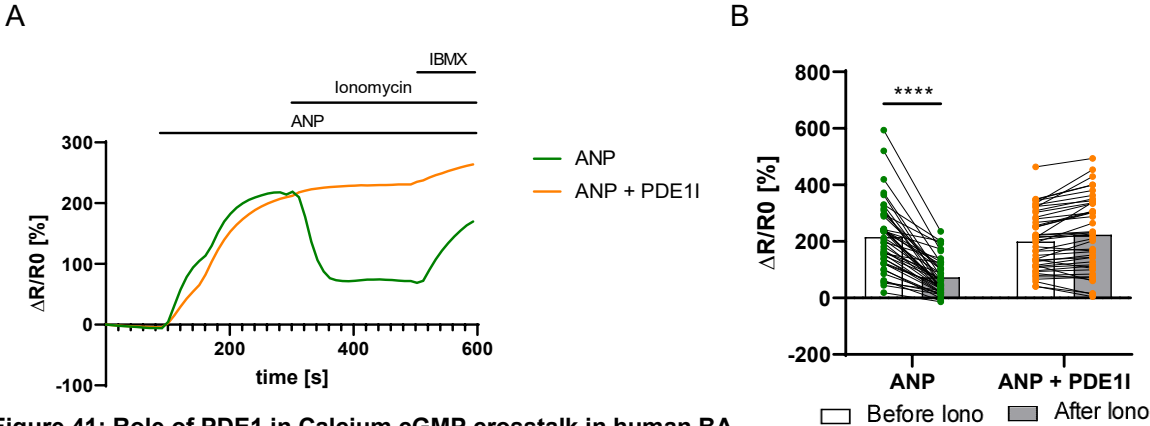


Figure 41: Role of PDE1 in Calcium cGMP crosstalk in human BA

A Representative fluorescence intensity traces from Green cGull expressing hBA perfused with ANP (100 nM) with or without previous PDE1I via Iti-214 (100 nM) treatment, and subsequent application of Ionomycin (1 μ M) and then IBMX (100 μ M) to elicit a maximum response. **B** Quantification of fluorescence intensity change to baseline from Green cGull expressing hBA treated with ANP with or without previous PDE1I via Iti-214 treatment. Paired results are connected and represent fluorescence intensity changes in % over baseline throughout the same measurement at different time points, either before or after Ionomycin addition. Two-way repeated-measures ANOVA followed by post-hoc Sidak correction for multiple comparisons. n = 44-45, p* \leq 0.05, p** \leq 0.01, p**** \leq 0.001, p**** \leq 0.0001.

4.16 Targeted cGMP sensors in hBA

To further scrutinize cGMP compartmentalization in human preBA, targeted single-fluorophore cGMP biosensors based on the Green cGull biosensor were developed. First, to create a nuclear-targeted cGMP indicator, the Green cGull biosensor was fused with a nuclear localization sequence to create Green cGull-NLS. Then the Green cGull-NLS biosensor sequence was subcloned into the rrl-CMV-lentiviral vector backbone. Ultimately, lentiviral particles were isolated and purified and used to transduce human preBA, as mentioned above. The nuclear localization of this sensor was confirmed by confocal imaging with a red nuclear stain via NucRed (Figure 44).

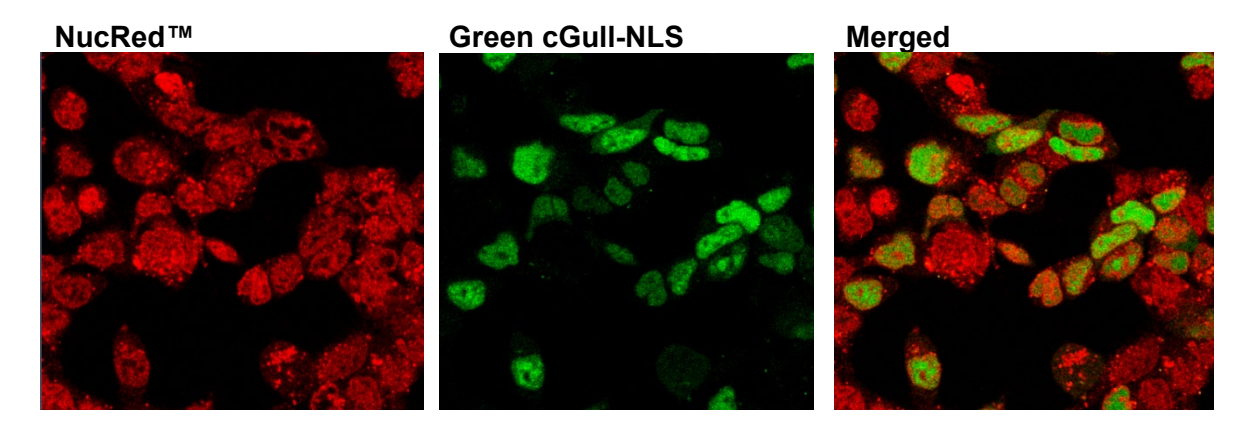


Figure 42: Fluorescence image of human preBA transduced with the Green cGull-NLS intensiometric biosensor

Cells were transduced via lentivirus for 72 hours before imaging took place. Nuclear staining was performed with NucRed according to the manufacturer's instructions. Images were acquired after CNP (100 nM) stimulation. Cells are shown at 63x magnification.

Next, the Green cGull biosensor was fused to the CAAX motif, a membrane localization sequence to create Green cGull-CAAX. The sensor sequence was again subcloned into the rrl-CMV lentiviral backbone to create lentiviral particles to transduce human preBA. The membrane-specific localization of this biosensor was then confirmed by confocal imaging using a red-membrane dye as a counterstain (Figure 45).

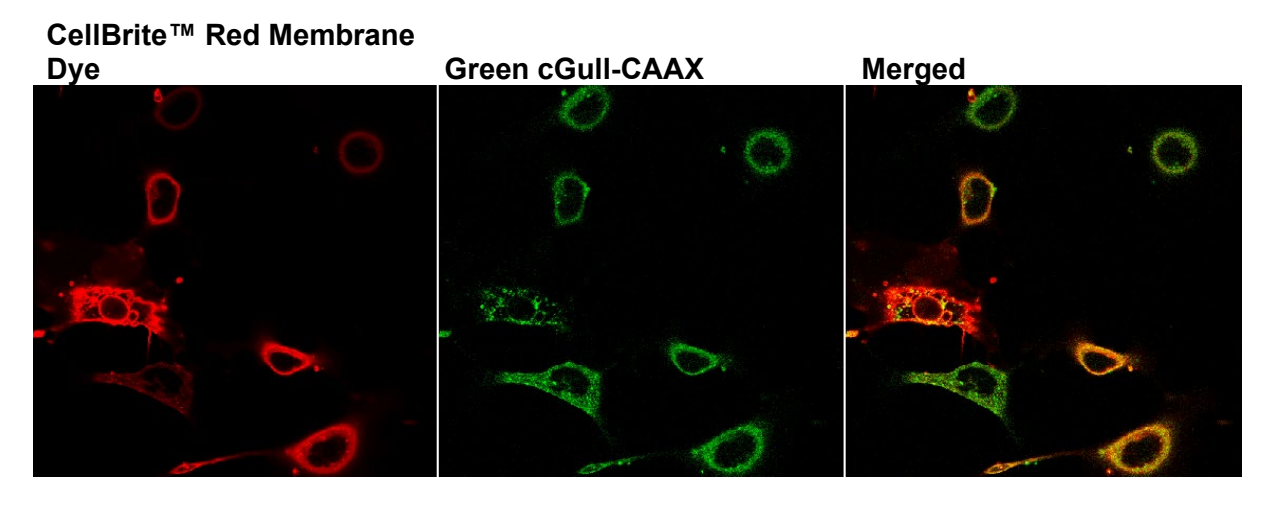


Figure 45: Fluorescence image from human preBA transduced with the Green cGull-CAAX intensiometric biosensor

Cells were transduced via lentivirus for 72 hours before imaging took place. Membrane staining was performed with the CellBrite™ Red Cytoplasmic Membrane Dye according to the manufacturer's instruction. Images were acquired after CNP (100 nM) stimulation. Cells are shown at 20x magnification.

Targeting sequences can alter the dynamic range of biosensors¹⁸⁶. Thus, the dose-response curves of the three different sensors to CNP, the main source of cGMP in human preBA were determined next. For this human preBA were transduced via lentivirus to express either Green cGull, Green cGull-NLS, or Green cGull-CAAX. 72 hours after transduction fluorescence measurements were performed. The transduced human preBA were perfused with CNP of

varying concentrations (1 nM, 10 nM, 30 nM, 60 nM, 100 nM, and 1000 nM), and the change in fluorescence was determined.

Green cGull-NLS had similar characteristics to the untargeted Green cGull biosensor in human preBA when treated with CNP (Green cGull EC $_{50}$: 67.6 nM, Green cGull-NLS EC $_{50}$: 36.6 nM; Green cGull 95% confidence interval (CI) of response: 226.0 to 276.8% signal intensity change, Green cGull-NLS 95% CI of response: 248.3 to 321.2 % signal intensity change) (Figure 46A, B).

Green cGull-CAAX on the other hand, also had similar EC_{50} for CNP but had reduced dynamic range (EC_{50} : 40.0 nM, 95% CI of response: 104.8 to 132.4% signal intensity change, 95% CI) (Figure 46C). Higher concentrations of CNP did not improve the fluorescence change for Green cGull-CAAX (Figure 46C).

In conclusion, the data show that Green cGull-NLS and Green cGull-CAAX can be utilized to study cGMP at distinct subcellular organelles. Green cGull-NLS demonstrates similar sensitivity and reactivity to CNP as the original Green cGull biosensor. Green cGull-CAAX however has a reduced dynamic range, but similar EC₅₀ for CNP.

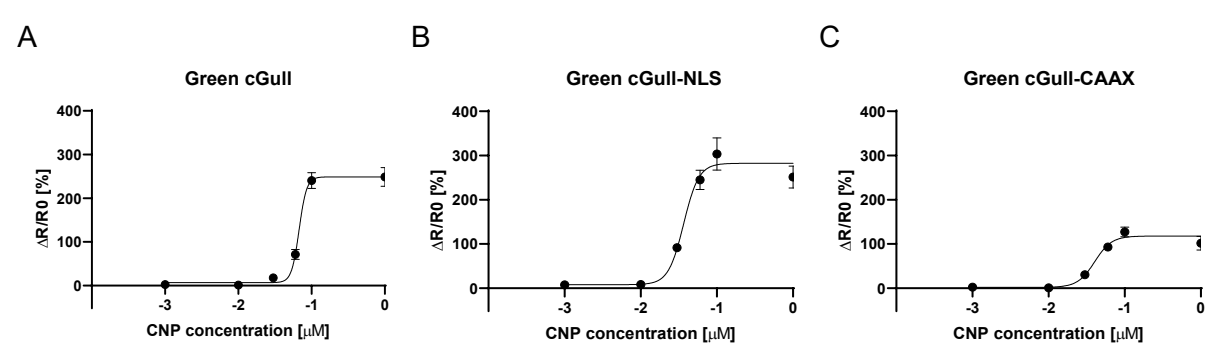


Figure 43: Targeted and untargeted Green cGull dose-response curves in human preBA to CNP A Dose-response curves for various CNP concentrations (1 nM, 10 nM, 30 nM, 60 nM, 100 nM, 1000 nM) in human preBA expressing either the Green cGull (A), Green cGull-NLS (B) or Green cGull-CAAX (C) cGMP biosensor. Data points are depicted as mean ± SEM. n = 19-39.

Table 46: Green cGull biosensors characteristics:

Sensor	EC ₅₀	Maximum Intensity Change (95% CI)
Green cGull	67.6 nM	226.0 to 276.8%
Green cGull-NLS	36.6 nM	248.3 to 321.2%
Green cGull-CAAX	40.0 nM	104.8 to 132.4%

Next, it was analyzed whether cGMP synthesis might differ at these organelles in human preBA.

CNP was the main source of cGMP in all three different compartments and the effect of CNP could be further enhanced by concomitant PDE inhibition by IBMX (Figure 47A-C). IBMX,

without concomitant GC stimulation, did not induce increases in cGMP in the cytosol or at the nucleus or membrane (Figure 47A-C). ANP induced significant cGMP signals in the cytosol and at the nucleus, albeit lower than CNP, but only induced a modest non-significant cGMP increase at the membrane (Figure 47A-C). Interestingly, NO induced a significant cGMP increase at the nucleus (Figure 47B), but not in the cytosol or at the membrane (Figure 47A, C, Figure 48). Furthermore, this nuclear cGMP signal was additionally enhanced by PDE inhibition via IBMX (Figure 47B).

Together, these data further substantiate the concept of cGMP compartmentalization in human preBA. Furthermore, they indicate that while NO may not induce significant cGMP increases in the cytosol, it does enhance cGMP levels at the nucleus, thus highlighting that cGMP synthesis within human preBA does not function in the same manner at every individual organelle.

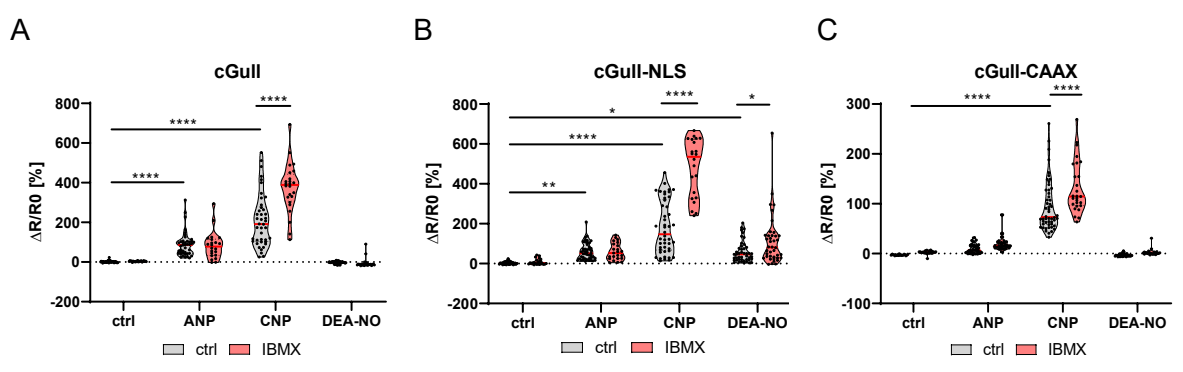


Figure 44: cGMP synthesis at different cell organelles in human preBA

A, B, C Quantification of fluorescence change in response to ANP (100 nM), CNP (100 nM), or DEA-NO (100 μ M) with or without concomitant IBMX (100 μ M) application in human preBA, expressing either the Green cGull (A), Green cGull-NLS (B) or Green cGull-CAAX (C) cGMP biosensor. Two-way ANOVA followed by post-hoc Holm-Sidak correction for multiple comparisons. n = 12-40, p* \leq 0.05, p** \leq 0.01, p*** \leq 0.001, p**** \leq 0.0001.

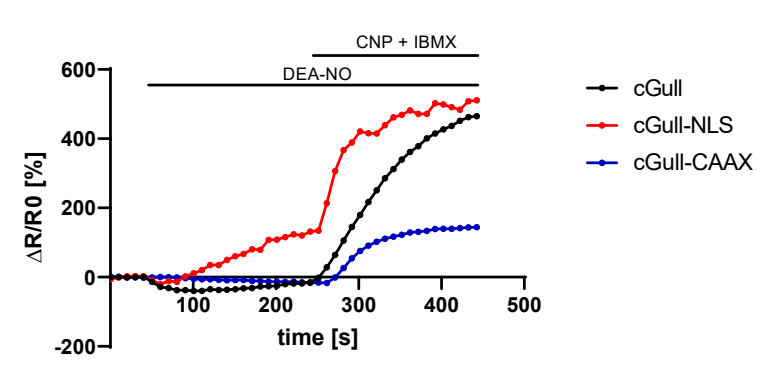


Figure 45: Fluorescence traces of DEA-NO induced cGMP synthesis at different cell organelles in human preBA

Representative fluorescence intensity traces from human preBA expressing either the Green cGull, Green cGull-NLS, or Green cGull-CAAX cGMP biosensor in response to DEA-NO (100 μ M) stimulation and later CNP+IBMX to elicit a maximum response.

5. Discussion

5.1 cGMP compartmentalization in murine BA and the role of PDE1

Mammals possess three canonical ways of synthesizing cGMP. Firstly, cGMP can be synthesized via the sGC in response to NO, which is released, for example, from endothelial cells in response to sheer stress^{115,280}. Secondly, cGMP can be synthesized via NPRA, and thirdly via NPRB. These receptors are activated via natriuretic peptides ANP or BNP and CNP, respectively²⁸¹. cGMP then affects downstream effectors, such as PKG, CNG channels, and PDEs^{148,151,152}.

Previous research has demonstrated that cGMP and its downstream effector PKG are vital for murine BA differentiation^{36,75,108}. preBA lacking PKG are unable to differentiate into lipid-laden functional brown adipocytes³⁶. Similar results were obtained in preBA lacking sGC, while, on the other hand, differentiation was potentiated when cells were treated with a sGC-stimulator⁷⁵. Furthermore, there has been ample evidence that the effects of cGMP are drastically different in murine versus primate adipocytes^{37,109–111,159}. The most prominent difference is that cGMP in primate adipocytes induces strong lipolytic responses, while no such effect can be observed in murine BA¹⁰⁹.

The concept of CN compartmentalization has been considered early in response to the observation that multiple cell types express more than one receptor linked to either ACs or GCs²³². Why should a cell express multiple receptors that lead to the generation of the same second messenger, if that second messenger freely diffuses within the cell without any degree of compartmentalization? How can a cell generate highly diverse responses, even opposing ones, such as proliferation or cell death, via the exact same second messenger²⁸²?

Recent research on cGMP and cAMP in cardiomyocytes has shed some light on this enigma. The authors demonstrated that cGMP does not freely diffuse within cardiomyocytes, but instead forms distinct subcellular clusters, so-called pools or signalosomes, which have distinct regulation patterns and functions^{231,240}. Specifically, only NPRB-cGMP led to positive inotropic effects, while NPRA-cGMP did not¹⁸⁵. This indicates that the same exact molecule, namely cGMP, has drastically different effects, depending on where and by which enzyme it is synthesized. In another publication, it was shown that CNP and BNP induce cGMP increases in different subcellular regions. In more detail, in adult rat cardiomyocytes CNP stimulation increases cGMP near phospholamban and troponin I, while BNP only induced cGMP at phospholamban¹⁸⁶.

Multiple studies, largely based on real-time imaging of cAMP or cGMP via genetically encoded biosensors (mainly FRET-based), have demonstrated that GC or AC activation does not result

in a homogenous increase of the respective CN throughout the entire cell, but instead leads to heterogeneous, locally confined signals^{153,186,254}.

Various hypotheses have been proposed on how such a subcellular compartmentalization could be achieved. Firstly, PDEs are believed to play a central role, with specific PDEs associating with specific compartments, acting as a barrier, thus preventing CNs from spilling outside of the individual pool^{185,186,229,254}. In addition to PDEs a physical phenomenon called liquid-liquid phase separation has recently been highlighted as a potential second mechanism central for cAMP compartmentalization²⁸³.

While the effects of total intracellular cGMP on BA are well understood it remains entirely unknown whether cGMP compartmentalization is also a factor in BA and, if so, how these cGMP pools are regulated and what their function is. Thus, the central aim of this thesis was to probe, whether cGMP is compartmentalized in BA and, if so, to characterize the different cGMP pools.

Importantly, the results presented here show that in preBA cGMP synthesized in response to the activation of different GCs, interacts with and is regulated by different subsets of PDEs. While cGMP from the sGC was mainly degraded via PDE3 and PDE9, cGMP from NPRB mainly interacted with PDE1 and PDE3. The fact that, depending on the cGMP-inducing stimulus, different PDEs are involved in regulating cGMP degradation, indicates that cGMP does not freely diffuse throughout the entire cell, but instead forms some sort of subcellular structure - signalosomes. Further evidence for this concept of compartmentalization in preBA was obtained by selectively activating PDE1 via calcium, a process that has been well-studied in other cell types^{214,284}. In these experiments calcium-induced either via G_□-DREADD and CNO or via Ionomycin exclusively interacted with NPRB-cGMP, but not sGC-cGMP. Importantly, this calcium to cGMP crosstalk could be entirely abolished by PDE1 inhibition. These observations fit the previous results, where PDE1 exclusively was involved in the regulation of NPRB-cGMP in murine preBA. Further substantiating the hypothesis of a specific interaction of PDE1 with NPRB-cGMP, and thus of cGMP compartmentalization, are the differentiation studies on murine BA presented here. It was found that, both on the mRNA and on the protein level, PDE1 inhibition enhanced specifically the NPRB-cGMP effect on the murine BA thermogenic and adipogenic program, while not potentiating the effect of the other cGMP stimuli. These observations highlight the functional relevance of cGMP compartmentalization in the regulation of murine BA differentiation.

These findings are of particular importance to the field of cGMP research, as improving our understanding of individual cGMP signalosomes could lead to the identification of distinct pools of cGMP which mediate particularly beneficial effects, thus leading to more precise development of future drugs. Understanding, which PDEs interact with these most

therapeutically desirable cGMP pools might lead to the discovery of promising targets for future obesity or diabetes treatments.

5.2 cGMP compartmentalization during BA differentiation

It is well understood that BA undergo significant changes during their differentiation process from fibroblast-like progenitor cells to fully mature, lipid-laden, thermogenic BA 31,34,36 . Changes in ligand sensitivity and receptor expression during this process are well documented for the cAMP signaling cascade 278 . Here previous studies have shown that the expression levels of β -AR change significantly during BA differentiation. As such β_3 -AR is only highly expressed in fully differentiated BA, but not in preBA. Consequently, fully differentiated BA respond strongly to specific β_3 -AR stimulation, while preBA do not 278 .

However, how the dynamics of cGMP synthesis and degradation change during BA differentiation remains unknown. Consequently, this thesis aimed to characterize the changes in cGMP synthesis, regulation, and compartmentalization during BA differentiation, thus probing whether cGMP compartmentalization is a phenomenon specific to preBA, or if it also exists in fully differentiated BA.

Interestingly, the data demonstrate that cGMP synthesis undergoes significant changes during BA differentiation. Firstly, the GC expression levels are drastically altered, with NPRB being significantly downregulated during BA differentiation, while NPRA and *Gucy1a1* and *Gucy1b1* are both upregulated. NPRA proved to be particularly interesting as its mRNA expression levels are overall rather low, but during day 4 of differentiation the mRNA expression levels transiently increase by approximately 74-fold. These results show that GC expression changes significantly between murine preBA and BA, but also that during the process of differentiation substantial, in part transient, gene expression alterations occur. A limitation of this study is that the BA differentiation was carried out *in vitro*, where cell culture artifacts cannot entirely be excluded. For example, a downregulation of various GCs was observable on day 2 of differentiation, where cells had been exposed to IBMX for 48 hours, possibly artificially leading to downregulation of all cGMP synthesizing enzymes. However, the results at other timepoints, such as day 4, appear more trustworthy, as no IBMX is present in the differentiation media.

Similar to the gene expression data, direct cGMP measurements via FRET revealed that cGMP synthesis is also altered during differentiation. In preBA, significant cGMP increases can be detected after CNP-NPRB and NO-sGC stimulation. However, no cGMP increase can be detected in the cytosol of murine preBA in response to ANP-NPRA stimulation. In fully differentiated BA, on the other hand, ANP, CNP, and NO all induced significant increases in cytosolic cGMP, with NO representing the main source of cGMP, followed by ANP. Thus, BA

switch from predominantly synthesizing cGMP via CNP-NPRB in preBA to mainly NO-sGC and ANP-NPRA mediated cGMP in BA.

What is surprising is the fact that ANP induces a larger increase in cytosolic cGMP in murine BA than CNP does, even though *Nprb* gene expression is considerably higher. A possible explanation might lie in cGMP compartmentalization, with NPRB-mediated cGMP possibly being confined to the membrane and consequently unable to reach the cytosolic cGMP FRET sensor. Alternatively, the NPRB-cGMP pool might be more tightly regulated by PDEs in mature BA. It might also be the case that the observed differences in mRNA expression don't completely translate into differences at the protein- or the functional level.

On the other hand, ANP does not induce cytosolic cGMP elevations in preBA, but still enhances adipogenic and thermogenic differentiation in adipocytes, as shown in this thesis and by other publications³⁷. A possible explanation for this phenomenon might lie in the transient strongly upregulated expression of *Npra* mRNA at day 4 of murine BA differentiation. Alternatively, it could be that ANP induces a non-cytosolic cGMP pool, which remains confined to certain organelles by PDEs, hence being undetectable in the cytosol, yet still exerting effects on differentiation.

The relevance of the NO-sGC pathway has already been demonstrated in murine BA⁷⁵. The findings of this thesis support the hypothesis that NO-mediated cGMP is of pivotal importance in murine BA, as NO induces significant cGMP elevations in both murine preBA and BA.

In summary, these findings suggest, that different drugs are effective at inducing cGMP elevation in murine preBA versus BA. Hence, if cGMP elevations are desired in preBA CNP should be used, while NO is most effective at inducing cGMP increases in fully differentiated murine BA. Via ANP a specific cytosolic cGMP elevation can be achieved in fully or, potentially, partially differentiated BA.

Importantly, the data indicate that cGMP compartmentalization is also observable in fully differentiated murine BA. Again, PDE1 was only associated with NPRB-cGMP, but not with sGC-cGMP. On the other hand, PDE9 was only associated with NPRA-cGMP, but neither with NO-cGMP nor with NPRB-cGMP. These results suggest that in murine BA there is not only a division between soluble sGC-associated cGMP and particular NPR-associated cGMP but also between NPRA and NPRB-mediated cGMP, thus indicating at least three distinct cGMP pools, each associated with one individual GC.

Further supporting the concept of cGMP compartmentalization in mature BA is again the NPR-specific calcium cGMP crosstalk. The data indicate that calcium in murine BA induced via lonomycin led to a reduction in cytosolic cGMP only after NPRA or NPRB stimulation, but not after NO-sGC stimulation, again demonstrating the specific interaction between PDE1 and

NPR-cGMP. Surprisingly, the calcium-activated PDE1 was involved in cGMP degradation from both NPRA and NPRB, even though PDE1 inhibition in the absence of calcium only enhanced NPRB-cGMP. A possible explanation might be that in a calcium-activated state PDE1 activity and subcellular location might change causing PDE1 to interact also with NPRA-cGMP, which it might not do in a non-activated calcium-free state. Another explanation might be that PDE1-mediated NPRA-cGMP degradation in its basal state is rather low and thus undetectable by the cGi-500 FRET biosensor, while in its activated state, this effect becomes measurable.

Additionally, not only did cGMP synthesis via GCs change during BA differentiation but instead also the regulation of individual cGMP pools by PDEs was also altered. While sGC-cGMP in preBA interacted with PDE3 and PDE9, sGC-cGMP in murine BA interacted mainly with PDE2 and PDE3.

In summary, these findings highlight that not only cGMP synthesis but also cGMP compartmentalization changes during BA differentiation. Consequently, pharmacological activation of specific compartments in distinct cell types appears feasible. In particular, PDE9 inhibition would selectively enhance sGC-cGMP only in preBA but not mature BA. This is especially interesting, considering recent publications highlighting PDE9 as a promising target to combat obesity, as mice lacking PDE9 or receiving a PDE9 inhibitor both were protected from obesity, due to enhanced cGMP signaling and adipose tissue function^{73,74}. The results of this thesis might suggest that this PDE9 inhibition could have selectively enhanced NO-sGC-cGMP in preBA leading to better-developed more active BAT. However, effects on WAT, or activation of NPRA-cGMP in fully differentiated BA, cannot be excluded and might also be responsible for some of the observed effects.

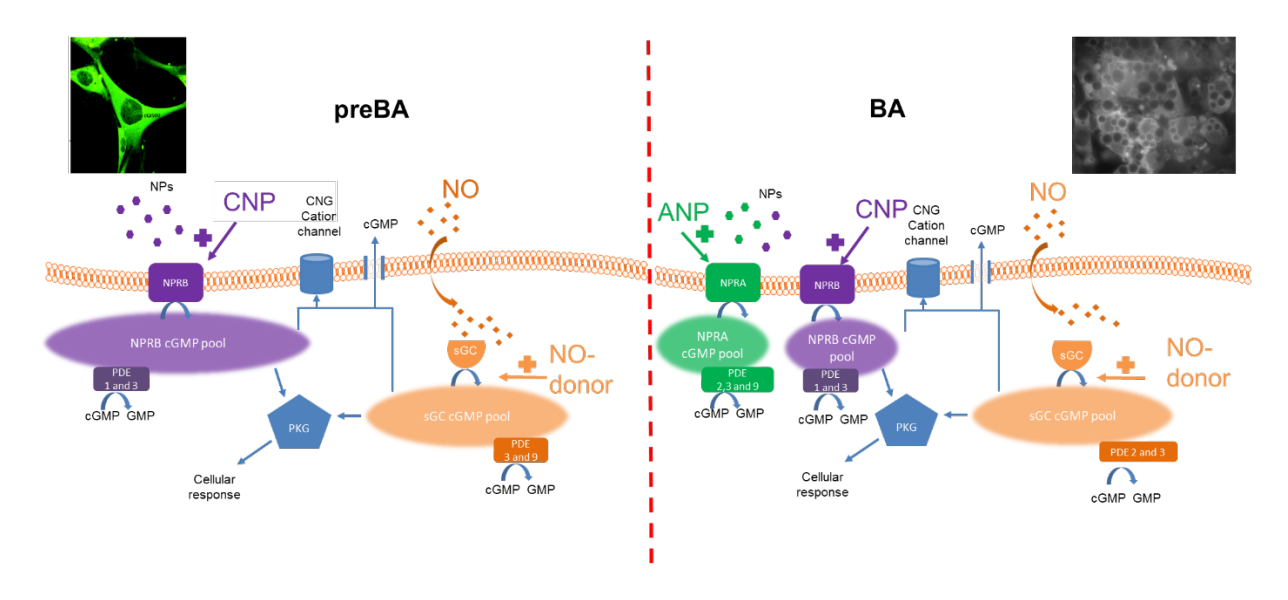


Figure 46: Schematic depiction of the association of different cGMP pools with their specific PDEs in murine preBA and BA

5.3 cGMP-cAMP crosstalk in brown adipocytes

Given the high expression levels of PDE2A, 3A, and especially 3B in adipocytes and their documented involvement in conveying the crosstalk between cGMP and cAMP, it was hypothesized that cGMP might influence cAMP levels in (pre-)BA and might thus also indirectly enhance lipolysis in murine BA. It is well established that PDE2 and PDE3 serve as important downstream effectors of cGMP^{129,153}. cGMP can either activate PDE2 thus reducing intracellular cAMP levels or inhibit PDE3 thus increasing intracellular cAMP levels^{129,153}.

In cardiomyocytes, this interaction has been previously described in more detail. Cardiomyocytes express two different isoforms of PKA. PKA-RI and PKA-RII, which localize to different subcellular compartments. Interestingly, the authors observed that sGC-cGMP can at the same time increase cAMP in the PKA-RI compartment while simultaneously decreasing cAMP in the PKA-RII compartment, by either inhibiting PDE3 or activating PDE2 in a spatially distinct manner¹⁵³. However, whether different pools of cGMP might also have different effects on distinct pools of cAMP, remains unknown. Additionally, the compartmentalization of cAMP in murine preBA and BA has already been demonstrated in a recent publication. Here the authors also found alterations in the regulation of different cAMP pools during BA differentiation²⁷⁸.

Considering previous results of this thesis that demonstrate cGMP compartmentalization, it was, thus, hypothesized that in murine preBA and BA distinct cGMP pools might also be able to modulate cAMP levels via PDE inhibition or activation and that this crosstalk might also be compartment specific. Yet which effect outweighs the other, either PDE2 activation or PDE3 inhibition remains unclear.

In the present work, the data demonstrate that cGMP-cAMP crosstalk is indeed observable in both murine preBA and BA. In preBA, FRET imaging revealed that cGMP elevations, via either NO or CNP, resulted in increases in cytosolic cAMP, while ANP did not show any effect on cAMP levels. This is potentially explained by ANP inducing no detectable increase in cytosolic cGMP in murine preBA, thus not significantly affecting either PDE2 or PDE3. Importantly, the results obtained from NO and CNP stimulation suggest that the cGMP-mediated inhibition of PDE3 outweighs the cGMP-induced activation of PDE2 in murine preBA, thus leading to increased cytosolic cAMP levels. Further substantiating this hypothesis are the results that show that PDE3 inhibition completely abolishes the CN crosstalk, while PDE2 inhibition did not alter the CN crosstalk significantly. Fitting the gene expression data, in which *Pde3* mRNA is shown to be more highly expressed than *Pde2* mRNA, it was also shown that PDE3 but not PDE2 has substantial basal activity in degrading cAMP. Also noteworthy is the more rapid cAMP increase detected in response to sGC-cGMP versus NPRB-cGMP. This faster response might be explained by the sGC-cGMP pool being located more closely than the

NPRB-cGMP pool to the cytosolic cAMP pool, thus, facilitating more rapid cAMP increases via PDE3 inhibition.

In summary, these experiments highlight the existence of a cGMP-cAMP crosstalk in murine preBA and characterize this as a positive crosstalk in which cGMP enhances cAMP signals primarily via PDE3 inhibition. The results regarding the role of PDE3A and PDE3B in CN crosstalk are of particular interest, as PDE3B is the most highly expressed PDE in murine preBA and BA. Furthermore, previous studies have shown the major importance of PDE3B in regulating BAT function and metabolism^{285–287}.

In fully differentiated murine BA the epac1-camps FRET indicator proved to be insufficiently selective for cAMP over cGMP. Previous studies have shown that cAMP levels increase upon BA differentiation²⁷⁸. This thesis found similar results for cGMP, where a more than 10-fold increase in basal cGMP was observed upon differentiation of BA. Hence, in fully differentiated BA cGMP levels are relatively high and are further enhanced via NO, ANP, or CNP stimulation. These very high levels of cGMP then activate the epac1-camps FRET sensor in a crosstalk-independent, nonspecific, manner. This is demonstrated in murine BA by complete inhibition of PDE2 and PDE3 not abolishing the FRET ratio change in epac1-camps expressing BA in response to a cGMP-inducing stimulus such as NO. Thus, demonstrating that the epac1-camps biosensor is unsuitable to characterize the CN crosstalk in fully differentiated murine BA.

However, by utilizing a highly selective ELISA the compartment-specific CN crosstalk could be studied in murine BA. In general, the CN crosstalk was again positive, with ANP and to a lesser extent CNP inducing cAMP elevations. However, the responses to NO were more nuanced. Indeed, the data indicate that sGC-cGMP can decrease cAMP levels, but only if cAMP was induced via β₂-AR stimulation. Surprisingly, if cAMP is induced by β₁-AR stimulation the opposite effect is observed. Here sGC-cGMP enhances cAMP levels, presumably via PDE3A and PDE3B inhibition. Concomitant inhibition of PDE2A completely abolished the negative crosstalk between sGC-cGMP and β₂-AR-cAMP. Interestingly, by measuring cGMP in murine BA via FRET a close association between sGC-cGMP and PDE2 as well as PDE3 was detected. This might explain why sGC-cGMP can at the same time enhance some cAMP pools while simultaneously reducing other cAMP pools associated with different β-AR. The interaction between sGC-cGMP and β₂-AR-cAMP might be mediated predominantly via PDE2, explaining why sGC-cGMP reduces β₂-AR associated cAMP. On the other hand, the interaction between sGC-cGMP and β₁-AR induced cAMP might be facilitated mainly via PDE3, resulting in cGMP-mediated PDE3 inhibition and thus elevating cAMP levels. This hypothesis is further substantiated by PDE2 inhibition completely abolishing the negative cGMP to cAMP crosstalk observed between sGC-cGMP and β₂-AR-cAMP.

Together these data suggest that simply looking at bulk cytosolic cGMP and cAMP is not sufficient to fully understand the dynamics of cGMP-cAMP crosstalk and that distinct individual pools of cGMP can interact via different PDEs with distinct individual pools of cAMP. Thus, cGMP can enhance cAMP signals from specific β -AR, while at the same time inhibiting cAMP signals from other β -AR, further underscoring the compartmentalization of these two CN.

It is well established that cGMP by itself cannot induce lipolysis in murine adipocytes, but only in primate BA. Different hypotheses have been proposed to explain this phenomenon. One widely spread explanation is that murine adipocytes in general express high levels of the NP clearance receptor NPRC. This hypothesis is supported by a publication that demonstrated that in WA, taken from mice lacking NPRC, NP treatment did indeed induce lipolysis³⁷. However, if this were the case for BA, then cGMP induced by non-NP sources, i.e. NO or 8-Br-cGMP, should induce lipolysis also in murine adipocytes. Yet the experiments presented in this thesis clearly show that neither ANP, CNP, NO nor 8-Br-cGMP itself induce any increases in lipolysis in murine BA. A possible explanation might be that high NPRC expression ablates NP-induced lipolysis only in WA, but not in BA, however, this seems unlikely as murine BA also express NPRC far more highly than human BA. The second hypothesis that might explain this species difference is that human PKG has a different phosphorylation pattern than murine PKG regarding its lipolysis-associated target proteins²⁸⁸. This hypothesis would explain why no source of cGMP, nor cGMP itself in the form of 8-Br-cGMP could induce lipolysis in murine BA.

In summary, the work presented here demonstrates the existence of a cGMP-cAMP crosstalk in both murine preBA and BA, in a similar fashion as it has been shown in other cell types such as cardiomyocytes. However, the data expands upon the concept of total cytosolic cGMP interacting with total cytosolic cAMP and instead paints a more compartmentalized picture with distinct cGMP pools interacting via different PDEs with distinct β -AR associated cAMP pools. Conclusively, cGMP can increase or decrease different individual cAMP pools at the same time via either PDE2 activation or PDE3 inhibition.

5.4 cGMP synthesis in human adipocytes

Extensive evidence has already been presented describing the differences between cGMP signaling and effects on adipocytes from mice versus primates^{109–111,129,159}. The most striking difference is clearly that acute cGMP exposure activates primate adipocytes by inducing PKG-mediated lipolysis, while no such effect can be observed in murine adipocytes^{37,109}. As mentioned above, explanations for this phenomenon, such as a high NPRC expression in murine adipocytes, are insufficient, as they don't explain why NO does not induce lipolysis in murine adipocytes. Even though the difference in cGMP downstream effects has been well characterized previously, little is known about how cGMP synthesis, degradation, and possibly

compartmentalization might differ between adipocytes from the two species. Therefore, this study aimed to analyze cGMP synthesis, degradation, and compartmentalization in human (pre-)BA and to compare the findings to murine (pre-)BA.

As no transgenic human adipocytes, expressing a cGMP biosensor, such as cGi-500, exist, a new transgenic cell line had to be created for these experiments. This was achieved by first isolating human brown adipocytes from the parathyroidal area from patients undergoing thyroid surgery and then using lentivirus to transduce these cells with the intensiometric cGMP indicator Green cGull²⁷¹. This non-immortalized cell line could then be used immediately for experiments.

The Green cGull biosensor was chosen because it has several advantages over the cGi-500 FRET sensor. Firstly, it is a single fluorophore biosensor, which makes it easier to add targeting sequences to it, allowing for later organelle-specific targeting. Secondly, the sensor is more resistant to photobleaching, as it is based on the citrine fluorophore instead of CFP. Thirdly, Green cGull has a remarkable dynamic range, facilitating intensity changes of up to 700%, while cGi-500 only shows far smaller FRET ratio changes (10 - 50%). Additionally, single fluorophore indicators are immune to the bleed-through phenomena. A major downside of this sensor is that it is very dim, making it impossible to identify transduced adipocytes before the start of the measurement, as basal cGMP levels don't sufficiently activate the sensor.

Yet, transduction via lentivirus yielded high transduction efficiencies (> 70%), allowing for the imaging of many transduced cells at the same time (10 - 20 cells per field of view). However, it was observed that if hBA were transduced early during their differentiation, the cells would no longer differentiate well into mature lipid-laden adipocytes. More specifically, with an early transduction approach, it was observed that the only cells fluorescing were the transduced, non-differentiated, fibroblast-like adipocyte progenitors, while the fully differentiated adipocytes showed no sensor expression. These results suggest that cells that are successfully transduced with Green cGull are unable to differentiate into fully mature BA. A possible explanation for this phenomenon might be that high expression of Green cGull leads to considerable cGMP buffering within the transduced cells. As cGMP is vital for adipocyte differentiation, both in murine and human adipocytes, this cGMP buffering might prevent the transduced cells from developing into mature BA. Instead, more success was achieved by transducing the adipocytes at a later time point, when the cells were already differentiated (day 9 of the 12-day protocol). Imaging then took place 72 hours after transduction to allow for high expression of Green cGull in fully differentiated mature human BA.

Strikingly, the dynamics of cGMP synthesis, degradation, and also compartmentalization were significantly different in human BA versus murine BA. Gene expression analysis via qRT-PCR already suggested that the mRNA expression of the genes coding for the sGC (*GUCY1A1* and

GUCY1B1) were drastically reduced in human BA, compared to murine preBA and BA. On the other hand, the mRNA expression of NPRs was far higher in human BA and the expression of the clearance receptor NPRC was, relative to the NPRA and NPRB expression, far lower in human BA than in murine BA. Indeed, neither in human preBA nor in hBA, did NO induce any detectable increase in cGMP. This fits the low GUCY mRNA expression data but is in stark contrast to murine BA, where NO induces cGMP in both preBA and BA. In human preBA, CNP was the main source of cGMP, similar to murine preBA. ANP induced significant increases in cytosolic cGMP, albeit less than CNP, in human preBA, while not inducing any detectable cGMP increases in murine preBA. Together these results suggest, that human preBA differ considerably from murine BA regarding cGMP synthesis.

Furthermore, in murine preBA, a switch in cGMP synthesis was observed during differentiation from cGMP synthesis being mainly CNP mediated to being mainly NO and ANP mediated. A switch in cGMP synthesis was also seen in hBA during differentiation, but not towards NO-sGC-cGMP. Instead, in fully differentiated hBA only ANP induced detectable cGMP increases, while both CNP and NO showed no change in cytosolic cGMP. These results are surprising, given the high mRNA expression of *NPRB* in fully differentiated hBA. Three possible explanations can be considered. Firstly, cGMP synthesized via CNP-NPRB could be tightly controlled by PDEs, resulting in the cGMP signal being suppressed in the absence of PDE inhibitors, such as IBMX. Secondly, the cGMP induced by CNP might be locally confined to a part of the cell, that is not the cytosol, i.e. a compartment where Green cGull is not expressed, such as the membrane. Alternatively, mRNA and protein expression might differ from one another.

In summary, these experiments showed that cGMP synthesis also changes during human BA differentiation. However, these changes are different compared to murine BA. In murine BA cGMP synthesis switched from CNP to NO and ANP, while in human BA it switched from CNP and ANP to only ANP. NO never induced detectable cGMP increases in human BA and the expression of sGC-related genes is low in human preBA and hBA. Together, these findings might suggest that NO is a less promising target to induce cGMP elevations in human preBA and hBA than NPs. Targeting NPRA might be especially promising as ANP stimulation induces cGMP increases in both human preBA and BA. Furthermore, other studies have shown that ANP also induced lipolysis in hBA and that PDE9 inhibition further potentiates this response⁷⁴.

5.5 cGMP compartmentalization in human brown adipocytes

cGMP compartmentalization has been investigated in various cell types. Most of these cell types stem from murine origin^{185,237}. However, some more recent publications have also investigated whether cyclic nucleotides, or cGMP specifically might also be compartmentalized

in human cells^{289,290}. Indeed, in human induced pluripotent stem cell-derived cardiomyocytes, cGMP compartmentalization has been described²⁹⁰.

Given the relatively close evolutionary relatedness of mice and humans and the highly conserved nature of second messenger signaling, it is to be expected that second messengers, like cGMP, should also be compartmentalized in human cells. Furthermore, considering that cGMP compartmentalization is present and functionally relevant in murine BA, as demonstrated in this thesis, it is likely that cGMP should also be compartmentalized in hBA.

Indeed, the data presented in this thesis demonstrate that in human preBA at least two separate cGMP pools exist. cGMP generated via CNP mainly interacted with PDE 5 and 9. On the other hand, NPRA-cGMP, induced via ANP, was mainly degraded via PDE 1 and 9, but not via PDE5. The association of these different cGMP pools with different subsets of PDEs indicates a spatial separation. Interestingly, the CNP-NPRB-cGMP pool was regulated by different PDEs compared to the same pool in mice, where PDE1 and PDE3 were the main contributors to cGMP degradation, highlighting species-specific differences in cGMP compartmentalization architecture.

Furthermore, organelle-targeted cGMP biosensors, created in this project, revealed that while NO does not induce significant increases in cytosolic cGMP, NO does induce significant increases in nuclear cGMP (see Figure 47 - 48) in human preBA. A caveat to this observation is the slightly increased dynamic range, as well as the slightly lower EC₅₀ value of the nuclear-targeted Green cGull-NLS biosensor. Due to these factors, it cannot be excluded that the sensor simply detects very minor increases in cGMP at the nucleus, which the non-targeted sensor could not detect in the cytosol.

Taken together, these findings demonstrate that cGMP is also compartmentalized in human preBA and that the subcellular architecture of cGMP compartmentalization differs between murine and human BA.

Based on the previous findings presented here, cGMP compartmentalization is also expected to be present in fully differentiated hBA. However, given that only ANP induces cGMP in human BA, no GC-specific cGMP compartmentalization could be explored. Beyond GC-associated cGMP compartmentalization, it could also be possible that cGMP from the same GC, namely NPRA, might diffuse into different subcellular compartments. For example, into a compartment associated with certain organelles, such as mitochondria or the cytoplasmic membrane. This hypothesis requires further investigation using the organelle-targeted cGMP sensors developed here.

However, the association between PDE1 and NPRA-cGMP in hBA could also be verified via calcium induction. Inducing calcium increases in hBA via Ionomycin caused a significant

decrease in NPRA-cGMP, which was completely dependent on PDE1. This potentially highlights PDE1 as a promising target to enhance ANP-mediated cGMP in fully differentiated hBA, thus inducing lipolysis and energy expenditure, and thus as a target for novel obesity treatments.

References

- 1. HEPATOLOGY, THE LANCET GASTROENTEROLOGY &., 'Obesity: another ongoing pandemic', *The Lancet Gastroenterology & Hepatology*, 6/6 (2021), 411.
- 2. 'Obesity and overweight', 2022 https://www.who.int/news-room/fact-sheets/detail/obesity-and-overweight, updated 15 Sep 2022, accessed 10 Apr 2022.
- 3. BLÜHER, MATTHIAS, 'Obesity: global epidemiology and pathogenesis', *Nature reviews*. *Endocrinology*, 15/5 (2019), 288–98.
- 4. GARROW, J. S., and WEBSTER, J., 'Quetelet's index (W/H2) as a measure of fatness', *International journal of obesity*, 9/2 (1985), 147–53.
- 5. POWELL-WILEY, TIFFANY M., POIRIER, PAUL, BURKE, LORA E. et al., 'Obesity and Cardiovascular Disease: A Scientific Statement From the American Heart Association', *Circulation*, 143/21 (2021), e984-e1010.
- 6. CERCATO, C., and FONSECA, F. A., 'Cardiovascular risk and obesity', *Diabetology & metabolic syndrome*, 11 (2019), 74.
- 7. 'World_Obesity_Atlas_2022' https://s3-eu-west-1.amazonaws.com/wof-files/World_Obesity_Atlas_2022.pdf, accessed 4 Oct 2022.
- 8. Vos, Theo, Lim, Stephen S., Abbafati, Cristiana et al., 'Global burden of 369 diseases and injuries in 204 countries and territories, 1990–2019: a systematic analysis for the Global Burden of Disease Study 2019', *The Lancet*, 396/10258 (2020), 1204–22.
- 9. Cannon, Barbara, and Nedergaard, Jan, 'Thermogenesis challenges the adipostat hypothesis for body-weight control', *The Proceedings of the Nutrition Society*, 68/4 (2009), 401–7.
- 10. MA, IRENE T., and MADURA, JAMES A., 'Gastrointestinal Complications After Bariatric Surgery', *Gastroenterology & Hepatology*, 11/8 (2015), 526–35.
- 11. CINTI, S., 'The adipose organ', *Prostaglandins, leukotrienes, and essential fatty acids*, 73/1 (2005), 9–15.
- 12. CANNON, BARBARA, and NEDERGAARD, JAN, 'Brown adipose tissue: function and physiological significance', *Physiological reviews*, 84/1 (2004), 277–359.
- 13. PFEIFER, ALEXANDER, and HOFFMANN, LINDA S., 'Brown, beige, and white: the new color code of fat and its pharmacological implications', *Annual review of pharmacology and toxicology*, 55 (2015), 207–27.
- 14. ROSEN, EVAN D., and SPIEGELMAN, BRUCE M., 'What we talk about when we talk about fat', Cell, 156/1-2 (2014), 20–44.
- 15. ZHANG, Y., PROENCA, R., MAFFEI, M. et al., 'Positional cloning of the mouse obese gene and its human homologue', *Nature*, 372/6505 (1994), 425–32.
- 16. PEIRCE, VIVIAN, CAROBBIO, STEFANIA, and VIDAL-PUIG, ANTONIO, 'The different shades of fat', *Nature*, 510/7503 (2014), 76–83.
- 17. ROSENWALD, MATTHIAS, and WOLFRUM, CHRISTIAN, 'The origin and definition of brite versus white and classical brown adipocytes', *Adipocyte*, 3/1 (2014), 4–9.
- 18. Wu, Jun, Boström, Pontus, Sparks, Lauren M. et al., 'Beige adipocytes are a distinct type of thermogenic fat cell in mouse and human', *Cell*, 150/2 (2012), 366–76.
- 19. SEALE, PATRICK, CONROE, HEATHER M., ESTALL, JENNIFER et al., 'Prdm16 determines the thermogenic program of subcutaneous white adipose tissue in mice', *The Journal of clinical investigation*, 121/1 (2011), 96–105.
- 20. Shao, Mengle, Wang, Qiong A., Song, Anying et al., 'Cellular Origins of Beige Fat Cells Revisited', *Diabetes*, 68/10 (2019), 1874–85.
- 21. PILKINGTON, ANNA-CLAIRE, PAZ, HENRY A., and WANKHADE, UMESH D., 'Beige Adipose Tissue Identification and Marker Specificity-Overview', *Frontiers in Endocrinology*, 12 (2021), 599134.

- 22. ZURIAGA, MARIA A., FUSTER, JOSE J., GOKCE, NOYAN et al., 'Humans and Mice Display Opposing Patterns of "Browning" Gene Expression in Visceral and Subcutaneous White Adipose Tissue Depots', *Frontiers in cardiovascular medicine*, 4 (2017), 27.
- 23. LAURY, M.C, CHAPEY, M.F, and PORTET, R., 'Involvement of the sympathetic nervous system in lipolytic activity in brown adipose tissue of cold acclimated rats', *Comparative Biochemistry and Physiology Part A: Physiology*, 87/1 (1987), 197–203.
- 24. LEE, MI-JEONG, WU, YUANYUAN, and FRIED, SUSAN K., 'Adipose tissue heterogeneity: implication of depot differences in adipose tissue for obesity complications', *Molecular aspects of medicine*, 34/1 (2013), 1–11.
- 25. Song, Anying, Dai, Wenting, Jang, Min Jee et al., 'Low- and high-thermogenic brown adipocyte subpopulations coexist in murine adipose tissue', *The Journal of clinical investigation*, 130/1 (2020), 247–57.
- 26. CHERNUKHA, IRINA, FEDULOVA, LILIYA, and KOTENKOVA, ELENA, 'White, beige and brown adipose tissue: structure, function, specific features and possibility formation and divergence in pigs', *Foods and Raw Materials*, 2022, 10–8.
- 27. PARK, KYE WON, HALPERIN, DANIEL S., and TONTONOZ, PETER, 'Before they were fat: adipocyte progenitors', *Cell metabolism*, 8/6 (2008), 454–7.
- 28. ROSEN, E. D., WALKEY, C. J., PUIGSERVER, P. et al., 'Transcriptional regulation of adipogenesis', *Genes Dev.*, 14/11 (2000), 1293–307.
- 29. MOTA DE SÁ, PAULA, RICHARD, ALLISON J., HANG, HARDY et al., 'Transcriptional Regulation of Adipogenesis', *Comprehensive Physiology*, 7/2 (2017), 635–74.
- 30. LEE, JI-EUN, SCHMIDT, HANNAH, LAI, BINBIN et al., 'Transcriptional and Epigenomic Regulation of Adipogenesis', *Molecular and cellular biology*, 39/11 (2019).
- 31. TANAKA, T., YOSHIDA, N., KISHIMOTO, T. et al., 'Defective adipocyte differentiation in mice lacking the C/EBPbeta and/or C/EBPdelta gene', *The EMBO journal*, 16/24 (1997), 7432–43.
- 32. BARAK, Y., NELSON, M. C., ONG, E. S. et al., 'PPAR gamma is required for placental, cardiac, and adipose tissue development', *Molecular cell*, 4/4 (1999), 585–95.
- 33. Wu, Z., Rosen, E. D., Brun, R. et al., 'Cross-regulation of C/EBP alpha and PPAR gamma controls the transcriptional pathway of adipogenesis and insulin sensitivity', *Molecular cell*, 3/2 (1999), 151–8.
- 34. GUO, LIANG, LI, XI, and TANG, QI-QUN, 'Transcriptional regulation of adipocyte differentiation: a central role for CCAAT/enhancer-binding protein (C/EBP) β ', *The Journal of biological chemistry*, 290/2 (2015), 755–61.
- 35. KAJIMURA, SHINGO, SEALE, PATRICK, and SPIEGELMAN, BRUCE M., 'Transcriptional Control of Brown Fat Development', *Cell metabolism*, 11/4 (2010), 257–62.
- 36. HAAS, BODO, MAYER, PETER, JENNISSEN, KATJA et al., 'Protein kinase G controls brown fat cell differentiation and mitochondrial biogenesis', *Science signaling*, 2/99 (2009), ra78.
- 37. BORDICCHIA, MARICA, LIU, DIANXIN, AMRI, EZ-ZOUBIR et al., 'Cardiac natriuretic peptides act via p38 MAPK to induce the brown fat thermogenic program in mouse and human adipocytes', *The Journal of clinical investigation*, 122/3 (2012), 1022–36.
- 38. HAMAN, FRANÇOIS, and BLONDIN, DENIS P., 'Shivering thermogenesis in humans: Origin, contribution and metabolic requirement', *Temperature (Austin, Tex.)*, 4/3 (2017), 217–26.
- 39. VAN MARKEN LICHTENBELT, WOUTER, 'Brown adipose tissue and the regulation of nonshivering thermogenesis', *Current opinion in clinical nutrition and metabolic care*, 15/6 (2012), 547–52.
- 40. FEDORENKO, ANDRIY, LISHKO, POLINA V., and KIRICHOK, YURIY, 'Mechanism of fatty-acid-dependent UCP1 uncoupling in brown fat mitochondria', *Cell*, 151/2 (2012), 400–13.
- 41. WIRSEN, C., 'ADRENERGIC INNERVATION OF ADIPOSE TISSUE EXAMINED BY FLUORESCENCE MICROSCOPY', *Nature*, 202 (1964), 913.

- 42. GERHART-HINES, ZACHARY, DOMINY, JOHN E., BLÄTTLER, SHARON M. et al., 'The cAMP/PKA pathway rapidly activates SIRT1 to promote fatty acid oxidation independently of changes in NAD(+)', *Molecular cell*, 44/6 (2011), 851–63.
- 43. TASKÉN, KJETIL, and AANDAHL, EINAR MARTIN, 'Localized effects of cAMP mediated by distinct routes of protein kinase A', *Physiological reviews*, 84/1 (2004), 137–67.
- 44. Granneman, James G., Moore, Hsiao-Ping H., Krishnamoorthy, Rukmani et al., 'Perilipin controls lipolysis by regulating the interactions of AB-hydrolase containing 5 (Abhd5) and adipose triglyceride lipase (Atgl)', *The Journal of biological chemistry*, 284/50 (2009), 34538–44.
- 45. MIYOSHI, HIDEAKI, PERFIELD, JAMES W., SOUZA, SANDRA C. et al., 'Control of adipose triglyceride lipase action by serine 517 of perilipin A globally regulates protein kinase Astimulated lipolysis in adipocytes', *The Journal of biological chemistry*, 282/2 (2007), 996–1002.
- 46. VAN DER LANS, ANOUK A. J. J., HOEKS, JORIS, BRANS, BOUDEWIJN et al., 'Cold acclimation recruits human brown fat and increases nonshivering thermogenesis', *The Journal of clinical investigation*, 123/8 (2013), 3395–403.
- 47. Yu, Xing Xian, Lewin, David A., Forrest, William et al., 'Cold elicits the simultaneous induction of fatty acid synthesis and beta-oxidation in murine brown adipose tissue: prediction from differential gene expression and confirmation in vivo', *FASEB j.*, 16/2 (2002), 155–68.
- 48. ISHIBASHI, JEFF, and SEALE, PATRICK, 'Medicine. Beige can be slimming', *Science (New York, N.Y.)*, 328/5982 (2010), 1113–4.
- 49. VILLARROYA, FRANCESC, CEREIJO, RUBÉN, VILLARROYA, JOAN et al., 'Brown adipose tissue as a secretory organ', *Nature reviews. Endocrinology*, 13/1 (2017), 26–35.
- 50. BECHER, TOBIAS, PALANISAMY, SRIKANTH, KRAMER, DANIEL J. et al., 'Brown adipose tissue is associated with cardiometabolic health', *Nature medicine*, 27/1 (2021), 58–65.
- 51. MERLIN, JON, EVANS, BRONWYN A., DEHVARI, NODI et al., 'Could burning fat start with a brite spark? Pharmacological and nutritional ways to promote thermogenesis', *Molecular nutrition & food research*, 60/1 (2016), 18–42.
- 52. LEITNER, BROOKS P., HUANG, SHAN, BRYCHTA, ROBERT J. et al., 'Mapping of human brown adipose tissue in lean and obese young men', *Proceedings of the National Academy of Sciences of the United States of America*, 114/32 (2017), 8649–54.
- 53. CINTI, SAVERIO, 'The role of brown adipose tissue in human obesity', *Nutrition, metabolism, and cardiovascular diseases : NMCD*, 16/8 (2006), 569–74.
- 54. CYPESS, AARON M., LEHMAN, SANAZ, WILLIAMS, GETHIN et al., 'Identification and importance of brown adipose tissue in adult humans', *The New England journal of medicine*, 360/15 (2009), 1509–17.
- 55. NEDERGAARD, JAN, BENGTSSON, TORE, and CANNON, BARBARA, 'Unexpected evidence for active brown adipose tissue in adult humans', *American journal of physiology. Endocrinology and metabolism*, 293/2 (2007), E444-52.
- 56. VAN MARKEN LICHTENBELT, WOUTER D., VANHOMMERIG, JOOST W., SMULDERS, NANDA M. et al., 'Cold-activated brown adipose tissue in healthy men', *The New England journal of medicine*, 360/15 (2009), 1500–8.
- 57. VIRTANEN, KIRSI A., LIDELL, MARTIN E., ORAVA, JANNE et al., 'Functional brown adipose tissue in healthy adults', *The New England journal of medicine*, 360/15 (2009), 1518–25.
- 58. SÖDERLUND, VELI, LARSSON, STIG A., and JACOBSSON, HANS, 'Reduction of FDG uptake in brown adipose tissue in clinical patients by a single dose of propranolol', *European journal of nuclear medicine and molecular imaging*, 34/7 (2007), 1018–22.
- 59. Parysow, Oscar, Mollerach, Ana M., Jager, Victor et al., 'Low-dose oral propranolol could reduce brown adipose tissue F-18 FDG uptake in patients undergoing PET scans', *Clinical nuclear medicine*, 32/5 (2007), 351–7.

- 60. ZHANG, ZHAOYUN, CYPESS, AARON M., MIAO, QING et al., 'The prevalence and predictors of active brown adipose tissue in Chinese adults', *European journal of endocrinology*, 170/3 (2014), 359–66.
- 61. YONESHIRO, TAKESHI, AITA, SAYURI, MATSUSHITA, MAMI et al., 'Age-related decrease in coldactivated brown adipose tissue and accumulation of body fat in healthy humans', *Obesity* (Silver Spring, Md.), 19/9 (2011), 1755–60.
- 62. BLONDIN, DENIS P., LABBÉ, SÉBASTIEN M., TINGELSTAD, HANS C. et al., 'Increased brown adipose tissue oxidative capacity in cold-acclimated humans', *The Journal of clinical endocrinology and metabolism*, 99/3 (2014), E438-46.
- 63. CYPESS, AARON M., WEINER, LAUREN S., ROBERTS-TOLER, CARLA et al., 'Activation of Human Brown Adipose Tissue by a β 3-Adrenergic Receptor Agonist', *Cell metabolism*, 21/1 (2015), 33–8.
- 64. CYPESS, AARON M., CHEN, YIH-CHIEH, SZE, CATHY et al., 'Cold but not sympathomimetics activates human brown adipose tissue in vivo', *Proceedings of the National Academy of Sciences of the United States of America*, 109/25 (2012), 10001–5.
- 65. BLONDIN, DENIS P., NIELSEN, SOREN, KUIPERS, ELINE N. et al., 'Human Brown Adipocyte Thermogenesis Is Driven by β2-AR Stimulation', *Cell metabolism*, 32/2 (2020), 287-300.e7.
- 66. CHAPPLE, CHRISTOPHER R., CARDOZO, LINDA, NITTI, VICTOR W. et al., 'Mirabegron in overactive bladder: a review of efficacy, safety, and tolerability', *Neurourology and urodynamics*, 33/1 (2014), 17–30.
- 67. GNAD, THORSTEN, SCHEIBLER, SASKIA, KÜGELGEN, IVAR von et al., 'Adenosine activates brown adipose tissue and recruits beige adipocytes via A2A receptors', *Nature*, 516/7531 (2014), 395–9.
- 68. GNAD, THORSTEN, NAVARRO, GEMMA, LAHESMAA, MINNA et al., 'Adenosine/A2B Receptor Signaling Ameliorates the Effects of Aging and Counteracts Obesity', *Cell metabolism*, 34/4 (2022), 649.
- 69. NIEMANN, BIRTE, HAUFS-BRUSBERG, SASKIA, PUETZ, LAURA et al., 'Apoptotic brown adipocytes enhance energy expenditure via extracellular inosine', *Nature*, 609/7926 (2022), 361–8.
- 70. BROEDERS, EVIE P.M., NASCIMENTO, EMMANI B.M., HAVEKES, BAS et al., 'The Bile Acid Chenodeoxycholic Acid Increases Human Brown Adipose Tissue Activity', *Cell metabolism*, 22/3 (2015), 418–26.
- 71. LI, YONGGUO, SCHNABL, KATHARINA, GABLER, SARAH-MADELEINE et al., 'Secretin-Activated Brown Fat Mediates Prandial Thermogenesis to Induce Satiation', *Cell*, 175/6 (2018), 1561-1574.e12.
- 72. LAURILA, SANNA, SUN, LIHUA, LAHESMAA, MINNA et al., 'Secretin activates brown fat and induces satiation', *Nature metabolism*, 3/6 (2021), 798–809.
- 73. CEDDIA, RYAN P., LIU, DIANXIN, SHI, FUBIAO et al., 'Increased Energy Expenditure and Protection from Diet-Induced Obesity in Mice Lacking the cGMP-Specific Phosphodiesterase PDE9', *Diabetes*, 2021, db210100.
- 74. MISHRA, SUMITA, SADAGOPAN, NANDHINI, DUNKERLY-EYRING, BRITTANY et al., 'Inhibition of phosphodiesterase type 9 reduces obesity and cardiometabolic syndrome in mice', *Journal of Clinical Investigation*, 2021.
- 75. HOFFMANN, LINDA S., ETZRODT, JENNIFER, WILLKOMM, LENA et al., 'Stimulation of soluble guanylyl cyclase protects against obesity by recruiting brown adipose tissue', *Nature communications*, 6 (2015), 7235.
- 76. GLÖDE, ANJA, NAUMANN, JENNIFER, GNAD, THORSTEN et al., 'Divergent effects of a designer natriuretic peptide CD-NP in the regulation of adipose tissue and metabolism', *Molecular metabolism*, 6/3 (2017), 276–87.
- 77. ACHESON, K. J., and BURGER, A. G., 'A study of the relationship between thermogenesis and thyroid hormones', *The Journal of clinical endocrinology and metabolism*, 51/1 (1980), 84–9.

- 78. IZMAIL-BEIGI, F., and EDELMAN, I. S., 'Mechanism of thyroid calorigenesis: role of active sodium transport', *Proceedings of the National Academy of Sciences of the United States of America*, 67/2 (1970), 1071–8.
- 79. BRENT, G. A., 'The molecular basis of thyroid hormone action', *The New England journal of medicine*, 331/13 (1994), 847–53.
- 80. JOHNSTONE, ALEXANDRA M., MURISON, SANDRA D., DUNCAN, JACKIE S. et al., 'Factors influencing variation in basal metabolic rate include fat-free mass, fat mass, age, and circulating thyroxine but not sex, circulating leptin, or triiodothyronine', *The American journal of clinical nutrition*, 82/5 (2005), 941–8.
- 81. LEE, JOO-YOUNG, TAKAHASHI, NOBUYUKI, YASUBUCHI, MIDORI et al., 'Triiodothyronine induces UCP-1 expression and mitochondrial biogenesis in human adipocytes', *American journal of physiology*. *Cell physiology*, 302/2 (2012), C463-72.
- 82. WEINER, JULIANE, KRANZ, MATHIAS, KLÖTING, NORA et al., 'Thyroid hormone status defines brown adipose tissue activity and browning of white adipose tissues in mice', *Scientific reports*, 6 (2016), 38124.
- 83. LEBON, V., DUFOUR, S., PETERSEN, K. F. et al., 'Effect of triiodothyronine on mitochondrial energy coupling in human skeletal muscle', *The Journal of clinical investigation*, 108/5 (2001), 733–7.
- 84. GUILHERME, ADILSON, YENILMEZ, BATUHAN, BEDARD, ALEXANDER H. et al., 'Control of Adipocyte Thermogenesis and Lipogenesis through β3-Adrenergic and Thyroid Hormone Signal Integration', *Cell Reports*, 31/5 (2020), 107598.
- 85. MARTÍNEZ-SÁNCHEZ, NOELIA, MORENO-NAVARRETE, JOSÉ M., CONTRERAS, CRISTINA et al., 'Thyroid hormones induce browning of white fat', *The Journal of endocrinology*, 232/2 (2017), 351–62.
- 86. Scott, Michelle A., Nguyen, Virginia T., Levi, Benjamin et al., 'Current methods of adipogenic differentiation of mesenchymal stem cells', *Stem cells and development*, 20/10 (2011), 1793–804.
- 87. BEAVO, J. A., 'Cyclic nucleotide phosphodiesterases: functional implications of multiple isoforms', *Physiological reviews*, 75/4 (1995), 725–48.
- 88. BERTHET, J., RALL, T. W., and SUTHERLAND, E. W., 'The relationship of epinephrine and glucagon to liver phosphorylase. IV. Effect of epinephrine and glucagon on the reactivation of phosphorylase in liver homogenates', *The Journal of biological chemistry*, 224/1 (1957), 463–75.
- 89. SUTHERLAND, EARL W., and RALL, T. W., 'FRACTIONATION AND CHARACTERIZATION OF A CYCLIC ADENINE RIBONUCLEOTIDE FORMED BY TISSUE PARTICLES', *Journal of Biological Chemistry*, 232/2 (1958), 1077–91 https://www.sciencedirect.com/science/article/pii/s0021925819774237.
- 90. ASHMAN, D. F., LIPTON, R., MELICOW, M. M. et al., 'Isolation of adenosine 3',5'-monophosphate and guanosine 3',5'-monophosphate from rat urine', *Biochemical and Biophysical Research Communications*, 11/4 (1963), 330–4.
- 91. Cyclic Phosphates. IV.1 Ribonucleoside-3',5' Cyclic Phosphates. A General Method of Synthesis and Some Properties (1961) https://pubs.acs.org/doi/pdf/10.1021/ja01464a039.
- 92. GHOFRANI, HOSSEIN-ARDESCHIR, D'ARMINI, ANDREA M., GRIMMINGER, FRIEDRICH et al., 'Riociguat for the treatment of chronic thromboembolic pulmonary hypertension', *The New England journal of medicine*, 369/4 (2013), 319–29.
- 93. HOLMES, S. J., ESPINER, E. A., RICHARDS, A. M. et al., 'Renal, endocrine, and hemodynamic effects of human brain natriuretic peptide in normal man', *The Journal of clinical endocrinology and metabolism*, 76/1 (1993), 91–6.
- 94. McMurray, John J. V., Packer, Milton, Desai, Akshay S. et al., 'Angiotensin-neprilysin inhibition versus enalapril in heart failure', *The New England journal of medicine*, 371/11 (2014), 993–1004.

- 95. TAKIMOTO, EIKI, CHAMPION, HUNTER C., LI, MANXIANG et al., 'Chronic inhibition of cyclic GMP phosphodiesterase 5A prevents and reverses cardiac hypertrophy', *Nature medicine*, 11/2 (2005), 214–22.
- 96. TSAI, EMILY J., and KASS, DAVID A., 'Cyclic GMP signaling in cardiovascular pathophysiology and therapeutics', *Pharmacology & therapeutics*, 122/3 (2009), 216–38.
- 97. PATRUCCO, ENRICO, DOMES, KATRIN, SBROGGIÓ, MAURO et al., 'Roles of cGMP-dependent protein kinase I (cGKI) and PDE5 in the regulation of Ang II-induced cardiac hypertrophy and fibrosis', *Proceedings of the National Academy of Sciences*, 111/35 (2014), 12925–9.
- 98. ARMSTRONG, PAUL W., PIESKE, BURKERT, ANSTROM, KEVIN J. et al., 'Vericiguat in Patients with Heart Failure and Reduced Ejection Fraction', *The New England journal of medicine*, 382/20 (2020), 1883–93.
- 99. HUANG, SHARON A., and LIE, JANETTE D., 'Phosphodiesterase-5 (PDE5) Inhibitors In the Management of Erectile Dysfunction', *P & T : a peer-reviewed journal for formulary management*, 38/7 (2013), 407–19.
- 100. McMahon, Chelsea N., Smith, Christopher J., and Shabsigh, Ridwan, 'Treating erectile dysfunction when PDE5 inhibitors fail', *The BMJ*, 332/7541 (2006), 589–92.
- 101. PYRGIDIS, NIKOLAOS, MYKONIATIS, IOANNIS, HAIDICH, ANNA-BETTINA et al., 'The Effect of Phosphodiesterase-type 5 Inhibitors on Erectile Function: An Overview of Systematic Reviews', *Frontiers in pharmacology*, 12 (2021), 735708.
- 102. HOEPER, MARIUS M., 'Pharmacological therapy for patients with chronic thromboembolic pulmonary hypertension', *European respiratory review : an official journal of the European Respiratory Society*, 24/136 (2015), 272–82.
- 103. BARNES, HAYLEY, BROWN, ZOE, BURNS, ANDREW et al., 'Phosphodiesterase 5 inhibitors for pulmonary hypertension', *The Cochrane database of systematic reviews*, 1 (2019), CD012621.
- 104. HATZIMOURATIDIS, KONSTANTINOS, 'A review of the use of tadalafil in the treatment of benign prostatic hyperplasia in men with and without erectile dysfunction', *Therapeutic Advances in Urology*, 6/4 (2014), 135–47.
- 105. HEMNES, ANNA R., and CHAMPION, HUNTER C., 'Sildenafil, a PDE5 inhibitor, in the treatment of pulmonary hypertension', *Expert review of cardiovascular therapy*, 4/3 (2006), 293–300.
- 106. ROEHRBORN, CLAUS G., MCVARY, KEVIN T., ELION-MBOUSSA, ALBERT et al., 'Tadalafil administered once daily for lower urinary tract symptoms secondary to benign prostatic hyperplasia: a dose finding study', *The Journal of urology*, 180/4 (2008), 1228–34.
- 107. WILKINS, M. R., WHARTON, J., GRIMMINGER, F. et al., 'Phosphodiesterase inhibitors for the treatment of pulmonary hypertension', *The European respiratory journal*, 32/1 (2008), 198–209.
- 108. MITSCHKE, MICHAELA M., HOFFMANN, LINDA S., GNAD, THORSTEN et al., 'Increased cGMP promotes healthy expansion and browning of white adipose tissue', *FASEB j.*, 27/4 (2013), 1621–30.
- 109. SENGENÈS, CORALIE, ZAKAROFF-GIRARD, ALEXIA, MOULIN, AGNÈS et al., 'Natriuretic peptide-dependent lipolysis in fat cells is a primate specificity', *American journal of physiology*. Regulatory, integrative and comparative physiology, 283/1 (2002), R257-65.
- 110. LAFONTAN, MAX, MORO, CÉDRIC, SENGENES, CORALIE et al., 'An unsuspected metabolic role for atrial natriuretic peptides: the control of lipolysis, lipid mobilization, and systemic nonesterified fatty acids levels in humans', *Arteriosclerosis, thrombosis, and vascular biology*, 25/10 (2005), 2032–42.
- 111. LAFONTAN, MAX, MORO, CÉDRIC, BERLAN, MICHEL et al., 'Control of lipolysis by natriuretic peptides and cyclic GMP', *Trends in endocrinology and metabolism: TEM*, 19/4 (2008), 130–7.
- 112. MATSUKAWA, N., GRZESIK, W. J., TAKAHASHI, N. et al., 'The natriuretic peptide clearance receptor locally modulates the physiological effects of the natriuretic peptide system',

- Proceedings of the National Academy of Sciences of the United States of America, 96/13 (1999), 7403–8.
- 113. POTTER, LINCOLN R., 'Guanylyl cyclase structure, function and regulation', *Cellular signalling*, 23/12 (2011), 1921–6.
- 114. Kuhn, Michaela, 'Molecular Physiology of Membrane Guanylyl Cyclase Receptors', *Physiological reviews*, 96/2 (2016), 751–804.
- 115. BUGLIONI, ALESSIA, and BURNETT, JOHN C., 'New Pharmacological Strategies to Increase cGMP', *Annual review of medicine*, 67 (2016), 229–43.
- 116. POTTER, LINCOLN R., 'Natriuretic peptide metabolism, clearance and degradation', *The FEBS journal*, 278/11 (2011), 1808–17.
- 117. POTTER, LINCOLN R., ABBEY-HOSCH, SARAH, and DICKEY, DEBORAH M., 'Natriuretic peptides, their receptors, and cyclic guanosine monophosphate-dependent signaling functions', *Endocrine reviews*, 27/1 (2006), 47–72.
- 118. POTTER, LINCOLN R., YODER, ANDREA R., FLORA, DARCY R. et al., 'Natriuretic peptides: their structures, receptors, physiologic functions and therapeutic applications', *Handbook of experimental pharmacology*, 2009, 341–66.
- 119. ROSE, ROBERT A., and GILES, WAYNE R., 'Natriuretic peptide C receptor signalling in the heart and vasculature', *The Journal of physiology*, 586/2 (2008), 353–66.
- 120. ALDERTON, W. K., COOPER, C. E., and KNOWLES, R. G., 'Nitric oxide synthases: structure, function and inhibition', *The Biochemical Journal*, 357/Pt 3 (2001), 593–615.
- 121. FÖRSTERMANN, ULRICH, and SESSA, WILLIAM C., 'Nitric oxide synthases: regulation and function', *European heart journal*, 33/7 (2012), 829-37, 837a-837d.
- 122. CRANE, B. R., ARVAI, A. S., GHOSH, D. K. et al., 'Structure of nitric oxide synthase oxygenase dimer with pterin and substrate', *Science (New York, N.Y.)*, 279/5359 (1998), 2121–6.
- 123. ZHOU, ZONGMIN, GROSS, STEFFEN, ROUSSOS, CHARIS et al., 'Structural and functional characterization of the dimerization region of soluble guanylyl cyclase', *Journal of Biological Chemistry*, 279/24 (2004), 24935–43.
- 124. KAMISAKI, Y., SAHEKI, S., NAKANE, M. et al., 'Soluble guanylate cyclase from rat lung exists as a heterodimer', *Journal of Biological Chemistry*, 261/16 (1986), 7236–41.
- 125. NAKANE, M., ARAI, K., SAHEKI, S. et al., 'Molecular cloning and expression of cDNAs coding for soluble guanylate cyclase from rat lung', *Journal of Biological Chemistry*, 265/28 (1990), 16841–5.
- 126. HARTENECK, C., WEDEL, B., KOESLING, D. et al., 'Molecular cloning and expression of a new alpha-subunit of soluble guanylyl cyclase. Interchangeability of the alpha-subunits of the enzyme', *FEBS letters*, 292/1-2 (1991), 217–22.
- 127. YUEN, P. S., POTTER, L. R., and GARBERS, D. L., 'A new form of guanylyl cyclase is preferentially expressed in rat kidney', *Biochemistry*, 29/49 (1990), 10872–8.
- 128. MUNDEL, P., GAMBARYAN, S., BACHMANN, S. et al., 'Immunolocalization of soluble guanylyl cyclase subunits in rat kidney', *Histochemistry and cell biology*, 103/1 (1995), 75–9.
- 129. FRIEBE, ANDREAS, SANDNER, PETER, and SCHMIDTKO, ACHIM, 'cGMP: a unique 2nd messenger molecule recent developments in cGMP research and development', *Naunyn-Schmiedeberg's archives of pharmacology*, 393/2 (2020), 287–302.
- 130. SHARINA, IRAIDA G., JELEN, FILIP, BOGATENKOVA, ELENA P. et al., 'Alpha1 soluble guanylyl cyclase (sGC) splice forms as potential regulators of human sGC activity', *Journal of Biological Chemistry*, 283/22 (2008), 15104–13.
- 131. MERGIA, EVANTHIA, RUSSWURM, MICHAEL, ZOIDL, GEORG et al., 'Major occurrence of the new alpha2beta1 isoform of NO-sensitive guanylyl cyclase in brain', *Cellular signalling*, 15/2 (2003), 189–95.

- 132. RUSSWURM, M., BEHRENDS, S., HARTENECK, C. et al., 'Functional properties of a naturally occurring isoform of soluble guanylyl cyclase', *The Biochemical Journal*, 335 (Pt 1) (1998), 125–30.
- 133. MONTFORT, WILLIAM R., WALES, JESSICA A., and WEICHSEL, ANDRZEJ, 'Structure and Activation of Soluble Guanylyl Cyclase, the Nitric Oxide Sensor', *Antioxidants & redox signaling*, 26/3 (2017), 107–21.
- 134. STASCH, JOHANNES-PETER, and HOBBS, ADRIAN J., 'NO-independent, haem-dependent soluble guanylate cyclase stimulators', *Handbook of experimental pharmacology*, 2009, 277–308.
- 135. STASCH, JOHANNES-PETER, PACHER, PÁL, and EVGENOV, OLEG V., 'Soluble guanylate cyclase as an emerging therapeutic target in cardiopulmonary disease', *Circulation*, 123/20 (2011), 2263–73.
- 136. FRITZ, BRADLEY G., Hu, XIAOHUI, BRAILEY, JACQUELINE L. et al., 'Oxidation and loss of heme in soluble guanylyl cyclase from Manduca sexta', *Biochemistry*, 50/26 (2011), 5813–5
- 137. SHARINA, IRAIDA G., and MARTIN, EMIL, 'The Role of Reactive Oxygen and Nitrogen Species in the Expression and Splicing of Nitric Oxide Receptor', *Antioxidants & redox signaling*, 26/3 (2017), 122–36.
- 138. RITCHIE, REBECCA H., DRUMMOND, GRANT R., SOBEY, CHRISTOPHER G. et al., 'The opposing roles of NO and oxidative stress in cardiovascular disease', *Pharmacological research*, 116 (2017), 57–69.
- 139. BOERRIGTER, GUIDO, COSTELLO-BOERRIGTER, LISA C., CATALIOTTI, ALESSANDRO et al., 'Targeting heme-oxidized soluble guanylate cyclase in experimental heart failure', *Hypertension (Dallas, Tex. : 1979)*, 49/5 (2007), 1128–33.
- 140. MANNA, PRASENJIT, and JAIN, SUSHIL K., 'Obesity, Oxidative Stress, Adipose Tissue Dysfunction, and the Associated Health Risks: Causes and Therapeutic Strategies', *Metabolic syndrome and related disorders*, 13/10 (2015), 423–44.
- 141. SCHMIDT, HARALD H. H. W., SCHMIDT, PETER M., and STASCH, JOHANNES-PETER, 'NO-and haem-independent soluble guanylate cyclase activators', *Handbook of experimental pharmacology*, 2009, 309–39.
- 142. HOFFMANN, L. S., SCHMIDT, P. M., KEIM, Y. et al., 'Distinct molecular requirements for activation or stabilization of soluble guanylyl cyclase upon haem oxidation-induced degradation', *British journal of pharmacology*, 157/5 (2009), 781–95.
- 143. STASCH, JOHANNES-PETER, SCHLOSSMANN, JENS, and HOCHER, BERTHOLD, 'Renal effects of soluble guanylate cyclase stimulators and activators: a review of the preclinical evidence', *Current opinion in pharmacology*, 21 (2015), 95–104.
- 144. STACY, REBECCA, HUTTNER, KENNETH, WATTS, JEN et al., 'A Randomized, Controlled Phase I/II Study to Evaluate the Safety and Efficacy of MGV354 for Ocular Hypertension or Glaucoma', *American journal of ophthalmology*, 192 (2018), 113–23.
- 145. THOONEN, ROBRECHT, CAUWELS, ANJE, DECALUWE, KELLY et al., 'Cardiovascular and pharmacological implications of haem-deficient NO-unresponsive soluble guanylate cyclase knock-in mice', *Nat Commun*, 6 (2015), 8482.
- 146. STASCH, J. P., BECKER, E. M., ALONSO-ALIJA, C. et al., 'NO-independent regulatory site on soluble guanylate cyclase', *Nature*, 410/6825 (2001), 212–5.
- 147. BUGLIONI, ALESSIA, and BURNETT, JOHN C., 'New Pharmacological Strategies to Increase cGMP', *Annual review of medicine*, 67 (2016), 229–43.
- 148. FRANCIS, SHARRON H., BUSCH, JENNIFER L., CORBIN, JACKIE D. et al., 'cGMP-dependent protein kinases and cGMP phosphodiesterases in nitric oxide and cGMP action', *Pharmacol Rev*, 62/3 (2010), 525–63.
- 149. HOFMANN, FRANZ, 'A concise discussion of the regulatory role of cGMP kinase I in cardiac physiology and pathology', *Basic research in cardiology*, 113/4 (2018), 31.

- 150. SANDNER, PETER, ZIMMER, DANIEL P., MILNE, G. TODD et al., 'Soluble Guanylate Cyclase Stimulators and Activators', *Handbook of experimental pharmacology*, 264 (2021), 355–94.
- 151. BIEL, MARTIN, and MICHALAKIS, STYLIANOS, 'Cyclic nucleotide-gated channels', *Handbook of experimental pharmacology*, 2009, 111–36.
- 152. PAQUET-DURAND, FRANÇOIS, BECK, SUSANNE, MICHALAKIS, STYLIANOS et al., 'A key role for cyclic nucleotide gated (CNG) channels in cGMP-related retinitis pigmentosa', Human molecular genetics, 20/5 (2011), 941–7.
- 153. STANGHERLIN, ALESSANDRA, GESELLCHEN, FRANK, ZOCCARATO, ANNA et al., 'cGMP signals modulate cAMP levels in a compartment-specific manner to regulate catecholamine-dependent signaling in cardiac myocytes', *Circulation research*, 108/8 (2011), 929–39.
- 154. CORBIN, J. D., TURKO, I. V., BEASLEY, A. et al., 'Phosphorylation of phosphodiesterase-5 by cyclic nucleotide-dependent protein kinase alters its catalytic and allosteric cGMP-binding activities', *European journal of biochemistry*, 267/9 (2000), 2760–7.
- 155. PELLIGRINO, D. A., and WANG, Q., 'Cyclic nucleotide crosstalk and the regulation of cerebral vasodilation', *Progress in Neurobiology*, 56/1 (1998), 1–18.
- 156. BOLD, A. J. de, BORENSTEIN, H. B., VERESS, A. T. et al., 'A rapid and potent natriuretic response to intravenous injection of atrial myocardial extract in rats', *Life Sciences*, 28/1 (1981), 89–94.
- 157. MATTINGLY, M. T., BRANDT, R. R., HEUBLEIN, D. M. et al., 'Presence of C-type natriuretic peptide in human kidney and urine', *Kidney international*, 46/3 (1994), 744–7.
- 158. Wong, Philip Ching Yat, Guo, Jun, and Zhang, Aldong, 'The renal and cardiovascular effects of natriuretic peptides', *Advances in physiology education*, 41/2 (2017), 179–85.
- 159. SENGENÈS, C., BERLAN, M., GLISEZINSKI, I. de et al., 'Natriuretic peptides: a new lipolytic pathway in human adipocytes', *FASEB j.*, 14/10 (2000), 1345–51.
- 160. MIYASHITA, KAZUTOSHI, ITOH, HIROSHI, TSUJIMOTO, HIROKAZU et al., 'Natriuretic peptides/cGMP/cGMP-dependent protein kinase cascades promote muscle mitochondrial biogenesis and prevent obesity', *Diabetes*, 58/12 (2009), 2880–92.
- 161. ENGELI, STEFAN, BIRKENFELD, ANDREAS L., BADIN, PIERRE-MARIE et al., 'Natriuretic peptides enhance the oxidative capacity of human skeletal muscle', *The Journal of clinical investigation*, 122/12 (2012), 4675–9.
- 162. WANG, THOMAS J., LARSON, MARTIN G., LEVY, DANIEL et al., 'Impact of obesity on plasma natriuretic peptide levels', *Circulation*, 109/5 (2004), 594–600.
- 163. COLLINS, SHEILA, and BORDICCHIA, MARICA, 'Heart hormones fueling a fire in fat', *Adipocyte*, 2/2 (2013), 104–8.
- 164. YASUE, H., YOSHIMURA, M., SUMIDA, H. et al., 'Localization and mechanism of secretion of B-type natriuretic peptide in comparison with those of A-type natriuretic peptide in normal subjects and patients with heart failure', *Circulation*, 90/1 (1994), 195–203.
- 165. PONIKOWSKI, PIOTR, VOORS, ADRIAAN A., ANKER, STEFAN D. et al., '2016 ESC Guidelines for the diagnosis and treatment of acute and chronic heart failure: The Task Force for the diagnosis and treatment of acute and chronic heart failure of the European Society of Cardiology (ESC)Developed with the special contribution of the Heart Failure Association (HFA) of the ESC', *European heart journal*, 37/27 (2016), 2129–200.
- 166. DEL RY, SILVIA, PASSINO, CLAUDIO, MALTINTI, MARISTELLA et al., 'C-type natriuretic peptide plasma levels increase in patients with chronic heart failure as a function of clinical severity', *European journal of heart failure*, 7/7 (2005), 1145–8.
- 167. SUDOH, T., MINAMINO, N., KANGAWA, K. et al., 'C-type natriuretic peptide (CNP): a new member of natriuretic peptide family identified in porcine brain', *Biochemical and Biophysical Research Communications*, 168/2 (1990), 863–70.
- 168. SUGA, S., NAKAO, K., ITOH, H. et al., 'Endothelial production of C-type natriuretic peptide and its marked augmentation by transforming growth factor-beta. Possible existence of

- "vascular natriuretic peptide system", *The Journal of clinical investigation*, 90/3 (1992), 1145–9.
- 169. DEL RY, S., CABIATI, M., VOZZI, F. et al., 'Expression of C-type natriuretic peptide and its receptor NPR-B in cardiomyocytes', *Peptides*, 32/8 (2011), 1713–8.
- 170. VIJAY, JINCHU, GAUTHIER, MARIE-FRÉDÉRIQUE, BISWELL, REBECCA L. et al., 'Single-cell analysis of human adipose tissue identifies depot and disease specific cell types', *Nature metabolism*, 2/1 (2020), 97–109.
- 171. SENGENÈS, C., MIRANVILLE, A., LOLMÈDE, K. et al., 'The role of endothelial cells in inflamed adipose tissue', *Journal of internal medicine*, 262/4 (2007), 415–21.
- 172. SUGA, S., NAKAO, K., HOSODA, K. et al., 'Receptor selectivity of natriuretic peptide family, atrial natriuretic peptide, brain natriuretic peptide, and C-type natriuretic peptide', *Endocrinology*, 130/1 (1992), 229–39.
- 173. COUÉ, MARINE, and MORO, CEDRIC, 'Natriuretic peptide control of energy balance and glucose homeostasis', *Biochimie*, 124 (2016), 84–91.
- 174. SANTHEKADUR, PRASANNA K., KUMAR, DIVYA P., SENESHAW, MULUGETA et al., 'The multifaceted role of natriuretic peptides in metabolic syndrome', *Biomedicine & pharmacotherapy = Biomedecine & pharmacotherapie*, 92 (2017), 826–35.
- 175. PEREZ-TERNERO, CRISTINA, AUBDOOL, AISAH A., MAKWANA, RAJ et al., 'C-type natriuretic peptide is a pivotal regulator of metabolic homeostasis', *Proceedings of the National Academy of Sciences*, 119/13 (2022), e2116470119.
- 176. MOYES, AMIE J., and HOBBS, ADRIAN J., 'C-type Natriuretic Peptide: A Multifaceted Paracrine Regulator in the Heart and Vasculature', *International journal of molecular sciences*, 20/9 (2019).
- 177. MOYES, AMIE J., CHU, SANDY M., AUBDOOL, AISAH A. et al., 'C-type natriuretic peptide co-ordinates cardiac structure and function', *European heart journal*, 41/9 (2020), 1006–20.
- 178. CHARLES, C. J., ESPINER, E. A., NICHOLLS, M. G. et al., 'Clearance receptors and endopeptidase 24.11: equal role in natriuretic peptide metabolism in conscious sheep', *The American journal of physiology*, 271/2 Pt 2 (1996), R373-80.
- 179. NALIVAEVA, N. N., ZHURAVIN, I. A., and TURNER, A. J., 'Neprilysin expression and functions in development, ageing and disease', *Mechanisms of Ageing and Development*, 192 (2020), 111363.
- 180. PFEFFER, MARC A., CLAGGETT, BRIAN, LEWIS, ELDRIN F. et al., 'Angiotensin Receptor-Neprilysin Inhibition in Acute Myocardial Infarction', *The New England journal of medicine*, 385/20 (2021), 1845–55.
- 181. SOLOMON, SCOTT D., McMurray, John J. V., Anand, Inder S. et al., 'Angiotensin-Neprilysin Inhibition in Heart Failure with Preserved Ejection Fraction', *The New England journal of medicine*, 381/17 (2019), 1609–20.
- 182. ZOIS, NORA E., BARTELS, EMIL D., HUNTER, INGRID et al., 'Natriuretic peptides in cardiometabolic regulation and disease', *Nature reviews. Cardiology*, 11/7 (2014), 403–12.
- 183. Chusho, H., Tamura, N., Ogawa, Y. et al., 'Dwarfism and early death in mice lacking C-type natriuretic peptide', *Proceedings of the National Academy of Sciences of the United States of America*, 98/7 (2001), 4016–21.
- 184. TAMURA, N., OGAWA, Y., CHUSHO, H. et al., 'Cardiac fibrosis in mice lacking brain natriuretic peptide', *Proceedings of the National Academy of Sciences of the United States of America*, 97/8 (2000), 4239–44.
- 185. SUBRAMANIAN, HARIHARAN, FROESE, ALEXANDER, JÖNSSON, PETER et al., 'Distinct submembrane localisation compartmentalises cardiac NPR1 and NPR2 signalling to cGMP', *Nature communications*, 9/1 (2018), 2446.
- 186. MANFRA, ORNELLA, CALAMERA, GAIA, FROESE, ALEXANDER et al., 'CNP regulates cardiac contractility and increases cGMP near both SERCA and TnI difference from BNP visualized by targeted cGMP biosensors', Cardiovascular research, 2021.

- 187. SAVARIRAYAN, RAVI, TOFTS, LOUISE, IRVING, MELITA et al., 'Safe and persistent growth-promoting effects of vosoritide in children with achondroplasia: 2-year results from an open-label, phase 3 extension study', *Genetics in medicine : official journal of the American College of Medical Genetics*, 23/12 (2021), 2443–7.
- 188. FIFER, M. A., MOLINA, C. R., QUIROZ, A. C. et al., 'Hemodynamic and renal effects of atrial natriuretic peptide in congestive heart failure', *The American journal of cardiology*, 65/3 (1990), 211–6.
- 189. Konishi, Masaaki, Ishida, Junichi, Springer, Jochen et al., 'Heart failure epidemiology and novel treatments in Japan: facts and numbers', *ESC Heart Failure*, 3/3 (2016), 145–51.
- 190. SACKNER-BERNSTEIN, JONATHAN D., KOWALSKI, MARCIN, FOX, MARSHAL et al., 'Short-term risk of death after treatment with nesiritide for decompensated heart failure: a pooled analysis of randomized controlled trials', *JAMA*, 293/15 (2005), 1900–5.
- 191. SACKNER-BERNSTEIN, JONATHAN D., SKOPICKI, HAL A., and AARONSON, KEITH D., 'Risk of worsening renal function with nesiritide in patients with acutely decompensated heart failure', *Circulation*, 111/12 (2005), 1487–91.
- 192. KAWAKAMI, RIKA, LEE, CANDACE Y. W., SCOTT, CHRISTOPHER et al., 'A Human Study to Evaluate Safety, Tolerability, and Cyclic GMP Activating Properties of Cenderitide in Subjects With Stable Chronic Heart Failure', *Clinical pharmacology and therapeutics*, 104/3 (2018), 546–52.
- 193. McDonagh, Theresa A., Metra, Marco, Adamo, Marianna et al., '2021 ESC Guidelines for the diagnosis and treatment of acute and chronic heart failure', *European heart journal*, 42/36 (2021), 3599–726.
- 194. IGNARRO, L. J., BUGA, G. M., WOOD, K. S. et al., 'Endothelium-derived relaxing factor produced and released from artery and vein is nitric oxide', *Proceedings of the National Academy of Sciences of the United States of America*, 84/24 (1987), 9265–9.
- 195. MITTAL, ANSHIKA, and KAKKAR, RITA, 'Nitric Oxide Synthases and Their Inhibitors: A Review', *LDDD*, 17/3 (2020), 228–52.
- 196. CARNICER, RICARDO, CRABTREE, MARK J., SIVAKUMARAN, VIDHYA et al., 'Nitric Oxide Synthases in Heart Failure', *Antioxidants & redox signaling*, 18/9 (2013), 1078–99.
- 197. ENGELI, STEFAN, JANKE, JÜRGEN, GORZELNIAK, KERSTIN et al., 'Regulation of the nitric oxide system in human adipose tissue', *J. Lipid Res.*, 45/9 (2004), 1640–8.
- 198. KIKUCHI-UTSUMI, KAZUE, GAO, BIHU, OHINATA, HIROSHI et al., 'Enhanced gene expression of endothelial nitric oxide synthase in brown adipose tissue during cold exposure', *American journal of physiology*. *Regulatory, integrative and comparative physiology*, 282/2 (2002), R623-6.
- 199. CINELLI, MARIS A., DO, HA T., MILEY, GALEN P. et al., 'Inducible nitric oxide synthase: Regulation, structure, and inhibition', *Medicinal research reviews*, 40/1 (2020), 158–89.
- 200. SCHMIDT, H. H., POLLOCK, J. S., NAKANE, M. et al., 'Ca2+/calmodulin-regulated nitric oxide synthases', *Cell calcium*, 13/6-7 (1992), 427–34.
- 201. HOFMANN, F., GENSHEIMER, H. P., and GÖBEL, C., 'cGMP-dependent protein kinase. Autophosphorylation changes the characteristics of binding site 1', *European journal of biochemistry*, 147/2 (1985), 361–5.
- 202. WERNET, W., FLOCKERZI, V., and HOFMANN, F., 'The cDNA of the two isoforms of bovine cGMP-dependent protein kinase', *FEBS letters*, 251/1-2 (1989), 191–6.
- 203. PFEIFER, A., ASZÓDI, A., SEIDLER, U. et al., 'Intestinal secretory defects and dwarfism in mice lacking cGMP-dependent protein kinase II', *Science (New York, N.Y.)*, 274/5295 (1996), 2082–6.
- 204. PFEIFER, A., KLATT, P., MASSBERG, S. et al., 'Defective smooth muscle regulation in cGMP kinase I-deficient mice', *The EMBO journal*, 17/11 (1998), 3045–51.
- 205. SCHLOSSMANN, JENS, FEIL, ROBERT, and HOFMANN, FRANZ, 'Signaling through NO and cGMP-dependent protein kinases', *Annals of medicine*, 35/1 (2003), 21–7.

- 206. NIKOLIC, DEJAN M., LI, YANZHANG, LIU, SHU et al., 'Overexpression of constitutively active PKG-I protects female, but not male mice from diet-induced obesity', *Obesity (Silver Spring, Md.)*, 19/4 (2011), 784–91.
- 207. SANYAL, ABHISHEK, NAUMANN, JENNIFER, HOFFMANN, LINDA SARAH et al., 'Interplay between Obesity-Induced Inflammation and cGMP Signaling in White Adipose Tissue', *Cell Reports*, 18/1 (2017), 225–36.
- 208. BENDER, ANDREW T., and BEAVO, JOSEPH A., 'Cyclic nucleotide phosphodiesterases: molecular regulation to clinical use', *Pharmacol Rev*, 58/3 (2006), 488–520.
- 209. THOMPSON, W. J., and APPLEMAN, M. M., 'Multiple cyclic nucleotide phosphodiesterase activities from rat brain', *Biochemistry*, 10/2 (1971), 311–6.
- 210. OMORI, KENJI, and KOTERA, JUN, 'Overview of PDEs and their regulation', *Circulation research*, 100/3 (2007), 309–27.
- 211. KERAVIS, THÉRÈSE, and LUGNIER, CLAIRE, 'Cyclic nucleotide phosphodiesterase (PDE) isozymes as targets of the intracellular signalling network: benefits of PDE inhibitors in various diseases and perspectives for future therapeutic developments', *British journal of pharmacology*, 165/5 (2012), 1288–305.
- 212. KOKKONEN, KRISTEN, and KASS, DAVID A., 'Nanodomain Regulation of Cardiac Cyclic Nucleotide Signaling by Phosphodiesterases', *Annual review of pharmacology and toxicology*, 57 (2017), 455–79.
- 213. GEREMIA, R., ROSSI, P., MOCINI, D. et al., 'Characterization of a calmodulin-dependent high-affinity cyclic AMP and cyclic GMP phosphodiesterase from male mouse germ cells', *The Biochemical Journal*, 217/3 (1984), 693–700.
- 214. EPSTEIN, P. M., FISS, K., HACHISU, R. et al., 'Interaction of calcium antagonists with cyclic AMP phosphodiesterases and calmodulin', *Biochemical and Biophysical Research Communications*, 105/3 (1982), 1142–9.
- 215. FLORIO, V. A., SONNENBURG, W. K., JOHNSON, R. et al., 'Phosphorylation of the 61-kDa calmodulin-stimulated cyclic nucleotide phosphodiesterase at serine 120 reduces its affinity for calmodulin', *Biochemistry*, 33/30 (1994), 8948–54.
- 216. HAGIWARA, M., ENDO, T., and HIDAKA, H., 'Effects of vinpocetine on cyclic nucleotide metabolism in vascular smooth muscle', *Biochemical pharmacology*, 33/3 (1984), 453–7.
- 217. JONES, G. H., VENUTI, M. C., ALVAREZ, R. et al., 'Inhibitors of cyclic AMP phosphodiesterase. 1. Analogues of cilostamide and anagrelide', *Journal of medicinal chemistry*, 30/2 (1987), 295–303.
- 218. MARTINS, T. J., MUMBY, M. C., and BEAVO, J. A., 'Purification and characterization of a cyclic GMP-stimulated cyclic nucleotide phosphodiesterase from bovine tissues', *Journal of Biological Chemistry*, 257/4 (1982), 1973–9.
- 219. YANG, Q., PASKIND, M., BOLGER, G. et al., 'A novel cyclic GMP stimulated phosphodiesterase from rat brain', *Biochemical and Biophysical Research Communications*, 205/3 (1994), 1850–8.
- 220. MARTINEZ, SERGIO E., BEAVO, JOSEPH A., and HOL, WIM G. J., 'GAF domains: two-billion-year-old molecular switches that bind cyclic nucleotides', *Molecular interventions*, 2/5 (2002), 317–23.
- 221. ŚWIEŻAWSKA-BONIECKA, BRYGIDA, DUSZYN, MARIA, KWIATKOWSKI, MATEUSZ et al., 'Cross Talk Between Cyclic Nucleotides and Calcium Signaling Pathways in Plants-Achievements and Prospects', *Frontiers in plant science*, 12 (2021), 643560.
- 222. ZACCOLO, MANUELA, and MOVSESIAN, MATTHEW A., 'cAMP and cGMP signaling cross-talk: role of phosphodiesterases and implications for cardiac pathophysiology', *Circulation research*, 100/11 (2007), 1569–78.
- 223. MENGES, LUKAS, KRAWUTSCHKE, CHRISTIAN, FÜCHTBAUER, ERNST-MARTIN et al., 'Mind the gap (junction): cGMP induced by nitric oxide in cardiac myocytes originates from cardiac fibroblasts', *British journal of pharmacology*, 176/24 (2019), 4696–707.

- 224. RASCÓN, A., LINDGREN, S., STAVENOW, L. et al., 'Purification and properties of the cGMP-inhibited cAMP phosphodiesterase from bovine aortic smooth muscle', *Biochimica et biophysica acta*, 1134/2 (1992), 149–56.
- 225. AMSALLEM, E., KASPARIAN, C., HADDOUR, G. et al., 'Phosphodiesterase III inhibitors for heart failure', *The Cochrane database of systematic reviews*, 2005, CD002230.
- 226. VECCHIS, RENATO de, CESARO, ARTURO, ARIANO, CARMELINA et al., 'Phosphodiesterase-5 Inhibitors Improve Clinical Outcomes, Exercise Capacity and Pulmonary Hemodynamics in Patients With Heart Failure With Reduced Left Ventricular Ejection Fraction: A Meta-Analysis', *Journal of clinical medicine research*, 9/6 (2017), 488–98.
- 227. WU, XIAOJING, YANG, TE, ZHOU, QI et al., 'Additional use of a phosphodiesterase 5 inhibitor in patients with pulmonary hypertension secondary to chronic systolic heart failure: a meta-analysis', *European journal of heart failure*, 16/4 (2014), 444–53.
- 228. FREDRIKSSON, ROBERT, and SCHIÖTH, HELGI B., 'The repertoire of G-protein-coupled receptors in fully sequenced genomes', *Molecular pharmacology*, 67/5 (2005), 1414–25.
- 229. ZACCOLO, MANUELA, ZERIO, ANNA, and LOBO, MIGUEL J., 'Subcellular Organization of the cAMP Signaling Pathway', *Pharmacol Rev*, 73/1 (2021), 278–309.
- 230. ARORA, KAVISHA, SINHA, CHANDRIMA, ZHANG, WEIQIANG et al., 'Compartmentalization of cyclic nucleotide signaling: a question of when, where, and why?', *Pflugers Archiv : European journal of physiology*, 465/10 (2013), 1397–407.
- 231. ZACCOLO, MANUELA, and POZZAN, TULLIO, 'Discrete microdomains with high concentration of cAMP in stimulated rat neonatal cardiac myocytes', *Science (New York, N.Y.)*, 295/5560 (2002), 1711–5.
- 232. Buxton, I. L., and Brunton, L. L., 'Compartments of cyclic AMP and protein kinase in mammalian cardiomyocytes', *Journal of Biological Chemistry*, 258/17 (1983), 10233–9.
- 233. CASTRO, LILIANA R. V., VERDE, IGNACIO, COOPER, DERMOT M. F. et al., 'Cyclic guanosine monophosphate compartmentation in rat cardiac myocytes', *Circulation*, 113/18 (2006), 2221–8.
- 234. HAYES, J. S., BRUNTON, L. L., and MAYER, S. E., 'Selective activation of particulate cAMP-dependent protein kinase by isoproterenol and prostaglandin E1', *Journal of Biological Chemistry*, 255/11 (1980), 5113–9.
- 235. BEAVO, JOSEPH A., and BRUNTON, LAURENCE L., 'Cyclic nucleotide research -- still expanding after half a century', *Nature reviews. Molecular cell biology*, 3/9 (2002), 710–8.
- 236. HOUSLAY, MILES D., 'Underpinning compartmentalised cAMP signalling through targeted cAMP breakdown', *Trends in biochemical sciences*, 35/2 (2010), 91–100.
- 237. BRESCIA, MARCELLA, CHAO, YING-CHI, KOSCHINSKI, ANDREAS et al., 'Multi-Compartment, Early Disruption of cGMP and cAMP Signalling in Cardiac Myocytes from the mdx Model of Duchenne Muscular Dystrophy', *IJMS*, 21/19 (2020), 7056.
- 238. STEINBERG, S. F., and BRUNTON, L. L., 'Compartmentation of G protein-coupled signaling pathways in cardiac myocytes', *Annual review of pharmacology and toxicology*, 41 (2001), 751–73.
- 239. OSTROM, RENNOLDS S., and INSEL, PAUL A., 'The evolving role of lipid rafts and caveolae in G protein-coupled receptor signaling: implications for molecular pharmacology', *British journal of pharmacology*, 143/2 (2004), 235–45.
- 240. NIKOLAEV, VIACHESLAV O., BÜNEMANN, MORITZ, SCHMITTECKERT, EVA et al., 'Cyclic AMP imaging in adult cardiac myocytes reveals far-reaching beta1-adrenergic but locally confined beta2-adrenergic receptor-mediated signaling', *Circulation research*, 99/10 (2006), 1084–91.
- 241. MÉRY, P. F., PAVOINE, C., BELHASSEN, L. et al., 'Nitric oxide regulates cardiac Ca2+ current. Involvement of cGMP-inhibited and cGMP-stimulated phosphodiesterases through guanylyl cyclase activation', *Journal of Biological Chemistry*, 268/35 (1993), 26286–95.

- 242. FEIL, ROBERT, LEHNERS, MORITZ, STEHLE, DANIEL et al., 'Visualising and understanding cGMP signals in the cardiovascular system', *British journal of pharmacology*, 179/11 (2022), 2394–412.
- 243. MOLTZAU, LISE ROMÁN, ARONSEN, JAN MAGNUS, MEIER, SILJA et al., 'Different compartmentation of responses to brain natriuretic peptide and C-type natriuretic peptide in failing rat ventricle', *The Journal of pharmacology and experimental therapeutics*, 350/3 (2014), 681–90.
- 244. WILSON, LINDSAY S., ELBATARNY, HISHAM S., CRAWLEY, SCOTT W. et al., 'Compartmentation and compartment-specific regulation of PDE5 by protein kinase G allows selective cGMP-mediated regulation of platelet functions', *Proceedings of the National Academy of Sciences*, 105/36 (2008), 13650–5.
- 245. ZHANG, LIANG, BOUADJEL, KAOUTER, MANOURY, BORIS et al., 'Cyclic nucleotide signalling compartmentation by PDEs in cultured vascular smooth muscle cells', *British journal of pharmacology*, 176/11 (2019), 1780–92.
- 246. ZHANG, MANLING, TAKIMOTO, EIKI, LEE, DONG-IK et al., 'Pathological cardiac hypertrophy alters intracellular targeting of phosphodiesterase type 5 from nitric oxide synthase-3 to natriuretic peptide signaling', *Circulation*, 126/8 (2012), 942–51.
- 247. LEE, DONG I., ZHU, GUANGSHUO, SASAKI, TAKASHI et al., 'Phosphodiesterase 9A controls nitric-oxide-independent cGMP and hypertrophic heart disease', *Nature*, 519/7544 (2015), 472–6.
- 248. FÖRSTER, TH., 'Zwischenmolekulare Energiewanderung und Fluoreszenz', *Ann. Phys.*, 437/1-2 (1948), 55–75.
- 249. FRET Förster resonance energy transfer: From theory to applications (Weinheim: Wiley-VCH, 2014).
- 250. SPRENGER, JULIA U., and NIKOLAEV, VIACHESLAV O., 'Biophysical techniques for detection of cAMP and cGMP in living cells', *International journal of molecular sciences*, 14/4 (2013), 8025–46.
- 251. SEKAR, RAJESH BABU, and PERIASAMY, AMMASI, 'Fluorescence resonance energy transfer (FRET) microscopy imaging of live cell protein localizations', *The Journal of cell biology*, 160/5 (2003), 629–33.
- 252. BÖRNER, SEBASTIAN, SCHWEDE, FRANK, SCHLIPP, ANGELA et al., 'FRET measurements of intracellular cAMP concentrations and cAMP analog permeability in intact cells', *Nature protocols*, 6/4 (2011), 427–38.
- 253. CHAO, YING-CHI, SURDO, NICOLETTA C., PANTANO, SERGIO et al., 'Imaging cAMP nanodomains in the heart', *Biochemical Society Transactions*, 47/5 (2019), 1383–92.
- 254. SURDO, NICOLETTA C., BERRERA, MARCO, KOSCHINSKI, ANDREAS et al., 'FRET biosensor uncovers cAMP nano-domains at β-adrenergic targets that dictate precise tuning of cardiac contractility', *Nat Commun*, 8/1 (2017).
- 255. GÖTZ, KONRAD R., SPRENGER, JULIA U., PERERA, RUWAN K. et al., 'Transgenic mice for real-time visualization of cGMP in intact adult cardiomyocytes', *Circulation research*, 114/8 (2014), 1235–45.
- 256. NIKOLAEV, VIACHESLAV O., BÜNEMANN, MORITZ, HEIN, LUTZ et al., 'Novel single chain cAMP sensors for receptor-induced signal propagation', *The Journal of biological chemistry*, 279/36 (2004), 37215–8.
- 257. PRASHER, D. C., ECKENRODE, V. K., WARD, W. W. et al., 'Primary structure of the Aequorea victoria green-fluorescent protein', *Gene*, 111/2 (1992), 229–33.
- 258. NARESH, VARNAKAVI., and LEE, NOHYUN, 'A Review on Biosensors and Recent Development of Nanostructured Materials-Enabled Biosensors', *Sensors (Basel, Switzerland)*, 21/4 (2021).
- 259. RODRIGUEZ, ERIK A., CAMPBELL, ROBERT E., LIN, JOHN Y. et al., 'The growing and glowing toolbox of fluorescent and photoactive proteins', *Trends in biochemical sciences*, 42/2 (2016), 111–29.

- 260. CALAMERA, GAIA, LI, DAN, ULSUND, ANDREA HEMBRE et al., 'FRET-based cyclic GMP biosensors measure low cGMP concentrations in cardiomyocytes and neurons', *Commun Biol*, 2/1 (2019), 2336.
- 261. RUSSWURM, MICHAEL, MULLERSHAUSEN, FLORIAN, FRIEBE, ANDREAS et al., 'Design of fluorescence resonance energy transfer (FRET)-based cGMP indicators: a systematic approach', *The Biochemical Journal*, 407/Pt 1 (2007), 69–77.
- 262. THUNEMANN, MARTIN, FOMIN, NATALIE, KRAWUTSCHKE, CHRISTIAN et al., 'Visualization of cGMP with cGi biosensors', *Methods in molecular biology (Clifton, N.J.)*, 1020 (2013), 89–120.
- 263. KOSCHINSKI, ANDREAS, and ZACCOLO, MANUELA, 'Activation of PKA in cell requires higher concentration of cAMP than in vitro: implications for compartmentalization of cAMP signalling', *Scientific reports*, 7/1 (2017), 14090.
- 264. THUNEMANN, MARTIN, WEN, LAI, HILLENBRAND, MATTHIAS et al., 'Transgenic mice for cGMP imaging', *Circulation research*, 113/4 (2013), 365–71.
- 265. BOCK, ANDREAS, ANNIBALE, PAOLO, KONRAD, CHARLOTTE et al., 'Optical Mapping of cAMP Signaling at the Nanometer Scale', *Cell*, 182/6 (2020), 1519-1530.e17.
- 266. MARGINEANU, ANCA, CHAN, JIA JIA, KELLY, DOUGLAS J. et al., 'Screening for proteinprotein interactions using Förster resonance energy transfer (FRET) and fluorescence lifetime imaging microscopy (FLIM)', *Scientific reports*, 6 (2016), 28186.
- 267. THUNEMANN, MARTIN, 'Generation and Characterization of Transgenic Mice for Noninvasive Cell Tracking with PET and for FRET-based cGMP Imaging'.
- 268. CALEBIRO, DAVIDE, NIKOLAEV, VIACHESLAV O., GAGLIANI, MARIA CRISTINA et al., 'Persistent cAMP-Signals Triggered by Internalized G-Protein—Coupled Receptors', *PLoS Biology*, 7/8 (2009), e1000172 http://dx.doi.org/10.1371/journal.pbio.1000172.
- 269. JESPERSEN, NAJA ZENIUS, LARSEN, THERESE JUHLIN, PEIJS, LONE et al., 'A classical brown adipose tissue mRNA signature partly overlaps with brite in the supraclavicular region of adult humans', *Cell metabolism*, 17/5 (2013), 798–805.
- 270. LIVAK, K. J., and SCHMITTGEN, T. D., 'Analysis of relative gene expression data using real-time quantitative PCR and the 2(-Delta Delta C(T)) Method', *Methods (San Diego, Calif.)*, 25/4 (2001), 402–8.
- 271. MATSUDA, SHOGO, HARADA, KAZUKI, ITO, MOTOKI et al., 'Generation of a cGMP Indicator with an Expanded Dynamic Range by Optimization of Amino Acid Linkers between a Fluorescent Protein and PDE5α', ACS sensors, 2/1 (2017), 46–51.
- 272. ZIMMERMANN, KATRIN, SCHEIBE, OLIVER, KOCOUREK, ANDREAS et al., 'Highly efficient concentration of lenti- and retroviral vector preparations by membrane adsorbers and ultrafiltration', *BMC biotechnology*, 11 (2011), 55.
- KOSUGI, SHUNICHI, HASEBE, MASAKO, MATSUMURA, NOBUTAKA et al., 'Six classes of nuclear localization signals specific to different binding grooves of importin alpha', *Journal* of Biological Chemistry, 284/1 (2009), 478–85.
- 274. APOLLONI, A., PRIOR, I. A., LINDSAY, M. et al., 'H-ras but not K-ras traffics to the plasma membrane through the exocytic pathway', *Molecular and cellular biology*, 20/7 (2000), 2475–87.
- 275. KEEFER, L. K., NIMS, R. W., DAVIES, K. M. et al., "NONOates" (1-substituted diazen-1-ium-1,2-diolates) as nitric oxide donors: convenient nitric oxide dosage forms', *Methods in enzymology*, 268 (1996), 281–93.
- 276. ARMBRUSTER, BLAINE N., LI, XIANG, PAUSCH, MARK H. et al., 'Evolving the lock to fit the key to create a family of G protein-coupled receptors potently activated by an inert ligand', Proceedings of the National Academy of Sciences of the United States of America, 104/12 (2007), 5163–8.
- 277. LIU, C., and HERMANN, T. E., 'Characterization of ionomycin as a calcium ionophore', *Journal of Biological Chemistry*, 253/17 (1978), 5892–4.

- 278. KANNABIRAN, SUKANYA ARCOT, GOSEJACOB, DOMINIC, NIEMANN, BIRTE et al., 'Real-time monitoring of cAMP in brown adipocytes reveals differential compartmentation of β1 and β3-adrenoceptor signalling', *Molecular metabolism*, 37 (2020), 100986.
- 279. PERDIKARI, ALIKI, LEPARC, GERMÁN GASTÓN, BALAZ, MIROSLAV et al., 'BATLAS: Deconvoluting Brown Adipose Tissue', *Cell Reports*, 25/3 (2018), 784-797.e4.
- 280. BALLIGAND, J-L, FERON, O., and DESSY, C., 'eNOS activation by physical forces: from short-term regulation of contraction to chronic remodeling of cardiovascular tissues', *Physiological reviews*, 89/2 (2009), 481–534.
- 281. *cGMP:* generators, effectors and therapeutic implications (Handbook of experimental pharmacology, Vol. 191, Berlin, Heidelberg: Springer, 2008) http://www.springerlink.com/content/p36541.
- 282. DI IORIO, PATRIZIA, RONCI, MAURIZIO, GIULIANI, PATRICIA et al., 'Pros and Cons of Pharmacological Manipulation of cGMP-PDEs in the Prevention and Treatment of Breast Cancer', *International journal of molecular sciences*, 23/1 (2022), 262 https://www.mdpi.com/1422-0067/23/1/262.
- 283. ZHANG, JASON Z., LU, TSAN-WEN, STOLERMAN, LUCAS M. et al., 'Phase Separation of a PKA Regulatory Subunit Controls cAMP Compartmentation and Oncogenic Signaling', *Cell*, 182/6 (2020), 1531-1544.e15.
- 284. HAN, P., WERBER, J., SURANA, M. et al., 'The calcium/calmodulin-dependent phosphodiesterase PDE1C down-regulates glucose-induced insulin secretion', *Journal of Biological Chemistry*, 274/32 (1999), 22337–44.
- 285. DIPILATO, LISA M., AHMAD, FAIYAZ, HARMS, MATTHEW et al., 'The Role of PDE3B Phosphorylation in the Inhibition of Lipolysis by Insulin', *Molecular and cellular biology*, 35/16 (2015), 2752–60.
- 286. Chung, Youn Wook, Ahmad, Faiyaz, Tang, Yan et al., 'White to beige conversion in PDE3B KO adipose tissue through activation of AMPK signaling and mitochondrial function', *Scientific reports*, 7 (2017), 40445.
- 287. Choi, Young Hun, Park, Sunhee, Hockman, Steven et al., 'Alterations in regulation of energy homeostasis in cyclic nucleotide phosphodiesterase 3B-null mice', *The Journal of clinical investigation*, 116/12 (2006), 3240–51.
- 288. KEICHER, CHRISTIAN, GAMBARYAN, STEPAN, SCHULZE, ELFRIEDE et al., 'Phosphorylation of mouse LASP-1 on threonine 156 by cAMP- and cGMP-dependent protein kinase', *Biochemical and Biophysical Research Communications*, 324/1 (2004), 308–16.
- 289. FEITEIRO, JOANA, VERDE, IGNACIO, and CAIRRÃO, ELISA, 'Cyclic guanosine monophosphate compartmentation in human vascular smooth muscle cells', *Cellular signalling*, 28/3 (2016), 109–16.
- 290. FALEEVA, MARIA, DIAKONOV, IVAN, SRIVASTAVA, PRASHANT et al., 'Compartmentation of cGMP Signaling in Induced Pluripotent Stem Cell Derived Cardiomyocytes during Prolonged Culture', *Cells*, 11/20 (2022).

Summary

Obesity is characterized by an imbalance between energy intake and expenditure, resulting in an abnormal accumulation of white adipose tissue (WAT), the primary form of energy storage in humans. Brown adipose tissue (BAT) possesses the unique ability to dissipate energy in the form of heat, making it a promising target for the development of novel obesity treatments.

Earlier studies have shown that the cyclic nucleotide cyclic guanosine monophosphate (cGMP) plays a pivotal role in BAT function. cGMP enhances brown adipocyte (BA) differentiation, mitochondrial biogenesis, thermogenesis, and energy expenditure and induces browning of WAT.

While previous research has focused on the role of cyclic adenosine monophosphate (cAMP) as well as its compartmentalization in various cell types, such as BA, the subcellular architecture of cGMP compartmentalization remains poorly understood in general and unexplored in BA.

Thus, the primary objective of this thesis was to provide a detailed characterization of the cGMP subcellular compartmentalization in murine and human BA, as well as their progenitors. To achieve this, a range of live-cell imaging techniques, such as Förster-resonance energy transfer and intensiometric biosensors, were employed and developed.

The experiments conducted in this study reveal that cGMP does not freely diffuse within BA. Instead, cGMP forms distinct subcellular pools that are regulated by different guanylate cyclases (GC) and phosphodiesterases (PDE). Moreover, the regulation of these pools by GCs and PDEs changes during the differentiation of BA progenitors into fully mature BA.

Additional experiments revealed a pivotal role of PDE1 in regulating exclusively natriuretic peptide-mediated cGMP in murine and human BA, while not interacting with nitric oxide induced cGMP. Moreover, PDE1 conveyed a cGMP-pool specific crosstalk between calcium and natriuretic peptide associated cGMP, while showing no interactions with nitric oxide associated cGMP. This observation underscores the potential druggability of individual subcellular cGMP pools by inhibiting specific associated PDEs.

While most research on cGMP in BA has focused on protein kinase G as a downstream effector, the findings presented in this thesis emphasize PDEs as important downstream effectors of cGMP. cGMP competitively inhibits the highly expressed PDE3, leading to increased intracellular cAMP levels, promoting lipolysis and energy expenditure in a synergistic manner to norepinephrine.

The differences between human and murine BA are well documented. However, the subcellular distinctions remain unclear. The data presented here reveal significant variations

in the subcellular architecture of cGMP compartmentalization in human versus murine BA. Different GCs mediate cGMP synthesis in human versus murine BA and different PDEs are involved in cGMP degradation. Nevertheless, cGMP compartmentalization, as well as the specific interaction of calcium with PDE1 and natriuretic peptide-derived cGMP, are consistent in both human and murine BA.

Lastly, the targeted sensors developed during this project revealed another dimension of cGMP compartmentalization in human BA progenitors. The data demonstrate that while nitric oxide does not induce detectable cGMP level increases in the cytosol it instead enhances cGMP levels specifically at the nucleus. Thus, cGMP appears to be compartmentalized into different cytosolic pools but also different organelle-associated pools.